Determination of Ligand Binding Conformations at α_1-Adrenergic Receptor Subtypes Based on NMR and MD studies

By

Tasneem M. Vaid

Submitted in total fulfilment of the requirements of the degree of Doctor of Philosophy

May 2019

Department of Biochemistry and Molecular Biology
Bio21 Molecular Science and Biotechnology Institute
The University of Melbourne

Under the supervision of:
A/Prof. Paul Gooley
Dr. Daniel Scott

“Because when it all comes together, it’s amazing. When it all comes together, the only thing you can do is bow down in gratitude, as if you have been granted an audience with the divine.
Because you have.”

Elizabeth Gilbert
Big Magic.

ABSTRACT

Adrenergic receptor (AR) subtypes (α_{1A}, α_{1B}, α_{1D}, α_{2A}, α_{2B}, α_{2C}, β_1, β_2, β_3) are G-protein coupled receptors (GPCRs) activated by the same endogenous catecholamines, adrenaline and nor-adrenaline. The two subtypes α_{1A}- and α_{1B}-AR maintain a complex balance in modulating the functions of the sympathetic and central nervous systems, whereby chronic activity can be either detrimental or protective for both heart and brain function. Regulation is believed to be mediated through the distinct activation of individual α_1-AR subtypes and thus, subtype selective activation or blocking may have major clinical implications.

Despite having tremendous clinical importance, there are no approved α_{1A}- or α_{1B}-AR selective marketed drugs. Firstly, the conservation of the orthosteric binding site within a GPCR family makes it challenging to achieve receptor subtype selectivity for competitive compounds. In such a case, allosteric modulators, which interact with binding sites that are topographically distinct from the binding site of the endogenous ligand, offer an alternative. Secondly, lack of structural information of a majority of GPCR members makes it difficult to predict ligand binding. Intrinsic instability of these receptors make crystallisation challenging and as yet, no crystal structure has been reported for α_1-AR subtypes while crystallising weakly binding ligands to GPCRs is difficult. The broad aim of the thesis was to gain molecular insight into the structures of weakly binding GPCR ligands by applying atomic resolution NMR methods.

In this study, we have used variants of α_{1A}- and α_{1B}-AR which were thermostabilised using the directed evolution method, Cellular high throughput encapsulation, solubilisation and screening (CHESS). The long-term stability of these receptors in detergents has enabled us to investigate binding of a variety of ligands including native agonists, adrenaline and noradrenaline, an α_{1A}-AR selective agonist A-61603, as well as allosteric modulators, benzodiazepines, by employing solution-based ligand-observed Nuclear Magnetic Resonance methods including STD-NMR (saturation transfer difference NMR), Water-LOGSY (water-ligand observed via gradient spectroscopy), Tr-NOESY (transferred nuclear overhauser effect spectroscopy) and INPHARMA (interligand noes for pharmacophore mapping) experiments. These are nuclear overhauser effect based methods, which rely on the transfer of magnetisation from the target protein or other molecules (such as bulk water and ligand) to

ligands through dipole–dipole interactions. STD-NMR and Water-LOGSY experiments are most commonly used to detect weak ligand binding and in fragment screening projects, while Tr-NOESY and INPHARMA are used to detect and map ligand binding conformations. The INPHARMA experiment takes advantage of known or expected orientations of a bound ligand, for example adrenaline bound to its GPCRs, to determine the respective orientation of novel ligands for which there are no known structures. We obtained experimental NMR data for the ligand A-61603 (α_{1A}-AR selective agonist) with respect to adrenaline for both α_{1A}- and α_{1B}-AR. These data were compared to the back-calculated spectra obtained from molecular dynamics simulations. The results helped mechanistically explain the selectivity of A-61603 towards α_{1A}-AR. Overall, we have shown that this solution-based methodology provides valuable information on ligand-binding poses inside the highly conserved orthosteric binding site of ARs, dissecting out subtle structural variations across the subtypes and thereby may aid in future subtype selective drug development.

DECLARATION

This is to certify that

- the thesis comprises of my original work towards the degree of Doctor of Philosophy,
- due acknowledgment has been made in the text to all other material used,
- the thesis is less than 100,000 words in length, exclusive of tables, maps, bibliographies and appendices.

Tasneem Vaid

PUBLICATIONS

- Williams, Lisa M., Xiaoji He, **Tasneem M. Vaid**, et al. “Diazepam Is Not a Direct Allosteric Modulator of A1-adrenoceptors, but Modulates Receptor Signaling by Inhibiting Phosphodiesterase-4.” Pharmacology Research & Perspectives 7 (1): (2019).

- Kelvin J. Yong, **Tasneem M. Vaid**, Patrick J. Shilling, et al. Determinants of Ligand Subtype-Selectivity at α1A-Adrenoceptor Revealed Using Saturation Transfer Difference (STD) NMR. ACS Chem. Biol. 13(4): 1090–1102 (2018).

ACKNOWLEDGEMENT

This Ph.D. has been an exciting journey. I owe my gratitude to many people I met on the way, and to those who were with me from the start. First and foremost, I would like to thank my supervisor Paul Gooley, for believing in my potential and accepting me into his group at the Bio21 Institute and providing me with this exciting project bundled with ideas and inspiration. His constant support and advice made this thesis possible. I would like to thank my co-supervisor Daniel Scott, for being a mentor more than a supervisor. His out of the box ideas and a keen interest in the project always fuelled my enthusiasm towards the work. Next, I would like to thank my "virtual" supervisor David Chalmers at the Monash institute of pharmaceutical sciences (MIPS). All MD simulation work presented herein was done in collaboration with him. I feel fortunate to have learned so much from him about biomolecular modelling, which I have always been interested in. The members of my thesis advisory committee Mike Griffin, Spencer Williams and Michael Kuiper are gratefully acknowledged for their duties during my Ph.D., providing valuable suggestions and ensuring timely completion of my work. Next, I would like to thank Christian Griesinger, Dirk Bockelmann and Pablo Trigo Mourino from the Max Planck Institute for Biophysical Chemistry, Göttingen, for kindly providing us the SpINPHARMA software, which has been tested in this work.

I owe my deepest gratitude to the lab-mate turned post-doc, Ashish Sethi, at the Bio21 Institute for his constant support from day one and for helping me solve every minor and major issue and for making me feel like nothing can go wrong. A big thank you to my lab mates, past and present. They are the most amazing people on earth. Thanks Kelvin, for helping me get hold of the basic experiments at the start of my Ph.D. Thanks Fabian, for all your help with the SEC, SAXS and for setting up the stage for the MD work by starting the collaboration with David at MIPS, which later turned out to be the significant chunk of my work. Thanks J (Feng-Jie) for all your minor and major help with the protein expression, purifications, SEC and what not. Thanks to Jingyu, for being a special friend and a constant support. Special thanks to Mohammad Tanipour, Fei Yan, Shatabdi Chakraborty, Samantha Lagaida, Shoni Bruell, Alamgir Hossain, Ericka Tudhope for being the nicest people ever. It was great to have you guys around! A special thanks go to Kathy Huang, who was an

honour's student in our lab. I happened to supervise her on her exciting and challenging work, which turned out to be a major promising project later on. That teaching taught me way more than I could teach her.

Special thanks go to the NMR facility at Bio21, especially Hamish Grant for all his help with major and minor issues. Shenggen, David, Paul and Sunnia have been very helpful. Thanks to Jim Dang from IT facility for his assistance. I am grateful to have received a Melbourne international fee remission (MIFRS) and a Melbourne international research scholarship (MIRS) from the University of Melbourne for my Ph.D. studies. I would like to thank the Department of Biochemistry and Molecular Biology for providing me the travel award which funded my visit to the GPCR Workshop at Hawaii. Further financial support covering the extensions of my Ph.D. course and conference attendances was generously provided by my supervisors at the Department of Biochemistry and Molecular Biology, the Bio21 Institute and the Florey Institute of Neuroscience and Mental Health.

I owe my deepest gratitude to my family. Without their support, blessings and spirit this would not have been possible. This is for them. Their "you can do it" attitude kept me inspired and encouraged always. My mom, Rehana and dad, Abbas are the loveliest people and the best parents one can have. I cannot thank them enough for all they have done for me, for believing in me, for supporting me no matter what and for being there for me always! Special thanks to my brother, Tayyab and sister Mariya, for their purest love; brother- and sister-in-law, Mohammed and Tasneem for their support and guidance; and my nieces, Jamila and Zahra, and nephew, Burhanuddin for just being adorable.

My relationship with my permanent housemate, my husband, Murtuza, is a Ph.D. old. The past four years nurtured our belief in each other's capabilities and our respect for each other's work. Thanks, for being the greatest support. I owe my deepest gratitude to my in-laws Abbas and Sakina, for taking care of me at the time when I needed it the most. Most of my thesis writing credit goes to them, they were at the back-stage taking care of the other things helping me focus on my work. They are the best people on earth!

Last but not least, I owe my gratitude to countless people at the Bio21 Institute and the Florey for making my time here in Melbourne, an experience I will keep dearly.

TABLE OF CONTENT

LIST OF TABLES

LIST OF FIGURES

LIST OF SUPPLEMENTARY FIGURES

LIST OF ABBREVIATIONS

[^{125}I]HEAT	2-[β-(4-hydroxyl-3-[^{125}I]iodophenyl)ethylamineomethyl]tetralone
1D	One-dimensional
2D	Two-dimensional
3D	Three-dimensional
5HT	5-hydroxytryptamine receptor
9AA	9-aminoacridine
$A_{2A}R$	Adenosine A2A receptor
ACO	Ant colony optimisation
ADGR	Adhesion GPCR
Adr-Nb-β_2AR	Adrenaline bound, nanobody stabilised β_2-AR
AP	Adapter Protein
BI-Nb-β_2AR	BI167107 bound, nanobody stabilised β_2-AR
BLT2	Leukotriene B4 receptor 2
BPH	Benign prostatic hyperplasia
BPTI	Bovine pancreatic trypsin inhibitor
BVES	Baculovirus expression system
C5aR1	Complement c5a receptor 1
cAMP	Cyclic-adenosine monophosphate
CAMs	Constitutively activating mutations
CAMt	Constitutively active mutant
Car-β_2AR	Carazolol bound β_2-AR structure
CCR	CC chemokine receptor
CHAPS	3-[(3-cholamidopropyl)dimethylammonio]-1-propanesulfonate
CHESS	Cellular high-throughput encapsulation, stabilisation and selection
CHS	Cholesterol hemi-succinate
CNS	Central nervous system
COPD	Chronic obstructive pulmonary disease
CORCEMA	Complete relaxation and conformational exchange matrix
CRD	Cysteine-rich domain
CRE	cAMP response element
CRHR	Corticotropin-releasing hormone receptor
CTF	C-terminal fragment
CXCR4	C-X-C chemokine receptor type 4
D2O	Deuterium oxide
DDM	N-Dodecyl-β-D-maltoside
DM	N-Decyl-β-D-maltoside
DMPC	1,2-dimiristoyl-SN-glycero-3-phosphocholine
DMSO	Dimethyl sulfoxide
DPPC	Dipalmitoylphosphatidylcholine
DR	Dopamine receptor

DRD_2	D_2 Dopamine receptor
DSS	2,2-Dimethyl-2-silapentane-5-sulfonate
DVL	Dishevelled (phosphoprotein)
E. coli	*Escherichia coli*
ECD	Extracellular domain
ECL	Extracellular
Eff	Effector proteins
EGFR	Epidermal growth factor receptor
epPCR	Error-prone PCR
FACS	Fluorescence-activated cell sorting
FBDD	Fragment-based drug discovery
FBS	Fragment-based screening
FDA	Food and drug administration
FF	Force field
FSHR	Follicle stimulating hormone receptor
FZDRs	Frizzled receptors
GABA	γ-aminobutyric acid
$GABA_AR$	γ-aminobutyric acid receptor type A
$GABA_BR$	γ-aminobutyric acid receptor type B
GAIN	GPCR-auto proteolysis inducing
GCGR	Glucagon receptor
GDP	Guanosine diphosphate
GEF	Guanosine exchange factor
GLP1R	Glucagon-like peptide 1 receptor
GPR40	G-protein-coupled receptor 40
GPRC	G-protein–coupled receptor family C
GPS	GPCR proteolysis site
GRKs	GPCR kinases
GTP	Guanosine triphosphate
HH	Hedgehog (protein)
HMQC	Heteronuclear multiple quantum correlation
HRH_1	Histamine H1 receptor
HRV	Human rhino virus
HSQC	Heteronuclear single quantum correlation
IC_{50}	Half-maximal inhibitory concentration
IL	Intracellular
ILOE	Inter-ligand NOE
IMAC	Immobilised metal affinity chromatography
INPHARMA	Interligand noes for pharmacophore mapping
IP3	Inositol-triphosphate
IPTG	Isopropyl β-D-1-thiogalactopyranoside
KO	Knockout
LB	Luria broth

LBDD	Ligand-based drug discovery
LHCGR	Luteinizing hormone receptor
LMNG	Lauryl maltose neopentyl glycol
mACHR	Muscarinic acetylcholine receptor
MBP	Maltose binding protein
MBPss	Maltose-binding protein signal sequence
MD	Molecular dynamics
mGluR	Metabotropic glutamate receptors
MUC-1	Mucin 1
muGFP	Monomeric ultrastable green fluorescent protein
NAM	Negative allosteric modulator
NCBI	National center for biotechnology information
NG	β-D-nonylglucopyranoside
NOE	Nuclear overhauser effect
NTF	N-terminal fragment
NTS_1	Neurotensin receptor type 1
OD_{600}	Optical density unit at 600 nm wavelength
OG	B-D-octylglucopyranoside
oGPCRs	orphan GPCRs
P2Y	Purinergic receptor
PAGE	Polyacrylamide gel electrophoresis
PAM	Positive allosteric modulator
PAR	Protease activated receptors
Pcc	Pearson correlation coefficient
PDEs	Phosphodiesterases
PI	Phosphatidylinositol
PKA	Protein kinase A
PLANTS	Protein-ligand ant system
PME	Particle-mesh Ewald
POPC	1-palmitoyl-2-oleoyl-*sn*-glycero-3-phosphocholine
Ptc	Patched (protein)
PTH1R	Parathyroid hormone receptor type 1
PTSD	Posttraumatic stress disorder
QAPB	Quinazoline piperazine bodipy
RF	Radio frequency
rHDL	Recombinant high density lipoproteins
RMSD	Root mean square deviation
RXFP	Relaxin family peptide receptors
SAM	Silent allosteric modulator
SARs	Structure-activity relationships
SDS	Sodium dodecyl sulphate
SEC	Size exclusion chromatography
sfGFP	Super-folded green fluorescent protein
SMOR	Smoothened receptor

SOS	Structural information using overhauser effects and selective labelling
StaRs(R)	Stabilised receptors (via alanine scanning mutagenesis)
STD	Saturation transfer difference
T2Rs	Taste2 receptors
T4L	T4 lysozyme
TINS	Target immobilised NMR screening
Tr-NOESY	Transferred NOE spectroscopy
TROSY	Transverse relaxation-optimised spectroscopy
TSHR	Thyrotropin receptor
VFT	Venus flytrap
Water-LOGSY	Water-ligand observed via gradient spectroscopy
WT	Wild-type
β-arr	β-arrestin
κOR	κ-opioid receptor
μOR	μ-opioid receptor

AMINO ACID NAME, THREE-LETTER CODE AND ONE-LETTER CODE

Ala	Alanine (A)
Arg	Arginine (R)
Asn	Asparagine (N)
Asp	Aspartate (D)
Cys	Cysteine (C)
Gln	Glutamine (Q)
Glu	Glutamate (E)
Gly	Glycine (G)
His	Histidine (H)
Ile	Isoleucine (I)
Leu	Leucine (L)
Lys	Lysine (K)
Met	Methionine (M)
Phe	Phenylalanine (F)
Pro	Proline (P)
Ser	Serine (S)
Thr	Threonine (T)
Trp	Tryptophan (W)
Tyr	Tyrosine (Y)
Val	Valine (V)

CHAPTER 1 : INTRODUCTION

1.1. G-protein-coupled receptors

One of the baffling questions in biology for almost over a century was how cells sense and respond to extracellular stimuli. The hypothesis that there are cell membrane spanning receptors capable of sensing and transducing signals might sound logical today but when it was first proposed, it was rejected[1]. Years of biochemical exploration later proved that such receptors exist, most of which are G-protein-coupled receptors (GPCRs) that share the typical architecture of seven transmembrane (TM) spanning helices.[2,3] GPCRs are widely represented in most life forms, including all of the major model organisms, from bacteria to fungi and animals[4]. In humans, they constitute by far the largest, most versatile and most ubiquitous of the several families of the cell surface receptors with over 800 encoded in the human genome[5,6]. GPCRs are involved in almost every aspect of human life, from early development and heart function to neuronal activity[7,8]. The first X-ray crystal structure of a GPCR, bovine rhodopsin provided a glimpse into the atomic structure confirming its heptahelical topology[9]. GPCRs are highly unstable when isolated from membranes and hence it took another seven years until advanced techniques were available that facilitated crystallisation of the first human GPCR, β_2-adrenergic receptor[10]. Since then, more than 60 different GPCR structures have been solved with over 200 of their complexes with different ligands[11]. Cryogenic electron microscopy (Cryo-EM) structures are also appearing rapidly[12–18] and a structure has been reportedly solved using solid-state nuclear magnetic resonance (NMR) spectroscopy[19]. In 2012, the Nobel Prize for Chemistry was awarded to Brian K. Kobilka and Robert J. Lefkowitz for their pioneering developments in the studies of GPCRs at the atomistic level[20].

1.2. GPCR signalling

All GPCRs share the typical architecture of seven transmembrane spanning α helices connected by three extracellular and three intracellular loop regions, an intracellular carboxyl-terminal and an extracellular amino-terminal. When an activating ligand (agonist) binds to the extracellular domains of the receptor, ligand-specific conformational changes are triggered leading to specific intracellular signalling responses (Figure 1.1). These responses are mediated through intracellular partner proteins, either heterotrimeric G-proteins or β-arrestins that selectively interact with particular receptor conformations.

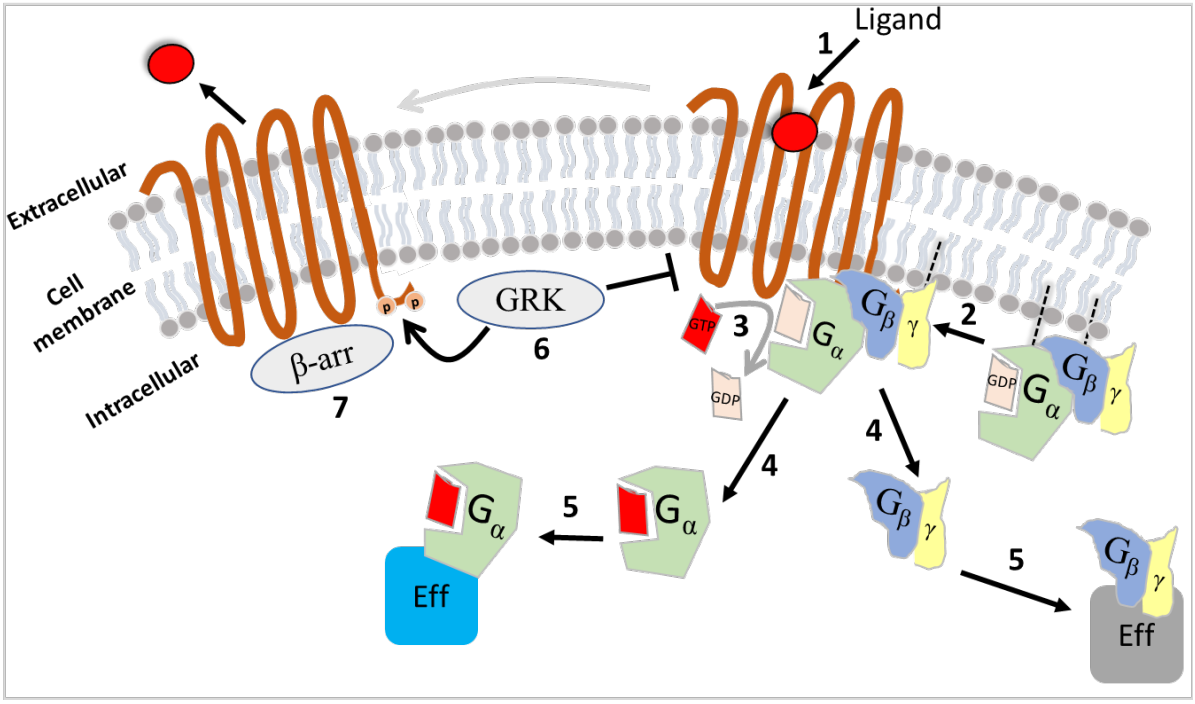

Figure 1.1. GPCR signalling events. (1) A ligand (agonist) induces an active-like conformational equilibrium that facilitates guanosine diphosphate (GDP) bound heterotrimeric G-proteins to couple to the intracellular domain of the GPCR (2). The fully activated GPCR acts as a guanosine exchange factor (GEF) triggering the exchange of GDP with guanosine-5'-triphosphate (GTP) (3). GTP-bound G-protein dissociates from the GPCR as a Gα-monomer and a Gβ/γ-dimer (4) which independently activate specific effector proteins (Eff, 5). G-protein coupling triggers phosphorylation of the GPCR C-terminus by G-protein coupled receptor kinases (GRKs, 6) which allows β-arrestins (β-arr) to bind to the intracellular domain of the GPCR and terminates GPCR signalling.

1.2.1. G-protein mediated signalling

The G-protein is a heterotrimeric guanine nucleotide binding protein consisting of Gα, Gβ and Gγ subunits tethered to the cell membrane. In mammals, Gα, Gβ and Gγ subunits are encoded by 16, 5 and 12 different genes respectively[21]. GPCRs interact primarily with the Gα subunit but have also been shown to interact with the Gβ and Gγ subunits[22]. Ligand binding promotes GPCR interaction with its cognate G-protein which catalyse the exchange of guanosine diphosphate (GDP) from the Gα in exchange for guanosine triphosphate (GTP), and dissociation of the GTP-bound Gα-subunit from the Gβγ-dimer[23,24] (Figure 1.1). The Gα-subunit family consists of four sub-families based on sequence similarity; $G\alpha_s$, $G\alpha_i$, $G\alpha_{q/11}$

and $G\alpha_{12/13}$. Both Gα subunits and Gβγ-dimers of the heterotrimeric G-proteins can couple to downstream effector molecules such as phospholipase C (activated by $G\alpha_q$ or $G\alpha_{11}$) or adenylyl cyclase (activated by $G\alpha_s$ and inhibited by $G\alpha_i$). This coupling regulates distinct cellular signalling cascades that involve second messengers such as cyclic adenosine monophosphate (cAMP) (with $G\alpha_s$ or $G\alpha_i$ activation) and intracellular Ca^{2+} (with $G\alpha_q$ or $G\alpha_{11}$ activation) leading to various downstream responses[25,26].

1.2.2. β-arrestin mediated signalling

The activated GPCR/G-protein signalling is terminated by the recruitment of GPCR kinases (GRKs)[27]. Gβγ recruits a GRK to the GPCR[28], GRKs then phosphorylate GPCRs at Ser or Thr residues in the intracellular loop (IL)3 or the C-terminal tail of the activated receptor[29]. This phosphorylation of the GPCR results in the binding of β-arrestin (mostly β-arrestin 1 and β-arrestin 2)[30], leading to desensitisation and subsequent recruitment of clathrin and its adaptor protein (AP)2, to internalize the GPCR via endocytosis[31]. Recently, it has been proposed that there is a possibility that after GPCR internalisation and dissociation from β-arrestin, a second G-protein signalling phase originates from GPCRs in endosomes[32]. Studies suggest that arrestins not only tag GPCRs for recycling but also connect GPCRs with a number of signalling pathways independent of G-proteins[33]. Also, it has been shown that GPCR phosphorylation can vary between cell-types leading to tissue specific signalling[34].

1.3. Classification of GPCRs

Historically the GPCRs have been classified on the basis of function and sequence similarity resulting in multiple classification systems. The following describes the three main classification systems in use for GPCRs:

1) The A-F system. This system of GPCR classifies GPCR sequences from both vertebrates and invertebrates, based on their amino acid sequence and functional similarities into six classes, A, B, C, D, E and F[35,36]. GPCRs from all classes contain characteristic seven hydrophobic TM helices. Class A or "rhodopsin-like family", is the largest group of GPCRs (accounting for around 80% of all GPCRs) and includes hormone, neurotransmitter and light receptors. Structurally, all class A GPCRs contain an eighth helix and a palmitoylated Cys at the C terminal region. Class B or the "secretin receptor family" consists of around 70 receptors and contains a long N-terminal domain of around 120 residues stabilised by

disulfide bonds. Class C includes the γ-aminobutyric acid (GABA) receptors, metabotropic glutamate family, calcium-sensing receptors and the taste receptors. These receptors are characterised by having a large extracellular N-terminal ligand binding domain of ~600 residues which is connected to the TM1 by a cysteine-rich loop. Class D includes fungal mating pheromone receptors, class E includes cAMP receptors and class F includes frizzled/smoothened receptors.

2) The "GRAFS" system. This system is based on phylogenetic-tree analysis of ~800 human GPCR sequences[37] and comprises five main families: Glutamate (G), Rhodopsin (R), Adhesion (A), Frizzled/Taste2 (F), and Secretin (S). The primary difference between the A-F system and the GRAFS system is the splitting of class B into two separate families, Secretin and Adhesion, in the GRAPHS system. This separation was based on the preliminary observation that the two families evolved distinctly from each other.

3) GPCRdb classification. The GPCR data base (GPCRdb) classifies human GPCRs into six classes (or families): A (Rhodopsin), B1 (Secretin), B2 (Adhesion), C (Glutamate), F (Frizzled) and Taste 2 based on evolutionary relationships[36,38]. The taste type 2 receptors were recently classified as a sixth class distinguishing it as having evolved from class A[39] and abbreviated with T. Classes A and B1 bind their endogenous ligands in the 7TM region, while for class B2, C and F GPCRs, 7TM is a site for allosteric modulation. Instead, these latter GPCRs have their orthosteric site in an extracellular domain[40]. Throughout this work, we have used the GPCRdb classification system. The following sections introduce each GPCR family in greater details.

1.3.1. Class A - The rhodopsin family

The rhodopsin family is by far the largest family of GPCRs consisting of 672 receptors of which 284 are non-olfactory receptors[41]. The GPCRs of this family are well-known for the diversity of their ligands[42], ranging from photons, ions to small-molecules and peptides like hormones and neurotransmitter to bigger proteins, for example, chemokines. For better referencing Ballesteros and Weinstein[43] have proposed a two-digit numbering system for amino acids in rhodopsin family GPCRs where the first number represents the transmembrane helix (1 to 7) in which the residue is located and the second number indicates its position relative to the most conserved residue in the corresponding helix which is given the value 50.

Starting from TM1, these conserved residues are Asn$^{1.50}$ (100% conservation), Asp$^{2.50}$ (94%), Arg$^{3.50}$ (96%), Trp$^{4.50}$ (96%), Pro$^{5.50}$ (77%), Pro$^{6.50}$ (100%), and Pro$^{7.50}$ (96%).

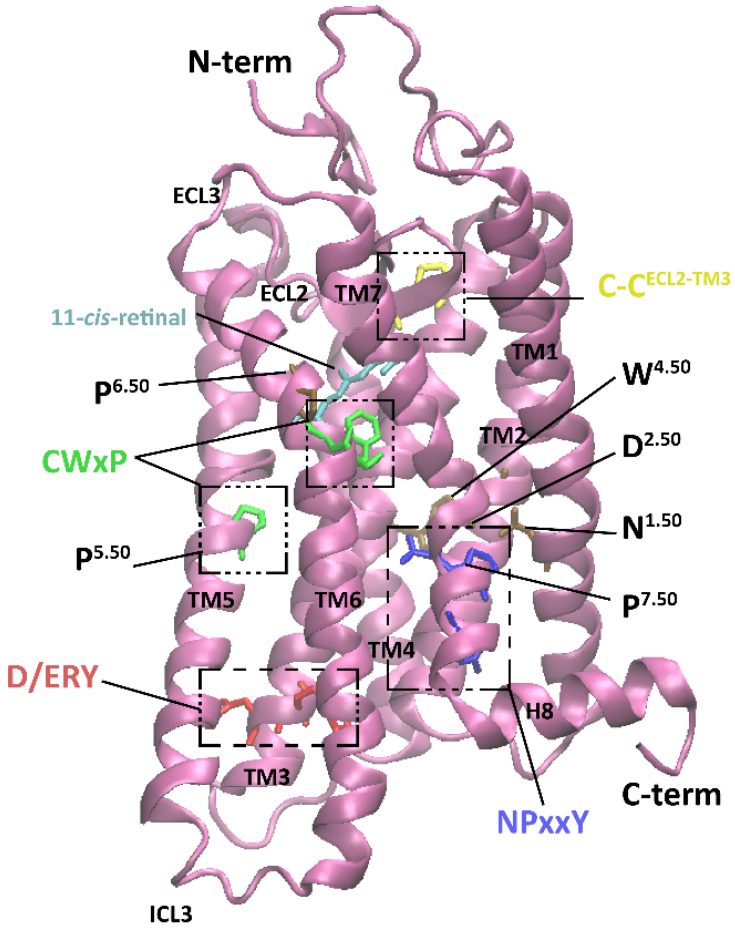

Figure 1.2. Conserved features of rhodopsin family GPCRs. Crystal structure of inactive bovine rhodopsin (PDB ID 1GZM, in pink) bound to its antagonist 11-*cis*-retinal (cyan). Highlighted in dashed boxes are the conserved features NPxxY (blue), D/ERY (red), CWxP (green) motifs and the disulphide bridge connecting TM3 and ECL2 (yellow). Other conserved residues which are not part of the conserved motif are colored brown.

This family has several characteristics, indicating their common evolutionary descent (Figure 1.2), first, NP$^{7.50}$xxY motif at the intracellular end of TM7 and the E/DR$^{3.50}$Y (or D(E)-R$^{3.50}$-Y(F)) motif at the border between TM3 and IL2[38]. Second, another common feature recently described is the molecular switch referred to as the "transmission switch" which links the movement of a CWxP motif on the extracellular sides of TM5 and TM6 to agonist binding[44,45]. And finally, another conserved feature is a disulphide bridge connecting extracellular loop (ECL)2 to the extracellular face of TM3. Furthermore, it has also been proposed that they share a conserved water network within the receptor core that mediates

activation[46]. Majority of GPCRs in this family have short N-terminal domains (≤63 amino acid residue long) with no conserved residues as such[40]. Exceptions include the luteinizing hormone receptor (LHCGR), the protease activated receptors (PAR)1-4, the thyrotropin receptor (TSHR), the follicle stimulating hormone receptor (FSHR) and the two relaxin family peptide receptors (RXFP)1 & 2. Because the rhodopsin family represents over 80% of human GPCRs[47], this family is the most extensively studied for potential therapeutic benefits.

1.3.2. Class B1 - The secretin family

One of the major changes that the GRAFS system introduced is to separate the secretin family from the adhesion family of GPCRs which are clustered together in the A-F classification system[37]. Historically, this family was named after the intestinal hormone secretin, which was the first hormone discovered[48] in the early 20th century, the receptor of which was first described nearly 80 years later[49,50]. The primary feature of the secretin family GPCRs is the large N-terminal extracellular domain (ECD)[51], which is important for recognition and binding of ligands, typically peptides or hormones. It is believed to be a two-step process[52]. Firstly, the 100-160 residue long N-terminal domain interacts with the ligand which, secondly, then triggers conformational changes, moving the tethered ligand into the extracellular orthosteric binding site of the receptor. This binding model was further supported by the molecular information revealed by the crystal structures of the human glucagon receptor (GCGR) TM domain[53] and its ECD[54]. In contrast, however, studies using antibodies targeting the ECD of the GCGR revealed that the ECD actually acts as a negative allosteric modulator that helps keep the agonist free receptor in an inactive state[54]. All members of this family are known to couple with Gαs and signal through activation of adenylate cyclase[55–58]. For this family, crystal structures have been reported for the TM domain of GCGR[53] and corticotropin-releasing hormone receptor (CRHR)1[59], which revealed that these receptors have the widest orthosteric binding pockets within the GPCR superfamily.

1.3.3. Class B2 - The adhesion family

Adhesion GPCR (ADGR) family is the second largest class of the GPCR family. They play important roles in processes like development[60,61], angiogenesis[62] and cell polarity[63,64]. All ADGRs share two unique features, first, the presence of two conserved cysteines in ECL1 and ECL2 that are assumed to form a disulphide bridge[65] and second, the exceptionally large and highly glycosylated N-termini[66], where the shortest is 394 (ADGRD1) and the largest is 3312

(ADGRC3) amino acids long in humans[66,67]. These large extracellular domains (ECDs) are believed to be associated with the evolution of cell adhesion. The signature of all ADGRs (except for ADGRA1) is the presence of ~320 amino acid long GPCR-auto proteolysis inducing (GAIN) domain which harbours the conserved GPCR proteolysis site (GPS)[68]. The conserved sequence motif within the GPS mediates autoproteolysis of ECD into the cleaved N-terminal fragment (NTF) which contains most of the ectodomain and the C-terminal fragment (CTF) consisting of a residual GPS portion, the 7-transmembrane helix domain (7TM), and the C terminus. NTF act as either a tethered agonist or tethered inverse agonist that interacts with the receptor's TM domain or an N-terminal ligand binding site that can be shed by means of auto proteolysis[69]. At present, no crystal structure of an adhesion family GPCR TM domain has been determined.

1.3.4. Class C - The glutamate family

The glutamate family of GPCRs includes many important subgroups such as the metabotropic glutamate receptors (mGluRs), the γ-aminobutyric acid receptor type B ($GABA_BR$) and other chemosensory receptors[70]. The mGluRs bind a diverse set of ligands, such as amino acids, pheromones and Ca^{2+} mediating major responses in the central and peripheral nervous system[71]. Glutamate, the major excitatory neurotransmitter in the brain[72], is an endogenous agonist of these receptors. mGluRs have been reported to play vital roles in neuropsychiatric disorders including depression, anxiety, and schizophrenia[73,74]. As for $GABA_BR$, there exists two subtypes, the $GABA_{B(1)}R$ and the $GABA_{B(2)}R$, which tend to assemble as heterodimers in neuronal membranes[75]. The major inhibitory neurotransmitter in the central nervous system (CNS), GABA, is the endogenous ligand of these receptors. The most striking structural feature that all members of this family except for G-protein–coupled receptor family C (GPRC)5A-D share, is a large N-terminal extracellular domain that is generally more than 600 amino acids long[70], around two-thirds of which form a structural motif popularly known as the Venus flytrap (VFT) module[76], which plays pivotal roles in ligand binding to these receptors[77,78]. To date two crystal structures of glutamate family receptor TM-domains, mGluR1[79] and mGluR5[80], have been solved.

1.3.5. Class F - The frizzled family and the taste2 family

Phylogenetic analyses across the two families, the frizzled and the taste2 family, have revealed the existence of three consensus motifs, IFL in TM2, SFLL in TM5 and SxKTL in TM7 that

are not observed in any other GPCR family[38]. The frizzled GPCR class comprises 10 frizzled receptors (FZDRs) and one smoothened receptor (SMOR)[81]. The frizzled receptors were originally identified in *Drosophila melanogaster* and the name frizzled is derived from a phenotype termed "frizzled" with irregularly growing, curly hairs on thorax, wings and feet while SMO refers to a segment polarity gene in *D. melanogaster*[82]. FZDRs are activated by secreted glycoproteins Wnt, and therefore play key roles in Wnt-signalling, which is important for various cellular processes including cell-fate decisions, differentiation, proliferation, migration and embryonic development[83]. Wnt is rich in post-translational modifications[83], most prominently glycosylation and acylation, which is necessary for its signalling[84]. Wnt binds to the conserved N terminal cysteine-rich domain (CRD) on FZDRs[82]. Upon ligand-binding, FZDRs signal through the phosphoprotein Dishevelled, DVL, which is part of the Wnt/β-cadenin signalling pathway[85–87] as well as heterotrimeric G-proteins. When it comes to SMOR, the activation of these receptors is not very similar to other GPCRs. SMOR has a 250-residue long CRD which interacts with a 12 TM protein termed patched (Ptc)[88]. Ptc is the actual receptor which after getting activated by its ligand hedgehog (HH), dissociates from SMO and then signals via G-proteins. The functional human taste2 receptors (T2Rs) are known to be expressed in taste buds in the tongue and the palate epithelium where they act as bitter taste sensors[89] and in cardiac tissue where they are proposed to have nutrient-sensing roles[90]. All T2Rs share exceptionally short N- and C-termini comprising a maximum of 8 and 25 amino acids respectively[89]. SMOR is the only receptor of this family with experimentally derived structures[91–93].

1.4. GPCR-ligand interactions

As mentioned before, all GPCRs contain a highly conserved seven TM core architecture. However, they utilize a remarkably diverse ligand binding pocket architecture and ligand receptor interactions, as shown by the reported crystal structures of GPCRs. The chemical nature of the ligands bound to the crystallised GPCRs includes a covalently attached chromophore, neurotransmitters, small molecule synthetic ligands, peptides, a lipid mimetic, and clinically-used drugs[94]. *In vivo*, these ligands act as inverse agonists, partial agonists, full agonists, biased agonists, and allosteric modulators. The divergent chemical structure and functional attributes of these ligands are reflected in their remarkably different binding modes, which range from strong interactions within the deep binding pocket to the weak interactions within the shallow binding pocket of the receptor. All these unique features are discussed in

further detail in the following sections, along with the potential applications for better drug design.

1.4.1. GPCRs as drug targets

GPCRs are involved in almost all physiological processes making them the most popular drug targets. As of July 2017, there are 475 approved drugs that target GPCRs[95], accounting for approximately 34% of all FDA approved drugs. New GPCR targeting drugs approved by the FDA since 2014 are used for the treatment of; hypotension (which targets β_1- β_2- and β_3-ARs, α_{2A}- α_{2B}- and α_{2C}-AR), type 2 diabetes (which targets Glucagon-like peptide 1 receptor (GLP1R)), schizophrenia (targeting 5-hydroxytryptamine receptor $(5HT)_{1A}$, $5HT_{2A}$ and D_2 dopamine receptor (DRD_2)), depression (targeting $5HT_{2A}$, $5HT_{1A}$, DRD_2 and $5HT_7$)), chronic obstructive pulmonary disease (COPD) (targeting β_2-AR)and others[95].

Moreover, there are currently 321 agents in clinical trials, which is 68% of the total number of approved drugs[95]. But unfortunately, the FDA approved GPCR targeted drugs, target only a small fraction of the potentially druggable GPCRs[96,97], 475 approved drugs target only about 100 GPCRs which is approximately 30% of all (365) non-olfactory human GPCRs, indicating a vast untapped pharmacological potential for this receptor family. Most of the drug development in the GPCR field is biased towards the GPCRs which have been extensively studied and are promising therapeutic targets[98], and usually exclude understudied or so-called orphan GPCRs (oGPCRs), for which there are no known endogenous agonists.[96] GPCRs have also been implicated in some monogenic diseases involving constitutively activating mutations (CAMs), such as uveal melanoma which occurs by CAMs of the cysteinyl leukotriene receptor 2[99], congenital stationary night blindness caused by rhodopsin CAMs[100] and others[101]. Furthermore, loss-of-function GPCR mutations have been linked to some human diseases for example, nephrogenic diabetes insipidus have been linked to mutations in V2-vasopressin receptor[102]. GPCRs are also shown to be involved in cell migration; for example neutrophils migrate through activation of a GPCR[103] and GPCR-regulated cell migration can also be detrimental for the organism, primarily during cancer[104]. Hyperactivation of GPCRs can cause unregulated growth and cell migration[105] by trans-activation of epidermal growth factor receptor (EGFR) and other receptors[105]. The progression of head, neck, lung, breast, colon, prostate and ovarian cancers have all been reported to be mediated, at least in part, by GPCR-EGFR crosstalk[105].

The primary challenge in targeting GPCRs is receptor specificity. GPCRs are often medication "off-targets", i.e., a drug known to bind to one specific GPCR can also bind to the other GPCRs, resulting in an off-target effect leading to an unpredicted interaction[106] or deleterious side-effects[107]. One of the infamous examples is fenfluramine, an anti-obesity drug, which was withdrawn from the market after it was discovered that the drug was an "off-target" activator of cardiac $5HT_{2B}$ serotonin receptors, leading to valvular heart disease[107,108]. Another example is hydroxyzine, an antihistamine, which is an inverse agonist for histamine H1 receptor (HRH_1), activates other GPCRs too[109] including muscarinic acetylcholine receptor (mACHR)[110], $5HT_{2A}$[111] and dopamine receptor (DR)[112]. Overall, the range of such off-target effects is vast[108,113].

1.4.2. Characteristics of orthosteric and allosteric GPCR ligands

In the 1920s, pioneering studies[114] led to the concepts of agonism and antagonism, where an agonist was defined as a ligand that induces or stabilizes an active state of the receptor while an antagonist is a ligand that blocks the access of the agonist to its receptor. The discovery that GPCRs may be active in the absence of ligands, i.e. they show basal/constitutive activity was made only after GPCRs were successfully cloned and expressed *in vitro*. Based on that observation, the following concepts have been developed (Figure 1.3)[115]:

1. **Full agonists**: ligands that maximally activate their respective GPCRs. Endogenous agonists such as hormones and neurotransmitters are generally full agonists.
2. **Partial agonists:** agonists that do not induce full (100%) activation.
3. **Antagonists:** ligands that block the activity of GPCRs by inhibiting the binding of agonists.
4. **Inverse agonist:** antagonists that decrease the basal activity of GPCRs.
5. **Neutral antagonists:** antagonists that inhibit the binding of agonists but do not interfere with the basal activity of GPCRs.

The binding site on the receptor where all agonists, partial agonists and antagonists interact with the GPCR is popularly known as the orthosteric binding site. The orthosteric binding site of GPCRs is towards the extracellular region of the receptors, between ECL2 and a highly conserved $W^{6.48x48}$ (Figure 1.4, shown in red). Numbering in superscript is the GPCRdb (GPCRdb.org) residue numbering[116] which is an extension of the Ballesteros and Weinstein[43] numbering scheme allowing referencing of amino acid positions across the members of

different GPCR families). Chan et al[117] recently superimposed all (>200) GPCR crystal structures and clustered the location of each ligand and found that the orthosteric ligands interact most frequently with the residues at the following positions (also shown in Figure 1.4):

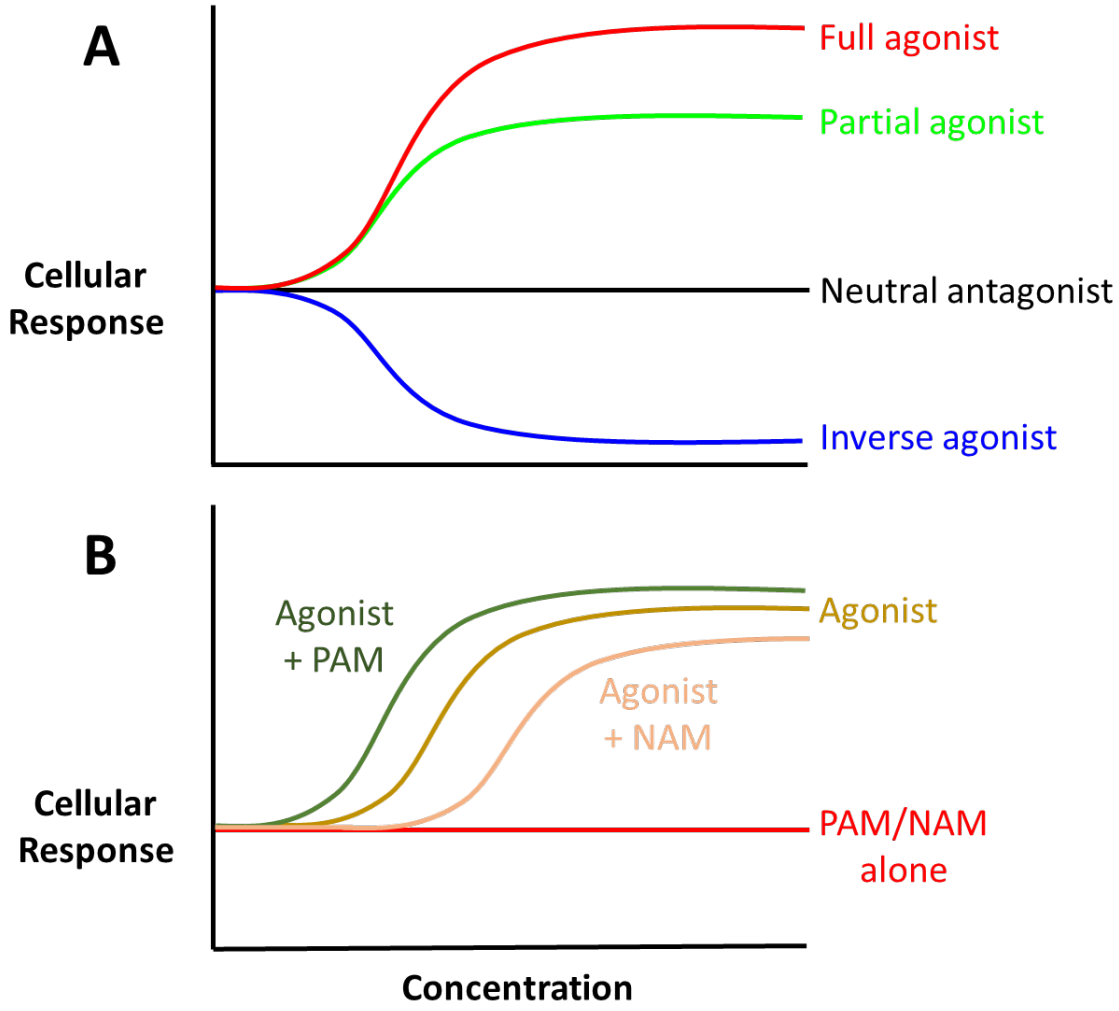

Figure 1.3. Activation profiles of GPCRs upon binding to orthosteric and allosteric ligands. (A) Full agonist and partial agonist activate the receptor leading to an increased cellular response. Neutral antagonist blocks the action of agonist and inverse agonist without eliciting a response of its own. Inverse agonist inactivates the receptor below the basal receptor activity. (B) Positive allosteric modulators (PAMs) and negative allosteric modulators (NAMs) modulate agonist (or inverse agonist) activation by increasing or decreasing ligand potency and/or efficacy respectively, but are unable to activate receptors on their own.

1. In TM3, positions 3.28x28, 3.29x29, 3.33x33, 3.36x36 and 3.37x37.
2. In TM5, positions 5.39x40, 5.40x41, 5.43x44, 5.44x45 and 5.47x47.
3. In TM6, positions 6.44x44, 6.51x51, 6.52x52, 6.55x55 and 6.58x58.
4. In TM7, positions 7.31x30, 7.34x33, 7.38x37, 7.41x40 and 7.42x41.

Importantly, the residues at positions 3.33x33, 4.52x52, 6.48x48, 6.51x51 and 6.55x55 shows the highest interaction frequencies (> 40%). All but 6.55 are highly conserved. In addition, interaction with TM2 and ECL2 residues at positions 2.60x60, 2.63x63 and 45.52x52 have also been observed.

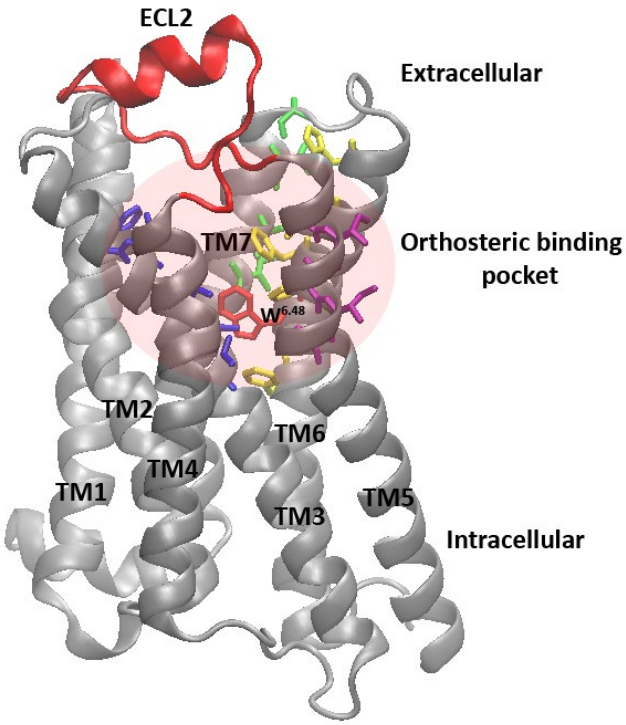

Figure 1.4. The orthosteric binding pocket of GPCRs. Orthosteric binding site residues mapped onto the crystal structure of β_2-AR. (PDB ID 5X7D). ECL2 and a highly conserved $W^{6.48x48}$ are coloured red. The side chains of all the protein residues which are known to interact frequently with the orthosteric ligand are shown, where residues from TM3 are coloured blue, TM5 are coloured violet, TM6 are coloured yellow and TM7 are coloured green.

In addition, the activity of the orthosteric site can be modulated remotely by molecules that bind at a site that is distinct from the orthosteric site, such molecules are known as allosteric modulators and the site at which they bind is known as the allosteric site[118]. Allosteric modulators can either be a positive allosteric modulator (PAM), a negative allosteric modulator (NAM) or a silent allosteric modulator (SAM)[119,120]. PAMs enhance the binding affinity and/or efficacy of the orthosteric agonist while NAMs inhibit the binding affinity and/or efficacy of the orthosteric agonist. SAMs, on the other hand, bind to the receptor but have no effect on the orthosteric agonist affinity or efficacy. Additionally, there are molecules that interact with both the orthosteric and allosteric sites and these are known as bitopic ligands. Allosteric modulators can be endogenous (for example, sodium[121], a NAM) and cholesterol[6] (which could be either a NAM or PAM) or exogenous synthetic compounds or natural

products[122]. The allosteric binding site residues were also clustered and classified into the following regions based on their location on the GPCRs[117] (as shown in Figure 1.5):

Region 1. Allosteric site next to the ECL2 surface. Allosteric ligands in this region have been observed in the crystal structures of the human purinergic receptor (P2Y) type 1 (PDB ID: 4XNW) and the M2 mACHR (PDB ID: 4MQT) (see Region I, Figure 1.5). ECL2 is a functionally important and hence therapeutically relevant region of GPCRs. It has been shown to play a pivotal role in cell-surface expression, ligand binding and activation of GPCRs [123–125]. ECL2 displays diverse folds between members of a GPCR subfamily as opposed to the TM region that is structurally conserved within a subfamily[126]. Therefore, this region offers more unique opportunities for drug design; antagonists in this region could effectively prevent agonist binding at the orthosteric site, acting as a "lid" blocking the entry in the orthosteric site[127]; while an allosteric modulator in this region can promote the binding or activity of an agonist via allosteric interaction[128].

Region 2. Allosteric site located at the receptor-lipid interface near the extracellular TM region. Allosteric ligands in this region have been observed in the crystal structure of the human G-protein-coupled receptor 40 (GPR40) (PDB ID: 4PHU)[129], protease activated receptor (PAR) type 2 (PDB ID: 5NDZ)[130], and P2Y1 (PDB ID: 4XNV)[131] (see Region II, Figure 1.5). Since the binding pockets at these sites are too shallow, with no obvious cavity, drug designing in these regions may prove challenging[132].

Region 3. Allosteric sites in the central TM region. Allosteric ligands in this region have been observed in the crystal structures of complement c5a receptor 1 (C5aR1) (PDB ID: 5O9H)[133] and GPR40 (PDB ID: 5TZY)[134](see Region III, Figure 1.5). Rational drug designing in this region with the elongated shape of the ligand might be useful, as it may act as a linker to connect the intracellular ends to the central TM regions, inducing conformational change near the hinge of the TM helix, mediating IL2 to achieve agonistic modulation.

Region 4. Allosteric sites in the intracellular regions. Recently, many such allosteric sites were observed, including the β_2-AR (PDB ID: 5X7D, purple)[135], CC chemokine receptor (CCR)2 (PDB ID: 5T1A)[136] and CCR9 (PDB ID: 5LWE, blue)[137] (see Region IV, Figure 1.5). These sites correspond to the highly conserved intracellular G-protein binding site and hence, for drug design approaches, achieving selectivity may be a challenge.

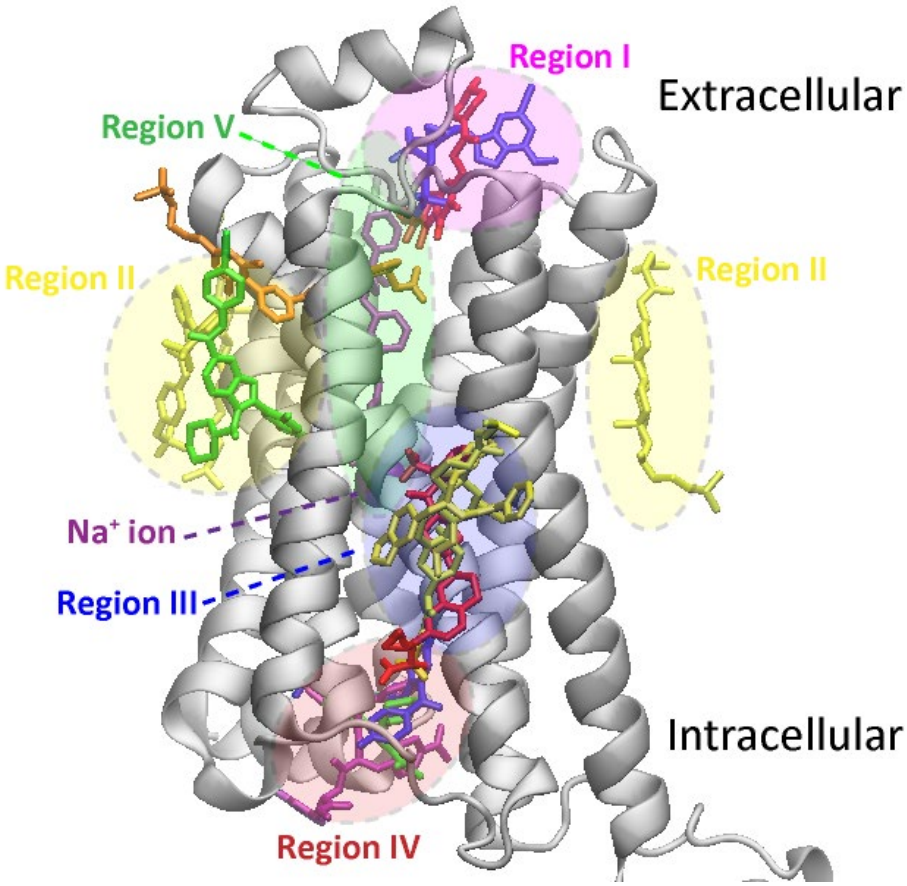

Figure 1.5. Allosteric binding pockets in GPCRs. Shown here are all the different allosteric ligands of which the crystal structures have been determined bound to their respective GPCRs. For clarity, only the receptor backbone structure of β_2-AR (PDB ID: 5X7D) is shown, onto which all the GPCR-allosteric ligand bound structures were superimposed. Based on that the allosteric binding sites can be classified into five regions (Region I - V) as highlighted by five different colours. Region I in purple (PDB ID: 4XNW and 4MQT in blue and red respectively). Region II in yellow (PDB ID: 4PHU, 5NDZ and 4XNV in orange, green and yellow respectively). Region III in blue (PDB ID: 5O9H and 5TZY in yellow and red respectively). Region IV in red (5X7D, 5T1A and 5LWE in purple, green and blue respectively). Region V in green (PDB ID: 4EIY and 5X33 in purple).

Region 5. Allosteric site next to the highly conserved residue $D^{2.50}$. In 2012, the structure of adenosine A2A receptor ($A_{2A}R$) (PDB ID: 4EIY)[138] showed for the first time, an allosteric sodium ion (labelled in Figure 1.5) coordinated with the highly conserved residues $D52^{2.50x50}$and $S91^{3.39x39}$, and three water molecules[138]. Allosteric sodium ions have been proposed to stabilize the inactive state of GPCRs[138,139] and facilitate the receptor activation

process as shown by MD studies[140]. Recently, a bitopic inverse agonist BIIL260, was observed in the crystal structure of Leukotriene B4 (LTB4) (PDB ID: 5X33, purple)[141]. This unique pocket has also been recently observed on M2 and M3 mACHRs[142].

Additionally, GPCR ligands also often display biased signalling or functional selectivity[143], a process by which ligands will direct or bias the signalling toward one pathway or another (either G-protein- or β-arrestin-mediated pathways). First insights into the structural details of biased ligand-GPCR interactions[144] were provided by the crystal structure of β_1-AR bound to a β-arrestin-biased ligand carvedilol[145] and structures of serotonin receptors $5HT_{2B}$[146] and $5HT_{2C}$[147] bound to a β-arrestin-biased ligand ergotamine. These structures have started to illuminate the ligand-receptor interactions that may contribute to generating bias at the receptor level, thereby dictating distinct signalling outcomes and opening whole new arenas for functionally selective GPCR drug discovery. Overall, these observations suggest that there might be many more unexplored binding sites that need to be identified by GPCR structures, unravelling of which would offer exciting new opportunities for GPCR drug discovery.

1.4.3. Challenges in targeting subtype selectivity in GPCRs

The majority of GPCR targeted approved drugs are designed to bind at the orthosteric binding sites on the receptors, which is simply because these sites are easily accessible and structurally well characterised when compared to the allosteric ligands. But at the same time these sites are highly conserved across the receptor subtypes making the selective drug development challenging. For example, all five subtypes of the mACHR (M1–M5), share almost identical orthosteric binding sites[128,148–151] and as a result, the orthosteric ligands of these receptors activate/inhibit all five subtypes. Another example is the adrenergic receptor (AR) subfamily (α_{1A}, α_{1B}, α_{1D}, α_{2A}, α_{2B}, α_{2C}, β_1, β_2, β_3) where all nine AR family members bind the same endogenous ligands, adrenaline and noradrenaline. Generally, poor subtype specificity by orthosteric ligands often leads to unexpected side effects in medical applications[152,153]. However, these problems can be circumvented by the use of allosteric ligands, which target less conserved sites compared to the orthosteric site and hence could specifically modulate orthosteric ligand activity[154–156] offering whole new opportunities for drug discovery and specifically for the subtype selective drug development.

1.5. The adrenoceptor family

The ARs belong to the Rhodopsin class of GPCRs. They mediate the functioning of the sympathetic nervous system by binding to the endogenous catecholamines, adrenaline and noradrenaline[157]. The initial concept of different subtypes of ARs (α and β) was put forward by Raymond Ahlquist[158]. Later studies divided α-ARs into two subtypes, α_1 and α_2, based on their anatomical location[159]. Years of pharmacological and biochemical characterisation led to the further characterisation of α-ARs into α_{1A}, α_{1B}, α_{1D}, α_{2A}, α_{2B}, α_{2C} and β-ARs into β_1, β_2 and β_3.[159–161] All nine adrenergic subtypes are activated by the same catecholamines. All α_1-ARs couple intracellularly with the G_q proteins[162], α_2-ARs couple with the G_i proteins[162], while all β-ARs are G_s coupled receptors[162].

In the late 1980s, α_1-ARs were subdivided into two subtypes α_{1A}- and α_{1B}-AR based upon the experimental competition binding data of the antagonists WB4101 and phentolamine in rat brain, which showed two-site competition or biphasic binding profile[163,164]. The subtype with the higher affinity (10-100 fold higher) was classified as α_{1A}-AR subtype, while the one with the lower affinity was called α_{1B}-AR subtype[163,164]. A third α_1-AR was cloned but did not fit into any of the pharmacological criteria of either α_{1A}-AR or α_{1B}-AR, and hence it was characterised as a novel subtype, α_{1C}-AR[165]. However, it was later demonstrated that the α_{1C}-AR was misclassified, and it actually represented the tissue-specific α_{1A}-AR[166,167]. Before reporting this "misclassification", another receptor was cloned, which was previously thought to be α_{1A}-AR, because of its high affinity for WB4101[168], but it was a novel subtype, not being previously described pharmacologically and it was characterised as α_{1D}-AR[169]. For these reasons, there are only three subtypes, α_1-AR; α_{1A}, α_{1B} and α_{1D}-ARs[170], that show distinct tissue localisation, amino acid sequence and pharmacology[171–173].

1.5.1. The significance of AR as a drug target

ARs are well-characterised GPCRs distributed across the sympathetic nervous systems and involved in many important physiological functions, in particular the regulation of cardiovascular homeostasis as well as the pathogenesis of cardiovascular diseases[171,174]. The α_1-AR subtypes mediate smooth muscle contraction and hypertrophic growth[175]. In humans, α_{1A}-ARs are known to be specifically expressed in the cerebellum, cerebral cortex, heart and prostate, α_{1B}-ARs in the aorta and spleen and α_{1D}-ARs in aorta[166,169,171,176,177]. While α_2-ARs are located in the nervous system in both pre- and post-synaptic neurons where they mediate

inhibitory responses, as opposed to the α_1-ARs[178]. β-ARs are located in cardiac muscles, airway muscles and the central nervous system[161]. β_1-AR activation increases heart rate and contraction force while activation of β_2-AR mediates vasodilation and bronchodilation[161]. β_3-ARs, unlike other subtypes, is involved in lipolysis and energy production in adipose tissues[161,179].

ARs are clinically targeted by α-blockers, β-blockers as well as sympathomimetic drugs for the treatment of several conditions[180–184]. α-blockers (i.e. α-adrenergic antagonists) can be classified into two categories, non-selective and selective α-blockers. Non-selective α-blockers, for e.g., phentolamine, phenoxybenzamine, tolazoline, trazodone and iobenguane, target all six types of α-ARs (α_{1A}, α_{1B}, α_{1D}, α_{2A}, α_{2B}, α_{2C}) and are used to treat high blood pressure[182] and Pheochromocytoma[182], a tumor of chromaffin cells of the adrenal medulla. While, selective α-blockers can be either α_1-AR selective (targeting α_{1A}-, α_{1B}- and α_{1D}-ARs) for e.g. prazosin, doxazosin, terazosin, tamsulosin, alfuzosin and silodosin, used specifically to lower the blood pressure[182], to treat benign prostatic hyperplasia (BPH, an enlargement of the prostate gland) or α_2-AR selective (targeting α_{2A}-, α_{2B}- and α_{2D}-AR) includes atipamezole, idazoxan, mirtazapine and yohimbine, mostly used for the treatment of hypotension[182] but overall have very limited clinical applications in human. α_1-AR selective blockers are associated with many adverse effects predominantly asthenia, dizziness, faintness and syncope[185]. Beta-blockers (i.e. β-adrenergic antagonists) are used to treat hypertension[186], to protect the heart from a second heart attack (myocardial infarction) after a first heart attack and to control abnormal heart rhythms[187]. Few β-blockers such as, carvedilol and labetalol have an additional α_1-AR blocking activity[186]. The sympathomimetic drugs that mimic the actions of epinephrine or norepinephrine include anti-hypotensive agonist methoxamine[183] and nasal decongestant agonist phenylephrine[184].

1.5.2. Insights from AR crystal structures and mutagenesis studies

From the AR family, the β_2-AR was the first hormone-activated GPCR of which crystal structure has been determined by X-ray crystallography[188]. This was also the first structure of a human GPCR; crystallisation was achieved by the use of soluble fusion protein, T4-lysozyme. The structure was in a complex with an inverse agonist, carazolol, which further stabilizes the receptor conformation[94]. A year after, the crystal structure of its closest homolog β_1-AR from Common turkey was published in complex with an antagonist[189]. These structures provided the

first insights into the inactive receptor conformations and ligand-binding pocket of the adrenergic receptors and most importantly, gave us the first insights into the challenges involved in developing subtype-selective ligands. As shown in Figure 1.6, the antagonist binding pocket between β_2-AR and β_1-AR differs by only one amino acid residue out of 15 residues that constitute the ligand binding pocket (defined as being within 4 Å of the inverse agonist carazolol). This high degree of binding pocket conservation extends even to the more distantly related α-ARs. For example, there are only four residues different between the ligand binding pockets of the α_{1A}-AR and β_2-AR and only three residues different between the ligand binding pockets of the α_{1B}-AR and β_2-AR (Figure 1.6).

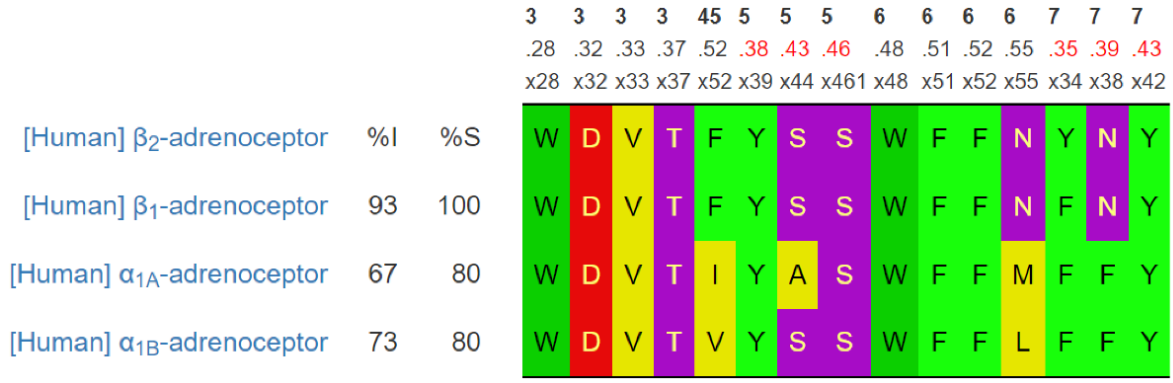

Figure 1.6. Ligand binding pocket residue similarity as calculated in GPCRdb[11]. The ligand binding pocket residues within 4 Å of the inverse agonist carazolol in the β_2-AR[188] crystal structure (PDB ID: 2RH1) are compared with the homologous residues in β_1-AR, α_{1A}-AR and α_{1B}-AR. To the right of the receptor names, two columns show the sequence identity (%I) and similarity (%S). The residue numbering at the top of the alignment table is based on the GPCRdb (GPCRdb.org) residue numbering scheme[116]. Alignment in red, yellow, green and purple denotes the presence of a negatively charged, hydrophobic aliphatic, hydrophobic aromatic and polar residue respectively.

Following that, a plethora of inactive state structures was published for β_1-AR and β_2-AR, as listed in the GPCRdb[11], and these are the only subtypes from AR family for which crystal structures are available so far. The major breakthrough came with the structure of the GPCR, β_2-AR in its active state[190], a state which was thought to be too unstable to be structurally determined.

It was rather challenging to get an active-state GPCR crystal structure due to the inherent instability of this state in the absence of a G-protein, but the use of a camelid antibody fragment (nanobody, Nb80) that exhibits G-protein-like behaviour enabled the crystallisation of the first agonist-bound, active-state GPCR[190]. The comparison of the structures in the active and inactive state provided useful insights into the activation process, including the subtle structural changes that facilitate the intracellular interaction of G-protein. Figure 1.7 compares the inactive inverse agonist (carazolol) bound β_2-AR structure[188] (Car-β_2AR) with the agonist (BI167107) bound, nanobody stabilised active β_2-AR[190] (BI-Nb-β_2AR). The cytoplasmic face of the receptor showed the largest differences, with an outward displacement of TM5 and TM6 and an inward movement of TM7 and TM3 in the BI-Nb-β_2AR complex when compared to the inactive structure. One of the most significant changes is observed in TM6, with an 11.4-Å movement of the helix at Glu $268^{6.30x30}$, destabilising the ionic lock with $Arg131^{3.50x50}$ of the DRY motif. The salt bridge between highly conserved $Asp130^{3.49x49}$ and $Arg131^{3.50x50}$ of the DRY motif in TM3 is also broken. The intracellular ends of TM3 and TM7 move towards the core by 4 and 2.5 Å, respectively, while TM5 moves outward by 6 Å. This large change is affected by a small clockwise rotation of TM6 in the turn preceding the conserved $Pro288^{6.50x50}$. In contrast to the large changes observed in the cytoplasmic domains of BI-Nb-β_2AR, the changes in the extracellular surface and the agonist-binding pocket are relatively subtle. Many of the interactions between the agonist BI167107 and the β_2-AR are similar to those observed with the inverse agonist carazolol. Interestingly, the changes observed between the inactive and active β_2-AR structures are remarkably similar to those observed between the inactive- and active-state structures of another class A GPCR, rhodopsin[191].

The next breakthrough came with the structure of an active-state GPCR bound to its native neurotransmitter, adrenaline, a catecholamine[192]. Before that, crystal structures of agonist-bound GPCRs relied mostly on the use of either exceptionally high-affinity agonists[193,194] or receptor stabilisation by mutagenesis[195–197]. Many endogenous agonists including adrenaline, which activates the β_2-AR, bind with relatively lower affinities and they are often chemically unstable. The use of directed evolution led to the engineering of a high-affinity camelid antibody fragment (Nb6B9) that stabilised the active state of the β_2-AR, leading to the successful crystallisation.

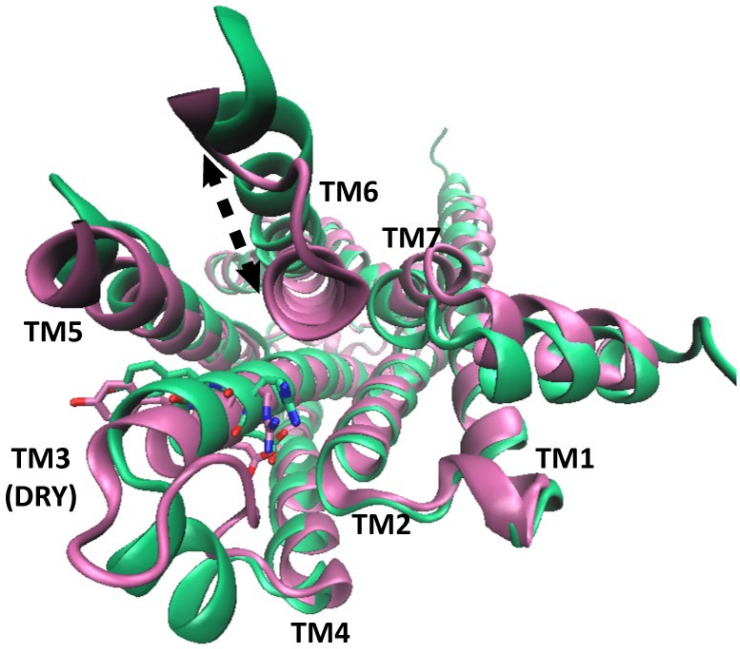

Figure 1.7. Comparison of the inactive- and active-state β2-AR crystal structure. The structure of the inverse agonist carazolol bound β_2-AR[188] (Car-β_2AR) is shown in pink. The structure of agonist BI167107 bound Nb80-stabilised β_2-AR[190] (BI-Nb-β_2AR) is shown in green. These two structures were aligned using the Multiseq tool in VMD. Cytoplasmic view showing the salt-bridge between Asp130$^{3.49x49}$ and Arg131$^{3.50x50}$ of the DRY motif in TM3 is broken in the BI-Nb-β_2AR structure; Intracellular end of TM6 is moved outward by 11.4 Å (change in distance calculated from α-carbon of the Glu$^{6.30x30}$); TM5 moves outward by 6 Å; while, TM3 and TM7 move inward towards the core of the receptor by 4 and 2.5 Å, respectively.

As shown in Figure 1.8, the adrenaline bound, nanobody stabilised active-state β_2-AR[192] (Adr-Nb-β_2AR) structure showed many similarities with the BI167107 bound active-state β_2-AR[190] (BI-Nb-β_2AR). Firstly, the agonist-induced rearrangements, in the Adr-β_2AR, at the intracellular surface and in the central portion of the transmembrane segments are virtually identical to that of the BI-Nb-β_2AR[190]. Secondly, consistent with prior mutagenesis studies, Ser203$^{5.42x43}$ and Ser207$^{5.46x462}$ make hydrogen bonds with the catecholamine phenoxy moeities[198] (Figure 1.8) and the conformation of these residues is also similar to that observed for the head group of BI167107[190]. Thirdly, the β-hydroxylamine moiety of adrenaline engages conserved residues Asp113$^{3.32x32}$ and Asn312$^{7.39x38}$ in a very similar manner to the BI167107[190]. Ser204$^{5.43x44}$, which was previously thought to interact with a

para-hydroxy group of the catecholamine directly[198,199], interacts indirectly with the head group of the catecholamine via Tyr308$^{7.35x34}$ and Asn293$^{6.55x55}$. And finally, BI-Nb-β_2AR and Adr-Nb-β_2AR structures show similar changes in the residues that connect the orthosteric binding pocket to the intracellular regions[192], indicating that the allosteric coupling mechanisms between the orthosteric and G-protein binding site might be a conserved feature of β_2-AR activation.

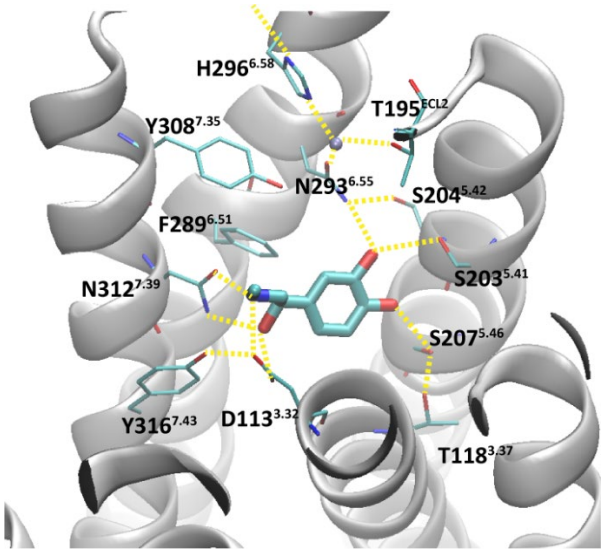

Figure 1.8. Bound conformation of adrenaline on β_2-AR. Shown here is the orthosteric binding pocket of adrenaline bound, nanobody stabilised β_2-AR crystal structure (Adr-Nb-β_2AR)[192] (PDB ID: 4LDO). The receptor is shown as a ribbon (grey), adrenaline is shown as a thick stick and the sidechains of the interacting receptor residues are shown as sticks (cyan). Yellow dots indicate the polar inter-residue and inter-ligand interactions.

Since both β-ARs and α-ARs recognize the same endogenous catecholamines, the ligand-binding pocket observed in the β-ARs is expected to be similar to the α-ARs. This notion is supported by the way the catechol hydroxyls interact with the β_2-AR serine residues in TM 5[192]. As shown in Figure 1.8, and discussed before, the phenyl group of catecholamine agonist, adrenaline, interacts with the β_2-AR via two hydrogen bonds one between the hydroxyl side chain of Ser203 in TM5 with the *meta*-hydroxyl group of adrenaline and a second being the hydroxyl side chain of Ser207 in TM5 with the *para*-hydroxyl group of adrenaline. Site-directed mutagenesis studies[200] have suggested that these interactions are conserved in α_1-ARs too, which could have been predicted as the equivalent positions of Ser203$^{5.42x43}$ and Ser207$^{5.46x461}$ in the β_2-AR are also Ser in the α_1-ARs (both α_{1A}-ARs and

α_{1B}-ARs, see Figure 1.9). When both Ser residues in α_{1A}-ARs were substituted in the double mutant to Ala, binding of epinephrine was significantly reduced[200] (10–100 fold). Furthermore, the studies suggested that for α_{1A}-ARs the interaction of Ser188$^{5.42x43}$ with the *meta*-hydroxyl of the catecholamine, is a key interaction for receptor activation[200], whereas, in the β-AR, each Ser residue accounts for roughly half of the activity.

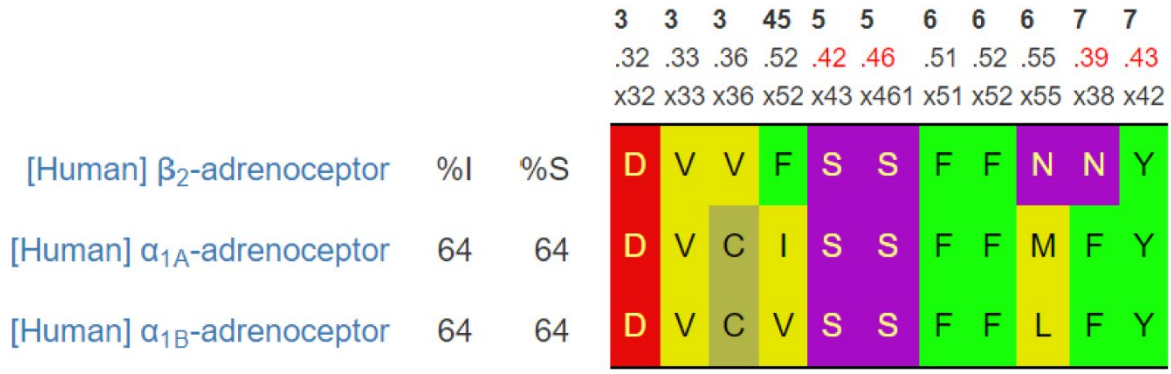

Figure 1.9. Conservation of the adrenaline binding pocket residues as calculated in GPCRdb[11]. The ligand binding pocket residues within 4 Å of the agonist adrenaline in the Adr-Nb-β_2AR[192] crystal structure (PDB ID: 4LDO) are compared with the equivalent residues in α_{1A}-AR and α_{1B}-AR. To the right of the receptor names, two columns show the sequence identity (%I) and similarity (%S). The residue numbering at the top of the alignment table is based on the GPCRdb (GPCRdb.org) residue numbering scheme[116]. Alignment in red, yellow, green and purple denotes the presence of a negatively charged residue, hydrophobic aliphatic residue, hydrophobic aromatic residue and polar residue respectively.

Other key interactions include the electrostatic interaction of adrenaline's β-hydroxylamine moiety with the highly conserved residue Asp113$^{3.32x32}$ and the hydrophobic interactions between the catechol ring of adrenaline and Phe289$^{6.51x51}$/Phe290$^{6.52x52}$. Mutagenesis studies on α_{1B}-AR indicate that a salt bridge is formed between Asp125$^{3.32x32}$ and Lys331$^{7.36x35}$, which constrain the receptor in an inactive state until broken by the binding of agonist[201]. Phe310$^{6.51x51}$ has been shown to be critically involved in both binding and activation of α_{1B}-AR[202], mutation of which showed affinity losses up to 1000-fold for the full agonists[202] and a significant decrease in both potency and efficacy of adrenaline stimulated phosphatidylinositol (PI) hydrolysis[202]. On α_{1A}-AR, two additional phenylalanine residues, Phe310$^{4.62x62}$ and Phe187$^{5.41x42}$, are known to be involved in the binding of agonists[203].

Mutation of these residues has been shown to decrease affinity by a 150-fold for the endogenous agonists. Interestingly, in β_2-AR, these aromatic residues are not conserved, illustrating one of the few distinct features in the agonist binding pocket across the two receptors.

AR binds their agonists including isoproterenol, adrenaline and noradrenaline in a stereospecific manner, with the (-)isomer being more potent than the (+)isomer[204]. Stereospecificity of AR agonists is defined by their β-OH-group, which is located at the chiral center. The α_{1A}-AR residues important for conferring the stereoselectivity have yet to be determined, while in the β_2-AR, it is attributed to an interaction between Asn293$^{6.55x55}$ and the β-hydroxyl group of the agonist[204]. However, α_1-ARs do not have Asn at 6.55x55 (α_{1A}-AR has Met and α_{1B}-AR has Leu) and yet the stereoselectivity of compounds is still conserved. The binding of an antagonist ([^{3}H]prazosin) on α_{1A}-AR is found to be severely affected by Asp106$^{3.32x32}$ mutations[205]. Another study found that the two conserved phenylalanine residues on TM7 (Phe308$^{7.35x34}$ and Phe312$^{7.39x38}$) are involved in π–π stacking with almost all α_{1A}-AR antagonists[206].

Another interesting motif explored is the ECL2, which have been proposed to regulate subtype specificity because of their low sequence conservation[207]. Mutation of ECL2 residues G196$^{45.51x51}$, V197$^{45.52x52}$ and T198 of hamster α_{1B}-AR to the corresponding residues (Q, I and N) in α_{1A}-AR changed the antagonist binding profile completely to that of the α_{1A}-AR[207]. Reversal of these three residues in the α_{1A}-AR to their corresponding residues in the α_{1B}-AR also entirely reversed the antagonist affinity to the wild-type (WT) α_{1B}-AR values indicating the roles of these positions in antagonist binding and subtype-selectivity[207]. Furthermore mutation of Asp191 to Ala in ECL2 of α_{1B}-AR resulted in 4 to 6-fold reduction in affinity for the agonists, adrenaline and noradrenaline, but with no significant effect on the signalling profile[208].

1.5.3. Distinct roles of α_1-AR subtypes

Studies on transgenic mice have demonstrated that α_{1A}-AR and α_{1B}-AR mediate different and sometimes opposing physiological responses in the regulation of cardiac and central nervous systems, whereby stimulation of α_{1A}-AR is cardio- and neuro-protective, while that of α_{1B}-AR is cardiac damaging and neurodegenerative[209,210].

In cardiac myocytes, α_{1A}- and α_{1B}-ARs mediate opposing cardiac physiology as they coupled to different G-proteins thereby activating differential signaling pathways[211,212]. Stimulation of both α_{1A}- and α_{1B}-ARs lead to cardiac hypertrophy or the thickening of the heart muscle. It is proposed that the α_{1A}-AR stimulation mediates adaptive and compensatory hypertrophy[175], while α_{1B}-AR stimulation mediates maladaptive and cardiac damaging hypertrophy[175]. A study on mice models has shown that the constitutively active mutant (CAMt) of α_{1A}-AR displayed cardiac hypertrophy with greater protection against cardiac ischemic injury[213]. Moreover, in mice, cardiac myocyte-targeted overexpression of WT α_{1A}-AR also mediated cardiac protection against pressure overload with fewer heart failure deaths[214]. Whereas myocyte-targeted CAMt of α_{1B}-AR in mice displayed hastened heart failure after ischemic damage and pressure overload[215] and cardiac-restricted overexpression of WT α_{1B}-AR also showed the development of dilated cardiomyopathy and systolic dysfunction which then led to heart failure and premature death[216].

Neuronal α_1-ARs are generally stimulatory and found on post-synaptic cell bodies. Constitutive stimulation of α_{1A}-AR has been demonstrated to be neuroprotective: increasing neurogenesis, exhibiting pro-epileptic effects, enhanced learning and memory and improving mood. It may also protect the brain from age-dependent neurodegeneration, anoxia, seizures and traumatic injury. In contrast, prolonged stimulation of α_{1B}-AR has been shown to be neurodegenerative, exhibiting pro-epileptic effects[175]. In mice, CAMt of α_{1A}-AR resulted in enhanced neurogenesis including the proliferation of neural stem cells[217], while CAM of α_{1B}-AR displayed age-related apoptotic neurodegeneration[218]. Additionally, mice with CAM of α_{1A}-AR exhibited similar behaviors as to those treated with anti-depressants[219]. Also, α_{1A}-AR knockout (KO) often shows spontaneous seizures while α_{1B}-AR KO confers resistance to the neurotoxicity-induced seizures[175,220].

All these studies, therefore, suggest that the therapeutic strategies to selectively block α_{1B}-ARs or/and selectively activate the α_{1A}-AR subtype may be cardioprotective and neuroprotective. Such protection may prove beneficial in cardiac-damaging conditions such as, during infarction or in the setting of heart failure and it may also be useful for the treatment of a number of neurological disorders. But subtype-selectivity has not been achieved yet, primarily, because α_{1A}- and α_{1B}-AR share high sequence similarities in both the TM region (~87%)[11] and the orthosteric binding region (~90%)[11] (Figure 1.9). Consequently, the

development of subtype selective ligands is challenging, which in turn has hindered research of subtype-specific localisation and understanding of the physiological roles of each subtype.

1.5.4. α_1-AR ligands and key features

Years of pharmacological studies have identified several α_1-AR selective and α_{1A}-AR subtype-selective ligands, however, there is a lag in the identification of α_{1B}-AR subtype-selective ligands. Table 1.1 lists most of the known α_1-AR selective and subtype selective ligands along with their affinities.

The α_1-AR selective ligands include anti-hypertensive antagonist prazosin[221], anti-hypotensive agonist methoxamine[183] and nasal decongestant agonist phenylephrine[184]. These ligands could selectively modulate smooth muscle contractility on α_1-ARs, but they do not show any significant level of selectivity between the different α_1-AR subtypes. The α_{1A}-AR selective ligands with weak subtype selectivity (10 to 50-fold) include methoxamine[183], oxymetazoline[222,223], tamsulosin[224], WB4101[206,222,225] and phentolamine[222]. This low subtype selectivity is observable in simple conditions such as radio-ligand binding assays on membrane preparations. In complex tissue or organ assays, where there are multiple subtypes present and the drug uptake is not under control, the selectivity is no longer observable or therapeutically useful[226]. Also, oxymetazoline has been shown to activate α_2-ARs[227]. The α_{1A}-AR selective ligands displaying higher subtype selectivity (>50-fold selectivity) include A-61603[228,229], silodosin[180], S(+)-niguldipine[224], which is also a potent dihydropyridine-type calcium channel blocker[230] and 5-methylurapidil[231], which is also a potent agonist of serotonin receptors[231]. Currently, silodosin, an antagonist, is the only approved α_{1A}-AR selective drug used for the treatment of BPH[180,181]. For α_{1B}-AR only a few selective ligands have been identified, including (+)cyclazosin[232] and chloroethylclonidine[225,227].

Table 1.1. List of α_{1A}- or α_{1B}-AR ligands along with their affinities

Ligand name	Action	p*Ki* α_{1A}-AR (human)	p*Ki* α_{1B}-AR (human)	Ref.
Endogeneous ligands				
Adrenaline (Approved)	Agonist	6.3	6.5	[222]
Noradrenaline (Approved)	Agonist	6.0	6.2	[222]
α_1-AR selective compounds				
[125I]-HEAT	Agonist	10.0 (K_D)	10.2 (K_D)	[222]
Prazosin (Approved)	Antagonist	9.0	9.6	[222,233]
Phenylephrine (Approved)	Agonist	5.4	6.3 (pIC_{50})	[224,234]
α_{1A}-AR selective compounds (10 to 50-fold)				
Methoxamine (Approved)	Agonist	5.0	4.0	[222]
Oxymetazoline (Approved)	Agonist	8.2	6.5	[222,223]
Tamsulosin (Approved)	Antagonist	10.4	9.6	[224]
WB4101	Antagonist	9.7	8.5	[206,222]
Phentolamine (Approved)	Antagonist	8.6	7.5	[222]
α_{1A}-AR selective compounds (>50-fold)				
A-61603	Agonist	7.9 - 8.1 (rat)	5.5 - 5.9 (hamster)	[228,229]
5-methylurapidil	Antagonist	9.1	7.4	[222,231]
S(+)-niguldipine	Antagonist	9.1	6.7	[222,224]
Silodosin (Approved)	Antagonist	10.4	7.7	[222]
α_{1B}-AR selective compounds				
(+)cyclazosin	Antagonist	7.48 (rat)	9.16 (rabbit)	[232]

There have been few ligands reported to be allosteric modulators of α_1-ARs. First, benzodiazepines including diazepam, lorazepam and midazolam have been reported to be potential allosteric modulators of α_{1A}-ARs[209], although a recent work from our group suggests that this modulation was not from a direct interaction of α_{1A}-AR with the benzodiazepines[235]. Another allosteric ligand is the conotoxin ρ-TIA, a peptide toxin found in the predatory marine

snail *Conus tulipa,* which has been demonstrated to be a NAM of α_1-ARs[236,237]. 9-aminoacridine (9AA) and its derivative tacrine have also been reported to be allosteric modulators of adrenergic receptors[238]. 9AA is a member of the aminoacridines and has a variety of roles including an anti-infective agent, an antiseptic drug, a mutagen.[239]. Tacrine (9-amino-1,2,3,4-tetrahydroacridine), the first FDA approved cholinesterase inhibitor for the treatment of Alzheimer's disease, is a positive allosteric modulator (PAM) at the muscarinic receptors[11] and negative allosteric modulator (NAM) at the α_{1A}-AR[238].

In essence, currently, there are no clinically approved (α_{1A}-or α_{1B}-AR) selective drugs that can discriminate between the subtypes, based on 100 to 1000-fold differences in affinity. And this has hindered the elucidation of specific biological roles of each of these subtypes and as a consequence, the selective targeting (blocking/activating) of these subtypes, which could be physiologically important and pharmacologically relevant (as discussed in the section 1.5.3), has been a great challenge.

1.6. GPCR structural studies using X-ray crystallography and cryo-EM

The biophysical techniques, other than NMR, used for structural characterisation of GPCRs include X-ray crystallography and cryo-EM. Using X-ray crystallography, ligand bound crystal structures of more than 50 different GPCRs have now been determined[11]. More recently, Cryo-EM structures of GPCRs in complexes with G-protein and agonists have been solved[12–18].

These GPCR crystal structures revealed the common architecture shared by all GPCRs including the evolutionarily conserved motifs (Figure 1.2) as well as the orthosteric and allosteric ligand binding pockets (Figure 1.4), giving us the atomic insights into the receptor–ligand interactions. Some high resolution structures (> 2.5 Å resolution) even revealed the presence of small molecules and ions giving us important insights into the allosteric modulation of GPCRs[121,138,240]. Such allosteric modulation by exogenous agents could be very useful for subtype selective drug development in GPCRs, where different subtype exhibits identical orthosteric ligand binding sites[241].

When it comes to the structure based drug designing these crystal structures have been extensively utilised. In-silico screening of compounds has resulted in the identification of many novel GPCR ligands[42,242]. The success of crystallographic techniques, however, relies heavily on the "stabilisation" strategies used to facilitate crystallisation. Such strategies include truncations of flexible domains and terminal regions, use of fusion proteins[243,244], introduction of stabilising mutations[196,245] and the use of the high binding affinity (K_i ≤10 nM) orthosteric ligand[94]. Crystallisation as well as Cryo-EM structures have been solved in complex with non-covalently interacting partner protein such as G-protein[246], antibody[247] and nanobody[190,248]. Other information which may be crucial for GPCR drug discovery such as allosteric modulation, biased signalling and partial agonism cannot be fully explained by these "snapshots" of conformational ensemble resulting in exclusion of "potentially recognisable" drug scaffolds. In essence, the success of GPCR crystallography and cryo-EM structures have revealed the need to complement these structures using other "orthogonal" techniques like NMR and molecular dynamics simulations.

1.7. Protein-ligand interaction study using NMR

The interaction of a receptor protein with a small-molecule ligand, in its simplest form (one binding site) follows a bimolecular association reaction with second-order kinetics. It is described by the equilibrium between the bound (protein-ligand complex, PL) and the free forms of the ligand (L) and protein (P).

$$\mathrm{P} + \mathrm{L} \underset{k_{\mathrm{off}}}{\overset{k_{\mathrm{on}}}{\rightleftharpoons}} \mathrm{PL}$$

Where k_{on} and k_{off} being the ligand association and dissociation rate constants. k_{on} depends mainly on the ligand diffusion rate and k_{off} is determined by the strength of protein-ligand interactions. The dissociation constant K_D and its reciprocal, the association constant K_A, are defined in terms of k_{off} and k_{on}:

$$K_{\mathrm{D}} = \frac{1}{K_{\mathrm{A}}} = \frac{[\mathrm{P}][\mathrm{L}]}{[\mathrm{PL}]} = \frac{k_{\mathrm{off}}}{k_{\mathrm{on}}}$$

The dissociation rates (k_{off} or off rates) can be approximated by assuming a diffusion controlled association (on rates) where k_{on} lies in the range of 1×10^7 to 3×10^7 M^{-1} s^{-1}.

When it comes to NMR, in the free state both protein and ligand retain their intrinsic NMR parameters (e.g., correlation coefficients, relaxation rates, chemical shifts, diffusion coefficients etc.). But when an interaction, as described in the binding equilibrium, occurs the spectral parameters of both the ligand and the receptor are modulated, as for ligand, it transiently adopts NMR parameters characteristic of the larger receptor and for the receptor, binding of the ligand transiently perturbs the receptor binding site microenvironment. This modulation of parameters forms the basis of all the NMR screening experiments. One of the key parameters governing the NMR experiments are the ligand dissociation rates i.e. off-rates (k_{off}). Based on that, there are three distinct cases:

1) Fast exchange regime: Where there is a fast exchange between the free and the receptor bound forms of the ligand which alternatively means, many cycles of protein–ligand association and dissociation occur within the "NMR timescale". This mostly holds true for the moderate to weak affinity ligands with a $k_{off} > 10^2$ s^{-1} (which typically corresponds to $K_D >$ 10 μM)[249].

2) Intermediate exchange regime: Where the exchange between the free and the receptor bound forms of the ligand (k_{off}) is roughly on the NMR timescale.

3) Slow exchange regime: Where the average lifetime of the protein–ligand complex is much longer than the NMR timescale, typically this may correspond to $k_{off} < 10$ s^{-1} and $K_D <$ 1 μM.

NMR methods that are suited for the analysis of the weak protein-ligand interactions (the fast exchange regime) can be classified into two broad categories: protein-observed NMR methods in which the protein component of the binding interaction is observed and ligand-based NMR methods, in which the ligand component is observed[250,251]. Ligand-based NMR methods are discussed in further details in the following sections.

1.7.1. Ligand-based NMR methods

Ligand-based methods rely on the differential behaviour of macromolecules and small molecules. For the binding ligand, the macromolecule-like properties are transferred from the

bound state of the ligand to the free state where they are readily observed. If the ligand is in the fast-exchange regime, the ligand resonances are modulated by the slower tumbling of the macromolecule. With these experiments, the ligand is in large molar excess over the receptor (> 10:1) and therefore interactions are observed on the signals of the free ligand[252]. The ligand-based approaches offer the following advantages: (1) isotope labelling of the target protein is not required; (2) sensitive and rapid NMR measurement can be achieved with lower protein concentrations, generally 5–50 μM. Indeed in some experiments such as target immobilised NMR screening (TINS)[253], the total amount of the sample can be reduced; (3) there is no upper limit on the size of the target protein. These experiments have been used to study interactions with monoclonal antibodies, intact viruses and even whole cells[254–257]; and finally (4) sample purity conditions are less stringent. However, impurities or buffer conditions that contain ^{1}H (for example, detergents) can obscure ligand signals and interfere with the analysis. Owing to these many advantageous factors, ligand-based NMR experiments have become one of the most widely used methods to detect ligand binding.

1.7.2. Types of ligand-based NMR methods

Ligand-based NMR binding experiments can be broadly divided into two categories:

1**. NOE-based methods**. These methods are based on the transfer of magnetisation from the target protein or other molecules (such as bulk water and ligand) to ligands through dipole-dipole interactions, i.e. through space known as the nuclear overhauser effect (NOE). These methods are widely used to characterise protein-ligand interactions and include saturation-transfer difference (STD)-NMR[258,259], structural information using overhauser effects and selective labelling (SOS)-NMR[260], water-ligand observed via gradient spectroscopy (Water-LOGSY) and its related methods[261,262], transferred NOE spectroscopy (Tr-NOESY)[263], interligand NOEs for pharmacophore mapping (INPHARMA)[264,265] and inter-ligand NOE (ILOE)[266].

As mentioned earlier, for NOE based methods, the only strict requirement is that the ligands should dissociate rapidly on the NMR timescale. In the slow exchange regime, when ligand exhibits strong affinity and lower dissociation rates (or off rates) from the target protein, the free ligand signals do not necessarily reflect the protein-bound form and hence the detection of ligand biding become challenging. In general, for efficient application of these methods, the

dissociation constant (K_D) between the target protein and ligand should be about 1 mM to 0.1 μM[252].

2. **Relaxation-based methods**. These experiments rely on the differential magnetisation relaxation properties of rapidly tumbling small molecules than that of the slowly tumbling macromolecules, which can be used to distinguish binders from non-binders. Examples include $T_{1\rho}$ or T_2 relaxation filtered 1D experiments[267,268]. The differential effect can be further enhanced by immobilising the receptor onto a solid support such as in the TINS method[253] or by the attachment of relaxation agents such as paramagnetic metals[269,270] and spin probes[268] to the binding site of the target protein.

Other experiments where the binding of the ligand is detected by the modulation of other physical properties have been reported. For example, magnetisation transfer following diffusion behaviour based selective purging of a population[271,272] or by using diffusion filters[267]. However, the NOE and relaxation based methods have been used to study GPCR-ligand interactions and are explained in greater detail in the following sections.

1.7.2.1 STD-NMR

The STD-NMR experiment[273,274] is based on the selective saturation of the receptor protons, from which it is then transferred to the binding molecules (Figure 1.10). Some of the receptor's protons are saturated by applying selective pulses in the region of the NMR spectrum corresponding to methyl groups of the protein (−0.5 to 0.3 ppm). During this saturation period, firstly, the magnetisation is transferred throughout the protein by dipole-dipole interactions between neighbouring ^{1}H nuclei and secondly, to any protons in ligands bound (i.e. in close proximity) to the protein. In this "on-resonance" spectrum, resonances from binding ligands are therefore partially or fully saturated, dependent on both binding kinetics and relaxation, while the resonances of non-binding molecules will remain unsaturated. Then the reference spectrum or the "off-resonance" spectrum is recorded, in which the selective pulses are set to a frequency which is far away from any chemical shift present in the sample, for e.g. −40 ppm.

Subtracting on-resonance (saturated) spectrum from the off-resonance (unsaturated) spectrum, generates the difference spectrum. The difference spectrum contains signals only from the saturated receptor and binding ligands, and not from the non-binding molecules

(Figure 1.10). Since, these experiments are performed with lower protein concentrations and higher concentrations of ligands, the most intense signals observed are from binding ligand molecules.

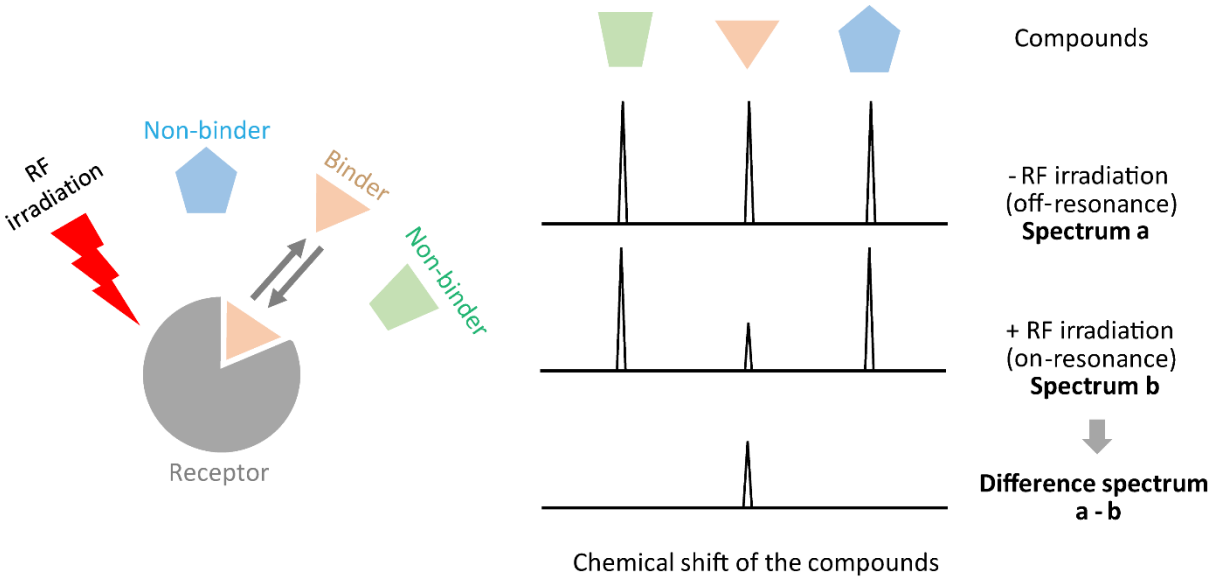

Figure 1.10. Schematic representation of the STD-NMR experiment. (Left) Triangle indicates a ligand that binds to the protein. Radio frequency (RF) irradiation selectively saturates the target protein. This saturation is specifically transferred to the bound ligand. (Right) Due to the interaction with the protein, transfer of saturation specifically modulates the signal intensity of the binding molecule. When the difference spectrum between the off-resonance (spectrum a) and on-resonance (spectrum b) saturation is calculated, NMR signals from the interacting compounds can be identified.

STD parameters (including saturation period, power of saturation pulse and frequency centre of saturating pulse) need to be optimised by using only the ligand in the absence of protein to confirm that the conditions are not directly saturating signals of the ligand. To some extent, as the k_{off} values are dependent on experimental conditions and hence, buffer conditions, protein and ligand concentrations should be finely tuned to obtain the best intensity in the difference spectrum while avoiding false-positives due to inter-ligand or protein-protein non-specific associations[275] or interactions with detergent molecules in case of detergent stabilised GPCRs. The protein and ligand concentrations are typically in the range of 2.0–20 µM and 0.2–2.0 mM, respectively.

1.7.2.2 SOS-NMR

SOS-NMR is an STD based method in which the target receptor is site-specifically ^{1}H-labelled, typically the methyls of Ile, Val, Leu or Met, while the other undesired non-labile protons are deuterated (^{2}H-substitution)[260]. Ligands that bind to the ^{1}H-labelled site of the receptor are detected, while the ligands bound to the undesired deuterated binding sites are excluded. By acquiring a trail of experiments with different ^{1}H-labelling at the target receptor site, a great deal of structural information on the receptor could be obtained. However, the sensitivity of this method is not very high because of the limited dipole-dipole interactions resulting from the low ^{1}H density on the target protein.

1.7.2.3 Water-LOGSY

Water-LOGSY[261,276] relies on the transfer of magnetisation between water molecules to proteins and small molecules via the NOE[261,276]. Water is present as both free and weakly ordered water around proteins as well as small molecules. Upon selective bulk water excitation, magnetisation gets transferred in a NOE manner via the exchange of bulk water with weakly ordered water to all molecules which are present in the solution.

It is the change in the sign of the NOE signal that differentiates binders from non-binders (Figure 1.11). Small molecules tumble fast, which translates into positive NOE while the larger protein tumbles slowly and exhibit negative NOE. Non-binders are surrounded by the weakly ordered water molecules (in fast exchange with bulk water). Upon selective bulk water excitation these unbound molecules will display positive NOE signal characteristic of small molecules. In the bound state, a ligand is associated with water molecules on its surface as well as water near or within the binding pocket. These water molecules experience the macromolecular tumbling properties of the protein and thus exhibit negative NOEs, which, upon selective excitation of the bulk water. In Water-LOGSY spectra, for better visualisation and understanding, positive NOE is phased negative and negative NOE is phased positive.

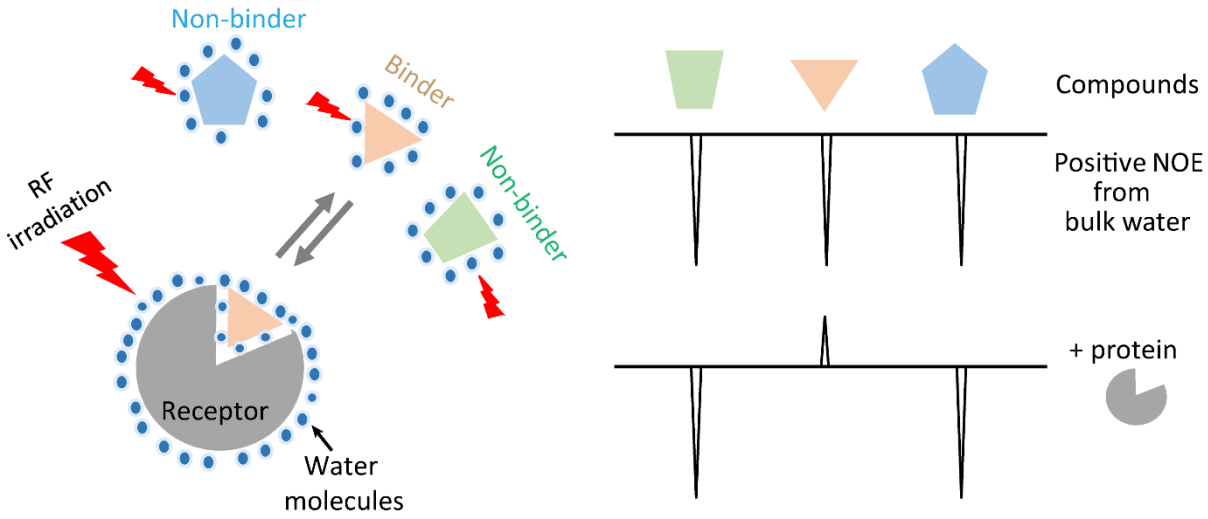

Figure 1.11. Schematic representation of the Water-LOGSY experiment. (Left) Light-blue dots indicate water molecules and a triangle indicates a ligand that binds. Non-binders display positive NOE with water. Protein and ligands binding to it display negative NOE with water. RF irradiation is used to selectively saturate the NMR signal of water. (Right) The phase of the signal of the binding ligand is inverted, compared to non-binding ligands, due to the interaction with protein.

The Water-LOGSY experiment is sensitive and rapid, but a number of caveats must be taken into consideration when analysing the data obtained. Firstly, exchangeable protons of the ligand (e.g., OH or NH groups) will give rise to positive NOEs and should be ignored in the analysis[277]. Secondly, some compounds can give rise to completely negative NOE and hence positive Water-LOGSY response, even in the absence of a macromolecular receptor. This might happen because of aggregation of the compound in the buffer used or due to interactions of a compound with microscopic precipitates and consequently, the ligand behaves like a macromolecule. To avoid these false positives, it is recommended to acquire Water-LOGSY spectra on only the ligand and in the absence of any macromolecule in the relevant buffer. Thirdly, the Water-LOGSY spectrum is the average of both bound and the free ligand populations. Thus, care in sample preparation must be taken to have a suitable molar ratio of ligand to protein, usually a ligand molar excess of 25 to 100-fold is used[277]. A high ratio of ligand to protein may result in a positive NOE. For these reasons, it is always better to analyse the experiments where relative populations of the bound and free state are perturbed, for example when a known potent competitor molecule is added, an increase in a

free population (more positive signal) can be observed, an indication of a depletion of the bound population.

1.7.2.4 Tr-NOESY

The Tr-NOESY method is used to define the conformation of the bound ligand by observing intra-ligand NOE peaks between protons of the free ligand[278–282]. The experiment is acquired as a two-dimensional spectrum where cross-peaks appear between the protons of the free ligand (Figure 1.12). The intensity of the cross-peak is related to the distance between the two protons and the correlation times of the molecule.

$$\mathrm{NOE} \propto \mathrm{r}^{-6} * f(\tau_{\mathrm{c}})$$

Where NOE is the NOE peak intensity, r is the distance between the two protons and $f(\tau_c)$ is a function of the correlation time τ_c.

The NOESY experiment has been widely used to describe the molecular structure of small and large molecules. If two protons are less than 5Å apart in space, it will be visible as an NOE peak and as described by the equation, closer the protons are higher will be the NOE intensity. Also, the NOE intensity depends on the correlation times (τ_c) of the molecule, which is governed largely by the molecular weight of the molecule (the higher the molecular weight, higher will be the correlation time) and to some extent, the temperature and viscosity of the sample solution[283]. Depending on the correlation times of the molecule, the NOE crosspeak can exhibit either positive (opposite sign to the diagonal peak) or a negative phase (same sign as that of the diagonal peak) as shown in Figure 1.12B. Positive NOEs are characteristic of small molecules, tumbling fast in the solution and hence showing lower correlation times. Negative NOEs are characteristic of macromolecules, tumbling slowly in the solution and hence showing longer correlation times. For the tr-NOESY, where a small molecule interacts with a macromolecule, generally on the fast exchange timescale, we expect the NOEs to be negative, reflecting the macromolecular condition. Hence the ligand retains the “memory” of the bound conformation, and the negative NOEs are consistent with the bound state.

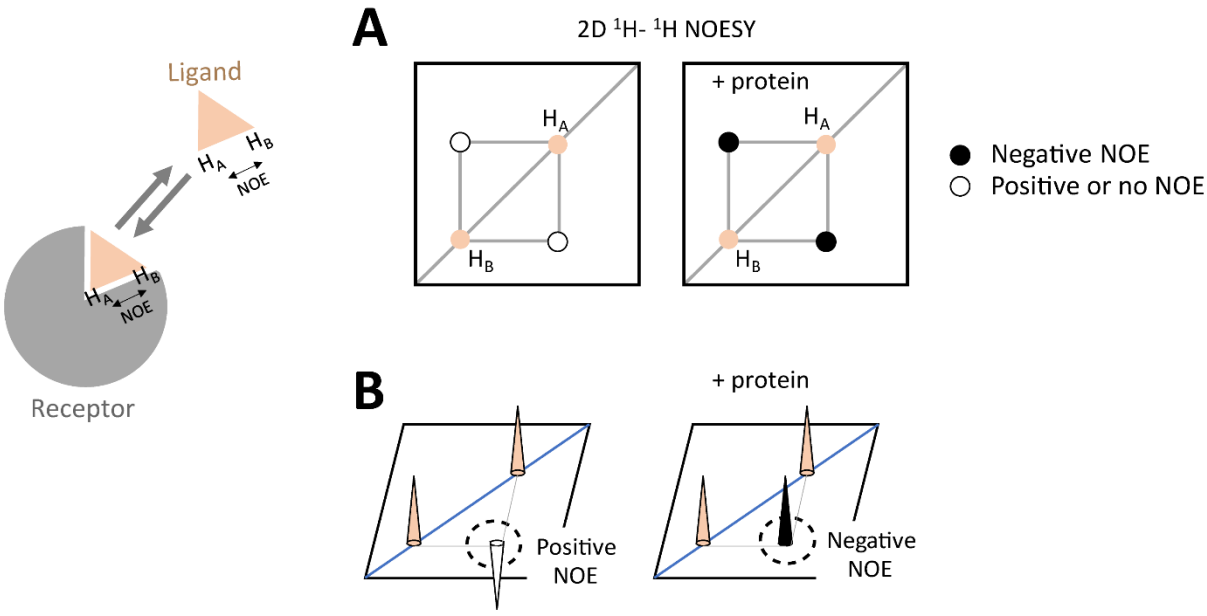

Figure 1.12. Schematic representation of the Tr-NOESY experiment. (Left) A triangle indicates a hit ligand. A. The orange and black circles indicate diagonal and cross peaks, respectively. The open and filled circles are positive and negative peaks respectively. B. (Left) Intra-ligand cross-peaks exhibit positive phase in the absence of a protein. (Right) Intra-ligand cross-peaks exhibit negative phase in the presence of a protein.

Tr-NOESY experiments use the sign inversion of the intra-ligand NOE cross-peaks to screen for the potential binding small ligands. These experiments can provide major insights into the ligand conformations and also into the binding induced conformational changes of the ligand. These experiments can provide information that can be used in hit-to-lead optimisation studies[284]

1.7.2.5 INPHARMA and ILOE

INPHARMA[264,265] and ILOE[266] methods are based on the observation of ligand-to-ligand NOEs or inter-ligand NOEs in the presence of the target protein (Figure 1.13) and are specific variations of the Tr-NOESY experiment describing conformations of two ligands binding to a protein target. Under these conditions both intra-ligand and inter-ligand NOEs are observed.

INPHARMA (Figure 1.13A) is based on the observation of inter-ligand NOEs that are target protein mediated and are observed between the two ligands binding competitively to the same binding site on the target protein such that ligand A binds first, transfers its magnetisation to

receptor protons and dissociates. During the same mixing time of the NOESY experiment, ligand B binds and the magnetisation, which was transferred from ligand A to the receptor, now gets transferred to ligand B. This leads to the inter-ligand peaks between the protons of two ligands although the two have never been spatially close at any given time during the experiment. The INPHARMA method determines the relative orientations of two individual ligands. If the protein bound conformation of one of the ligands is known, the conformation of the other ligand can be determined[264,265]. The ILOE method is also based on the observation of inter-ligand NOEs. In this scenario the two individual ligands bind to the target protein simultaneously and in close proximity, thereby forming a ternary complex (Figure 1.13B). Both ligands are not expected to bind to the same binding site nor sterically hinder binding[266].

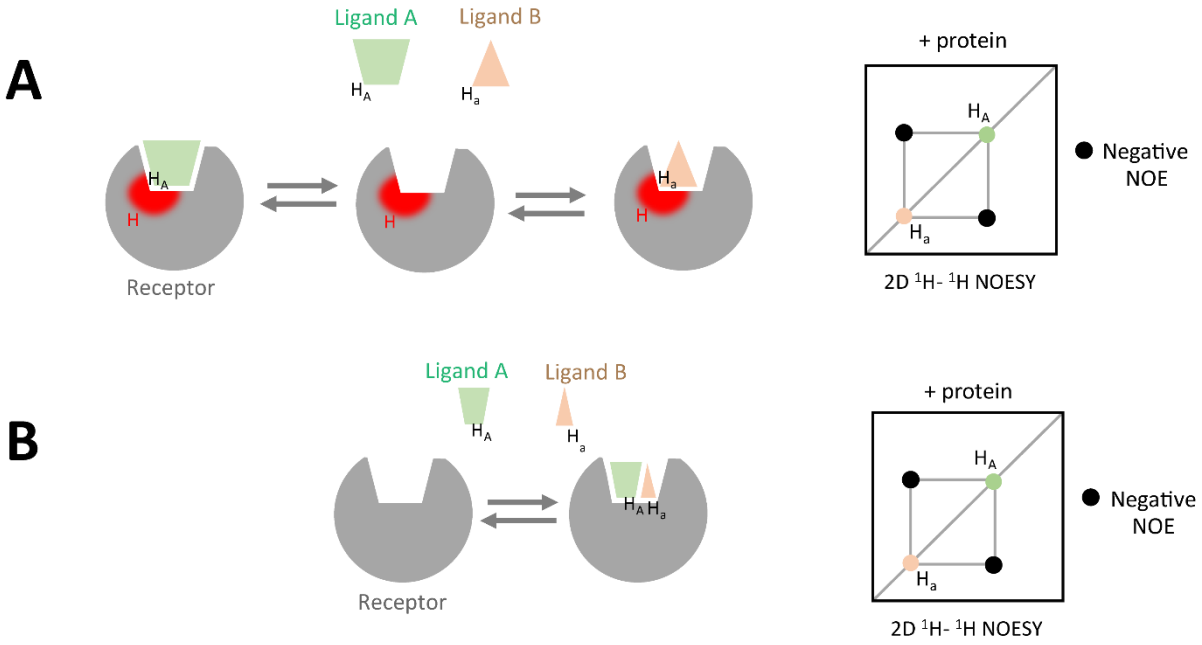

Figure 1.13. Schematic representation of the INPHARMA and ILOE methods. A. INPHARMA method. (Left) Ligand A (a trapezoid) and ligand B (a triangle) indicate two different ligands binding to the same site such that ligand A binds first, transfers its magnetisation (coloured in red) to the receptor and dissociates. The ligand B then binds to the same site and receives the transferred magnetisation from the protein. (Right) The pink and green circles indicate diagonal peaks of competitive binding ligands (pink triangle and green trapezoid) and the black-filled circles indicate negative inter-ligand NOE cross-peaks. B. ILOE method. (Left) A green trapezoid and a pink triangle indicate two different hit ligands binding to the adjacent sites on the protein forming a ternary complex. (Right) The pink, green, and

black-filled circles indicate diagonal peaks of adjacently binding ligands (pink triangle and green trapezoid) and negative inter-ligand NOE cross-peaks respectively.

Superficially NOEs generated by INPHARMA and ILOE do not distinguish between the proposed binding schemes. There are three ways to differentiate INPHARMA peaks from ILOEs: First, INPHARMA peaks are typically observed at mixing times ranging from 50–100 ms[264,284], while ILOEs have been reported at longer mixing times, typically 600–800 ms. Second, by performing competition experiments with a third strong binding specific molecule, where for INPHARMA, the inhibitor is expected to displace both molecules[285]. Thirdly, deuteration of the receptor has been proposed to differentiate INPHARMA from ILOE[284,285]. As mentioned before INPHARMA relies on the passage of magnetisation between the two ligands via receptor protons, contrary to ILOEs, in which receptor has no role in the transfer of saturation between the two ligands. So, if the inter-ligand peaks observed in the Tr-NOESY spectra are INPHARMA peaks, upon deuteration of the receptor, the intensities of these peaks should be quenched because the deuterated receptor would no longer be able to retain the magnetisation.

The ILOE and INPHARMA methods may be used to develop new "known drug-novel fragment hybrid compounds" with higher affinities by optimising drugs through growing and chemical linking identified binders, also known as SAR-by-NMR and fragment-growing[250,284]. These methods also allow the characterisation of novel variants of the known binders.

1.7.2.6 Relaxation based methods

The relaxation based methods, as the name suggests, are based on the differential relaxation rates (T_1 and T_2) of the rapidly tumbling small molecule and the slowly tumbling macromolecular complex. T_1, the longitudinal relaxation time is dependent on the molecular tumbling, the chemical nature of the group and field strength. T_2, the transverse relaxation time, is significantly dependent on the molecular tumbling and protein dynamics. In general, the protons of small molecules (<1 kDa) exhibit slow relaxation (i.e. long T_1 and T_2 relaxation times, T_1 = 1-2 s and T_2 = 1s) while a macromolecule (>10 kDa) exhibit fast relaxation (i.e. short T_1 and T_2 relaxation times, T_1 = 20 - 50 ms and T_2 = 5 - 20 ms[286]). And hence, if a ligand binds to the protein, forming a macromolecular complex, it retains the memory of the complex, exhibiting fast relaxation. Due to fast relaxation, the protein (or macromolecule) and the binding ligand signals are selectively attenuated, so the observed spectrum contains signals

from only the nonbinding compounds. Subtracting the observed spectrum from the control spectrum (in the absence of the protein) results in a spectrum which contains only the signals from the ligand. These methods have been widely used to distinguish ligands from non-binding compounds[267,268]. The differential effect can be enhanced by immobilising the receptor onto a solid support such as on the Sepharose resin as used in the TINS method[253] (shown in Figure 1.14).

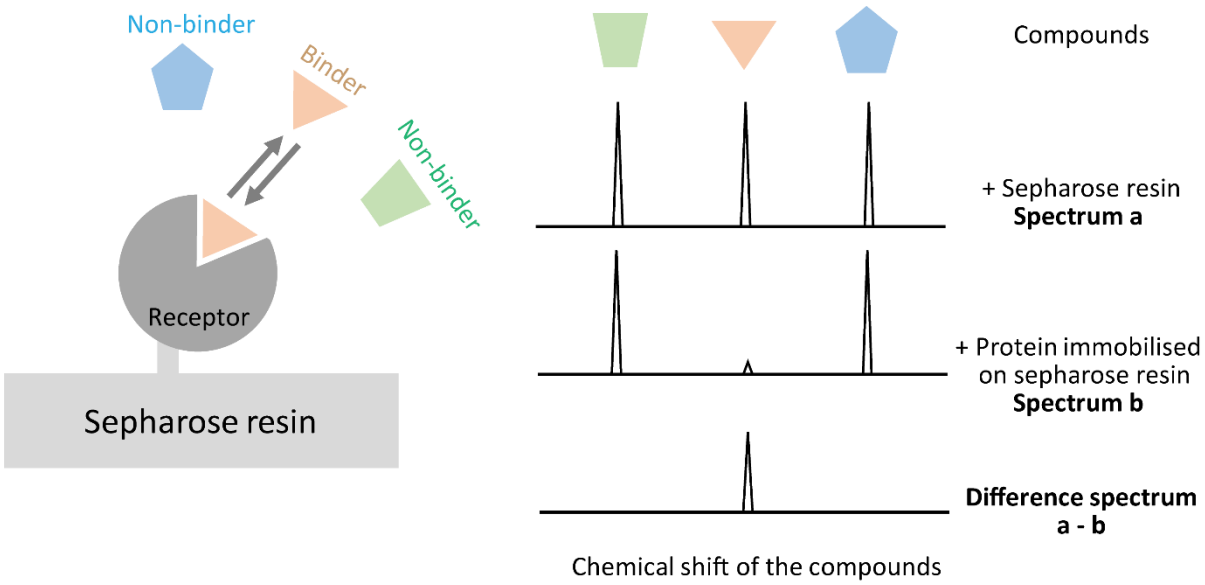

Figure 1.14. Schematic representation of the TINS method. (Left) Triangle indicates hit ligand. (Right) Spectrum a, ^{1}H spectrum of ligands in the presence of sepharose resin and no receptor. Spectrum b, the ^{1}H spectrum of ligands in the presence of protein immobilised on sepharose resin. Interaction of a ligand with Sepharose-bound protein specifically modulates the signal intensity (or broadens the signal) of the binding molecule. When the difference spectrum between the spectrum a and spectrum b is calculated, NMR signals from the interacting compounds can be identified.

1.7.3. Ligand-based NMR methods used to study GPCR-ligand interactions

NMR has been utilised for fragment-based screening (FBS) targeting thermostabilised GPCRs[287]. Ligand-based NMR methods, such as STD-NMR and TINS have been used on $A_{2A}AR$[288,289] and β_1AR[290] where fragments have been determined that inhibited the binding of tritium labelled ligands with IC_{50} (i.e., half-maximal inhibitory concentration) values ranging from 5 μM to 5 mM. STD-NMR[291–293] has also been applied to determine the bound

conformations and binding epitope of ligands on C-X-C chemokine receptor (CXCR) type 4[291], Human Sweet Receptor[293], α_{1A} and α_{1B}-AR[292] and others[294–297].

An advantage these methods offer is their capability to monitor the relatively weak interactions of low-molecular-weight compounds with GPCRs and hence can support fragment-based lead discovery approaches. The crucial stage in FBS is the lead optimisation, in which the structural information is needed to decide on where to link, merge or grow a given fragment[298]. NMR methods could be particularly useful in providing such information. Tr-NOESY[299–301] and INPHARMA[302,303] provide information on how to link or merge fragments in lead optimisation processes. Tr-NOESY experiments led to the determination of the bound conformations of ligands on the leukotriene B4 receptor 2 (BLT2), pituitary adenylyl cyclase-activating polypeptide receptor and κ-opioid receptor (κOR)[294,299,301] and INPHARMA has been applied for the selection of docking models on $A_{2A}R$[303] and GPR40[302].

1.7.4. Implementation of ligand-based NMR experiments in molecular docking protocols

To be able to predict the ligand bound conformation with higher confidence or to screen large numbers of docked conformations, many docking algorithms can now implement information generated by experimental NMR methods[304–307]. Several are described in further detail in the following sections.

1.7.4.1 PLANTS

Protein-ligand ANT System (PLANTS) molecular docking program is based on the ant colony optimisation (ACO) algorithm[304]. The intensity data obtained from STD-NMR and Tr-NOESY experiments[304] are implemented as distance restraints[305] during the docking step reducing the degrees of freedom of the ligand, resulting in an experimentally correlated ligand docked conformation. The method has been verified on three different systems: the inhibitor SBi279 bound to S100B protein (PDB 3GK2), T-antigen disaccharide bound to *Maclura pomifera* agglutinin and mucin 1 (MUC-1) pentapeptide bound to monoclonal antibody SM3.[304]

1.7.4.2 CORCEMA-ST

CORCEMA-ST protocol is based on the complete relaxation and conformational exchange matrix (CORCEMA) theory,[282] coupling a simulated annealing procedure to the CORCEMA

calculation.[273,308] The protocol[306] uses STD peak intensities for the refinement of the receptor bound conformation of a weak ligand. This implies that the prior protein-ligand complex coordinates should be available either from NMR techniques, X-ray crystallography or molecular docking. The protocol is developed to determine the global minimum conformation of the ligand and unlike traditional molecular docking programs, it is not developed for exploration of a wide energy landscape. Rather, this tool is useful for refinement of predicted/approximated complex structures derived from NMR data with distance constraints or low resolution crystallographic data.

The CORCEMA-ST protocol works by varying the ligand torsion angles based on STD peak intensities to iteratively minimize the "NOE-R" factor. NOE-R factor is a pseudo-energy function which measures the agreement between the CORCEMA predicted STD intensities and the experimental STD intensities. The CORCEMA-ST protocol was able to reproduce the experimental complex conformations of the glutathione tripeptide (PDB ID: 2GSR) and a trisaccharide (PDB ID: 2KMB) using simulated STD-NMR experimental intensities[309].

1.7.4.3 SpINPHARMA

SpINPHARMA is a program for quantitative evaluation of the INPHARMA experiments[307]. The core functionality of the program is the theoretical back-calculation of the NOESY spectra from the set of two competitive ligands and the protein of interest.

The program uses complete relaxation matrix approach:

$$\frac{dI(\tau_m)}{dt} = -(R + K) \cdot I(\tau_m)$$

where

$$I(\tau_m) = e^{-(R+K)\tau_m} I(0)$$

K and R are the kinetic and relaxation matrices. $I(0)$ is the initial magnetisation and τ_m is the mixing time. The peak integrals are calculated using eigen decomposition.

The methodology has been particularly useful in rescoring docking poses[310]. A number of protein-ligand docked conformations are first generated by a classical molecular docking protocol and then for every docked ligand pose an INPHARMA score is calculated, relative to

the known conformation of another ligand. The INPHARMA score is a correlation coefficient between the theoretically calculated and experimentally measured INPHARMA NOEs where closer the score is to 1, higher the correlation of that pose with the experimental NOE. In this way, the docking poses of a ligand are filtered relative to the known bound conformation of another ligand. The method was tested on protein kinase A (PKA) with two inhibitors (L_1, PDB ID: 3DNE and L_2, PDB ID: 3DND) where the authors reported a remarkable increase in accuracy (i.e. similarity of the predicted docked conformation to the crystal structure) compared to a traditional docking protocol[310]. It is better to use a large number of protein-ligand complex conformations for SpINPHARMA calculations[307] because the INPHARMA intensities observed in the Tr-NOESY spectra do not result from a single structure but form the conformational ensemble of structures. Ideally, one could generate such ensembles using molecular dynamics simulations and hence, the comparison of back-calculated volumes averaged over all complex structures taken from the MD simulation with the experimental intensities, would result in a more accurate prediction. This approach has been used for the determination of a bound conformation of a low-affinity ligand 3-pyrrolidin-1-ylquinoxalin-2-amine on human $A_{2A}R$, based on the receptor bound crystal structure of ligand ZM-241,358[303].

1.8. Structural modelling and dynamics of protein

There are approximately 150,000 experimentally solved structures of proteins currently available in the worldwide protein data bank (wwPDB), which includes multiple structures of the same proteins. When it comes to the sequences, the national center for biotechnology information (NCBI) nonredundant database contains >3,000,000 sequences from different species. Advancements in the gene sequencing technologies have led to the exponential increase in the known sequences but the rate of submission of determined structures has slowed[311]. Consequently, the gap between the sequences available and the experimentally solved structures is widening rapidly. Moreover, high-resolution structures are basically ‘snapshots’ of a single protein conformation and hence, the information on conformational changes that are essential for stability, function, ligand binding and modulation is not possible to obtain from these structures. Due to the complexities of solving structures of membrane proteins, including GPCRs, they are underrepresented in the structural databases. Membrane proteins represent >30% of a genome and are targeted by ~50% of the therapeutic drugs[312] and yet only ~ 1% of the experimentally solved structures are from membrane proteins. This lack in

structural information is mostly because of their inherent instability making it difficult to express, purify and crystallise these proteins compared to the other water-soluble proteins[313].

To fill this ever-widening gap, when no experimentally derived structure of protein exists, the structures of the protein can be modelled *in silico* using computational structure prediction methodologies. Even when an experimentally determined structure is available, computational methods can be used to estimate binding energies, predict protein conformational changes required for/resulting from ligand binding or signalling events, predict the ligand binding conformations and model the effects of mutations.

1.8.1. Protein structure prediction

Protein structure prediction methods can be broadly classified into two groups, template-based and free-modelling. Template-based methods include homology modelling and threading. Homology modelling, is based on the fact that the proteins related by divergent evolution exhibit similar structures and hence using the known structure of a related protein (the template), the unknown structure of a 'target' protein can be modelled[314]. In general, the sequence identity between the template and the target protein needs to be 25% or greater to be successfully employed for homology modelling[315,316]. Some of the widely-used programs for the model building include MODELLER[317,318], SWISS-MODEL[319], 3D-JIGSAW[320], BUILDER[321] and NEST[322]. Threading methods, on the other hand, can be used to model structures of the target protein when the homologous proteins with known structure do not exist. The target protein, however, is required to have the same fold as proteins of known structures. It is based on the rationale that proteins with no obvious sequence relationship can still adopt the same fold because the structure is more conserved than the sequence[323]. These methods are, therefore, constrained to the availability of known folds[324,325] and while we may expect that we have representatives of all possible folds, threading must be considered low-resolution. Commonly used threading programs are THREADER[326,327] and RAPTOR[328].

Clearly, in the absence of template structures, the structures of the target sequences of homologous proteins cannot be predicted with confidence. To partly address this problem and the fact that a homology model is likely to look more like the template structure than their actual "native" structure, template free modelling techniques have been developed. These algorithms are based on the Anfinsen's thermodynamic hypothesis, according to which, in a

given environment the structure of a protein is based on its sequence, corresponding to the global minimum of the potential energy of the system. Free-modelling approaches build 3D structures of the target sequence employing iterative processes where the conformation keeps changing until the conformation exhibiting the lowest potential energy is found. Commonly used methods include ASTRO-FOLD[329,330] and UNRES[331,332]. In general, these methods are limited to the high computational cost of searching the energy landscape and the difficulty in selecting the 'native' i.e., global minima structure from the numerous conformations "trapped" at local minima. Therefore, most of the modelling strategies now incorporate features from multiple approaches.

1.8.2. Force field-based modelling methods

The molecular modelling process relies on finding the global minimum of the energy landscape by starting with an initial conformation and then changing it in accordance with the rules of the method. In these approaches, atoms are treated as a series of balls linked by springs (the covalent bonds). The energy of the whole system is defined by a function consisting of a set of terms describing these covalent, but also non-covalent (van der Waals and electrostatic) interactions. This function is known as the 'force field'[333]. In biomolecular modelling, three types of force fields are commonly used:

1) **All atom force fields** treat every atom separately and the parameters, which includes bonded, non-bonded and charge interactions, are described for each and every atom in the system. Examples include OPLS-AA[334,335], CHARMM[336–338] and AMBER[339].

2). **United atom force fields** do not treat non-polar hydrogens as separate atoms, these are merged with the carbon as 'united atoms'. This reduces the particle size of the system significantly, hence requiring less computer power. Examples include OPLS-UA[340] and GROMOS[341].

3). In the **coarse-grained force fields,** individual atoms are grouped into 'super atoms' where one particle constitutes 2-5 atoms, reducing the computational requirement considerably. Examples include MARTINI[342,343] and its extension for proteins[344]. These models have been used frequently to study protein–protein complexes[345,346], protein folding[347–349], vesicle fusion[350,351] and to simulate membrane proteins[352–356] for a longer time scale.

1.8.2.1 Energy minimisation

In molecular mechanics, energy minimisation implies the approaches used to "walk-downhill" the energy surface of a molecule to find a structure (or structures) close to or at the global minimum. The process is iterative, i.e. the conformation keeps changing until the structure with the lowest energy is found. Three commonly used energy minimisation algorithms are Newton–Raphson, conjugate gradient and steepest descent. Minimisation can also be used to resolve steric clashes, to get rid of unfavourable interactions and also to analyse the effect of a point mutation or a set of mutations on a protein structure.

1.8.2.2 Molecular dynamics

In molecular dynamics (MD), the behaviour of the system is observed over time, as measured by the force field value, using rules that are based on the Newton's equations of motion. The resulting trajectory of a molecule represents conformational changes of a protein over time. In 1977, the first MD simulation of a protein was reported, which consisted of a 9.2 ps trajectory of a small protein, bovine pancreatic trypsin inhibitor (BPTI) in vacuum[357]. Around a decade later, a longer 210 ps simulation was reported for the same protein in water[358]. The substantial increase in computing power since then led to the first MD simulation of a membrane protein, bacteriorhodopsin, a GPCR in 1995[359]. Following that, many different studies using MD simulations have been performed which includes determination of ligand–protein interactions[360], study of protein dynamics[361], simulation of lipid surfaces[362,363], structure refinement[364–366], sampling protein conformations[367] and modelling of membrane embedded proteins[368–370]. A variety of MD simulation program packages are available for study of biological macromolecules including CHARMM[336], Amber[339], NAMD[371], GROMACS[372,373] and Schrödinger software packages[374]. One of the key questions is how long the system should be simulated? The simulation time scales range from ns to ms[375,376] (Figure 1.15) depending on what information one wants to extract out of these simulations and off course the available computer power.

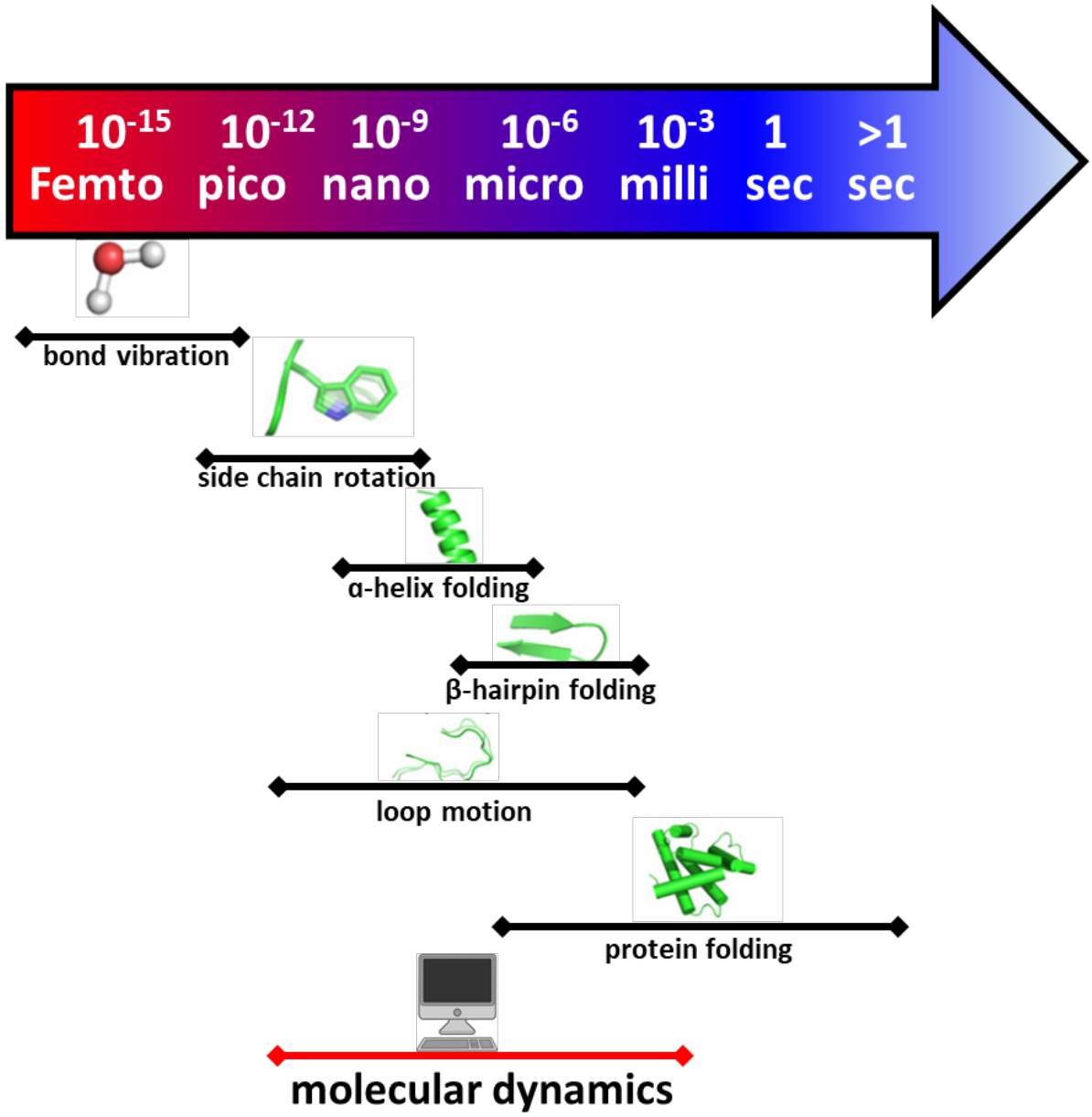

Figure 1.15. Time scales of different motions in protein. Graphical comparison of the timescales of protein motions ranging from femtosecond to seconds. The region of the dynamic range in a protein for which MD is best suited is shown.

1.8.3. Computational modelling of GPCRs

In recent years, MD simulations have been applied to many GPCRs to explore various dynamic properties such as modes and kinetics of ligand binding as well as the activation mechanism of the receptor[377–379]. The first GPCR crystal structure of bovine rhodopsin paved the way for tremendous growth in GPCR MD studies attempting to analyse various aspects of rhodopsin function[380–382]. It also resulted in more reliable homology models for other

rhodopsin-like GPCRs. The coordinates of bovine rhodopsin were used to build homology models of the $5HT_{1A}$ receptor[383] and protein dynamics induced by ligand binding were studied, illustrating how binding of a ligand to a GPCR, transfers information to the G-protein binding site[383]. MD was also used to study signal transduction of the CXCR4 receptor[384]. Homology models of the μ-opioid receptor (μOR) have also been built based on the bovine rhodopsin structure, determining the key residues in the binding of an antagonist naltrexone[385]. The study also reported for the first time; the MD simulations of an opioid receptor embedded in a membrane (1,2-dimiristoyl-SN-glycero-3-phosphocholine (DMPC)) mimicking a lipid bilayer. Another study reported simulations of the κOR in a dipalmitoylphosphatidylcholine (DPPC) bilayer[386] bound to dynorphin, an endogenous ligand.

It is well established now, that GPCRs undergo conformational changes to be able to interact with a G-protein or an arrestin. Most of these changes occur in TM6 but also in TM3 and TM7[387–391]. Exploration of these conformational changes, specifically the activation mechanism of GPCRs upon binding to a variety of ligands has been the focus of most of the MD studies, using both conventional long-time scale simulations[193,387,392,393] as well as methods employing advanced sampling tricks[394–396].These studies have shown the significance of capturing intermediate conformations which might not be achievable using X-ray crystallography, which is generally biased towards capturing low-energy states. Thorough understanding of the GPCR drug binding kinetics has been another major focus. Ligand binding pathways i.e. the entry of a ligand into the receptor binding site from the bulk solution has been studied by both conventional MD[393,397] and enhanced sampling methods[398–400] providing molecular insights into the GPCR ligand binding and modulation. Another recent area of focus is the interactions of GPCRs with lipids, such as cholesterol, which is reported to modulate the receptor stability and ligand binding activity[401–408].

MD simulations have made a phenomenal impact in the world of GPCRs, by providing extremely useful insights into ligand binding, protein dynamics and modulatory aspects of GPCR functioning[409] at the molecular level. Undoubtedly, the advancements in computing power and the algorithmic approaches will lead to deeper insights into GPCR functioning and modulation, opening new opportunities for GPCR drug development.

1.9. Aims of the project

1.9.1. Preparation and characterisation of the thermostabilised variants of α_1-AR subtypes (chapter 2).

Unlabelled thermostabilised α_{1A}- and α_{1B}-AR variants were expressed and purified as fusion proteins using the existing optimised protocols[292]. The purified receptors were then tested for their binding competency using saturation binding assays. Next, the competition binding experiments were performed to assess the binding affinities of various ligands to test their suitability for the ligand-based NMR experiments. One key experiment reported in this thesis is the use of deuterated receptors to differentiate INPHARMA NOEs from ILOEs. Hence, for this purpose, existing protocols were optimised to get sufficient amounts of the purified deuterated α_{1A}-ARs.

1.9.2. Probing benzodiazepine binding to α_{1A}-ARs using NMR (chapter 3).

Benzodiazepines are reported to be the allosteric modulators on α_{1A}-ARs[209], and hence the binding of a variety of benzodiazepines such as diazepam, lorazepam, bromazepam, temazepam and oxazepam, was tested against the stabilised α_{1A}-ARs, using ligand-based NMR methods including STD-NMR, Water-LOGSY and Tr-NOESY experiments. Furthermore, different control experiments were performed to test the binding specificity of these highly lipophilic compounds. The results validate our recently published work[235], which claims that the reported modulation of α_1-ARs activity by benzodiazepines is not a result of direct ligand binding to α_1-ARs.

1.9.3. Determination of the bound conformation of A-61603 on α_{1A}- and α_{1B}-ARs based on NMR and MD studies (chapter 4).

In this chapter, the ligand-based NMR method, INPHARMA, is primarily used in combination with the extensive MD simulation studies, based on which the bound conformation of A-61603 (an α_{1A}-AR selective agonist) was determined, on both α_{1A}- and α_{1B}-ARs, relative to adrenaline (an endogenous agonist) the conformation of which is predicted based on the extensive SAR studies and crystal structures of the homologous receptor. Most importantly, the enantiomeric forms of A-61603 were studied separately in MD studies, shedding light on the importance of treating isomers as separate drugs. We believe this a great methodology for rapid determination

of the bound conformation of ligands and application of which could contribute remarkably to the subtype selectivity in drug development for GPCRs.

CHAPTER 2 : PREPARATION AND CHARACTERISATION OF α_{1A}-AR and α_{1B}-AR MUTANTS

2.1. Introduction

While GPCRs are integral membrane proteins, they also possess inherent conformational and structural flexibility, which is crucial for diverse signalling mechanisms as well as coupling to multiple effectors. This flexibility and membrane location make it difficult to isolate GPCRs, and thus, expression and purification of GPCRs have always been challenging. The very first crystal structure of a GPCR was reported in 2000[9] and it was of bovine rhodopsin which, contrary to typical GPCRs, is inherently stable and shows high native expression. The second GPCR structure, of human β_2-adrenoceptor[3], was seven years later and since then remarkable progress with X-ray crystallography has occurred with structures for more than 60 different GPCRs being available in the Protein Data Bank[11],which includes structures from all classes except B2/adhesions and T/taste2[11]. Cryo-EM structures of GPCRs are also appearing at a rapid rate, including tertiary complexes of receptors with agonists and G-proteins of the A_1 adenosine receptor[12], GLP1R[13], μOR[14], the calcitonin receptor[15], the serotonin $5HT_{1B}$ receptor[16], rhodopsin[17] and the latest one of M1 and M2 mACHR[18]. Series of methodological and technological developments including protein engineering, use of new detergents, use of lipidic cubic phase-based crystallisation methods and microfocus synchrotron beamlines have enabled these GPCR structures to be determined[410].

2.1.1. GPCR protein engineering

When it comes to protein engineering, several approaches have been developed including removal of the structurally dynamic carboxyl and amino termini of GPCRs and the IL3 which is highly heterogeneous in conformation[411,412], the use of antibodies[10,247,413–418], in particular nanobodies[248], the fusion of receptors with small, easily crystallizable proteins[53,59,80,138,150,151,188,243,244,419–429] and finally GPCR thermostabilisation[80,129,189,195,245,430–432].

GPCR thermostabilisation was first used for the crystallisation of the β_1-adrenoceptor and then, has been used for many other GPCRs[189,431,432]. A series of mutants are made and tested for ligand binding at increasing temperatures using radioligand binding assays, to identify the mutants with enhanced thermostability than that of the WT receptor. One of the widely used ways to generate systematic mutant libraries of GPCRs is alanine scanning[189,431,432] which has been used in a process referred to as StaR (stabilised receptor), which stabilizes the receptors in a particular conformation by reducing the conformational flexibility. StaR has been used in crystallisation of many GPCRs[245]. Another method is cellular high-throughput encapsulation, stabilisation and selection (CHESS), a directed evolution method that can evolve populations of GPCR mutants for improved stability in detergents[433]. In this method, a randomly mutated library of the GPCRs, created using error-prone PCR (epPCR), are expressed in the *Escherichia coli* (*E. coli*) inner membrane. The *E. coli* cells are then encapsulated into microcapsules, yielding a semi-permeable container that is permeable for solubilising detergents and fluorescently-labelled ligands but impermeable for large molecules such as proteins and plasmids. When *E. coli* cells are exposed to a solubilising detergent it disintegrates within the microcapsule containing the plasmid DNA, including the gene coding for that particular GPCR, detergent solubilised recombinant GPCRs and several endogenous *E. coli* proteins too big to diffuse through the pores. GPCRs are then probed for stability using receptor-specific fluorescent ligands which are small enough to freely diffuse through the semi-permeable membrane of a microcapsule. Those mutants which are detergent stable and can bind fluorescent ligands can be separated using fluorescence-activated cell sorting (FACS) as they confer high fluorescence to the associated microcapsules. Since the genetic material is retained within the microcapsules, the plasmids corresponding to detergent stable receptors can be extracted for identification and the process can be repeated in an evolutionary manner until the expected receptor stability is achieved.

Several GPCR structures have been obtained in complexes with diverse sets of ligands[434], ranging from inverse agonists, which "locks" the receptor in an inactive conformation, to full agonists[434], which in the presence of G-protein, shift the equilibrium between active and inactive states toward the active state. These structures provide some basic understanding of ligand-induced conformational changes and ligand specificity[435,436]. Moreover, these crystal structures paved a path for structure-based drug design for these important proteins[437–441] with a plethora of studies reported on the *in silico* screening of GPCR ligands, with several characterising novel chemical scaffolds[42,242]. Most importantly, for the first time, the crystal

structure of a GPCR (rhodopsin carrying the disease-causing mutation G90D[442]) enabled us to understand the structural basis of disease-causing mutations[442].

The crystallography of GPCRs have been progressed enormously, however, there are outstanding key questions about the receptor functioning that are of significant interest to drug discovery, such as the basis for selectivity of the ligand; the mechanisms of receptor activation; the structural basis for biased signalling, basal activity, allosteric modulation and partial agonism by small molecules and ions, that cannot be completely answered from crystallography data. These limitations mostly result from the modifications of the WT GPCR structure which facilitates crystallisation but stabilize the receptor into a low energy state and hence in large part affect functionally important conformational equilibria. A classic representation of these limitations came from the structures of β_1-ARs, which showed highly similar conformations for complexes with either full, biased or partial agonists and also antagonists[196,443]. The similar structures were probably due to the thermostabilisation trapping the receptor in an inactive state. To date, all of the GPCR crystal structures have been solved complexed with ligands, selection of which plays an important role in GPCR crystallography. So far, most of the ligands used have a strong binding affinity ($K_i \leq 10$ nM)[94] and similar chemical properties and thus providing information on only a fraction of the potentially recognisable drug scaffolds. In summary, all these limitations necessitate the use of alternative techniques to complement crystal structures. In that respect, solution NMR is particularly promising.

2.1.2. GPCR expression

The primary challenge in studying the structure and solution behaviour of GPCRs is the production of enough recombinant protein. Several recombinant protein expression hosts have been used such as *E. coli*; yeast (more specifically *Saccharomyces cerevisiae* and *Pichia pastoris*); baculovirus expression system (BVES) in insect cells; and mammalian cells (listed in the decreasing order of achievable protein yields per litre of culture). The most cost effective recombinant expression system in general is *E. coli*. while the most suitable expression system, in terms of quality of expression for human/mammalian integral membrane proteins, are the mammalian cells[444] as it represents the closest alternative to their native environment.

Due to high molecular weight, NMR structural and dynamic analysis of GPCRs requires either site specific isotopic labelling (for example, $^{13}CH_3$-methionine[445–449] and ^{15}N-valine[450]) or uniform ^{13}C,^{15}N labelling[451,452], which benefits from perdeuteration to improve or slow the relaxation of the NMR signal[453,454]. Deuteration, however, requires back-protonation of the amide or "unlabelling" (with ^{1}H) of deuterated proteins which is difficult for proteins dissolved in a hydrophobic detergent or lipid environment. Nevertheless, deuteration of the protein can significantly enhance the sensitivity and resolution of the isotopic signals, thereby rendering proteins larger than 20 kDa amenable to structural NMR studies[455–457]. As is observed with $^{13}CH_3$-methionine labelled dynamics studies on the β_2-AR, where perdeuteration improved the spectral quality dramatically and made it possible to see resonances that are not otherwise observable at low protein concentrations[446]. Fractional deuteration benefits NOESY-based experiments by providing some protons for distance measurements[455]. Deuteration of the receptor could be particularly useful for the Tr-NOESY experiments as spin-diffusion from receptor protons is prevented or reduced[458]. Importantly, deuteration provides a means to differentiate INPHARMA signals from ILOEs[285].

When it comes to the expression of deuterated GPCRs, *E. coli* appears to be the popular choice[459] because of its well understood metabolism and remarkable capacity to tolerate hostile conditions of 100% D_2O solutions. Although other organisms, such as yeast[460], insect[446] or mammalian cells[461], have been used to produce deuterated proteins, the major limitation is that they are intolerant to D_2O and hence, the production of perdeuterated proteins is limited. Yeast expression systems such as *P. pastoris* have been used for high-level deuterated GPCR expression (~70%[462] to 90%[451]), achieved in the presence of deuterated carbon sources by gradually (in ~7 to 9 days) adapting the cells to deuterated media.[451,462–464] For example, deuteration of the WT human ^{15}N labelled $A_{2A}R$, which enabled the studies of ^{1}H–^{15}N backbone and side chain dynamics[451]. But the protein production yields are lower when compared to *E. coli* at an equivalent cost. Other organisms, like some algae, can thrive in 100% D_2O solutions[465], but the production of recombinant proteins by genetic engineering has not been exploited much in these organisms. Deuteration in mammalian and insect cells have been achieved by adding deuterated digests from lower organisms (as used for β_1-AR[460] and CCR5[466] expression) or deuterated amino acids (used for β_2-AR[446] and μOR[445] expression) in the cell culture media. But the extent of deuteration is lower. In insect cells, the efficiency of deuteration is reported to be amino acid dependent[446]. In essence, in terms of protein production yields and genetic engineering, *E. coli* offers the best compromise.

2.1.3. GPCR purification

Once a robust expression strategy has been identified, the GPCRs need to be extracted from the phospholipid bilayer of their recombinant host cells in a functional state and reconstituted in a membrane mimetic environment that facilitates efficient purification and is suitable for biophysical and biochemical analysis. For NMR studies, use of a variety of membrane mimetics has been reported[467] including bilayers (of various shapes, sizes and lamellarity), bicelles (aligned or isotropic), detergent micelles, nanodiscs, amphipols, reverse micelles. As to detergent micelles, the most common ones used for GPCR solubilisation are the mild non-ionic alkylglucosides such as N-dodecyl-β-D-maltoside (DDM)[10,421], N-decyl-β-D-maltoside (DM)[59,189,468], β-D-nonylglucopyranoside (NG) and β-D-octylglucopyranoside (OG)[191]; and the amphiphile, lauryl maltose neopentyl glycol (LMNG)[195]. Generally, the longer the detergent's alkyl chain, the gentler its effect on the receptor[469]. Often, other agents are used in combination with these detergents such as the anionic bile acid salt sodium cholate[423]; the zwitter-ionic surfactant 3-[(3-cholamidopropyl)dimethylammonio]-1-propanesulfonate (CHAPS)[421,468,470] and the synthetic cholesterol derivative, cholesterol hemi-succinate (CHS)[468].

After solubilisation and reconstitution, GPCRs need to be purified using reproducible protocols to obtain high quality protein samples. One of the most commonly used techniques for GPCR purification is immobilised metal affinity chromatography (IMAC) purification that employs the affinity tags attached to the recombinantly expressed GPCR. The basis of IMAC purification is the coordinate bonding of metals with specific amino acids, mostly histidine. On proteins, IMAC is mediated through a poly-histidine-tag. Commonly used tags are hexa-histidine tags (6xHis) used for purification of β_1-AR[189,471], CXCR1[472], M_3 mACHR[150] and μOR[421,473] and deca-histidine (10xHis) tags used for purification of $A_{2A}R$[474,475], β_2-AR[447], cannabinoid receptor type 2[476], δOR[423], human orexin receptor 2[470], mGluR[477], neurotensin receptor type 1 (NTS_1)[478], orexin receptor type 2 (OX_2R)[479], PAR1[422] and SMOR[91]. Considerations need to be taken to choose the size and position of His-tags, as these can have an influence on the protein expression levels as well as the capturing efficiency of the IMAC.[480] Two types of IMAC resins are widely used: Ni^{2+}-NTA resin (Ni^{2+}-nitrilotriacetate) and Co^{2+} or Talon resin (Co^{2+}-carboxymethylaspartate). Although both resins can tolerate detergents in amounts used for solubilisation, Talon resin is always a first choice for GPCR purification because of its less non-specific binding and higher elution purity[481]. Other affinity

chromatography techniques include antibody affinity chromatography, for example, Flag M1 which comprises a resin immobilised monoclonal anti-Flag M1 antibody that recognizes the free N-terminus of the Flag peptide tag (DYKDDDDK)[482] and an anti-rhodopsin ID4 monoclonal antibody that recognizes a 9 amino acid C-terminal peptide ID4 which is naturally present in rhodopsin and related photoreceptors[483]. Other techniques include receptor specific affinity chromatography which assumes that ligands only bind correctly folded variants of their cognate receptors and thus using "ligand columns" that is, columns with these ligands chemically attached to the support, allow to selectively capture correctly folded receptor. This form of chromatography has been used in the purification of many GPCRs[2,15,16,38–47].

As a final polishing step, size exclusion chromatography (SEC) is used to ensure homogeneity and monodispersity of the final protein as either a monomeric GPCR due to their tendency to form oligomers/aggregates, for example β_2-AR[243], CXCR1[472], M_3 mACHR[150], $mGluR_5$[80], NTS_1[468,470], OX_2R[479], PAR1[422], δOR[423] and μOR[421,473]; as a part of macromolecular complexes such as the A_{2A}R-Fab[247], the β_2-AR-G_s[10,484], and β_2-AR-nanobody[190,490] complexes; or reconstituted into recombinant high density lipoproteins (rHDL)[491].

To impart additional stability to the receptor, certain additives such as glycerol[474] and ligands[94] (mostly inverse agonists and antagonists) have been used during different protein production steps. The choice of the buffer is another consideration, which it seems is dependent on the receptor, but overall HEPES is often the first choice, probably because of its superior buffering capacity at low temperatures when compared to most salt-based buffers[492].

2.1.4. CHESS stabilisation and characterisation of α_{1A}-AR and α_{1B}-AR.

Stabilisation of α_{1A}-AR was conducted with three rounds of error-prone PCR and eleven rounds of CHESS whereas α_{1B}-AR was subjected to two rounds of error-prone PCR and six rounds of CHESS[292]. Single clones isolated from these populations, when expressed, purified, and screened for detergent and temperature stability, identified two variants α_{1A}-AR A4 and α_{1B}-AR #15 to be the most stable of each subtype. α_{1A}-AR A4 contained fifteen and α_{1B}-AR #15 nine amino acid substitutions, compared to the respective WT receptors. The locations of these mutations mapped onto homology models of both the receptors are shown in Figure 2.1.

α_{1A}-AR A4 contains two mutations in the N-terminal extracellular domain (C14S and T15I), one mutation in TM1 (L36I), four mutations in TM2 (I65V, N67Y, L80M, and F86Y), one mutation in TM3 (G127A) and TM4 (W151F), one mutation in ECL2 (E171V), three mutations in TM7 (F312L, N322K, and P327L), and one mutation between TM7 and helix 8 (S329Y). The F86Y, F312L and L80M mutations lie within or near the predicted orthosteric binding pocket. The N322K mutation is in the NPxxY motif, which is important for receptor activation. α_{1B}-AR #15 contains one mutation in the N-terminus (G27D), one mutation in TM2 (L105Q), one mutation in ICL2 (S150Y), two mutations in ECL2 (D191Y and E194G), one mutation in each of TM6 (T295M) and TM7 (F334L). F334L is located at the top of the orthosteric binding pocket and is analogous to the F312L mutation found in α_{1A}-AR A4.

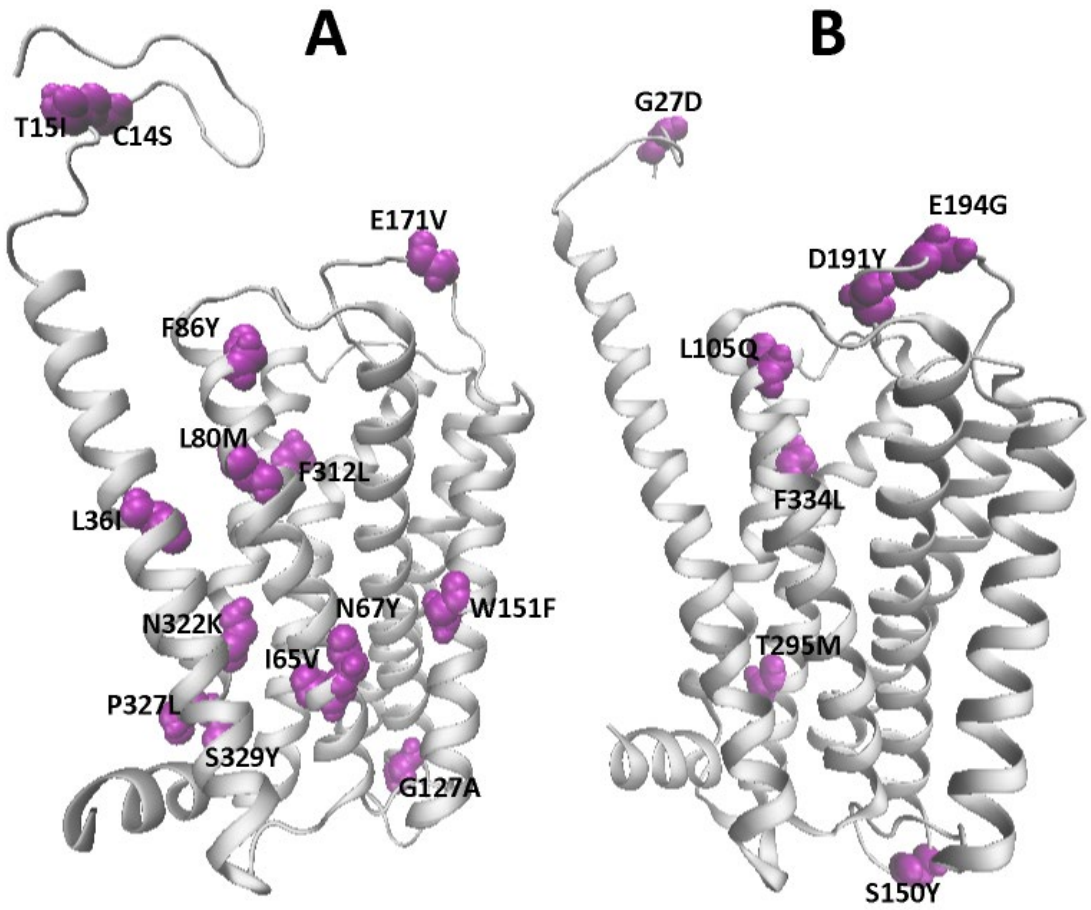

Figure 2.1. Mutation map of the thermostabilised α_{1A}-AR A4 and α_{1B}-AR #15. Location of mutations mapped onto the homology models of A. α_{1A}-AR A4 and B. α_{1B}-AR #15. ICL3, N- and C- terminal regions which do not contain any mutation are not shown.

2.2. Materials and methods

2.2.1. Expression system

Expression vectors, pDS15 and pDS11, were used for recombinant expression of CHESS stabilised α_{1A}-AR A4 and α_{1B}-AR #15.

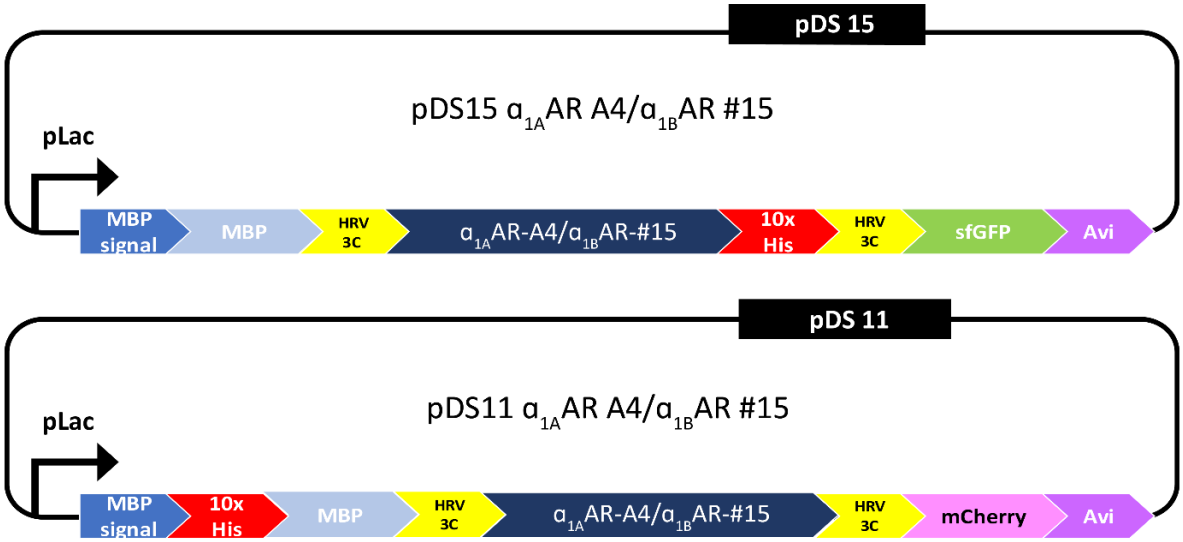

Figure 2.2. Expression constructs. Vector maps of the expression constructs used for recombinant expression of α_{1A}-AR A4 and α_{1B}-AR #15.

The expression vector pDS15 (Figure 2.2) encodes an N-terminal maltose-binding protein signal sequence (MBPss) which is used for targeting the receptor to the inner periplasmic membrane of *E. coli*[493], maltose binding protein (MBP), a NNNNNNNNNG (Asp_{10}) linker prior to a human rhino virus (HRV) 3C protease site (LEVLFQGP) which are linked via a BamHI restriction site to residue V2 of α_{1A}-AR A4 or N2 of α_{1B}-AR #15. C-terminal residues S351 of α_{1A}-AR A4 or G383 of α_{1B}-AR #15 are linked via a NheI restriction to deca-histidine (His_{10}) tag followed by a HRV 3C protease site, a GGGSGGGS linker, a super-folded green fluorescent protein (sfGFP)[494] for improved expression and fluorescence-based quantification of expression and an Avi-tag for in vivo biotinylation in *E. coli*. The expression of recombinant protein is driven under the control of the lac operon. The expression vector pDS11 is essentially similar to pDS15, except that sfGFP is replaced by the mCherry for improved fluorescence-based assessment of protein quality and that there is a slight difference in the frame sequence, which is as follows: maltose binding protein (MBP) signal peptide, His_{10} tag,

MBP, Asp_{10} linker, HRV 3C protease site, receptor cloning site (BamHI − NheI), a second HRV 3C protease site, 2 x GGGS linker, mCherry, and Avi-tag. Same expression and purification protocols were followed for both the constructs. All of the major experiments reported in this thesis were performed on GFP fusion proteins (pDS15 expression construct), and for all the fluorescence based saturation and competition binding assays, mCherry fusion proteins (pDS11) were used because of the spectral overlap of GFP with that of the fluorescent ligand used in these experiments.

2.2.2. Transformations and pre-cultures

The transformation was carried out by thawing 100 µL of chemically competent *E. coli* C43(DE3) cells on ice and adding ~1 µg of plasmid miniprep. The transformation mixture was then incubated for 30 min on ice and subsequently heat shocked for 1 min at 42 °C. The transformed cells were then recovered by adding 250 µL of Luria broth (LB) medium and incubating with shaking for 40 min at 37 °C before plating on LB agar plates (100 mg/L ampicillin, 1% (w/v) Glucose). A colony was picked to inoculate a 5 mL LB pre-culture containing 100 mg/L ampicillin and 1% (w/v) glucose which was incubated at 37 °C at 225 rpm in an orbital shaker overnight (for approximately 16 h).

2.2.3. Recombinant expression of α_{1A}-AR A4 and α_{1B}-AR #15

For expression of the α_{1A}-AR A4 and α_{1B}-AR #15 in *E. coli* C43(DE3), protocols from Marley et al[495] were modified. The minimal medium (M1) consisted of an autoclaved basal salts solution (30 mM KH_2PO_4, 23 mM K_2HPO_4, 16 mM Na_2HPO_4, 17 mM NaCl, 37 mM NH_4Cl, adjusted to pH 7.4 with NaOH) that was supplemented with sterile filtered 100x trace metal stock solution (1% v/v), 2 mM $MgSO_4$, 0.4% w/v Glucose, 50 mg/L Thiamine and 100 mg/L Ampicillin immediately before use. The 100x trace metal stock solution was prepared as described by Cai *et al.*[496]

For 2 L LB expression, two 5 mL LB pre-cultures were inoculated to 1 L LB each, supplemented with 100 mg/L ampicillin and 1% (w/v) glucose and incubated at 37 °C, 220 rpm until an OD_{600} of 0.9 – 1.0 was reached. Cells were then harvested by centrifugation at 3000 rpm, 20 °C for 10 min. The cells were washed by resuspending in M1 minimal solution and re-pelleting at 3000 rpm, 10 min at 20 °C. The pellet was resuspended in 500 mL M1 solution. The expression cultures were incubated for 1 h to allow adaptation of the culture to media.

Recombinant protein expression was then induced with isopropyl β-D-1-thiogalactopyranoside (IPTG, 250 μM) and protein expression was carried out for 4 h (37 °C, 220 rpm). The cells were then pelleted by centrifugation (3800 rpm, 4 °C, 20 min), snap frozen in liquid nitrogen and stored at -80 °C.

The expression of the deuterated receptor was essentially the same, except that the M1 minimal solution was prepared in 75% D_2O and protein expression was carried out for 5.5 hours after IPTG induction and the inoculated 500 mL minimal media was split into five 2 L flasks, containing 100 mL media each, for better aeration.

2.2.4. Purification of α_{1A}-AR A4 and α_{1B}-AR #15

Protonated and deuterated α_{1A}-AR A4 fusion proteins (MBP-α_{1A}-AR A4-sfGFP) and protonated α_{1B}-AR #15 fusion protein (MBP-α_{1B}-AR#15-sfGFP) were purified using a protocol as previously reported.[292] Harvested cells were resuspended in 20 mL of IMAC solubilisation buffer (50 mM potassium phosphate, 1% DDM, 150 mM NaCl, 0.12% CHS, 0.5% CHAPS, 1 mg mL^{-1} lysozyme, 0.1 mg mL^{-1} DNaseI, 1 Roche cOmplete protease inhibitor tablet, pH 8.0) and sonicated for 15 cycles (10 s on, 20 s off, 30% power) at 4 °C. The sonicated cells were mixed at 4 °C for 2 h after adding an additional 30 mL of IMAC solubilisation buffer. Cell debris was pelleted by centrifugation at 10000 rpm for 30 min at 4 °C and the lysate (supernatant) was filtered by passing through a 0.45 μm syringe filter. To capture full-length α_1-ARs fusion proteins, 1.5 mL of TALON metal affinity resin (Clontech) equilibrated with 10 column volumes (CV) of equilibration buffer (50 mM potassium phosphate, 0.05% DDM, 150 mM NaCl, pH 8.0) was added to the clarified lysate and mixed gently for 2 h at 4 °C. The lysate-resin mix was then washed with 30 CV of IMAC wash buffer (50 mM potassium phosphate, 0.05% DDM, 500 mM NaCl, 10 mM imidazole, pH 8.0) and the fusion receptors were eluted with 10 CV of IMAC elution buffer (50 mM potassium phosphate, 0.05% DDM, 500 mM NaCl, 300 mM imidazole, pH 8.0). Elutions were concentrated to 0.5 mL and buffer exchanged (50 mM potassium phosphate, 0.05% DDM, 100 mM NaCl, pH 7.4) by either passing it through the PD-10 desalting columns (GE Healthcare) or performing size exclusion chromatography (SEC) using a Superdex 200 Increase 10/300GL column (GE Healthcare). The PD-10 elutions or SEC collected fractions were concentrated again to a final volume of 0.2 mL. Protein concentrations were determined by Direct Detect (Merck Millipore). Deuterated glycerol was added to 20%, and aliquots of the proteins were snap-frozen in liquid nitrogen and

stored at -80 °C. For all concentration steps, Amicon Ultra-15 100 kDa molecular weight cut-off (MWCO) centrifugal concentrators (Merck Millipore) were used.

For purification of the cleaved α_{1A}-AR A4 and α_{1B}-AR #15, proteolytic cleavage was carried out by adding 100 mM of Na_2SO_4, 50 mM of NaCl, 1 mM TCEP and 100 mM of HRV 3C protease to the PD-10 eluate (resulting in a total volume of approx. 2.5 mL) and leaving the mixture gently rocking for 16 h at 4°C. The cleavage mixture was then topped-up with approx. 10 mM Imidazole, then transferred to a gravity flow column and incubated gently rocking for 1.5 h at 4°C with 1.5 mL of Talon resin equilibrated with 5 CV of equilibration buffer. The flow through containing cleaved receptors (either α_{1A}-AR A4 or α_{1B}-AR #15) was collected and concentrated to approximately 450 µL using an Amicon Ultra 15 concentrator with 30 kDa cutoff (Millipore). The concentrated sample was then loaded onto a Superdex 200 10/300 Increase column (GE Healthcare) equilibrated with SEC buffer (50 mM potassium phosphate, 0.05% DDM, 100 mM NaCl, pH 7.4)

2.2.5. Saturation and competition binding on stabilised α_{1A}-AR A4 and α_{1B}-AR #15

All binding assays were performed on stabilised α_1-AR fusion proteins following the protocols as previously reported[292] by immobilising the purified Avi-tagged receptors onto the Dynabeads (Streptavidin T1). Saturation binding was performed using specific α_1-AR binder QAPB (BODIPY-FL-prazosin) and competition binding assays were performed using α_1-AR agonists adrenaline, noradrenaline, A-61603 and antagonist prazosin as displacers of specific QAPB binding.

2.3. Results and discussion

2.3.1. Purification of α_{1A}-AR A4 and α_{1B}-AR #15

The SDS-PAGE gels of the purifications of α_{1A}-AR A4 and α_{1B}-AR #15 fusion proteins are shown in Figure 2.3. The protocol involved one IMAC step to capture the fusion protein from the solubilised *E. coli* lysate followed by PD-10 or SEC to exchange buffers or to remove larger aggregates, ensuring monodispersity of the sample. The SEC profile revealed a peak centered at an elution volume of 11.5 mL to be the main species for α_{1A}-AR A4 fusion protein and at around 8.5 mL for α_{1B}-AR #15 fusion protein (Figure 2.4). The purification yields for

protonated α_{1A}-AR A4 and α_{1B}-AR #15 fusion proteins were ~1 mg/L and ~0.5 mg/L, respectively.

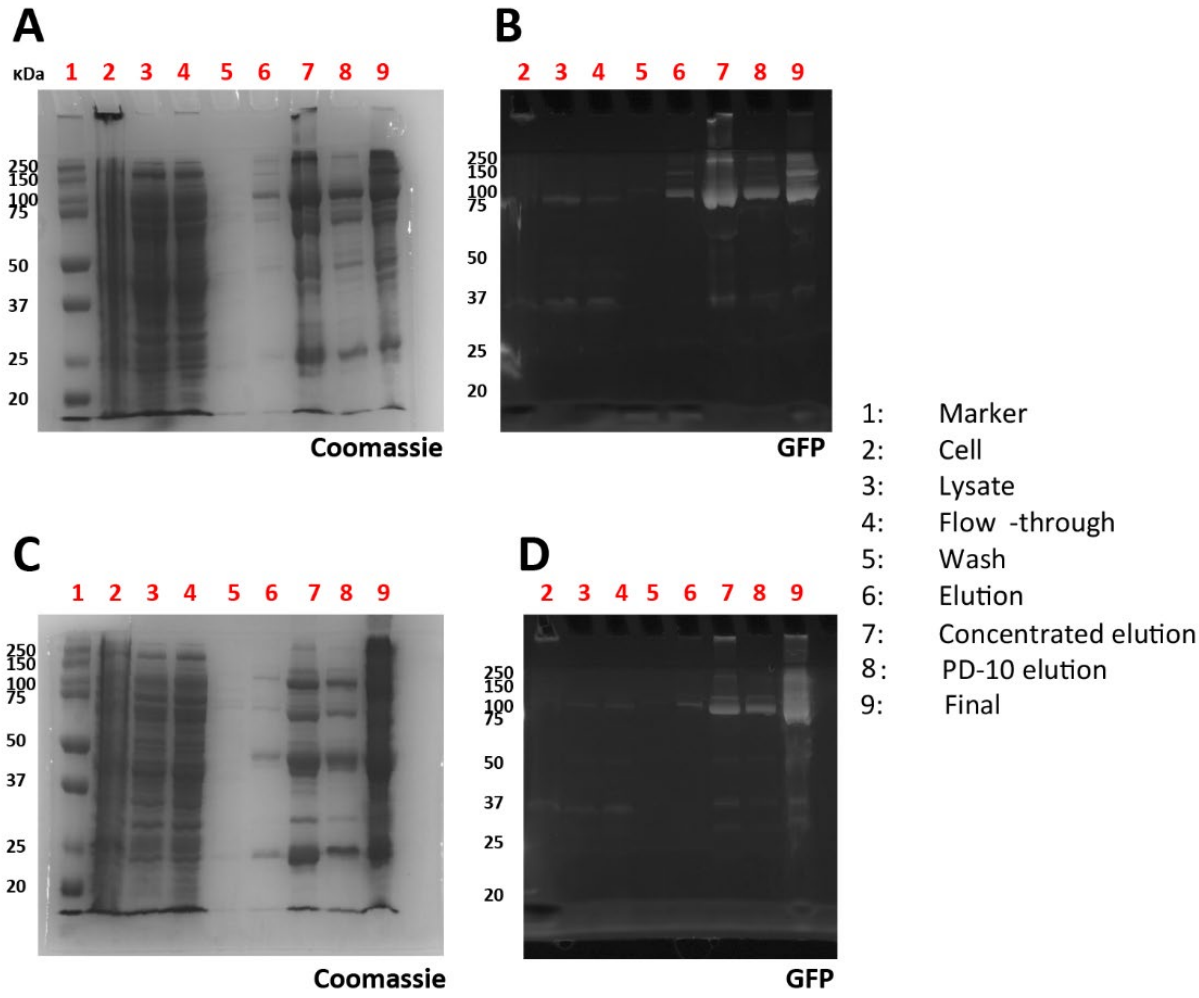

Figure 2.3. SDS-PAGE gels of purification of α_{1A}-AR A4 and α_{1B}-AR #15 fusion proteins. A. 10% SDS-PAGE gel with coomassie blue staining. Samples were denatured in loading buffer, but not heated. B. GFP-fluorescence reading of the same SDS-PAGE gel prior to coomassie blue staining. Lane 1, Marker (Precision Plus Protein™ Dual Color Standards #1610374). Lane 2, DM/CHS/CHAPS solubilised *E. coli* cells. Lane 3, clarified *E. coli* cell lysate prior to incubation with IMAC resin. Lane 4, flow-through of IMAC. Lane 5, wash of IMAC resin using DDM containing buffer. Lane 6, elution from IMAC resin. Lane 7, concentrated elution using 100 kDa cut-off concentrators. Lane 8, elution from PD-10 column (buffer exchange). Lane 9, final concentrated fusion protein mixture.

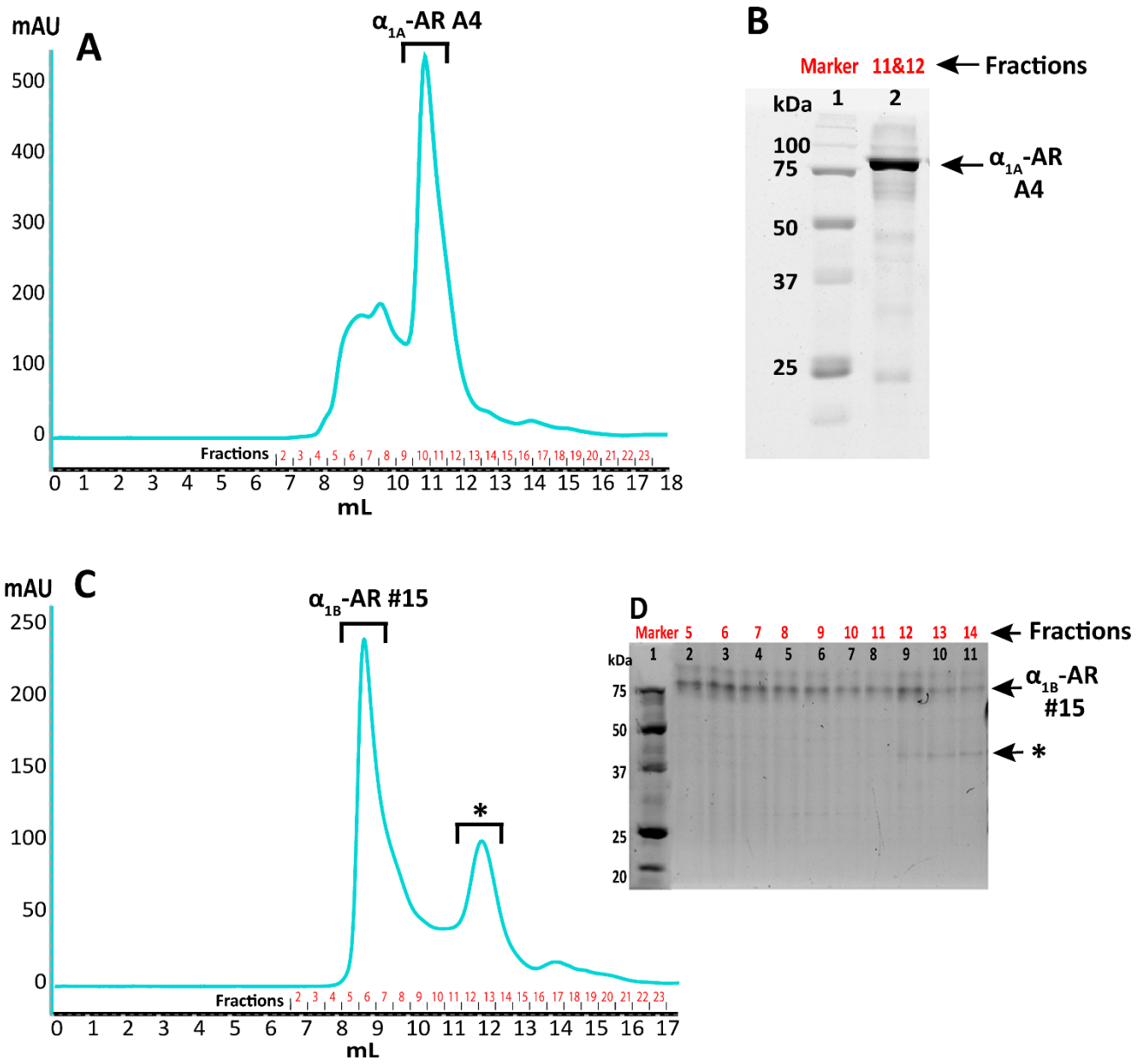

Figure 2.4. Preparative SEC of α_{1A}-AR A4 and α_{1B}-AR #15 fusion proteins. A. SEC of concentrated elution from IMAC (Figure 2.3 A & B, lane 7) for MBP-α_{1A}-AR A4-sfGFP B. SDS-PAGE gel of the collected SEC fractions are shown; Lane 1: Marker (Precision Plus Protein™ Protein Standards #1610373). Lane 2: Purified MBP-α_{1A}-AR A4-sfGFP fusion protein (MW: 116.31 kDa, appears between 75 to 100 kDa[497]) combined SEC fractions from 11.2 – 12.2 mL C. SEC of concentrated elution from IMAC (Figure 2.3 C & D, lane 7) for MBP-α_{1B}-AR #15-sfGFP D. SDS-PAGE gel of SEC fractions 5-14. Lane 1, marker. Lanes 2-4: collected SEC fractions 5-7. Lanes 5-11: SEC fractions 8-14. The SEC signal marked * and the respective band in the SDS-PAGE gel correspond to the cleaved MBP (MW: 39.92 kDa).

2.3.2. Expression and purification of deuterated α_{1A}-AR A4

Expression in deuterated media is an additional metabolic burden on *E. coli* cells to produce recombinant protein incorporated with deuterium in place of the naturally abundant hydrogen atoms. We aimed to maximally deuterate the receptor and hence M1 media made in 100% D_2O was used for protein expression. Using SDS-PAGE gel, when the deuterated and protonated protein expressions were compared, as shown in Figure 2.5A & B, the expression yields were critically low and insufficient receptor was being produced. For these reasons, the M1 media prepared in 75% D_2O was tested with different expression times (Figure 2.5C & D) and again compared with the expression of the protonated receptor. The SDS-PAGE gel analysis indicated that cells could thrive well in the 75% deuterated M1 media with ~5.5 - 6 h optimal for the expression of sufficient deuterated α_{1A}-AR A4.

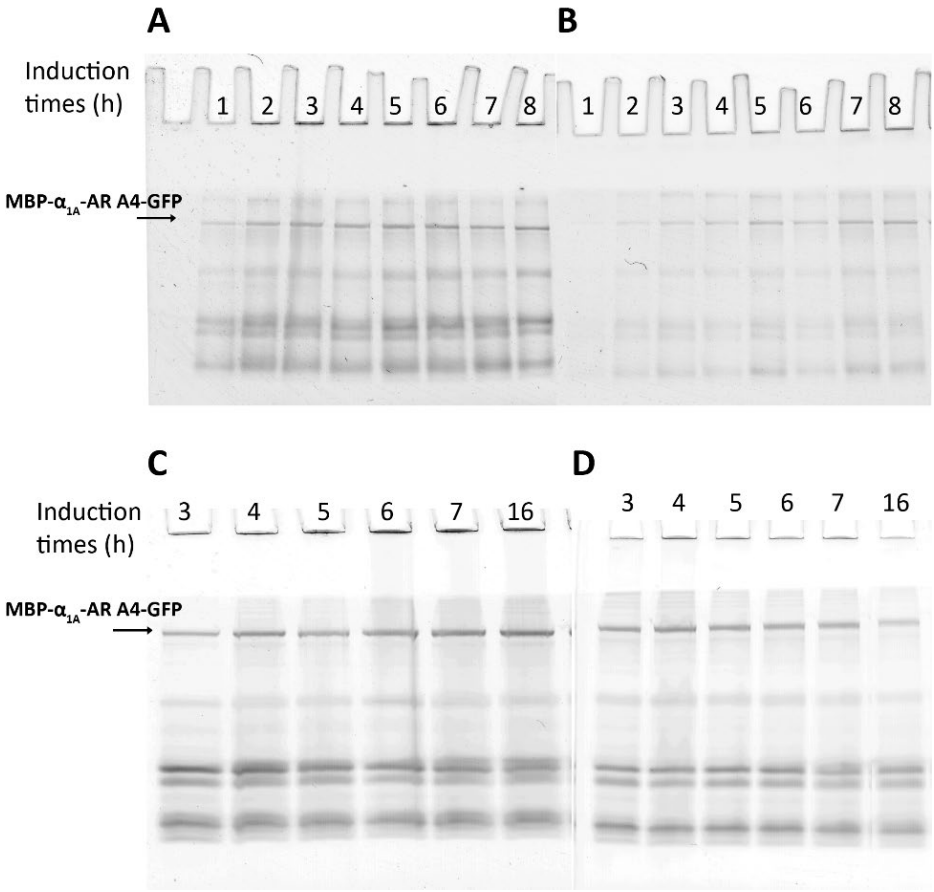

Figure 2.5. SDS-PAGE gels of the recombinant expression of the deuterated α_{1A}-AR A4 fusion protein. GFP-fluorescence reading of the SDS-PAGE gel of the α_{1A}-AR A4 fusion

protein expression in A & B, protonated and 99.9% deuterated M1 media respectively. C & B. protonated and 75% deuterated M1 media respectively, tested at different induction times.

The deuterated α_{1A}-AR A4 fusion protein was purified in the same way as that of the protonated receptor (Figure 2.6). The purification yields for the deuterated α_{1A}-AR A4 was ~0.7 mg/L.

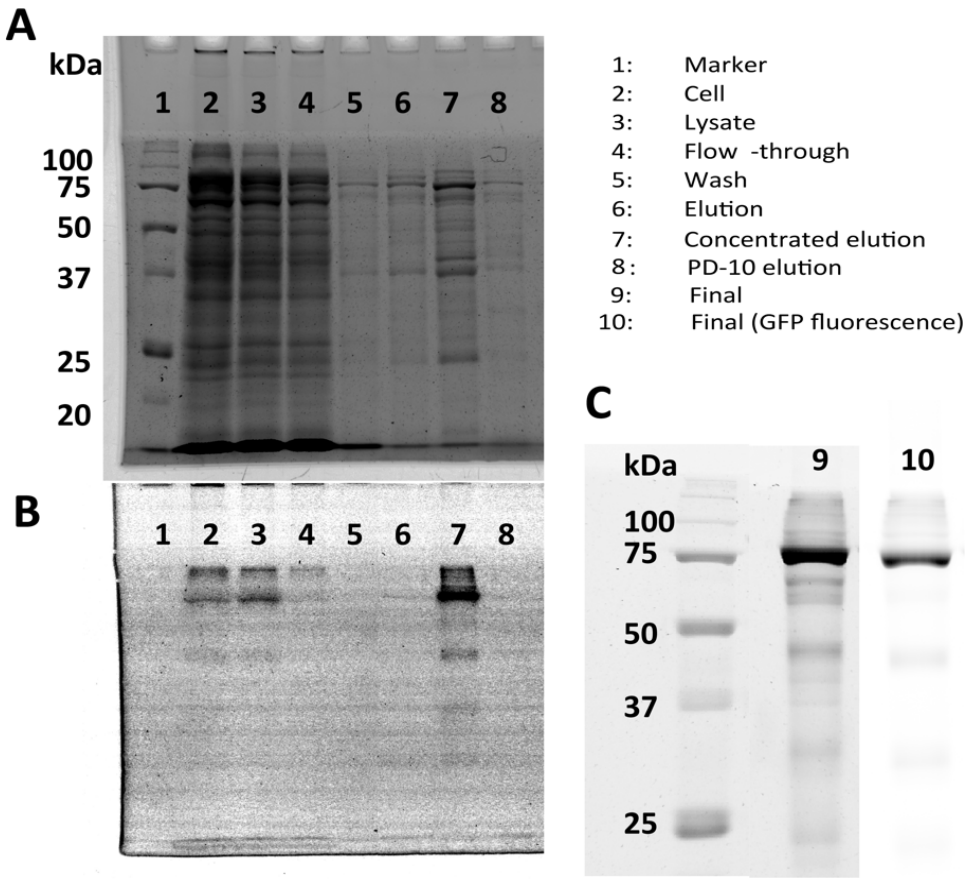

Figure 2.6. SDS-PAGE gels of purification of deuterated α_{1A}-AR A4 fusion proteins. A) 10% SDS-PAGE gel with coomassie blue staining. Samples were denatured in loading buffer, but not heated. B) GFP-fluorescence reading of the same SDS-PAGE gel prior to coomassie blue staining. Lane 1, Marker (Precision Plus Protein™ Protein Standards #1610373). Lane 2, DM/CHS/CHAPS solubilised *E. coli* cells. Lane 3, clarified *E. coli* cell lysate prior to incubation with IMAC resin. Lane 4, flow-through of IMAC. Lane 5, wash of IMAC resin using DDM containing buffer. Lane 6, elution from IMAC resin. Lane 7, concentrated elution using 100 kDa cut-off concentrators. Lane 8, elution from PD-10 column (buffer exchange).

Lane 9, final concentrated protein mixture and Lane 10, GFP fluorescence of the final concentrated protein mixture.

2.3.3. Saturation and competition binding assays using α_{1A}-AR A4 and α_{1B}-AR #15

Saturation binding assays against QAPB were performed to assess the purity and binding competency of the purified thermostabilised receptors. The streptavidin coated beads were used to capture and retain the purified Avi-tagged receptors during the QAPB binding and subsequent wash steps. QAPB is a fluorescent ligand which binds specifically to α_1ARs with nM affinity. Two parameters are reported: the K_D which is the radioligand concentration needed to achieve a half-maximum binding at equilibrium and a measure of receptor affinity; and B_{max}, the maximum specific binding, an indication of the binding competent population of the receptor. Saturation binding assays (Figure 2.7) revealed that the QAPB bound to the solubilised thermostabilised receptors with slightly weaker affinities (~5 nM) than the reported K_D of around 2 nM for this ligand on WT α_{1A}-AR and α_{1B}-AR expressing mammalian cells[498].

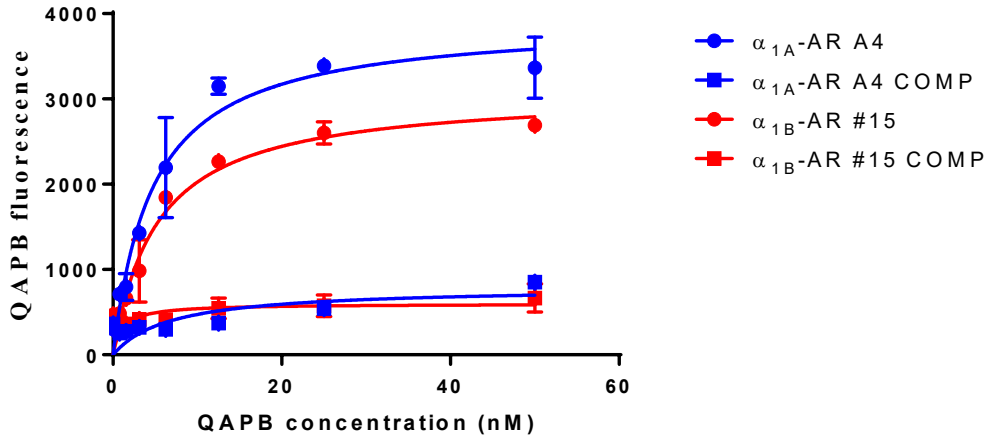

Figure 2.7. Saturation binding experiments. Saturation binding of QAPB to purified α_{1A}-AR A4 (blue circles) and α_{1B}-AR #15 (red circles) fusion proteins. Non-linear regression of specific QAPB binding revealed a single population of binding sites with the equilibrium dissociation constant (K_D) 4.7 ± 0.9 nM for α_{1A}-AR A4 and K_D = 5.2 ± 1.1 nM for α_{1B}-AR #15. Comparison of maximal binding capacity (B_{max}) upon competition (COMP) with 10 µM prazosin (blue squares for α_{1A}-AR A4 and red squares for α_{1B}-AR #15) revealed that in both cases around ~80% of the receptor was binding competent.

In the next step, competition binding studies were performed using α_1-AR agonists adrenaline, noradrenaline, A-61603 and antagonist prazosin as displacers of specific QAPB binding. As shown in Figure 2.8, all ligands were able to displace the bound QAPB in a concentration-dependent manner. The displacement curves were monophasic and were best evaluated using a one-site competition curve fit. Competition binding determined that the endogenous α_1-AR agonists adrenaline and noradrenaline, as well as the α_{1A}-AR-selective agonist A-61603 (reported to have a 2-fold higher affinity for WT α_{1A}-AR than WT α_{1B}-AR[228]) could all bind both stabilised detergent solubilised receptors α_{1A}-AR and α_{1B}-AR. Although, the binding affinities were around two-orders of magnitude weaker compared with the reported affinities on the respective WT receptors.[228] However, the subtype selectivity for A-61603 was retained, evident by the higher p*Ki* values of A-61603 on α_{1A}-AR A4 than α_{1B}-AR #15.

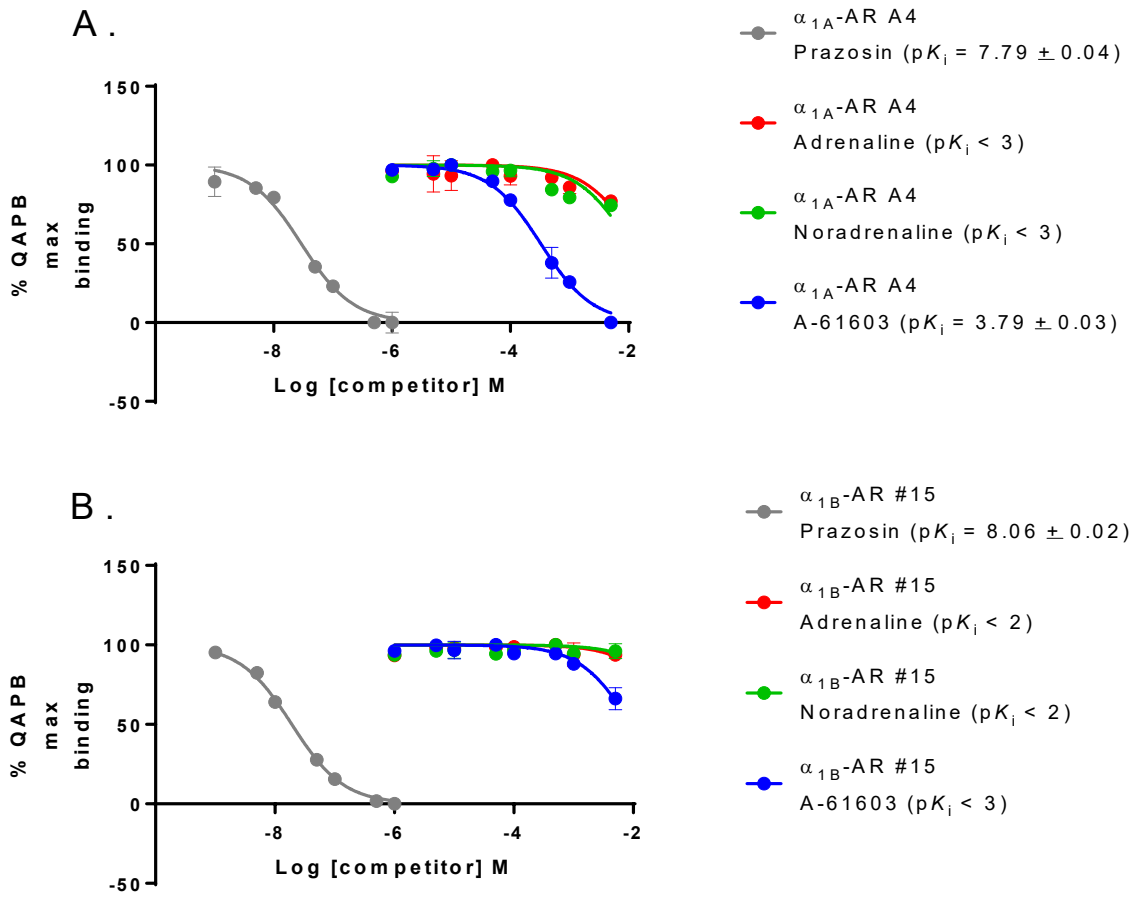

Figure 2.8. QAPB competition binding experiments. QAPB competition binding against purified (A). α_{1A}-AR A4 and (B). α_{1B}-AR #15 fusion proteins. Grey, red, green and blue lines/symbols indicate competition with prazosin, adrenaline, noradrenaline and A-61603 respectively.

As discussed in subsequent chapters, we aim to use ligand-based NMR methods to characterise ligand binding to the stabilised α_{1A}-AR A4 and α_{1B}-AR #15. These methods are NOE based methods that work through magnetisation transfer through space. These experiments rely on fast dissociation of bound ligands which carry into their free state, magnetisation originating from its receptor bound conformation, and so typically works best for weak binding systems, such as those with dissociation constants in the high μM to mM region. The inhibition constant (K_i) values we are observing on α_{1A}-AR A4 and α_{1B}-AR #15 with adrenaline, noradrenaline and A-61603 seems to be ideal for application of such ligand-based NMR methods.

CHAPTER 3 : PROBING BENZODIAZEPINE BINDING TO STABILISED α_{1A}-AR USING LIGAND-BASED NMR METHODS

In the following chapter, the contribution the author made to the following paper has been explained in detail:
Lisa M. Williams, Xiaoji He, **Tasneem M. Vaid**, *et al.* "Diazepam Is Not a Direct Allosteric Modulator of A1-adrenoceptors, but Modulates Receptor Signaling by Inhibiting Phosphodiesterase-4." Pharmacology Research & Perspectives 7 (1) (2019).

3.1. Introduction

3.1.1. Benzodiazepines and its therapeutic uses

Benzodiazepines are one of the most widely used drugs known for their tranquilising, antianxiety and muscle relaxant activities. In addition to their well-known anxiolytic actions, benzodiazepines also show activities as antiarrhythmic agents[499–503]; antagonists of α_2-adrenoceptor[504] and cholecystokinin[505–508]; non-nucleoside inhibitors of HIV-1 reverse transcriptase[509–512]; compounds that affect the hunger centre[513,514]; compounds with muscarinic[515] and κ-opioid[516–519] receptors activity; inhibitors of cholesterol absorption[520]; act as antibacterial[521], antifungal[521], antimalarial[522], anticancer[523,524] and anti-inflammatory agents[524]. Finally, benzodiazepines have been reported to act as a partial agonist of α_1-adrenergic receptors[209] and therefore, the purpose of this chapter was to investigate their selectivity.

The basic activity of benzodiazepines is associated with a CNS, and their key molecular target is the γ-aminobutyric acid receptor type A ($GABA_AR$), an ionotropic pentameric transmembrane receptor, and ligand-gated ion channel. GABA, the major inhibitory neurotransmitter in the CNS is the endogenous ligand of this receptor. $GABA_AR$ activation causes a chloride ion influx resulting in hyperpolarisation of the cell and thereby facilitating the sedative or inhibitory actions of benzodiazepines in the central nervous system. Benzodiazepines, as such, do not activate the $GABA_AR$, but instead act as PAMs increasing the affinity and efficacy of the endogenous ligand, GABA, to bind and activate the receptor[525].

Positive allosteric modulation of the $GABA_AR$ is the mechanism whereby diverse chemical classes of therapeutic agents such as pyrazoloquinolinones[526], barbiturates[526,527] and benzodiazepines[526] act to reduce seizures, induce conscious sedation, reduce anxiety, induce and maintain sleep[526].

The benzodiazepines; diazepam and lorazepam, have been shown to attenuate intracellular calcium oscillations in pulmonary artery smooth muscle cells, suggested to be due to off-target interactions with adrenergic receptors.[4] As mentioned before, it has been postulated[209] that benzodiazepines directly bind to COS-1 cells expressing $\alpha_{1A/B/D}$-AR. Diazepam, lorazepam, and midazolam have been shown to compete with the radioligand α_1-AR antagonist [^{125}I]HEAT (2-[β-(4-hydroxyl-3-[^{125}I]iodophenyl)ethylamineomethyl]tetralone) on these cells and functional inositol-triphosphate (IP_3) assays also showed potentiation of agonist responses by these benzodiazepines at $\alpha_{1A/B/D}$-AR expressing cells[209], suggestive of allosteric interaction. However, no further studies have been reported supporting direct binding of these benzodiazepines to the α_1-ARs.

In this work, we sought to use the purified thermostabilised mutant of α_{1A}-AR to determine the binding epitope of selected benzodiazepines using a similar NMR approach as we used to study binding epitope of orthosteric ligands on these receptors[292]. Our aim was to understand how benzodiazepines bind to α_1-ARs and eventually to apply this information for the development of more selective modulators targeting the speculated allosteric site.

3.1.2. A panel of clinically-used benzodiazepines under study

The action of benzodiazepines on $GABA_ARs$ has been widely studied. Most of the benzodiazepines are 1,4-benzodiazepine derivatives (Figure 3.1).

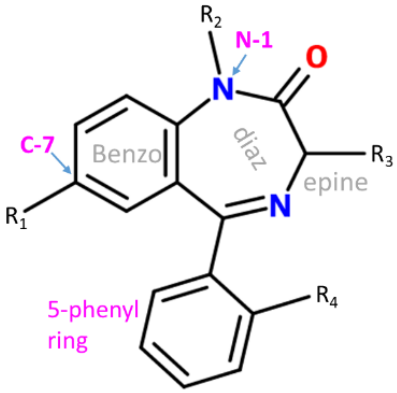

Figure 3.1. The core structure of benzodiazepine. "R" labels denote common locations of side chains, which give different benzodiazepines their unique properties. Key positions in the structure (C-7, N-1 and 5-phenyl ring), substitutions at which have been shown to be important for the sedative and tranquilising activities, are marked.

The core chemical structure of benzodiazepines is the fusion

of a diazepine ring and a benzene ring (Figure 3.1). It has been reported that the substituent on C-7 is of paramount importance; electron-withdrawing functional groups on C-7 generally impart high sedative and tranquilising activities, whereas electron-donating groups have the opposite effect[528]. Also, substitution on N-1 and in the 5-phenyl ring affected the activity decisively, as evident by the significant changes in sedative and tranquilising properties[528]. A halogen in the *o*-position of the phenyl ring and a methyl group on N-1 potentiated the activity; while a substituent in the *p*-position of the phenyl ring decreased the activity dramatically[528]. Since we ultimately aim to selectively modulate α_1-ARs, it is desirable to reduce the effect of benzodiazepines on $GABA_AR$. Keeping the above information in mind, we assembled a panel of benzodiazepines with structural relationships to diazepam, lorazepam and midazolam to explore structure-activity relationships at α_1-adrenergic receptor[292].

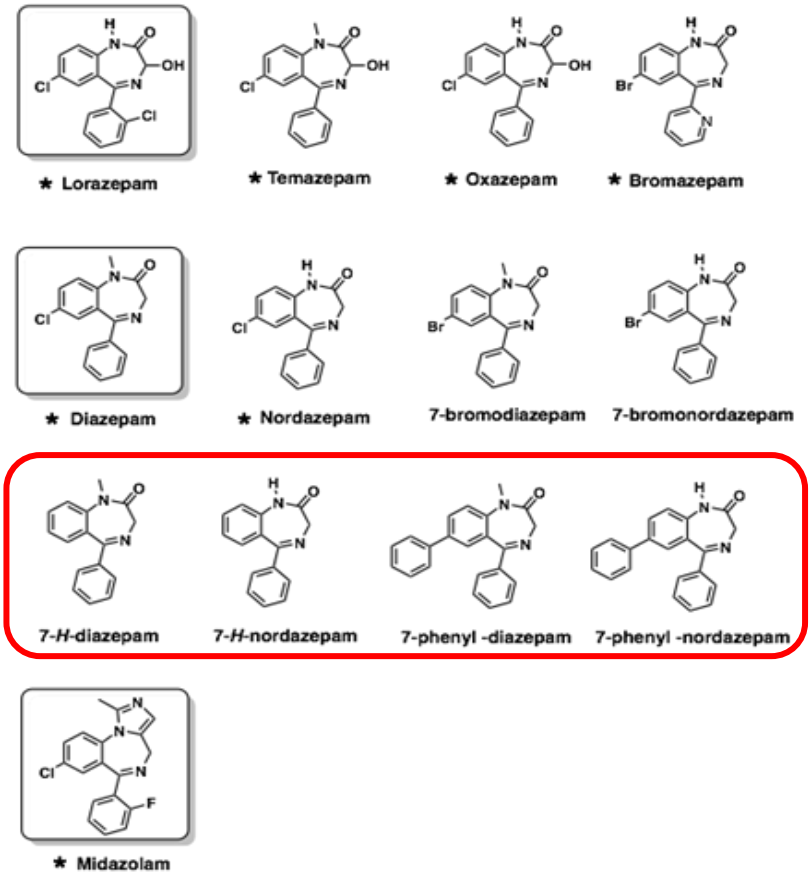

Figure 3.2. Structures of 1-4 benzodiazepines derivatives. Clinically-used compounds are starred. Compounds highlighted in black boxes have been reported to modulate $\alpha_{1A/B/D}$-AR activity. Compounds in the red box, are also based on the known SAR of benzodiazepines, but are expected to show reduced/no $GABA_AR$ activity.

Structures of 1-4 benzodiazepine derivatives which have been assembled by Xiaoji He (Prof. Spencer Williams's lab) are listed in Figure 3.2. To start with, we selected the first five compounds, i.e. lorazepam, temazepam, oxazepam, bromazepam and diazepam, to investigate receptor binding using NMR. Primarily, we wanted to confirm whether these compounds are showing binding to the thermostabilised purified receptors and if so, how specific the binding is. And eventually, we wanted to study those compounds showing reduced/no $GABA_AR$ activity. As mentioned earlier, electron-withdrawing groups on C-7 generally impart high $GABA_AR$ activity[528], whereas electron donors have the reversed effect, and hence the compounds in the third row (highlighted in a red box in Figure 3.2) are expected to show reduced or no $GABA_AR$ activity.

3.2. Material and methods

3.2.1. Materials

n-Dodecyl-β-D-maltopyranoside (DDM) was purchased from Anatrace. *(R)*-adrenaline, prazosin hydrochloride, 9AA, spiperone, tacrine hydrochloride and DSS (2,2-Dimethyl-2-silapentane-5-sulfonate) were purchased from Sigma Aldrich. All benzodiazepines were prepared by Xiaoji He from Spencer Williams lab. Stock solutions of 50 mM adrenaline was prepared in 0.1 M HCl, 5 mM prazosin was prepared in deuterated methanol, 100 mM benzodiazepines (diazepam, lorazepam, oxazepam, temazepam and bromazepam), 100 mM 9AA, and 10 mM spiperone were prepared in d_6-DMSO while 100 mM tacrine and 25 mM DSS were prepared in MilliQ water.

3.2.2. Protein expression and purification

The α_{1A}-AR was evolved for high stability in detergents using cellular high-throughput encapsulation, solubilization and screening (CHESS) as described elsewhere[292]. The resultant stabilised α_{1A}-AR variant, α_{1A}-AR A4, contains 15 amino acid substitutions over the wild-type human α_{1A}-AR (as shown in Figure 2.1). Unlabelled MBP-sfGFP fusion receptor was transformed into *Escherichia coli* C43 (DE3) and expressed using protocols of Marley et al[495]. and was purified in DDM using Immobilised Metal Affinity Chromatography as described elsewhere[292]. For purification of the cleaved α_{1A}-AR A4, proteolytic cleavage was carried out by adding 100 mM of Na_2SO_4, 50 mM of NaCl, 1 mM TCEP and 100 mM of HRV 3C protease to the PD-10 eluate and leaving the mixture gently rocking for 16 h at 4°C. The cleavage mixture was then topped-up with 10 mM imidazole, then transferred to a gravity flow column

and incubated gently rocking for 1.5 h at 4°C with 1.5 mL of Talon resin equilibrated with 5 CV of equilibration buffer. The flow through containing cleaved receptors was collected and concentrated to approx. 450 µL using an Amicon Ultra 15 concentrator with 30 kDa cutoff (Millipore). The concentrate was then loaded onto a Superdex 200 10/300 Increase column (GE Healthcare) equilibrated with SEC buffer (50 mM potassium phosphate, 0.05% DDM, 100 mM NaCl, pH 7.4). The cleaved α_{1A}-AR A4, used for the Water-LOGSY experiments, was a kind gift from the lab of Prof. Andreas Plückthun, University of Zurich. It was purified by Mattia Deluigi.

3.2.3. NMR spectroscopy and data processing

Unless mentioned otherwise, all NMR samples were made up in 500 µL of DDM buffer (50 mM potassium phosphate, 100 mM NaCl, 0.05% DDM, 10% ^2H_2O, pH 7.4) in 5-mm standard NMR tubes. For Water-LOGSY experiments, 100 µL DSS was added to the samples as an internal standard. All NMR experiments were performed on a 700 MHz Bruker Avance III HD spectrometer using a cryogenically cooled triple resonance probe and the resultant spectra were analysed using Topspin (version 3.5pI7).

STD-NMR data were acquired with saturation time of 3 s, using a train of 50 ms Gaussian pulses with a B1 field of about 130 Hz, separated by 4 µs delays[529]. The on- and off-resonance frequencies were −1 and 71.4 ppm, respectively. To suppress residual protein and water signals, a spin-lock pulse of 40 ms and excitation sculpting[530] with gradients were employed, respectively. The relaxation delay between transients was set to 3.5 s. A total of 512 transients were averaged over 32 K data points and a spectral width of 16 ppm. Prior to Fourier transformation, data were multiplied by an exponential function with 2 Hz line-broadening and zero-filled once. 2D transferred-NOESY (Tr-NOESY) experiments were acquired using standard pulse sequences with water suppression using excitation sculpting with gradients[530], 56 scans as 2048 (t2) × 400 (t1) data points at mixing time of 150 ms and relaxation delay (D1) of 1.2 s. Prior to Fourier transformation, the data were zero-filled to 4096 × 4096 points and apodised with a cosine-squared function in both dimensions. For the Water-LOGSY experiment[276,531], a total of 152 transients were averaged over 32 K data points and a spectral width of 16 ppm. The relaxation delay and mixing times were set to 2.0 s. To suppress residual protein and water signals, a spin-lock pulse of 30 ms and excitation sculpting[530] with gradients

were employed, respectively. Prior to Fourier transformation, data were multiplied by an exponential function with 2 Hz line-broadening and zero-filled once.

3.3. Results

3.3.1. STD-NMR experiments in the presence of α_{1A}-AR A4

STD-NMR experiments were done to characterise the binding of five benzodiazepines, namely lorazepam, oxazepam, temazepam, bromazepam and diazepam to the thermostabilised, purified α_{1A}-AR A4. As shown in Figure 3.3 A-E, for all the compounds, STD signals can be observed. Also shown, are the signals of adrenaline (Figure 3.3 F), an α_{1A}-AR endogenous ligand, the binding of which is well characterised using STD-NMR on the CHESS stabilised α_{1A}-AR A4[292].

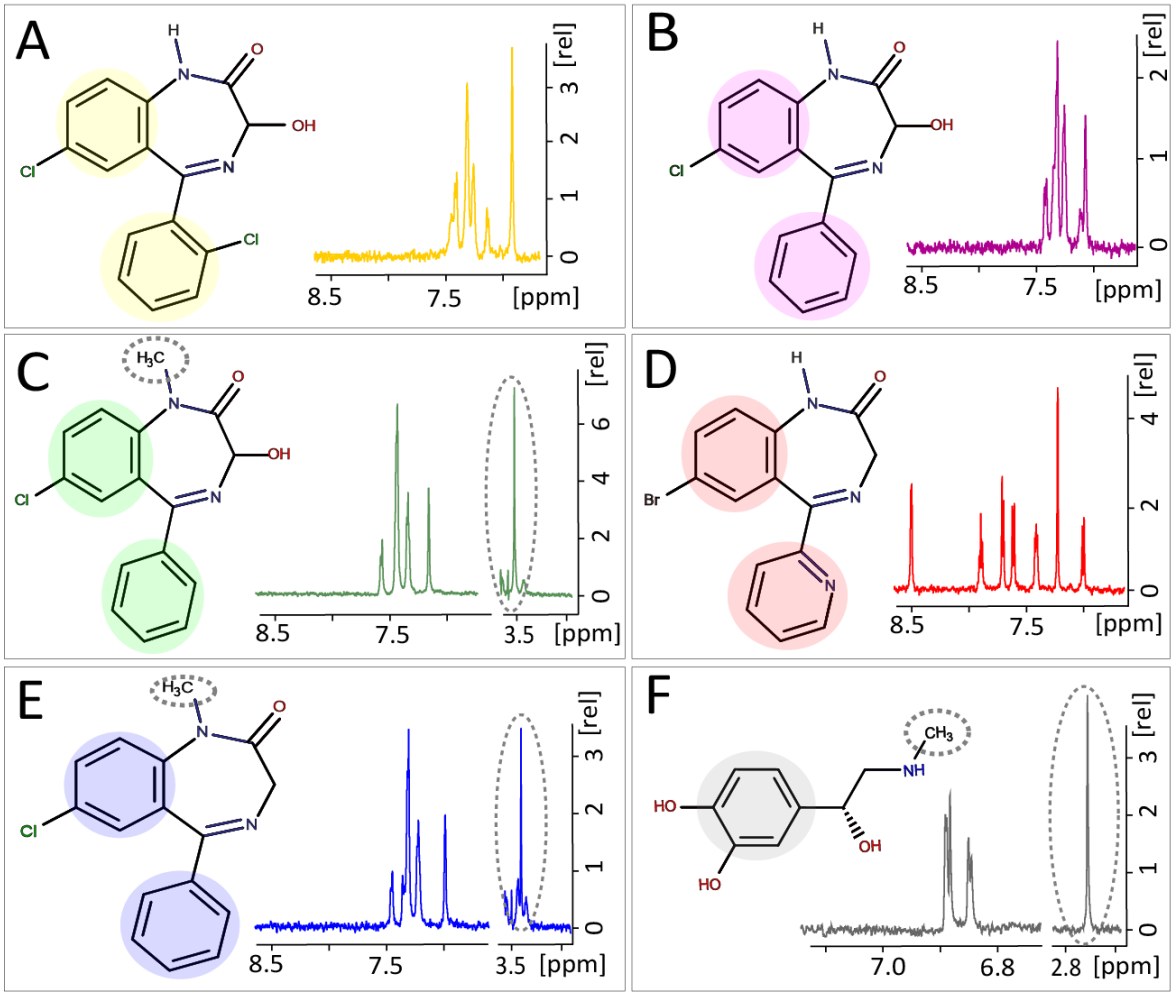

Figure 3.3. STD-NMR spectra of benzodiazepines in the presence of α_{1A} AR A4. Starting from the top, A. Lorazepam, B. Oxazepam, C. Temazepam, D. Bromazepam, E. Diazepam and

F. Adrenaline. The concentration used: 5µM α_{1A} AR A4 and 500 µM compound. STD signals correspond to compounds' phenyl protons (the region highlighted in the same coloured circles onto the structures as the corresponding STD peaks) are shown. Methyl protons in the structures and corresponding peaks in the spectrum are highlighted using a dashed circle.

The appearance of STD signals suggested the transfer of saturation to the bound ligands. Apart from the specific binding of these compounds to the receptor, this transfer can also result from the non-specific binding of the compound mostly via hydrophobic interactions to the receptor or to the detergent micelles in which receptors are embedded. Aggregation of compounds too can give rise to the STD signals.

3.3.2. Water-LOGSY experiments in the presence of α_{1A}-AR A4

Next, Water-LOGSY was performed as an alternative method to characterise the binding of benzodiazepines to α_{1A}-AR A4. The method is based on the selective saturation of the bulk water signal, magnetisation is then transferred to the bound ligand via different pathways[261,276]. (section 1.6.2.3).

In the Water-LOGSY experiment, as shown in Figure 3.4, compounds that bind to the target protein give positive resonances (i.e. have the same sign as protein resonances), and compounds that do not interact with the protein give negative resonances.[276]. Figure 3.4 shows Water-LOGSY spectra of three benzodiazepines; Oxazepam, Temazepam and Diazepam, and adrenaline in the presence of the receptor. Protons from all three compounds exhibiting positive phase indicate the transfer of magnetisation to the ligands via saturated water molecules, which in turn suggest interaction of these molecules to the receptor embedded in a detergent micelle. But again, these signals can also occur in case of compound aggregation where water molecules get trapped and receive the selective inversion.

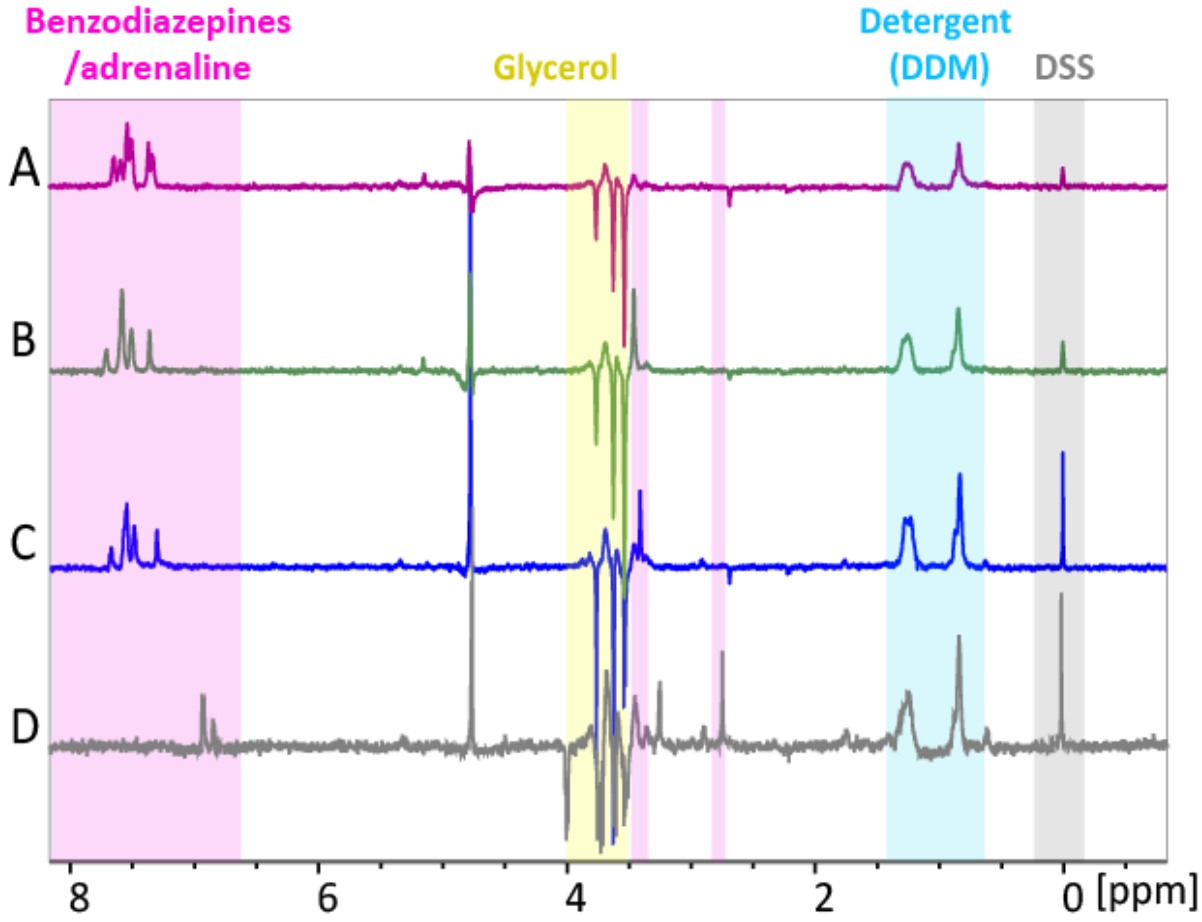

Figure 3.4. One-Dimensional Water-LOGSY spectra for ligands A. Oxazepam, B. Temazepam, C. Diazepam and D. Adrenaline (all 250 µM) in the presence of 5 µM α_{1A}-AR A4. Positive and negative signals identify receptor interacting and non-interacting molecules, respectively. The signals between 3.5-4 ppm (highlighted in yellow) belong to glycerol, which was used as a cryoprotectant and was present at mM concentration. Glycerol is not expected to interact with the receptor and hence its phase acts a reference signal. Signals from DDM, benzodiazepines/adrenaline and DSS are highlighted in cyan, pink and grey bands respectively. All spectra were calibrated against the DSS signal at 0 ppm.

3.3.3. Control Experiments

With all benzodiazepines giving STDs and positive Water-LOGSYs, we had a suspicion that we might be observing non-specific interactions with these highly hydrophobic molecules. Various control experiments were performed to confirm whether the STD-NMR and Water-LOGSY observed ligand interactions are indeed with the receptor. In the following sections, experiments were performed with the empty detergent micelles to check if the

compounds interact with the detergent molecules; with another CHESS stabilised receptor, to see how specific these interactions are for the α_{1A}-ARs; in the presence of reported antagonists and allosteric ligands to see if we get any competition which would implicate specificity of ligand binding and finally the ligand binding was tested in the presence of the thermally denatured receptor. A non-promiscuous ligand will only bind to the intact ligand binding pocket on the receptor, the disruption of which should inhibit the binding of the ligand. As an alternative method to test the binding of benzodiazepines to α_{1A}-AR A4, Tr-NOESY experiments were also performed.

3.3.3.1 Control 1: STD-NMR in the presence of a detergent

For all the five selected benzodiazepines, STD-NMR spectra were recorded with the samples containing the same detergent buffer, but no receptor protein to test whether the STD signals we are observing in the presence of the receptor is a result of the specific binding to the receptor or is it just the interaction of these compounds with the detergent micelle. As shown in Figure 3.5 A-E, for all the compounds except for bromazepam, we could see weak STD signals, indicating interactions with the empty detergent micelles. Also, as a control, a similar experiment was performed with adrenaline (Figure 3.5 F), with which, as expected, we did not see any STD signals.

When these spectra (Figure 3.5) were compared with the spectra in the presence of the receptor (Figure 3.3), we can clearly see that the STD signals are present in the presence of the detergent, implying detergent-ligand interactions. Now, this could be accounted for by subtracting these STD intensities from those in the presence of a receptor. But that might not be the best approach because the size and density of the micelle, when protein is embedded in it, might be higher than that of the empty micelle. As a result, these detergents, when forming a micelle around the receptor, might show more interactions with the ligands. All benzodiazepines gave STD signals in the presence of the detergent except for bromazepam. But again, one can argue that the interaction of bromazepam with the detergent might accentuate or become more evident when it is present with the detergents forming a bigger micellar complex in the presence of the receptor. Hence, more control experiments are needed to find out if bromazepam is indeed the odd one out.

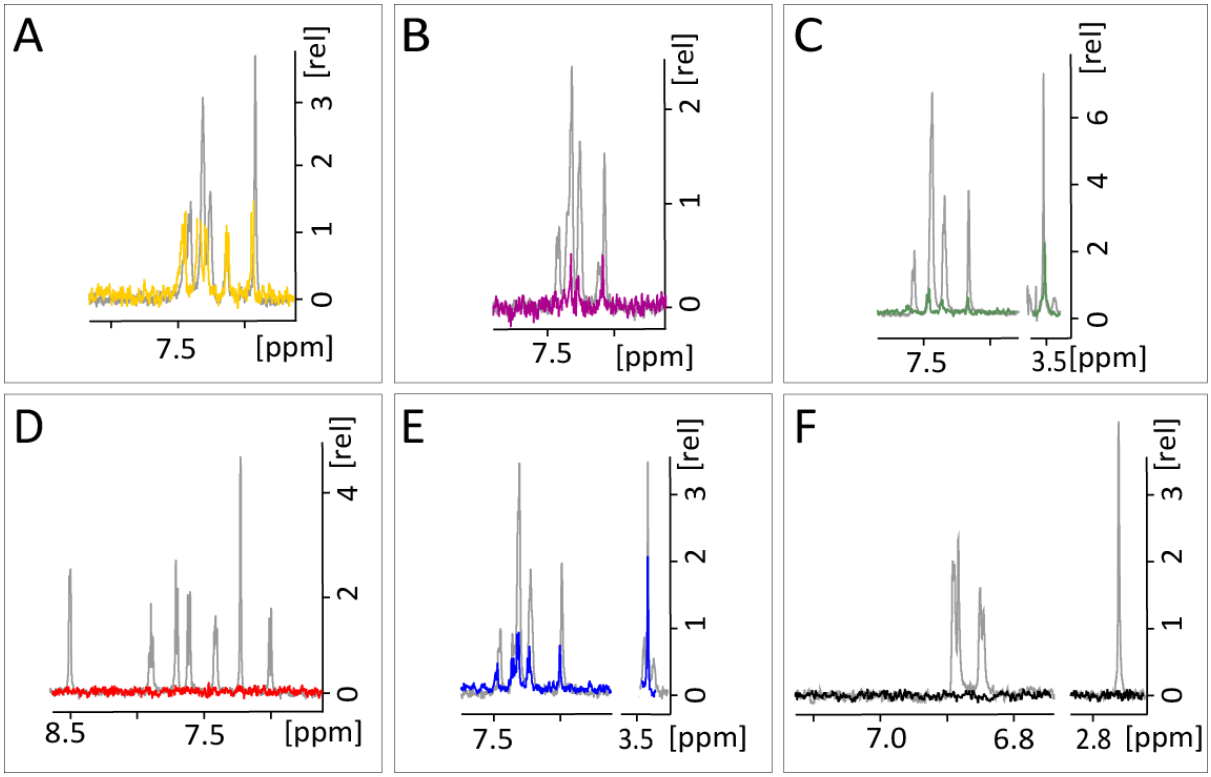

Figure 3.5. STD-NMR spectra of benzodiazepines in the absence of α_{1A} AR A4 and in the presence of DDM. Starting from the top, A. Lorazepam, B. Oxazepam, C. Temazepam, D. Bromazepam, E. Diazepam and F. Adrenaline. The concentration used: 5µM α_{1A}-AR A4, 500 µM benzodiazepines/adrenaline and 1 mM DDM. All signals correspond to the phenyl region and methyl groups of ligands (as shown in Figure 3.3). The spectra in grey represent the STD signals in the presence of the receptor (as shown in Figure 3.3).

3.3.3.2 Control 2: Water-LOGSY experiment in the absence and presence of a detergent.

Again, to assess the binding we observed in the presence of a receptor (Figure 3.3 & 3.4), few control Water-LOGSY experiments were performed in the absence and presence of detergent molecules, to confirm if the detergent interactions we observed with STD-NMR experiments (i.e. control # 1) are consistent with the Water-LOGSY experiments too. Also, as a control similar experiments were performed with adrenaline, an α_{1A}-AR endogenous ligand, the binding of which is well characterised using STD-NMR on the CHESS stabilised α_{1A}-AR A4[292].

As shown in Figure 3.6, all ligands show a negative phase i.e. free molecule condition in the absence of the detergent molecules (spectra in magenta, green, blue and grey), but when there is a detergent present in the buffer, all benzodiazepines show positive phase, most probably resulting from the interaction of these compounds with the empty detergent micelles. While our control experiment with adrenaline (Figure 3.6 D) shows the negative phase or unbound small molecule condition even in the presence of the detergent molecules. These experiments further confirm the non-specific interactions of benzodiazepines with the empty detergent micelles.

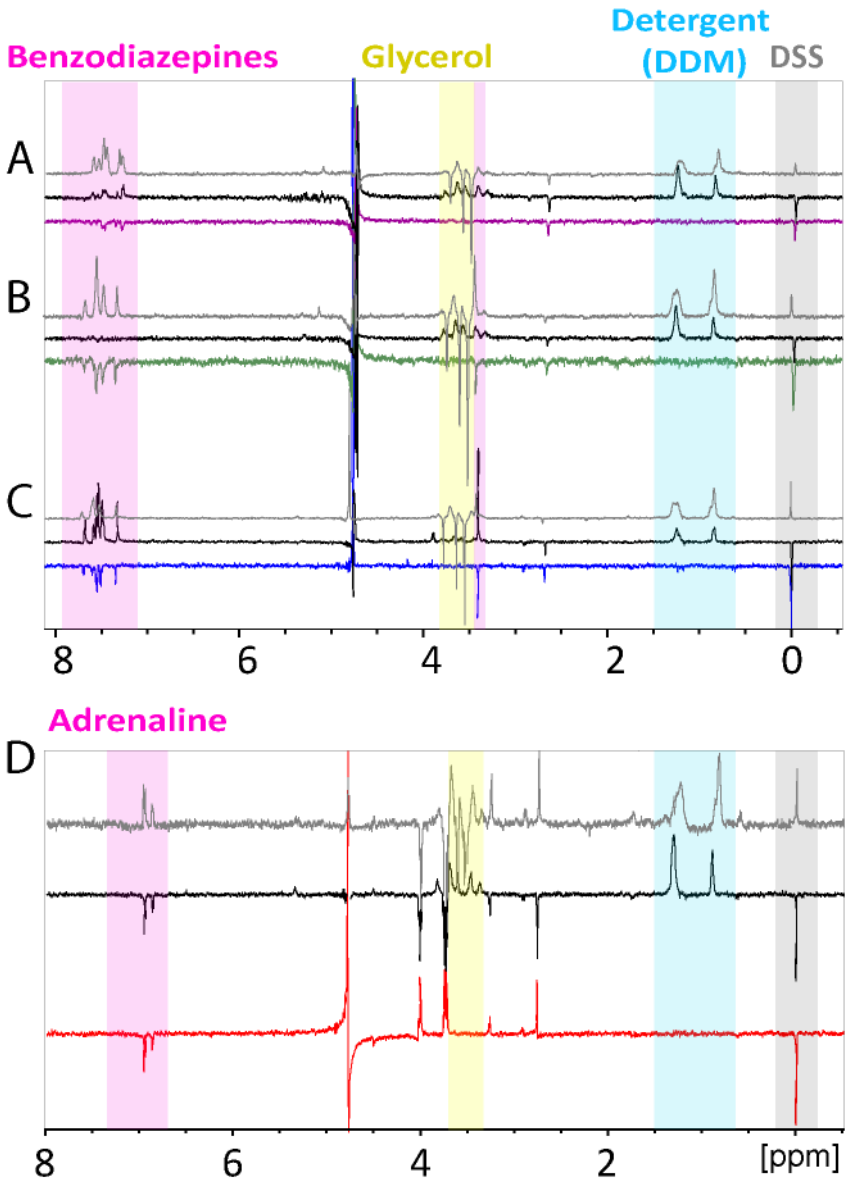

Figure 3.6. Water-LOGSY spectra in the absence and presence of a detergent. Spectra were recorded in the absence (magenta, green, blue and red) and the presence (in black) of a

detergent. A. Oxazepam, B. Temazepam, C. Diazepam and D. Adrenaline. Ligand and DDM concentrations were 250 µM and 1 mM respectively. Signals from DDM, benzodiazepines/adrenaline and DSS are highlighted in cyan, pink and grey bands respectively. All spectra were calibrated against the DSS signal at 0 ppm. All spectra in grey represent the Water-LOGSY signals in the presence of the receptor (as shown in Figure 3.4).

3.3.3.3 Control 3: STD-NMR in the presence of thermostabilised neurotensin receptor (enNTS$_1$).

The STD-NMR experiments of benzodiazepines were recorded in the presence of another CHESS stabilised GPCR (Figure 3.7 A-E), i.e. neurotensin receptor variant (enNTS$_1$)[532]. For all five benzodiazepines, STD signals can be observed in the presence of enNTS$_1$. As a control again we used adrenaline (Figure 3.7 F), to see whether we observe any STD signals with this well characterised orthosteric ligand of the adrenergic receptors too.

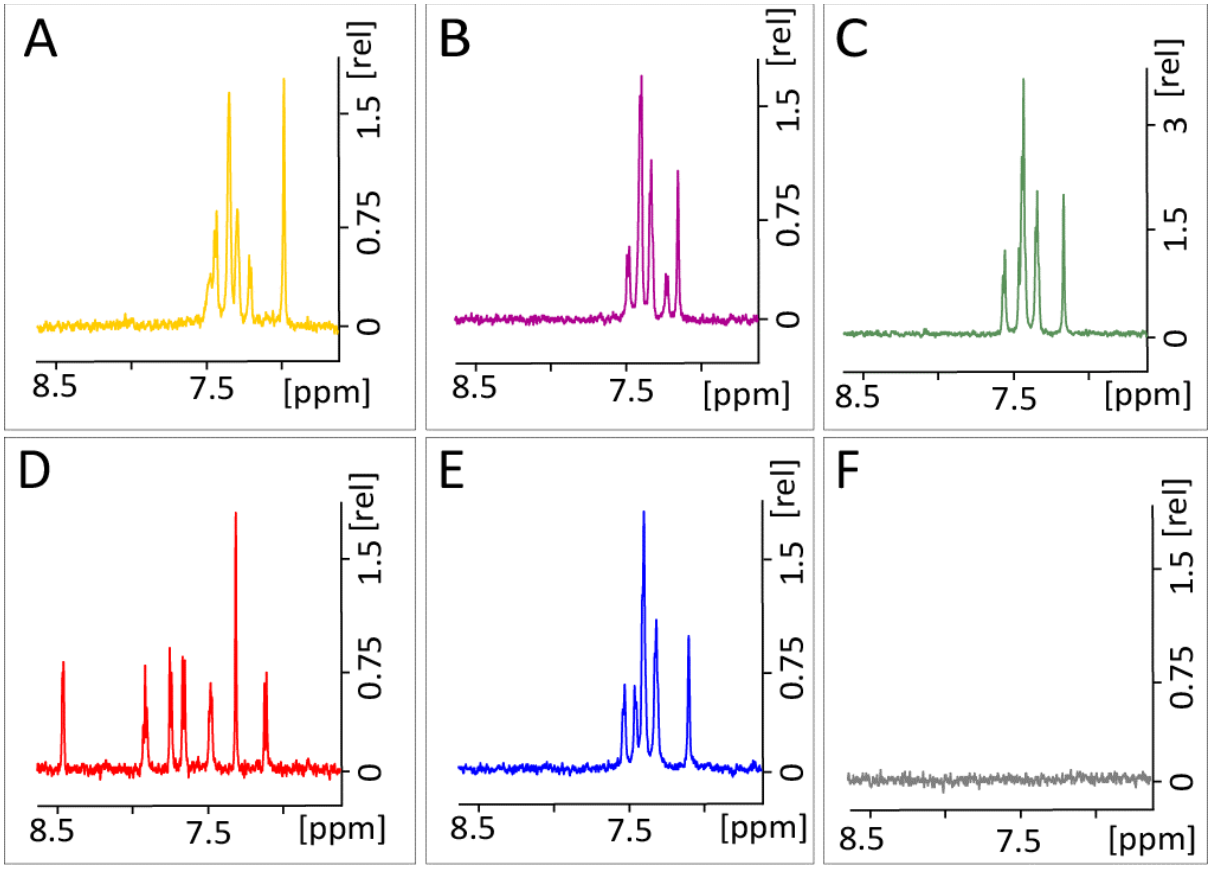

Figure 3.7. STD-NMR spectra in the presence of enNTS$_1$. A. Lorazepam, B. Oxazepam, C. Temazepam, D. Bromazepam, E. Diazepam and F. Adrenaline. Receptor and ligand

concentrations were 5 μM and 500 μM respectively. All signals correspond to the phenyl region of the compounds (as shown in Figure 3.3).

As shown in Figure 3.7, in the presence of the enNTS$_1$ receptor, we observed STD signals for all five benzodiazepines (including bromazepam) and no STD signal for adrenaline. The interactions of benzodiazepines or related compounds with neurotensin receptors have never been reported in the literature before, and hence we now strongly believe that these STDs are resulting from the interaction of benzodiazepines to the bigger and more denser detergent micelle incorporating the receptor.

3.3.3.4 Control 4: STD-NMR competition experiments in the presence of prazosin, 9AA, spiperone and tacrine.

Prazosin is a high affinity (nM) specific α_1-adrenergic receptor antagonist[222,533] (α_1 blocker) used to treat anxiety, high blood pressure and posttraumatic stress disorder (PTSD). 9AA is a member of aminoacridines and has a variety of roles including anti-infective agent, an antiseptic drug, a fluorescent dye, a MALDI matrix material, an acid-base indicator and a mutagen[239]. 9AA and its derivative tacrine have been reported to be allosteric modulators of adrenergic receptors[238]. Tacrine (9-amino-1,2,3,4-tetrahydroacridine) was the first FDA approved cholinesterase inhibitor for the treatment of Alzheimer's disease. It has been reported to act as a PAM at the muscarinic receptors[11] and NAM at the α_{1A}-AR[238]. Spiperone, a spiro butyrophenone analogue has been reported to be an α-adrenergic antagonist as well as dopaminergic antagonist, a serotonergic antagonist, an antipsychotic agent, and a psychotropic drug[534,535]. Also, it has been recommended for the treatment of schizophrenia.

Although bromazepam gave weaker STD signals with eNTS1, it was the only compound with which we did not observe any STD signals in the presence of detergent molecules and hence most of the following study (except for the prazosin) was focused on this compound to further validate the lack of specific binding on α_{1A}-ARs. As shown in Figure 3.8, competition STD-NMR experiments were acquired in the presence of antagonists (prazosin and spiperone) as well as allosteric compounds (9AA and tacrine). All compounds including prazosin, 9AA, spiperone and tacrine were added to 1:100 molar complex of α_{1A}-AR A4/bromazepam.

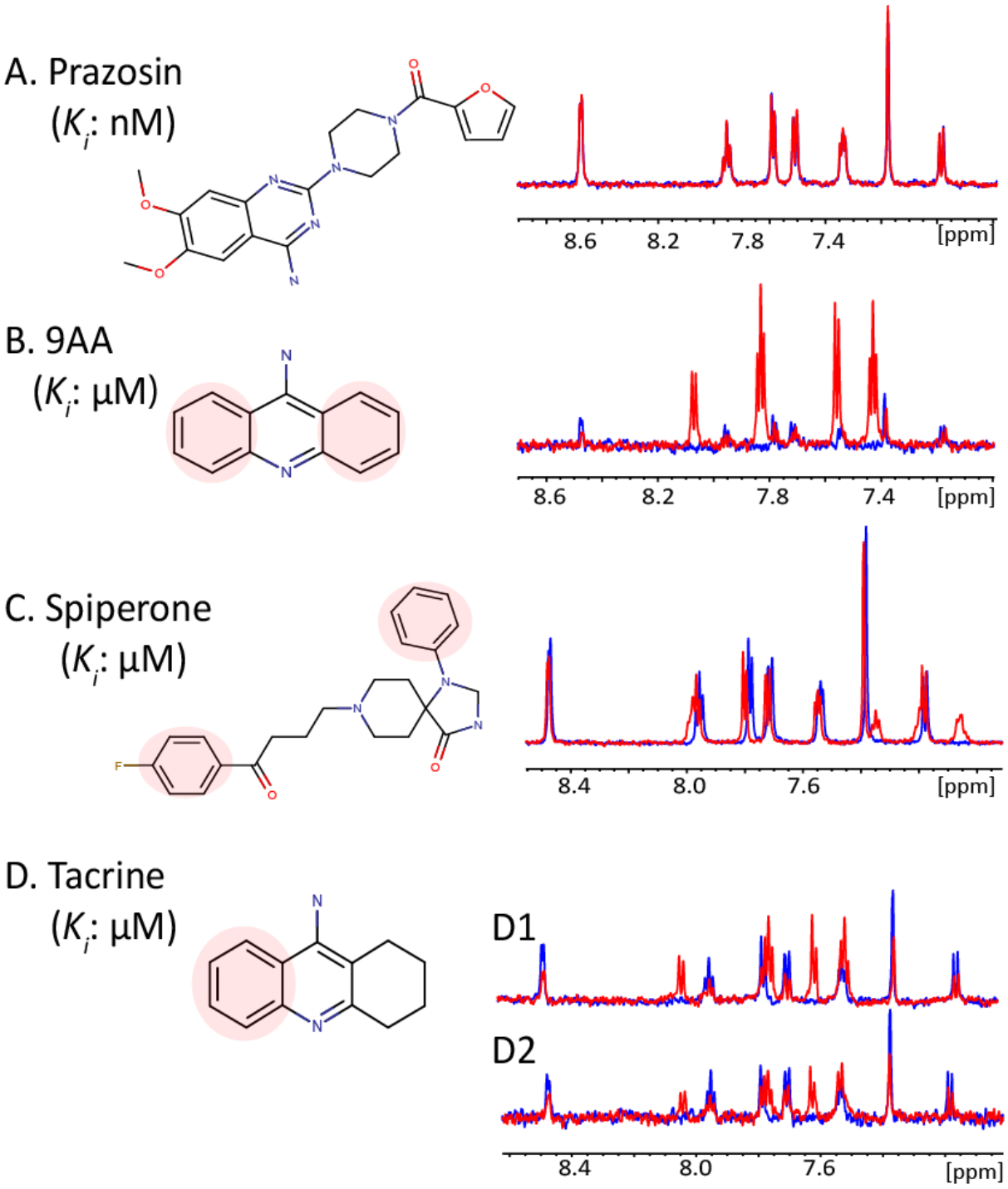

Figure 3.8. Competition STD-NMR experiments with a variety of known α_{1A}-AR antagonists and allosteric ligands. A. STD of 500 μM bromazepam with 5 μM α_{1A}-AR A4 (blue) and upon addition of 10 μM prazosin (red). B. STD of 250 μM bromazepam with 2.5 μM α_{1A}-AR A4 (blue) and upon addition of 500 μM 9AA (red). C. STD of 500 μM bromazepam with 5 μM α_{1A}-AR A4 (blue) and upon addition of 500 μM spiperone (red). D. STD of 250 μM bromazepam with 2.5 μM α_{1A}-AR A4 (blue) and upon addition of 500 μM

tacrine (red). E. STD of 250 µM bromazepam with 2.5 µM enNTS$_1$ receptor (blue) and upon addition of 500 µM tacrine (red). All bromazepam STDs (in blue) correspond to the phenyl region as shown in Figure 3.3 D. While, the phenyl region of the allosteric compounds that is giving rise to the new STD peaks are highlighted onto the structure.

Upon addition of prazosin, no competition was observed for all five benzodiazepines. Spectrum in Figure 3.8A is shown for bromazepam. The 9AA signals are quite strong (Figure 3.8 B) and the bromazepam signals after the addition of 9AA showed a decrease in the intensity (for most of the peaks) but also appeared slightly shifted, suggesting an interaction between these compounds. Upon addition of spiperone, small chemical shift difference was observed, with a slight decrease in the signal intensities of bromazepam (Figure 3.8 C), which might again indicate the interaction between the two compounds. With tacrine, we saw ~50% decrease in intensity for signals belonging to bromazepam, which might indicate overlapping binding epitope of bromazepam and tacrine on the α_{1A}-AR. To know how specific these interactions are with the α_{1A}-ARs, we performed similar STD competition where tacrine was added to 1:100 molar complex of enNTS$_1$/bromazepam. In this case, also, the addition of tacrine resulted in a similar reduction in intensity for signals belonging to bromazepam. Now, this could either mean that bromazepam and tacrine both bind to the overlapping pockets at the two the CHESS stabilised receptors or that both the compounds are non-specifically interacting with the detergent micelles. Further study needs to be done to explain what information these experiments might contain.

3.3.3.5 Control 5: Thermal denaturation experiment.

A thermal denaturation experiment, where the receptor was denatured by heating it up to 60 °C (reported melting temperature of α_{1A}-AR A4 is ~50 °C)[292], was performed to determine if binding of bromazepam is dependent on the native fold of the receptor indicating its binding specificity. STD experiments of bromazepam with a mixture of adrenaline/α_{1A}-AR A4 were recorded at 25 °C. Then, the NMR tube was heated at 60 °C for 30 min. A STD spectrum was recorded again on the same sample. Reference/Difference spectra were observed for a change in intensity of signals after heating.

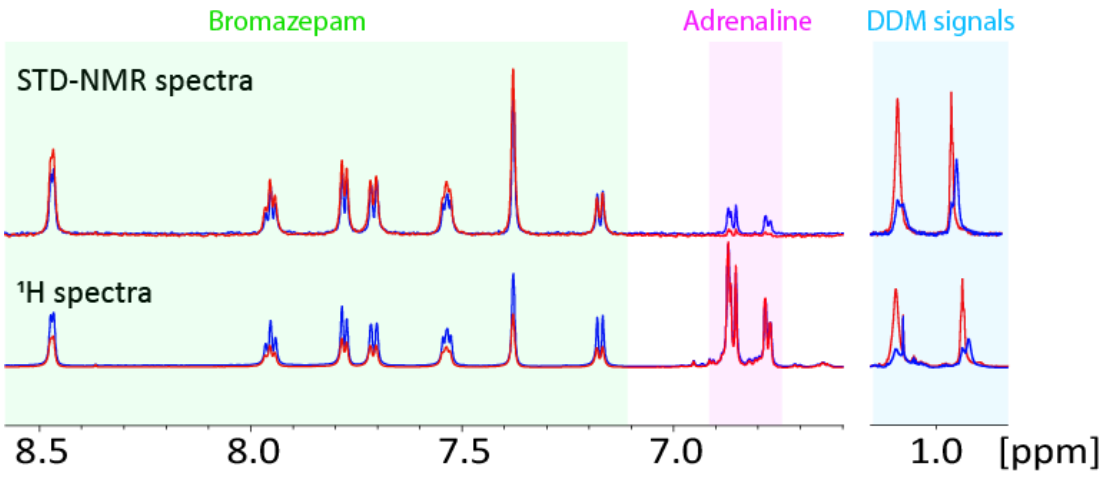

Figure 3.9. Thermal denaturation experiment. STD-NMR experiments with 5µM α_{1A}AR(A4), 500 µM adrenaline and 500 µM bromazepam at 25 ºC (in blue) compared with the same experiment with the sample heated at 60 ºC (in red). All bromazepam and adrenaline STDs correspond to the phenyl region as shown in Figure 3.3. Signals of adrenaline, bromazepam and DDM are highlighted in a pink, green and cyan band respectively. Top trace: Difference spectra. Lower trace: ^{1}H NMR spectra are showing signals before and after heating.

As per the difference spectra shown in Figure 3.9, bromazepam signals intensify after heating, suggesting hydrophobic interactions of bromazepam with the denatured receptor while the adrenaline signals lose intensity suggesting the specific binding of adrenaline, which was disrupted upon denaturation of the receptor and the disruption of the orthosteric binding pocket. Furthermore, upon heating free DDM signals are increasing, suggesting a low aggregation number of DDM micelles. The aggregation number (that is, the number of detergent monomers per micelle) is reported to decrease with increase in temperature[536].

3.3.3.6 Control 6. 2D Tr-NOESY in the absence and presence of detergent

To confirm benzodiazepines interactions with the detergent molecules, 2D Tr-NOESY experiments were performed in the absence and presence of DDM with no receptor. NOE cross-peaks are positive (opposite sign to the diagonal peaks) for a small molecule in the free unrestricted state. While when a ligand interacts with a macromolecular complex with sufficiently long residence times, it exhibits negative NOEs (same sign as the diagonal peaks).

As shown in Figure 3.10 (A and C), in the absence of the detergent, we observe few positive NOEs corresponding to the small molecule condition while in the presence of detergent

molecules, we observed strong negative NOEs of bromazepam with the detergent (NOEs upfield of 2 ppm correspond to DDM). Such interactions, most likely with the detergent micelles, indicates the formation of macromolecular complexes/aggregation in the presence of the detergent. As a control, similar experiments were recorded with adrenaline, which showed small molecule condition, both in the absence and presence of the detergent (Figure 3.10, B and D) and no NOEs with the detergent could be observed.

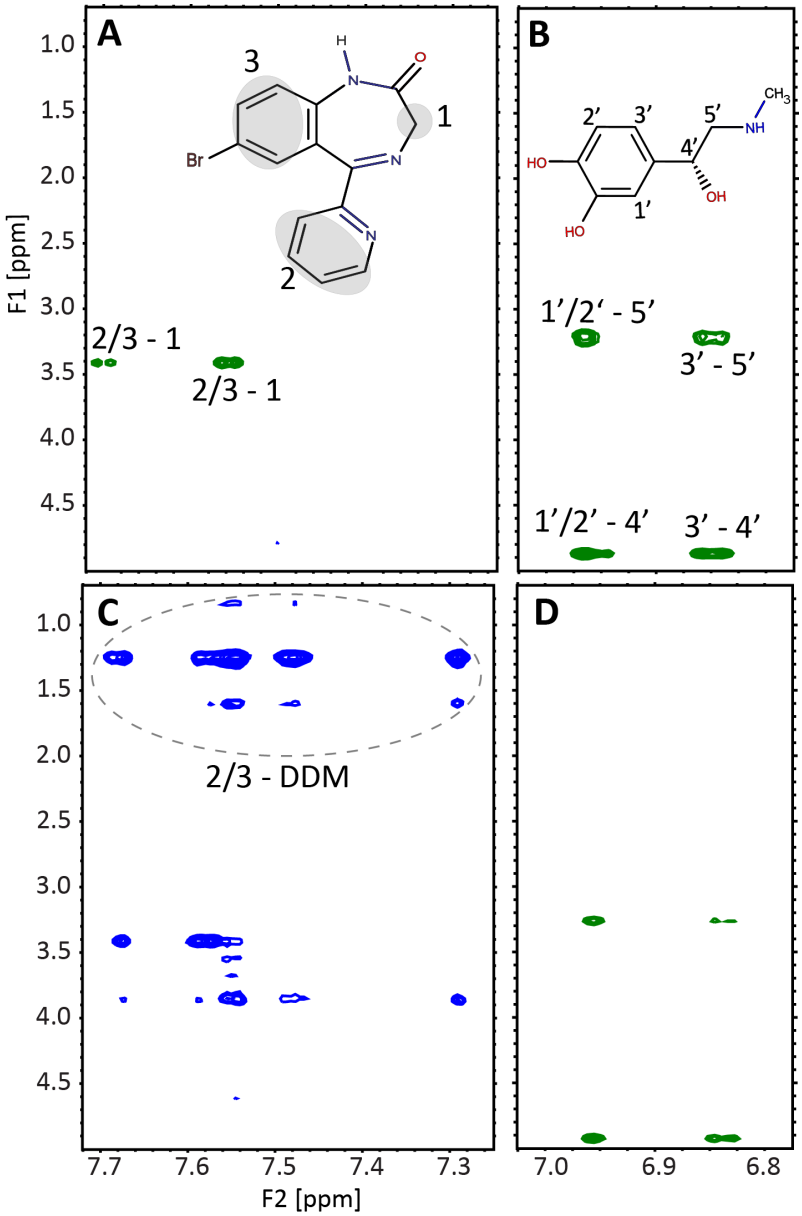

Figure 3.10. 2D tr-NOESY experiment. A section of the Tr-NOESY spectra comparing the signals in the absence and the presence of the detergent, DDM. The colour of the cross peak indicates the phase, positive peaks: green; negative peaks: blue. A. 500 µM diazepam in the

absence of DDM at 800 ms mixing time. B. 1 mM adrenaline in the absence of DDM at 800 ms mixing time. C. 500 µM diazepam in the presence of 0.05 % DDM at 150 ms mixing time and D. 375 µM adrenaline in the presence of 0.05 % DDM. At 800 ms mixing time.

3.4. Discussion

This work aimed to characterise the binding of a variety of benzodiazepines to a purified, thermostabilised α_{1A}-AR variant using ligand-based NMR methods. Benzodiazepines chosen for this study were structurally related to diazepam, lorazepam and midazolam because these have been reported to be positive allosteric modulators at the α_1-ARs. Indirect radioligand binding and signalling assays on receptor-overexpressing cell lines were used to demonstrate positive modulation of these benzodiazepines on α_{1A}-AR, α_{1B}-AR and α_{1D}-AR[209]. Despite that, we observed no indication of the specific binding of benzodiazepines to the purified α_{1A}-AR. Our studies with benzodiazepines suggest that the binding of these compounds is mostly driven by non-specific/hydrophobic interactions to itself or with the detergent molecules owing to the highly lipophilic nature of these compounds. The high lipophilic nature of the benzodiazepines is also evident by their high ClogP values, which are listed in Table 3.1 along with adrenaline and noradrenaline. A negative ClogP means a compound is hydrophilic as is the case with adrenaline and noradrenaline while a positive/higher value indicates the compound is more lipophilic.

Compound name	ClogP values
Adrenaline	-0.06
Noradrenaline	-1.04
Lorazepam	2.47
Oxazepam	1.84
Temazepam	2.08
Bromazepam	2.41
Diazepam	2.74

Table 3.1. ClogP of adrenaline, noradrenaline and benzodiazepines.

ClogP of a ligand is the calculated logarithm of its partition coefficient between n-octanol and water and is a well-established measure of the lipophilicity of a compound. A negative value for ClogP means the compound has a higher affinity for the aqueous phase (it is more hydrophilic); when ClogP = 0 the compound is equally partitioned between the lipid and aqueous phases; a positive value for ClogP denotes a higher concentration in the lipid phase (i.e., the compound is more lipophilic).

In recently published work from our group[235], these thermostabilised α_1-AR mutants were used to study whether diazepam and lorazepam positively modulate α_1-AR signalling via direct binding to the receptors. None of the results indicated that diazepam or lorazepam could directly bind to purified α_1-AR subtypes. As reported[235] calcium signalling and cell-based binding assays with WT α_1-ARs also could not detect any direct modulatory effects of diazepam on these receptors. Interestingly, diazepam was found to positively modulate cAMP response element (CRE) reporter stimulation through α_1-AR activation, but this was found to be driven through the ability of diazepam to inhibit phosphodiesterases (PDEs), a known target of some benzodiazepines.

3.4.1. The applicability of ligand-based NMR methods

The ligand-based NMR experiments have emerged as a tool to study GPCR-ligand interactions. TINS and STD-NMR have been used for fragment screening on $A_{2A}R$[288,289] and β_1-AR[290]; fragments were identified that inhibited the binding of tritium-labelled ligands with half-maximal inhibitory concentration (IC_{50}) values ranging from 5 μM to 5 mM. In a recently published work, STD-NMR, Water-LOGSY and Tr-NOESY experiments were used to determine the receptor-bound conformation of a peptide to CXCR4[300] directly on living cancer cells. STD-NMR has been used for the determination of the ligand bound conformations and epitope mapping on Human Sweet Receptor[293] and CXCR4[291] using membrane preparations. The use of membrane preparations greatly increased signal-to-noise while preserving functional binding, when compared to whole cell analysis. Moreover, the use of purified stabilised GPCRs increases the signal-to-noise of the experiments, as demonstrated in this work and also in a published work from our lab, where STD-NMR was used to map the binding epitope of adrenaline and A-61603 on α_{1A} and α_{1B}-AR[292]. These experiments also show promise in understanding G-protein interactions. For example, the conformation and orientation of a C-terminal fragment of the IL3 of the PTH1R bound to $G\alpha_s$ were determined by a combination of Tr-NOESY and STD-NMR[537] which were then incorporated into MD simulations to provide atomic insights into the mechanism of activation of this receptor.

False-positives in STD-NMR and Water-LOGSY experiments. It is important to acknowledge that the ligand-based NMR methods are prone to produce false-positive results that are mostly driven by compound aggregation[538]. With STD, the receptor-micelle is irradiated to where the entire complex is excited and some of the magnetisation is transferred

via NOE mechanisms to bound ligands. The magnetisation is retained after the ligands dissociate and hence the NMR signals of the ligands decrease appearing as a peak in the difference spectrum. If a ligand does not bind, then STD is not observed. But in case of aggregation, firstly, the aggregates of a compound can receive selective saturation (because aggregation results in broadening of peaks[539]) and secondly, the compound aggregates can non-specifically interact with the hydrophobic residues on protein surfaces[540] and thereby receive selective magnetisation, resulting in a false-positive signal. In Water-LOGSY experiments, magnetisation transfer to the bound ligands occurs via irradiated solvent water molecules trapped either in the binding pocket or at the protein surface. Compounds that aggregate also contain trapped water molecules or water is involved in the hydrogen bond formation, and hence selective excitation of bulk water will result in the transfer of saturation to the aggregate protons too, resulting in a false-positive signal[541], even in the absence of protein.

Although these ligand-based techniques are easy to use and are compliant to high molecular weight unlabelled targets, there are major shortcomings: the techniques can identify both specific and nonspecific binders, and it is usually difficult to discriminate between the desired site-specific binding and promiscuous binding due to compound aggregation[540,542]. Therefore, control experiments are required to discriminate between specific and nonspecific binders. One of the key experiments is to repeat the experiments in the presence of a high affinity competitor ligand and when such competitive reference compounds are not available, another biophysical technique is required for validation[249,543–546]. To overcome aggregation related potential false STD hits, STDs have been performed in the presence of a detergent Tween-20 (0.01%)[538], the addition of these detergents in some cases eliminates aggregation. Cala and Crim[545] reported the use of "STD effect" based epitope mapping to differentiate specific ligands from nonspecific ligands. The protons of a binding molecule that is closest to the receptor will show stronger "STD effects (I_{STD}/I_0)" than ones which are more solvent exposed. They argued that if a ligand binds non-specifically to a binding site, this will result in similar STD effects for all protons of a ligand indicating nonspecific binding. However, they did mention that there are certain limitations, such as, if a compound can bind in two different, but even so specific binding modes, it might show uniform STD effects and thus be a false negative. In general, there is a need to be aware that these commonly used ligand-based NMR techniques can generate false-positive hits. This situation is exacerbated when high concentrations of ligands or ligands with high hydrophobicity are tested for binding, which promotes aggregation.

Therefore, proper and multiple control experiments should be implemented to decrease the possibility of observing nonspecific hits.

3.5. Conclusion

In conclusion, this work with benzodiazepines and thermostabilised α_{1A}-ARs employing ligand-based NMR methods, confirms that the benzodiazepines do not specifically interact with α_{1A}-ARs. The results were very useful, in the sense that it validates our recently published work[235] which claims that the reported modulation of α_1-ARs activity by benzodiazepines[209] in cell-based assays is not a result of direct ligand binding to α_1-ARs.

CHAPTER 4 : DETERMINATION OF THE BOUND CONFORMATION OF A-61603 ON α_{1A}-AR AND α_{1B}-AR BASED ON NMR AND MD STUDIES

Tasneem M. Vaid[1,2,3], David K. Chalmers[4], Daniel J. Scott[1,3], Paul Gooley[1,2]

[1]Department of Biochemistry and Molecular Biology, University of Melbourne, Parkville, VIC, Australia

[2]Bio21 Molecular Science & Biotechnology Institute, University of Melbourne, Parkville, VIC, Australia

[3]The Florey Institute of Neuroscience & Mental Health, University of Melbourne, Parkville, VIC, Australia

[4]Monash Institute of Pharmaceutical Sciences, Monash University, Parkville, VIC, Australia

4.1. Introduction

Owing to their involvement in a diverse array of biological and pathological processes, G-protein-coupled receptors (GPCRs) are one of the largest membrane-protein classes to which drugs are targeted[547,548]. All GPCRs share a typical architecture of seven transmembrane (TM) spanning helices, connected by three extracellular and three intracellular loops. Binding of an activating ligand to the extracellular half of the receptor promotes interactions with a cognate heterotrimeric G-protein at the intracellular regions of the receptor[435], leading to further downstream effects. Based on sequence similarity, GPCRs are commonly divided into five families in vertebrates[38], which are further grouped into sub-families consisting of various closely related receptor subtypes which exhibit major differences in the mode of ligand binding[549], cellular localisation[550], second messenger utilisation[551] and physiological effects[552,553].

The adrenergic receptor (AR) subfamily consists of nine subtypes (α_{1A}, α_{1B}, α_{1D}, α_{2A}, α_{2B}, α_{2C}, β_1, β_2, β_3) which bind the same endogenous ligands, adrenaline and noradrenaline. The α_1-AR subtypes are the prime mediators of smooth muscle contraction and hypertrophic growth[175] and

are clinically targeted by non-selective and selective α-blockers (i.e. α-adrenergic antagonists) as well as sympathomimetic drugs for the treatment of several conditions[180–184]. Non-selective α-blockers, for e.g. phentolamine, phenoxybenzamine, tolazoline and trazodone, as the name suggests, targets all six types of α-ARs (α_{1A}, α_{1B}, α_{1D}, α_{2A}, α_{2B}, α_{2C}) and are used to treat high blood pressure[182]. The α_1-selective blockers such as prazosin, doxazosin, terazosin, tamsulosin, alfuzosin and silodosin are used to treat hypertension[182] and benign prostatic hyperplasia[180,181] (BPH, an enlargement of the prostate gland). The sympathomimetic drugs that mimic the actions of epinephrine or norepinephrine include anti-hypotensive agonist methoxamine[183] and nasal decongestant agonist phenylephrine[184].

In humans, α_{1A}-ARs are known to be specifically expressed in the cerebellum, cerebral cortex, heart and prostate; α_{1B}-ARs in the aorta and spleen and α_{1D}-ARs in aorta[166,169,171,176,177]. The lack of subtype-selective ligands has hindered research of subtype-specific localisation and understanding of the physiological roles of each subtype. Moreover, studies on transgenic mouse models demonstrate that α_{1A}-AR and α_{1B}-ARs mediate opposing responses to adrenaline and noradrenaline release, in relation to cardioprotection, seizures and neurogenesis[175]. Such opposing responses suggest that subtype selective activation (of α_{1A}-AR) or blocking (of α_{1B}-AR) will have clinical implications for conditions such as heart failure, epilepsy and neurodegenerative diseases[175]. Molecular targeting of α_{1A}-AR and α_{1B}-AR has been hindered substantially due to their highly similar sequences (amino acid similarity in the TM region is ~87% and in the orthosteric binding region is ~90%) and a lack of high resolution structural knowledge on how ligands bind α_1-ARs, which means that any differences between the two receptors remain unexploited. Majority of the crystal structures available for the AR family receptors are solved complexed with high affinity ligands[189,484], which tends to stabilize the receptor, facilitating crystallisation. But most of the AR agonists are weak binding ligand and hence studying them is challenging.

NMR is one of the widely used biophysical techniques for investigation of weak protein-ligand interactions[554] with two alternative experimental setups: protein-observed NMR and ligand-based NMR. In protein-observed NMR, the binding of the ligand is observed by the intensity and chemical shift perturbations of protein resonances and information on the binding epitope of the protein and the dissociation constant (K_D) can be inferred. But, unlike ligand-based NMR methods, such measurements are limited as large milligram amounts of isotopically labelled proteins are required. In ligand-based NMR, the focus is on the NMR

signals of the ligand. Interactions are manifested as through space (and not through-bond, scalar or *J coupling*) magnetisation transfer i.e. the nuclear Overhauser effect (*NOE*) between protons of the protein to those of the ligand. The interaction is typically requiring a fast off-rate ($k_{off} > 10^2$ s^{-1}). These experiments are performed with an excess of ligand over protein (>10:1) and therefore, interactions are observed on the signals of the free ligand. Typical experiments performed include saturation transfer difference (STD) NMR[273,274], water-ligand observed via gradient spectroscopy (Water-LOGSY)[261,276] and transferred nuclear overhauser effect spectroscopy (Tr-NOESY)[278,279]. STD-NMR and Water-LOGSY are based on the transfer of NOEs to the protons of the weakly binding ligand. In the case of STD, receptor protons are selectively saturated. The magnetisation is then transferred to the bound ligands via NOE[273,274]. In the case of Water-LOGSY, protons of bulk water are excited, and magnetisation is transferred from transiently bound water molecules to the ligands[261,276]. These experiments have been used for the study of GPCR-ligand interactions; STD-NMR has been used for fragment screening on $A_{2A}R$[288,289] and β_1-AR[290] and for the determination of the bound conformations and epitope mapping of ligands on Human Sweet Receptor[293], CXCR4[291], α_{1A} and α_{1B}-AR[292] and few more [294–297]; both STD-NMR and Water-LOGSY have been used to determine the receptor-bound conformation of a peptide to the CXCR4[300] directly on a living cell; STD-NMR and Tr-NOESY have been used for the determination of structural features involved in the activation of $G\alpha_s$ by the parathyroid hormone receptor type 1 (PTH1R)[537].

The Tr-NOESY method is used to define the conformation of the bound ligand by observing intra-ligand NOE peaks between protons of the free ligand[278–282]. These experiments use the sign inversion of the intra-ligand NOE cross-peaks to screen for the potential binding small ligands. Providing the ligand experiences sufficiently long residence times the observed negative NOEs in the Tr-NOESY are consistent with the macromolecular condition and provide structural (intraligand ^{1}H NOEs) information describing the conformation of the bound ligand[278,279]. A situation can occur if this experiment is conducted on two ligands binding to a receptor. If the ligands bind simultaneously with similar residence times in adjacent sites on the protein surface forming a ternary complex, negative interligand NOEs can be observed, referred to as ILOEs (intermolecular ligand-ligand noe)[555]. In another scenario, when two ligands bind competitively (and not simultaneously) with similar residence times to the same protein binding pocket, again NOEs can be observed between ligand protons. Such NOESY cross-peaks are referred to as INPHARMA (interligand noe for pharmacophore mapping) NOEs[556]. Importantly, ILOEs are generated by direct dipolar interactions between

ligand protons, whereas INPHARMA NOEs are generated via magnetisation passing from ligand protons to protein protons and subsequently to protons of the second ligand. Using these methods, if the binding mode of one of the compounds is known, the protein-bound orientation and structure of the other can be inferred. For GPCRs, such INPHARMA experiments were first reported on GPR40 containing cell membrane preparations[302] and more recently on human $A_{2A}R$ reconstituted in nanodiscs[303].

The binding of catecholamines, adrenaline and noradrenaline, to α_{1A}-ARs has been widely explored with contributions from the pioneering work on the adrenaline bound structure of the β_2-AR[557] as well as a number of biophysical and structure-function studies[203,205,292,558,559]. A-61603 is an α_{1A}-AR selective agonist and unlike adrenaline, the structure-activity relationships (SARs) for binding of A-61603 to α_1-ARs is largely unexplored, with only one recently published study from our group where the A-61603 binding epitope was mapped using STD-NMR experiments[292]. Here, we have used INPHARMA to characterise the binding of A-61603[228] relative to adrenaline/noradrenaline using thermostabilised variants of the α_{1A}- and α_{1B}-ARs. The INPHARMA measurements are complemented with molecular docking and atomic-level molecular dynamics (MD) simulations. These studies have enabled us to identify "subtle distinctness" of the ligand binding pockets across the closely related subtypes, information that can be used to guide structure-based and ligand-based drug design (SBDD and LBDD).

4.2. Materials and methods

4.2.1. Materials

n-Dodecyl-β-D-maltopyranoside(DDM), 3-[(3-cholamidopropyl)-dimethylammonio]-1-Prop aneSulfonate]•N,N-dimethyl-3-Sulfo-N-[3-[[3α,5β,7α,12α)-3,7,12-trihydroxy-24-oxocholan-24-yl]Amino]propyl]-1-propanaminium hydroxide (CHAPS) and cholesterol hemi-succinate (CHS) were purchased from Anatrace. *(R)*-adrenaline, *(R)*-noradrenaline, prazosin hydrochloride and A-61603 hydrate were purchased from Sigma Aldrich. BODIPY-FL-prazosin (QAPB [quinazoline piperazine bodipy]) was purchased from ThermoFisher Scientific. Noradrenaline and adrenaline were dissolved to 50 mM in 0.1 M HCl, prazosin was dissolved to 10 mM in 100% d_4-methanol and A-61603 was dissolved to 50 mM in water. The bacterial expression vectors were designed as described elsewhere[292].

4.2.2. Protein expression and purification

α_{1A}-AR and α_{1B}-AR were evolved for high stability in detergents using CHESS as described elsewhere[292]. The resultant stabilised α_{1A}-AR variant, α_{1A}-AR A4, contains 15 amino acid substitutions over the wild type human α_{1A}-AR and the stabilised α_{1B}-AR variant, α_{1B}-AR #15, contains 9 mutations (Figure 2.1). Plasmids for the fusions of the receptors (MBP- α_{1A}-AR A4-sfGFP and MBP-α_{1B}-AR #15- sfGFP) were transformed into *Escherichia coli* C43 (DE3). The proteins were expressed using protocols of Marley *et al.*[495] and were purified as MBP-sfGFP fusions in DDM containing buffer using immobilised metal affinity chromatography as described elsewhere[292]. Expression and purification of the fractionally deuterated α_{1A}-AR were essentially the same, except that the transformed cells were expressed in 75% ^2H_2O minimal media for an induction period of 5.5 hours and for better aeration 500 ml of minimal media was split into five 2 L flasks, containing 100 ml media each.

4.2.3. NMR spectroscopy and data processing

Unless mentioned otherwise, all NMR samples were prepared containing 20 μM receptor, 1 mM of adrenaline/noradrenaline and/or 600 μM of A-61603 hydrate in 500 μL of phosphate buffer (50 mM Potassium Phosphate, 100 mM NaCl, pH 7.4) containing 0.05% DDM and 10% ^2H_2O in 5 mm NMR tubes. To avoid oxidation, all samples containing adrenaline/noradrenaline were supplemented with 1 mM ascorbic acid. To all samples containing α_{1B}-AR #15, 2 mM CHAPS and 1 mM CHS were added to improve receptor stability over longer time periods. All spectra were acquired at 25 ºC on a 700 MHz Bruker Avance IIIHD spectrometer equipped with a cryogenically cooled triple resonance probe.

2D Tr-NOESY experiments were acquired using standard pulse sequences with water suppression using excitation sculpting with gradients[530], 56 scans as 2048 (t2) × 400 (t1) data points at mixing times ranging from 70−800 ms and a relaxation delay of 1.2 s. STD-NMR data were acquired with saturation time of 3 s, using a train of 50 ms Gaussian pulses with a B1 field of about 130 Hz, separated by 4 μs delays[529]. The on- and off-resonance frequencies were −1 and 71.4 ppm, respectively. To suppress residual protein and water signals, a spin-lock pulse of 40 ms and excitation sculpting[530] with gradients were employed, respectively. The relaxation delay between transients was set to 3.5 s. A total of 512 transients were averaged over 32,000 data points and a spectral width of 16 ppm. Prior to Fourier transformation, data were multiplied by an exponential function with 2 Hz line-broadening and zero-filled once.

Data were processed and analysed using Bruker Topspin 3.5 or NMRFAM-SPARKY 1.4. The data were apodised with cosine-squared functions in both dimensions and zero-filled to 4096 × 4096 points prior to Fourier transformation. For all 2D Tr-NOESY experiments, data were prepared in the following steps: Based on the assignments[292] all cross and diagonal peaks were assigned and integrated. This measure presented a few difficulties due to peak overlap. Two of these were the 1′ and 2′ resonances of adrenaline/noradrenaline (numbering shown in Table 4.1). In the direct dimension, both are overlapping but still distinguishable. Therefore, the volumes were approximated based on the two integration areas (Supp. Figure 1). The resonance arising from 1′ is a singlet overlapping with a component of the doublet from 2′. Also evident from 1D ^{1}H NMR and Tr-NOESY experiments is the roofing effects between resonances of protons 2′ and 3′ of adrenaline/noradrenaline, and as a result the outer two transitions have lower intensities than the middle ones, and as calculated for resonance of 3′ the downfield peak intensity is 1.25 times the upfield peak. Therefore, the area of the upfield peak of 2′ near 6.84 ppm (B) was divided by 1.25, and the obtained value (x) was then added to B to obtain the full integral of the resonance of 2′. Accordingly, x was subtracted from the integral around 6.86 ppm (A) to obtain the integral of the resonance of 1′. This was done for all diagonal intra- and inter- molecular peaks involving these resonances. In the indirect dimension, both resonances cannot be distinguished. Therefore, the overall integral of both was taken and split relative to the intensity ratios of the corresponding signals on the other side of the diagonal. In this manner we analysed 11, 6 and 5 diagonal peaks of A-61603, adrenaline and noradrenaline respectively; 54, 13 and 8 intramolecular NOEs of A-61603, adrenaline and noradrenaline respectively; and 19 intermolecular NOES for the adrenaline/A-61603 pair and 14 intermolecular NOES for the noradrenaline/A-61603 pair. For the comparison of protonated and deuterated receptor Tr-NOESY data, each cross-peak was normalised by the diagonal peak intensity at 70 ms mixing time in the indirect dimension (F1). All the cross-peaks were then plotted and fitted using Graphpad PRISM 6.01. The initial build-up rates i.e. cross-relaxation rates for all proton pairs (except the ones showing scalar coupling) were then calculated. For α_{1B}-AR #15, the difference of the normalised signals between the samples without prazosin and with prazosin was taken into account for all the calculations to remove the contributions which are unrelated to the binding pocket.

4.2.4. Computational modelling

4.2.4.1 Protein structure preparations

Homology models of α_{1A}-AR A4 and α_{1B}-AR #15 were built with I-TASSER[560] using the crystal structure of β_2 adrenergic receptor[561] (PDB ID: 5JQH) as the template. The N- and C-terminal regions and IL3, which have no sequence similarity to the template, were deleted from the model. In the α_{1A}-AR A4 the deleted residues are: residues 1 to 20, 215 to 265 and 342 to 366 and in the α_{1B}-AR #15 model, the deleted regions are: residues 1 to 37, 234 to 284 and 364 to 520. The protein models were processed and refined using the Schrödinger Maestro software suite (version 2018.3) and using the OPLS-2005 force field (FF). The Protein Preparation Wizard was used to add hydrogen atoms consistent with a pH of 7.0. Missing side chains in the α_{1B}-AR #15 model were added using Prime. When comparing receptors, the GPCRdb (GPCRdb.org) residue numbering[116] has been used.

4.2.4.2 Ligand structure preparations and docking

The three ligands used in this study: adrenaline, noradrenaline and A-61603 each contain a single chiral center and thus have (*R*) and (*S*) enantiomers. For adrenaline and noradrenaline, the (*R*) enantiomer is the only active and commercially available form; hence it was used for all the experimental and computational studies. Commercially available A-61603 is racemic (*R*/*S*)-A-61603 and was used for all the NMR experiments while both enantiomers were studied separately *in silico*. All ligand structures were obtained from the PubChem[562]. The Schrodinger LigPrep was used for geometric optimisation of ligands with the OPLS-2005 FF. Ligand ionisation states were calculated with Epik[563]. The adrenaline docked complex structures were prepared by merging the coordinates of adrenaline from the crystal structure of β_2 adrenergic receptor bound to adrenaline[561] (PDB ID: 4LDO) with the backbone aligned α_{1A}-AR A4 and α_{1B}-AR #15 apo state models. For *(R)*- and *(S)*-A-61603, induced fit docking was performed on both α_{1A}-AR A4 and α_{1B}-AR #15 models using Molsoft ICM-Pro 3.8. Thirty docked conformations were generated for each enantiomer at the two subtypes. The docked structures were energy minimised using Minimize tool in Maestro version 11.7.012 under OPLS-2005 FF.

4.2.4.3 Comparison of experimental and back-calculated INPHARMA spectra

The Pearson correlation coefficient (Pcc) between the experimental and back-calculated volumes of the INPHARMA signals for each pair of an adrenaline and A-61603 complex

structures was calculated. The back-calculated values were obtained with the SpINPHARMA[307] program using the two-state model,

$$TL_1+L_2 \rightleftarrows TL_2+L_1$$

Kinetic rate constants k_{L1} and k_{L2}

The affinity values of adrenaline and A-61603 used are taken from Yong *et al.*[292] as listed in Table 4.1. The correlation times τ_c of the receptor-ligand complexes and free ligands were calculated using Stoke's law:

$$\tau_c = \frac{4\pi\eta_W r_H^3}{3k_B T}$$

where η_W is the viscosity of the protonated solvent (0.8903 cP); k_B is the Boltzmann's constant; T is the temperature (298 K) and r_H is the effective hydrodynamic radius, the value of which was approximated from the molecular mass[564] of the protein/ligand complex embedded in a detergent micelle. The molecular mass of fusion proteins; MBP-α_{1A}-AR A4-sfGFP and MBP-α_{1B}-AR #15-sfGFP were calculated to be 116.7 kDa and 120.6 kDa respectively, each embedded in a 72 kDa DDM micelle[565]. The molecular mass of adrenaline is 183.204 Da and A-61603 is 390.3 Da. Pcc values were calculated for all the docked conformations of A-61603 (30 conformations of each enantiomer), against one adrenaline bound conformation.

4.2.4.4 Molecular dynamics simulations

The System Builder module of the Desmond package[374] was used to embed each receptor model in an explicit water-bilayer-water environment. Approximately 100 POPC (1-palmitoyl-2-oleoyl-*sn*-glycero-3-phosphocholine) lipids and 6680-8660 SCP water molecules were placed around the protein in an orthorhombic box of approximately 10 Å x 10 Å x 10 Å dimensions. The whole system was modelled using the OPLS-2005 FF. The receptor models were neutralised by adding 8-14 chloride ions. Additional Na^+ and Cl^- ions were added, corresponding to a concentration of 150 mM NaCl. The receptor models were relaxed using a minimisation and successive MD simulations using a protocol modified from that developed by Dmitry Lupyan in collaboration with Schrödinger Inc.[566]. The MD steps were: a 50 ps NVT simulation with harmonic constraints of 50 kcal/mol on the protein heavy atoms; two NPT simulations of 20 and 10 ps with harmonic constraints of 20 kcal/mol on the protein heavy

atoms and gradual restraining of membrane to 5 kcal/mol; a 100 ps MD simulation was performed to raise the temperature from 50 to 300 K in the NPT ensemble while retaining the restraints on the protein heavy atoms and membranes; 25 ns MD simulation with restraints on backbone and ligand atoms in the NPγT ensemble at 300 K; and last, a relaxation step was performed in the same ensemble for 25 ns at 300 K removing all restraints. Production runs used a 2 fs time step, a temperature of 300 K and pressure of 1.0132 bar in the NPγT ensemble (with $\gamma = 0$) using a Nose-Hoover thermostat and a Martyna–Tobias–Klein barostat with a 2.0 ps relaxation time. Van der Waals and short-range electrostatic interactions were cut off at 9 Å and long-range electrostatic forces were modelled using the particle-mesh Ewald (PME) approach[567].

4.2.4.5 Computational analysis scheme

The computational workflow is illustrated in the flow chart shown in Figure 4.1. Thirty docked conformations of each enantiomer of A-61603 were generated and the Pcc (Pearson correlation coefficient) scores were calculated using SpINPHARMA[307] for each docked conformation with respect to the docked conformation of adrenaline. A-61603 docked structures exhibiting high Pcc values as well as the one with the lowest value, as a control, were selected as starting structures for 100 ns MD simulations. Conformations that were stable or stabilising during the 100 ns MD were selected for a 500 ns of MD. One hundred conformations were sampled from the last 250 ns simulations of the 500 ns MD simulations (i.e. every 2.5 ns). Pcc values were calculated between the experimental and back-calculated volumes of the INPHARMA signals for each pair of an adrenaline and A-61603 complex structure resulting in 10000 values for each conformation. Heatmap plots of the Pcc values were produced. The structures exhibiting the highest overall score was selected as the final bound conformation of each ligand. MD trajectories were analysed with VMD[568] and the RMSD plots were generated using "trajectory visualizer tool". Root mean square deviation (RMSD) data and heatmaps were plotted in SigmaPlot 14.0.

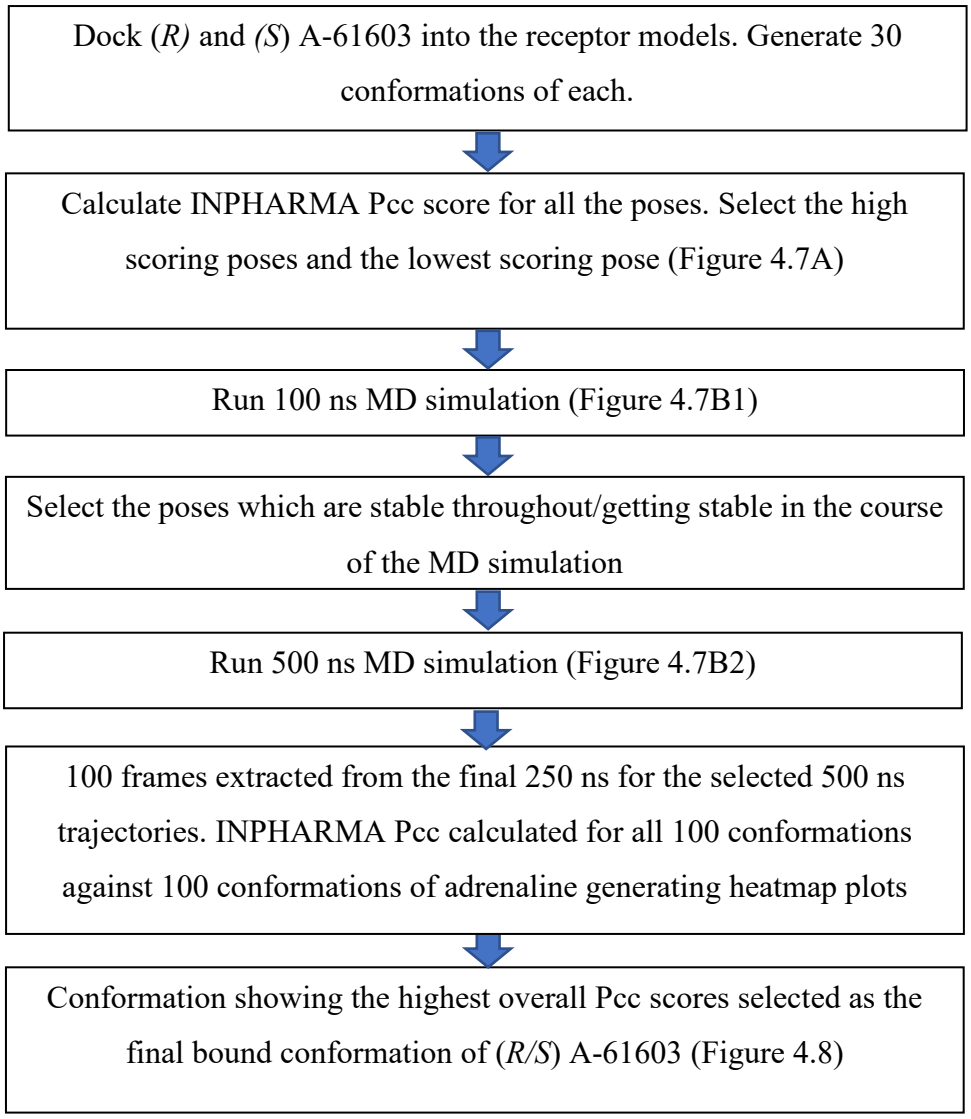

Figure 4.1. Flow chart illustrating the computational procedure.

4.3. Results

4.3.1. Tr-NOESY of ligands binding to α_{1A}-AR and α_{1B}-AR

The test ligands selected for the study are displayed in Table 4.1. Adrenaline and noradrenaline are endogenous ligands for α_1-ARs, whereas A-61603 is an α_{1A}-AR selective agonist. Tr-NOESY spectra were recorded for each ligand separately, in the absence or presence of either α_{1A}-AR A4 or α_{1B}-AR #15 (Figure 4.2). In the absence of receptor, all ligands exhibited cross-peaks that were of the opposite sign to the diagonal peaks (positive NOEs) indicating fast tumbling, as is expected for small molecules, while upon addition of the receptor (either α_{1A}-AR A4 or α_{1B}-AR #15) negative NOEs were observed, characteristic of the bound macromolecular condition. NOEs between the ligand protons and water were observed,

suggesting the presence of bound water molecules in the binding pocket of the receptor. The variations in the intensities of the NOEs upon binding to the receptors may indicate conformational preferences of the bound ligand at the two receptor subtypes.

Table 4.1. Chemical structures and affinities of the ligands: noradrenaline, adrenaline and A-61603.

Ligand	Structure[a]	~K_i (μM)[b] α_{1A}-AR A4	~K_i (μM)[b] α_{1B}-AR #15
(R) - Noradrenaline	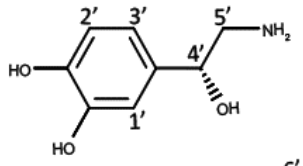	>1000	>1000
(R) - Adrenaline	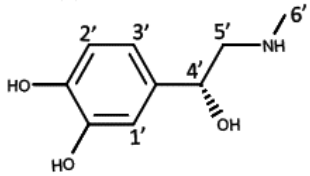	>1000	>1000
(R/S) - A-61603	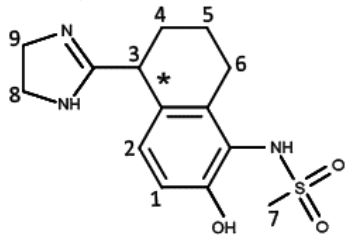	40	250

[a.] Numbering indicates positions of the assigned protons in the NMR spectra. An asterisk denotes chiral center**.**

[b.] The affinity of the ligands for thermostabilised α_{1A}-AR A4 and α_{1B}-AR #15 was determined for the detergent solubilised receptor [8].

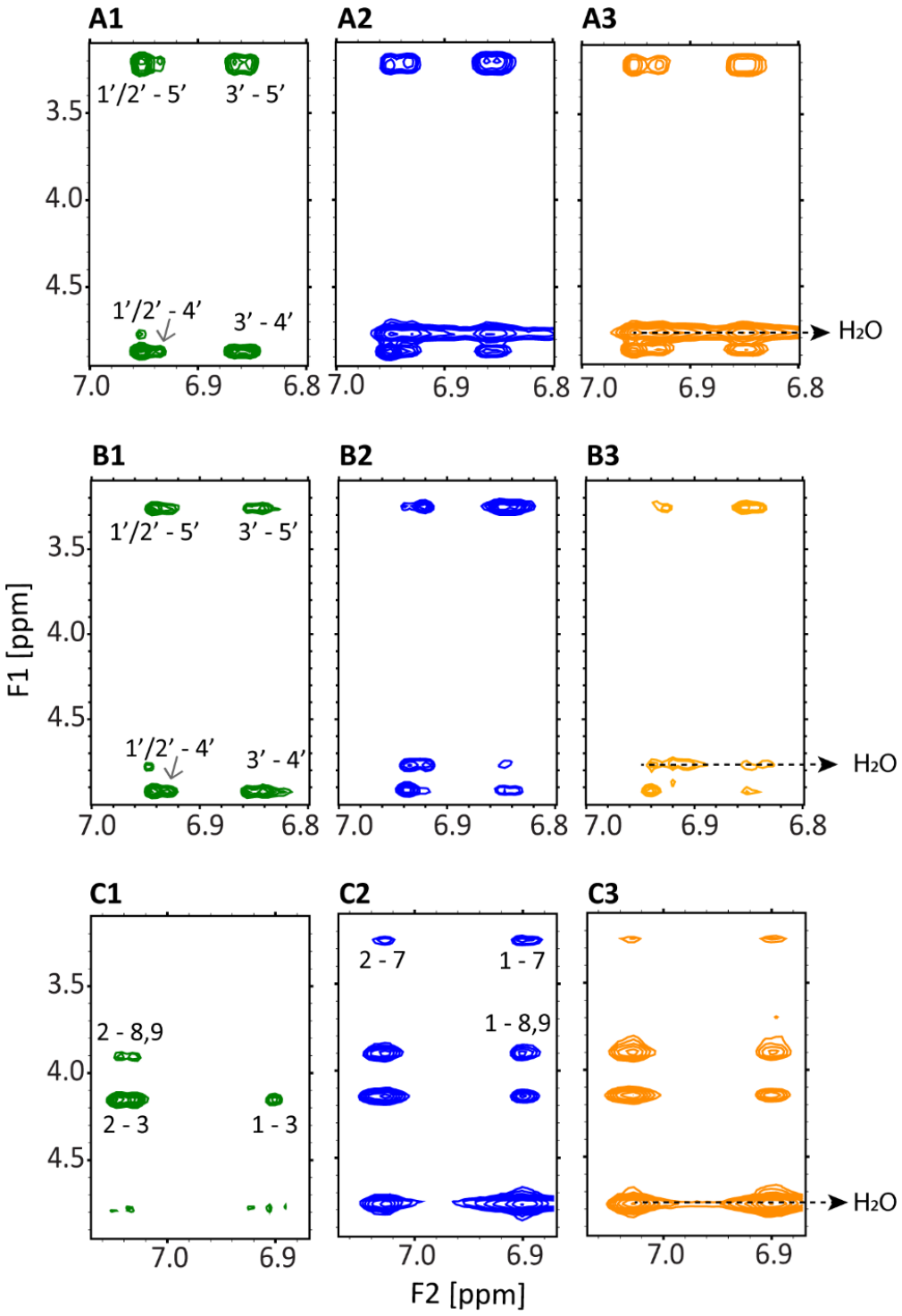

Figure 4.2. 2D Tr-NOESY experiments showing conformational preferences of ligands binding to the receptor. The colour of the cross peak indicates the phase, positive peaks: green; negative peaks: blue (α_{1A}-AR A4) and orange (α_{1B}-AR #15). Noradrenaline in the absence of receptor (A1), in the presence of α_{1A}-AR A4 (A2) and in the presence of α_{1B}-AR #15 (A3). Adrenaline in the absence of receptor (B1) in the presence of α_{1A}-AR A4 (B2) and in the presence of α_{1B}-AR #15 (A3). A-61603 in the absence of receptor (C1), in the presence of

α_{1A}-AR A4 (C2) and in the presence of α_{1B}-AR #15 (C3). All resonances are labelled according to the structures in Table. 4.1. Spectra in the absence of the receptor were recorded with mixing times 800 ms while in the presence of the receptor, the spectra were acquired at 300 ms (for noradrenaline) and 150 ms (for adrenaline). the proton from noradrenaline or adrenaline is denoted by the prime symbol (′) whereas the proton from A-61603 is not.

4.3.2. Catecholamine and A-61603 INPHARMA at α_{1A}-AR and α_{1B}-AR

The STD-NMR recorded in the presence of adrenaline or noradrenaline with A-61603, in the presence of either α_{1A}-AR A4 or α_{1B}-AR #15 show well resolved STD signals for both ligands (Figure 4.3), indicating binding of both ligands to the receptor. Reduction of the STD signals of one ligand upon addition of another suggests that both the ligands bind weakly (affinity in µM – mM range, consistent with the measured K_i values listed in Table 4.1) to the same binding site on the receptors.

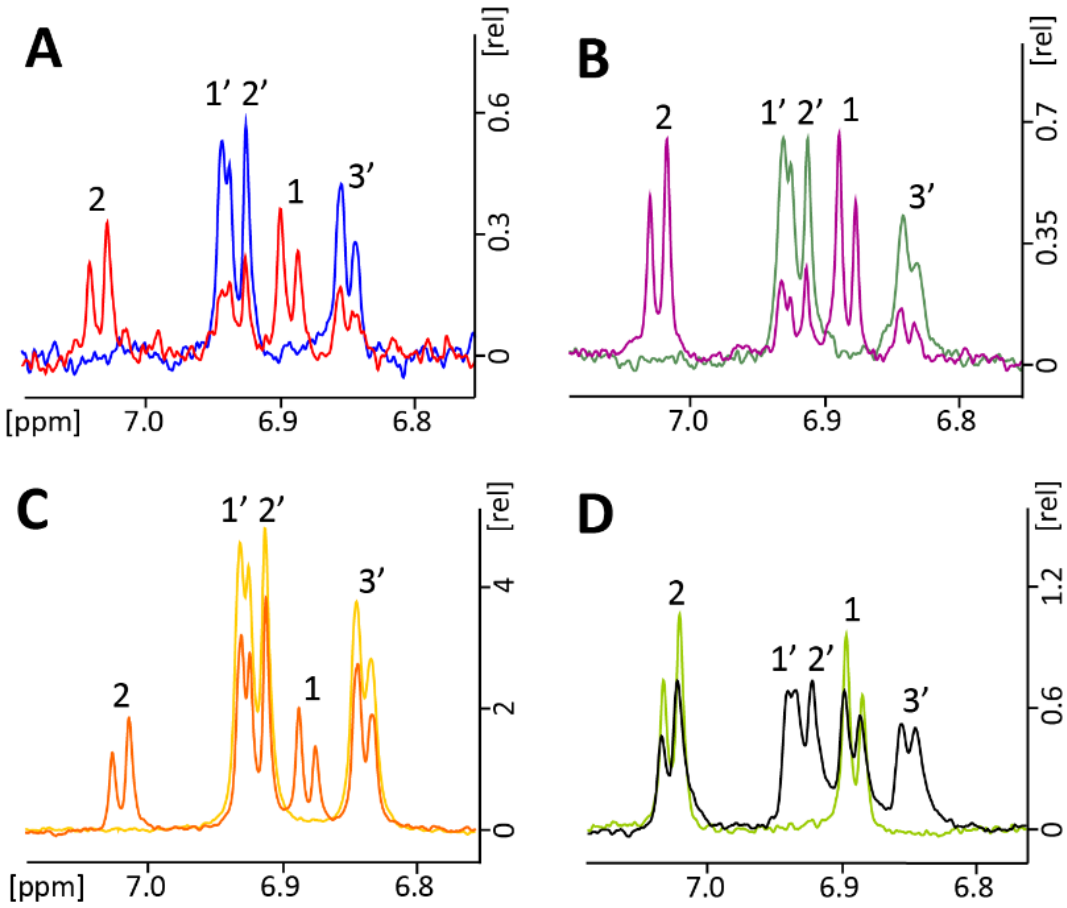

Figure 4.3. STD competition experiments of adrenaline and noradrenaline with A-61603. A. STD of 375 µM adrenaline with 2 µM α_{1A}-AR A4 (blue) and upon addition of 375 µM

A-61603 (red). B. STD of 375 μM adrenaline with 10 μM α_{1B}-AR #15 (dark green) and upon addition of 375 μM A-61603 (magenta). C. STD for 1 mM noradrenaline with 20 μM of α_{1A}-AR A4 (yellow) and upon addition of 500 μM A-61603 (orange). D. STD of 500 μM A-61603 with 10 μM α_{1B}-AR #15 (green) and upon addition of 1000 μM noradrenaline (black). All resonances are labelled according to the structures in Table. 4.1. The proton from noradrenaline or adrenaline is denoted by the prime symbol (′) whereas the proton from A-61603 is not.

Build-up tr-NOESY experiments were then acquired in the presence of two ligands, A-61603 with either adrenaline or noradrenaline and the two receptors (either α_{1A}-AR A4 or α_{1B}-AR #15). In addition to the intramolecular NOEs (as shown in Figure 4.2), several interligand NOE cross-peaks were now observed between the resonances of the two ligands for both receptors (Figure 4.4). The appearance of the interligand NOEs between these ligand pairs binding competitively to the receptor is consistent with INPHARMA. It is important, however, to confirm and differentiate it from ILOE. In ILOE experiments[555], the two ligands bind simultaneously to neighbouring protein pockets and a ternary complex is formed. By contrast, in the INPHARMA experiment, the ligands bind consecutively to the protein and only a binary complex is formed. The transfer of magnetisation is clearly different: the INPHARMA NOEs originate from a spin-diffusion process mediated by the protons of the protein-binding pocket, while ILOEs originate from a direct transfer of magnetisation between the two ligands. Consequently, if protein protons are replaced by deuterium, INPHARMA NOEs (and not ILOEs) should be specifically attenuated. Therefore, Tr-NOESY build-up experiments were performed on a fractionally deuterated receptor under the same experimental conditions. Resulting build-up data and cross-relaxation rates for the intra- and intermolecular NOEs were compared against that of the protonated receptor (Figure 4.5 and Supp. Figure 2). Here we expect for INPHARMA that intermolecular NOEs will be quenched, a consequence of loss of receptor protons, whereas for ILOE intermolecular NOEs will be similar in the presence of deuterated receptor. Indeed, for the deuterated receptor intermolecular NOEs were considerably weaker and thereby built-up more slowly, consistent with INPHARMA. Intramolecular NOEs, however, exhibited similar or faster buildup rates, a consequence of fewer pathways for magnetisation transfer to the deuterated proteins[458]. To confirm that the NOE cross-peaks form only upon ligand binding to the protein and not from the interaction between the ligands, NOESY experiments of the ligand pairs, adrenaline/A-61603 and

noradrenaline/A-61603, were recorded in the absence of a protein (Supp. Figure 3), both the compounds exhibited only positive intramolecular NOEs, characteristic of small molecules, indicating the absence of any aggregation or interaction between the two compounds.

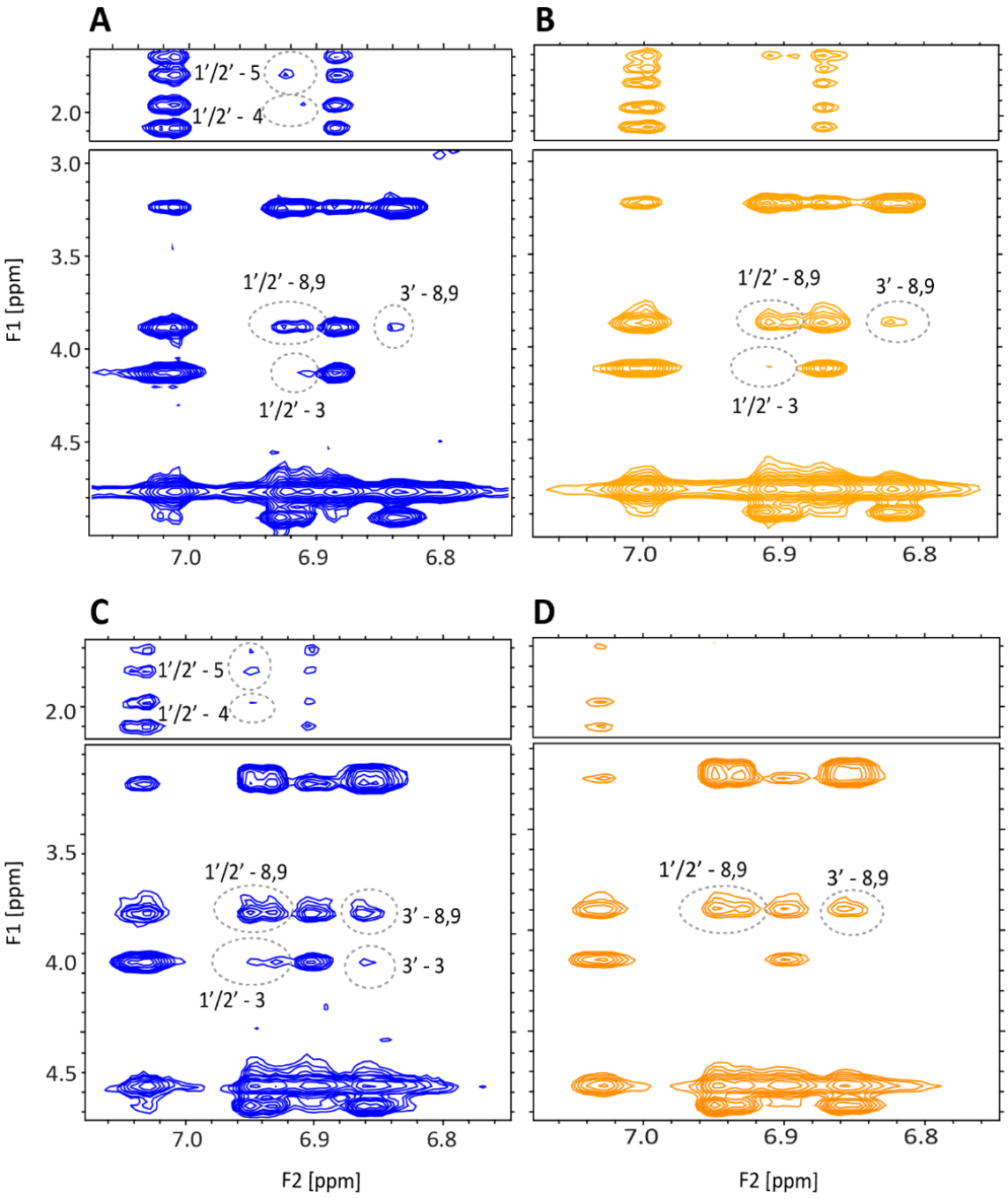

Figure 4.4. Tr-NOESY experiments of adrenaline and noradrenaline with A-61603. 2D Tr-NOESY spectra of a mixture of 1 mM adrenaline and 0.6 mM A-61603 in the presence of 20 µM receptor α_{1A}-AR A4 (A) and α_{1B}-AR #15 (B) at 300 ms mixing time. 2D Tr-NOESY spectra of a mixture of 1 mM noradrenaline and 0.6 mM A-61603 in the presence of 20 µM

receptor α $_{1A}$-AR A4 (C) and α $_{1B}$-AR #15 (D) at 300 ms mixing time. The intermolecular NOEs are circled, and the proton from noradrenaline or adrenaline is denoted by the prime symbol (') whereas the proton from A-61603 is not. The colour of the cross peak indicates the phase, positive peaks: green; negative peaks: blue (α_{1A}-AR A4) and orange (α_{1B}-AR #15).

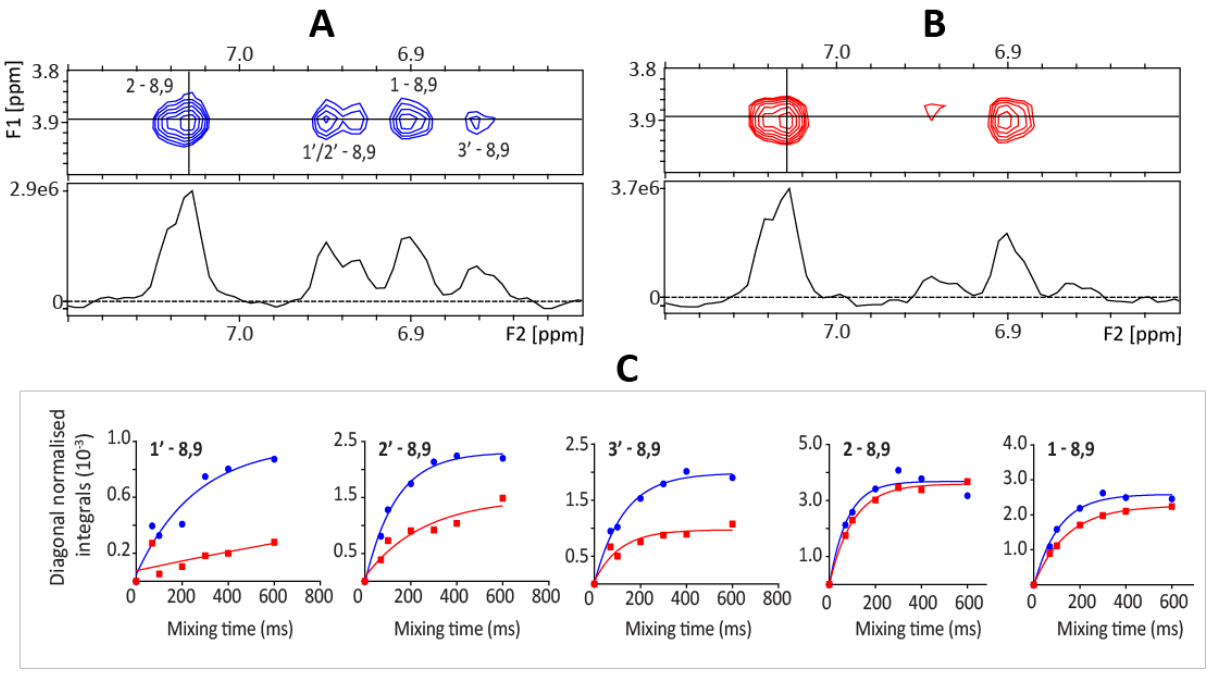

Figure 4.5. Tr-NOESY experiments with the deuterated receptor. Slices of Tr-NOESY spectra (mixing time 300 ms) for the mixture of 1 mM noradrenaline and 0.6 mM A-61603 in the presence of (A) 20 μM protonated α $_{1A}$-AR A4 and (B) 20 μM fractionally deuterated α $_{1A}$-AR A4. (C) Comparison of buildup data between the intramolecular and intermolecular proton pairs, shown in A and B, of noradrenaline and A-61603 with protonated (in blue) and deuterated (in red) α $_{1A}$-AR A4. All resonances shown here exhibit a negative phase and are labelled according to the structures in Table. 4.1.

4.3.3. Confirming the INPHARMA signals are from orthosteric binding

The occurrence of INPHARMA suggests that the two ligands, adrenaline (or noradrenaline) and A-61603, are binding subsequently at the same site. This site can either be an orthosteric site or an allosteric site. To study that, Tr-NOESY experiments were repeated under the same conditions as INPHARMA but in the presence of a high affinity (nM) α_1-selective antagonist prazosin, the binding of which is suggested by various SAR[205,569] and computational studies[570] to be at the orthosteric site. With α_{1A}-AR A4, all intermolecular NOEs disappeared, while

intramolecular NOEs turned positive, depicting an unbound small molecule condition and consistent with the orthosteric binding of the two ligands at α_{1A}-AR (Figure 4.6A). For α_{1B}-AR #15, upon addition of prazosin intermolecular NOEs were not observed, but in contrast to α_{1A}-AR A4, negative intramolecular NOEs from both ligands were still observed (Figure 4.6B). This might indicate either non-specific or allosteric binding of the ligands at two separate sites distant from each other. Nonetheless, the absence of intermolecular NOEs supports that the INPHARMA is resulting from the binding of the two ligands at the orthosteric site on α_{1B}-AR #15.

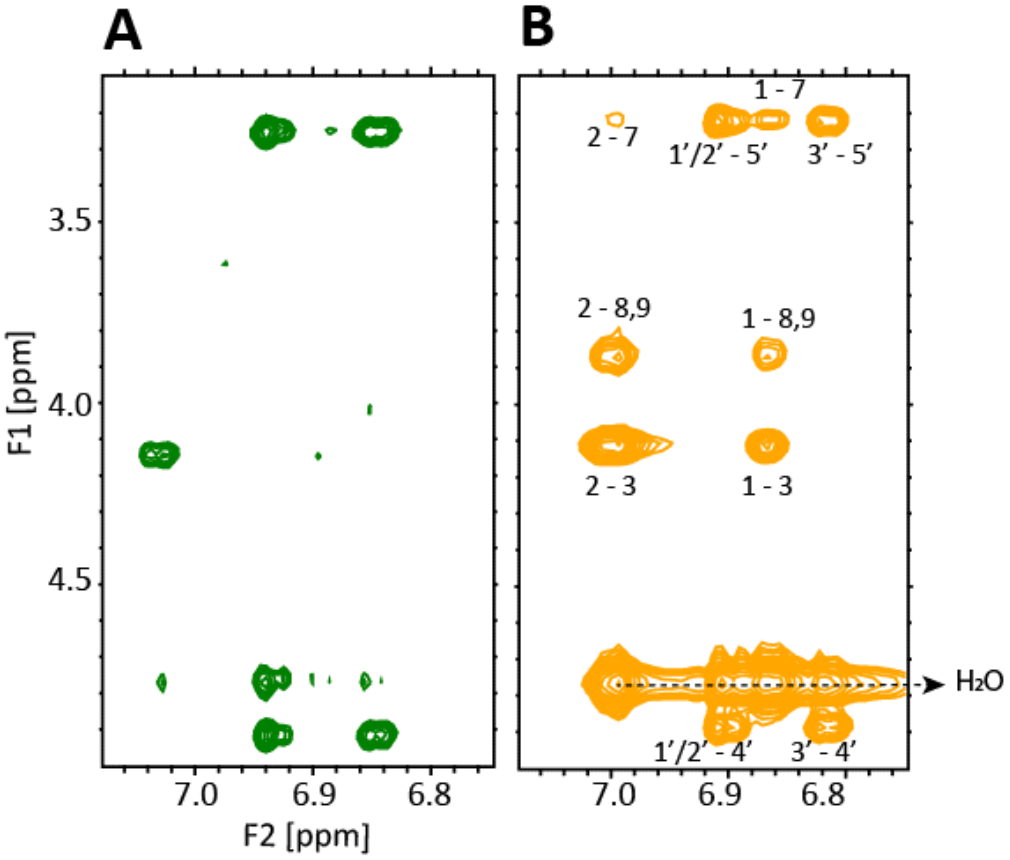

Figure 4.6. Tr-NOESY experiment in the presence of high affinity antagonist prazosin. Spectra of a ligand pair adrenaline (1 mM)/A-61603 (0.6 mM) in the presence of 20 µM prazosin with (A) 20 µM α_{1A}-AR A4 and (B) 20 µM α_{1B}-AR #15 at 300 ms mixing time. The colour of the cross peak indicates the phase, positive peaks: green; negative peaks: blue (α_{1A}-AR A4) and orange (α_{1B}-AR #15). All resonances are labelled according to the structures in Table. 4.1.

4.3.4. Determining the binding pose of A-61603 at α_{1A}-AR and α_{1B}-AR

In order to determine the bound conformations of A-61603 on α_{1A}- and α_{1B}-AR, the INPHARMA data with adrenaline and A-61603 on both α_{1A}-AR A4 and α_{1B}-AR #15 were quantitatively analysed with the SpINPHARMA[307] software. The analyses were performed using the computational models of docked complexes of adrenaline and A-61603 on α_{1A}-AR A4 and α_{1B}-AR #15. Homology models of α_{1A}-AR A4 and α_{1B}-AR #15 were prepared and the adrenaline was docked to them based on the adrenaline bound structure of the β_2-AR[557] and other structure-function studies[558]. Our adrenaline docked models are in good agreement with reported studies where: the *meta*-hydroxyl substituent of the aromatic ring makes hydrogen bonds with $Ser^{5.42x43}$; the *para*-hydroxyl interacts with $Ser^{5.46x461}$; and the protonated amine interacts with $Asp^{3.32x32}$ [558]. The phenyl group contributes significant hydrophobic contacts (Supp. Figure 4). The stability of the adrenaline docked poses was established by running MD simulations. As indicated by the RMSD plots (Supp. Figure 5), the docked poses of adrenaline were stable under MD on both the α_{1A}-AR A4 and α_{1B}-AR #15 for 500 ns.

Initial bound conformations of both enantiomers of A-61603 were created by induced-fit docking into the of α_{1A}-AR A4 and α_{1B}-AR #15 homology models. For each model, 30 poses of each enantiomer were quantitatively scored using SpINPHARMA[307], which back calculates the INPHARMA spectra and generates the Pearson correlation coefficient (Pcc) values for a pair of ligands based on its agreement with the experimental INPHARMA NOEs. The Pcc values of all A-61603 docked poses were calculated against adrenaline docked receptor models (Figure 4.7A and Supp. Figure 6A, 7A and 8A). For both α_{1A}-AR and α_{1B}-AR, the top- and lowest scoring poses of (*R*)- and (*S*)- A-61603 (marked in red in Figure 4.7A, Supp. Figure 6A, 7A and 8A) were subjected to all-atom 100 ns MD simulations to gauge the stability of these receptor-ligand complexes. Ligand RMSD values were analysed and models where the ligand position was stable or stabilising in the course of 100 ns MD simulation were selected for longer 500 ns MD simulations (Figure 4.7B, Supp. Figure 6B, 7B and 8B). Hundred frames were sampled from the final 250 ns from each 500 ns simulation. For each receptor subtype, INPHARMA Pcc scores were then recalculated between the sampled frames from the A-61603 simulations and the adrenaline simulations, producing a total of 10,000 individual scores for each system. These data, plotted as heat maps, are shown in Figure 4.7C (and Supp. Figure 6C, 7C and 8C).

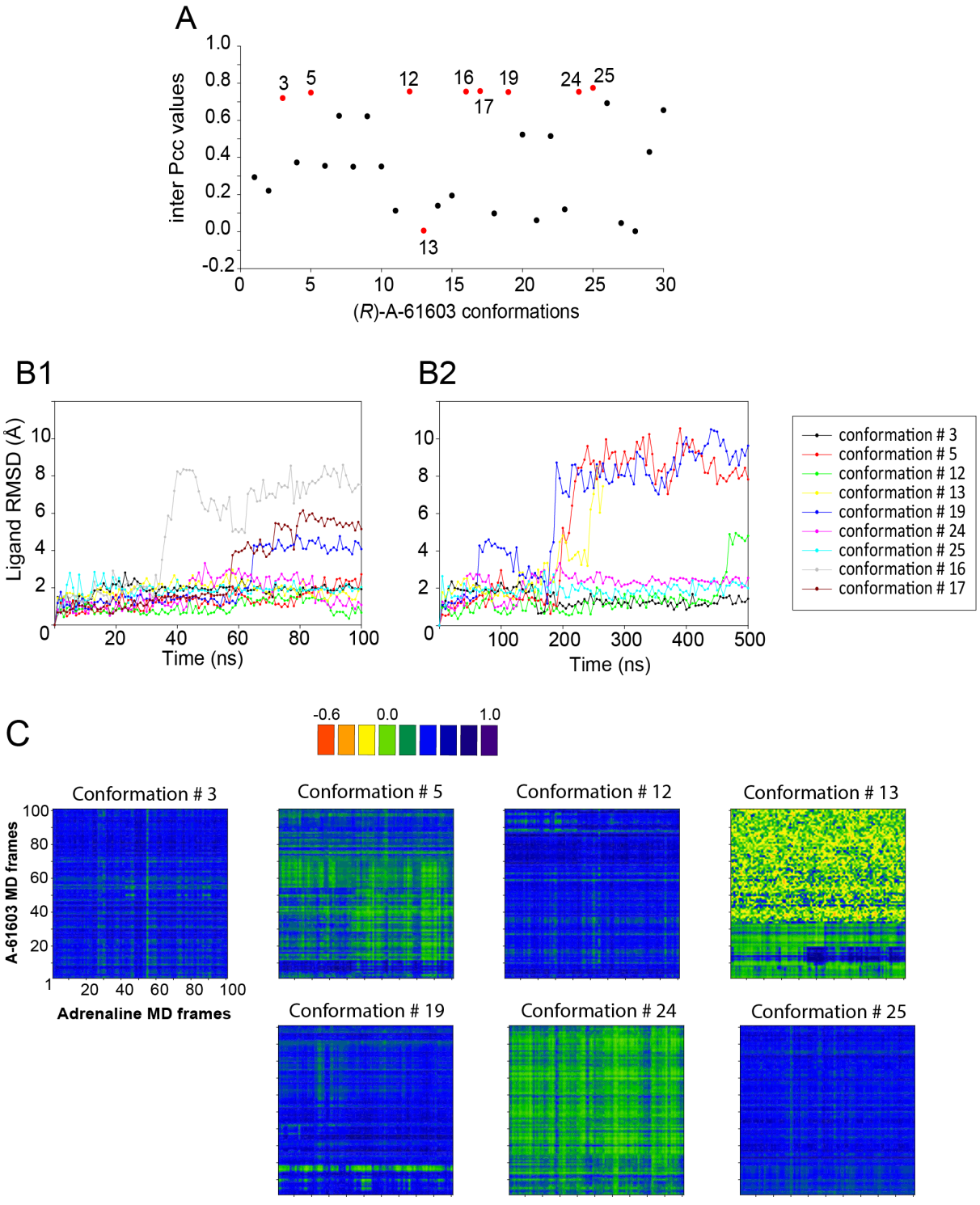

Figure 4.7. Computational analysis of (*R*)-A-61603 binding to α_{1A}-AR A4. (A) A plot showing INPHARMA Pcc (Pearson correlation coefficient) score for each of the 30 (*R*)-A-61603 docked conformations on α_{1A}-AR A4. Selected conformations are marked in red and numbered. (B) RMSD plots of the selected (*R*)-A-61603 conformations. (B1) RMSD across 100 ns MD simulation. (B2) RMSD of the selected stable conformations across 500 ns

MD. (C) Heat map representing the Pcc scores between the extracted MD frames. The values are arranged in the temporal order of the adrenaline and A-61603 simulation in the x- and y-dimension, respectively.

For α_{1A}-AR A4 receptor models, (*R*)-A-61603 conformations, #3, #12 and #25 exhibited overall good Pcc values while the low scoring conformation #13 was not stable in the MD simulations. As shown in the Supp. Figure 9, all three poses (#3, #12 and #25) were oriented similarly. Conformation #3 was stable for 500 ns and gave both the highest Pcc value (PS_{Max}) of 0.82 and the highest median score (PS_{Median}) of 0.43. For (*S*)-A-61603, only conformation #18 exhibited overall good Pcc values (Supp. Figure 6). The conformation was initially the lowest scoring conformation tested for stability, but during the relaxation phase of MD, the ligand moved to a different position in the receptor (Supp. Figure 10), stabilising and exhibiting the highest PS_{Max} and PS_{Median} values of 0.58 and 0.27 respectively. The five highest scoring snapshots from the simulations of each of the selected conformations i.e. (*R*)-A-61603 #3 and (*S*)-A-61603 #18 are shown in Figure 4.8 B and C respectively with the key interacting residues of the receptor along with the histograms showing the overall distribution of the Pcc scores. Based on the overall higher Pcc values (PS_{Max} and PS_{Median}) for (*R*)-A-61603 compared to (*S*)-A-61603, the NMR data reflects mostly the binding of the (*R)* enantiomer to α_{1A}-AR. This is consistent with the published work where radioligand binding and functional assays showed that the (*R*) enantiomer of A-61603 is the highly selective enantiomer at WT α_{1A}-AR[571]. Also, the selected conformation #3 of (*R*)-A-61603 on α_{1A}-AR is in a good agreement with the proposed orientation based on STD-NMR build-up studies[292].

A similar analysis was performed for A-61603 binding to the α_{1B}-AR #15 receptor. In this case, (*R*)-A-61603 conformation #23 and (*S*)-A-61603 conformation #17 exhibited the highest Pcc values (PS_{Max} of 0.74 for both and PS_{Median} of 0.51 and 0.54 respectively). The lowest scoring conformation of (*R*)-A-61603 was conformation #9 while the lowest scoring pose of (*S*)-A-61603 was conformation #11, both of which were unstable in the simulations (Supp. Figure 7B and 8B). The top 5 high scoring snapshots of the selected conformations, (*R*)-A-61603 #23 and (*S*)-A-61603 #17, are shown in Figure 4.8 (E and F) with the key interacting residues of the receptor highlighted. With α_{1B}-AR #15, the Pcc values were similar for both top ranked poses for (*R*) and (*S*) A-61603, which is consistent with binding studies where each enantiomer exhibited similar affinity at on WT α_{1B}-AR [571].

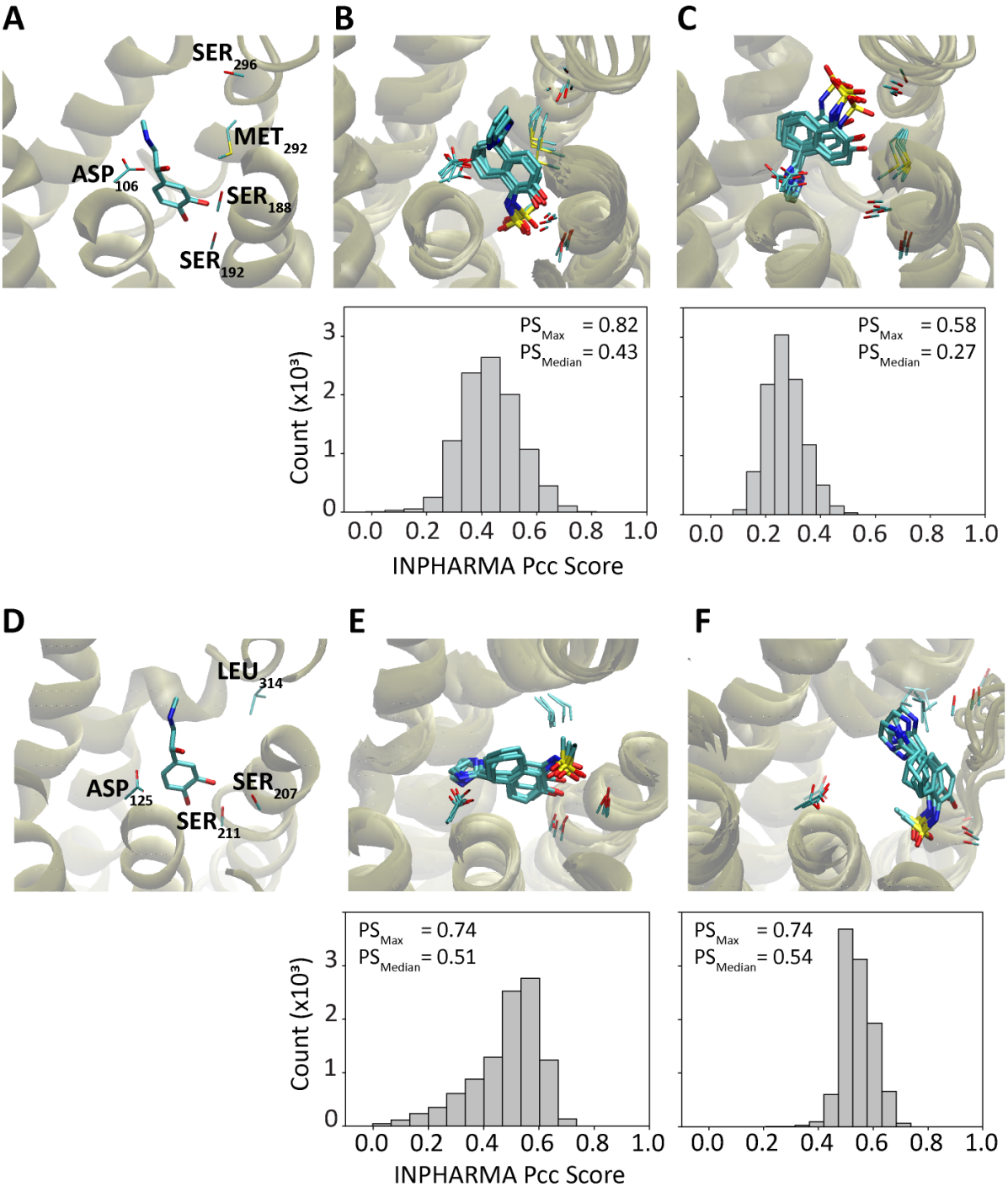

Figure 4.8. Final predicted conformations of (*R*)- and (*S*)-A-61603 on α_{1A}-AR A4 and α_{1B}-AR #15. Predicted protein-ligand complex structures of the α_{1A}-AR A4 with (A) adrenaline, (B) (*R*)-A-61603 and (C) (*S*)-A-61603. And of the α_{1B}-AR #15 with (D) adrenaline, (E) (*R*)-A-61603 and (F) (*S*)-A-61603. Key protein residues are labelled. Histograms of the INPHARMA Pcc scores evaluated for the extracted MD frames are shown for the corresponding (*R*)- and (*S*)-A-61603 conformations, where PS_{Max} is the maximum Pcc score and PS_{Median} is the median of the distribution. For all A-61603 poses, the top five high scoring

conformations were selected from five equal intervals i.e. from every 50 ns run (out of final 250 ns of 500 ns MD). In other words, from the 100 sampled frames of final 250 ns MD, instead of selecting the five top scoring conformations (which are likely to be clustered together), these 100 frames were sequentially split into five sets of 20 frames. From each set, the highest scoring conformation was selected.

4.3.5. Effects of mutating residue at position 6.55x55

The proposed conformational poses of A-61603 on α_{1A}-AR A4 (Figure 4.8 & Supp. Figure 11), and α_{1B}-AR #15 suggest that the non-conserved position 6.55x55 (Met292 in α_{1A}-AR and Leu314 in α_{1B}-AR) may play a role in A-61603 sub-type selectivity. Our models suggest that Leu314 in α_{1B}-AR sterically hinders optimal binding of the benzyl group of (*R*)-A-61603, probably explaining the weaker affinity compared to α_{1A}-AR (Supp. Figure 12). The hypothesis was validated by shortening the residue at position 6.55x55 in α_{1B}-AR #15 by mutating it to Ala, which resulted in an increased affinity for A-61603, making it similar to α_{1A}-AR A4 as shown in Table 4.2 and Supp. Figure 13. As mutating Leu314 to Met in α_{1B}-AR exhibits an increase in the binding affinity of two other α_{1A}-AR selective agonists oxymetazoline and methoxamine[559], we investigated the effect of this mutation on the binding of A-61603 to α_{1B}-AR #15 and observed similar stronger binding affinities for A-61603. We also investigated the effect of mutating Met292 on α_{1A}-AR A4 to Leu, and as expected, it resulted in a weaker affinity for A-61603. Effects of these and other mutations on the affinities of A-61603 (as listed in Table 4.2) indicates the importance of the residue at position 6.55x55 in imparting selectivity to A-61603. Furthermore, our results suggest that Met292 is not the sole contributor, as upon mutating it to Leu on α_{1A}-AR A4 or mutating Leu314 to Met in α_{1B}-AR does not necessarily bring the affinity to the same level as observed for the respective receptor.

Table 4.2. Ligand-binding profiles of α_{1A}-AR and α_{1B}-AR mutants.

RECEPTOR MUTANT	PK_i PRAZOSIN	PK_i A-61603
α_{1A}-AR A4	7.8 ± 0.04	3.8 ± 0.03
α_{1A}-AR A4 M292L	7.7 ± 0.03	3.1 ± 0.05
α_{1A}-AR A4 M292A	7.0 ± 0.07	3.7 ± 0.04
α_{1B}-AR #15	8.1 ± 0.02	2.4 ± 0.05
α_{1B}-AR #15 L314M	7.8 ± 0.04	2.7 ± 0.03
α_{1B}-AR #15 L314A	7.8 ± 0.03	**3.5 ± 0.07**

QAPB competition binding (with prazosin/A-61603) against purified α_{1A}-AR and α_{1B}-AR mutants were performed to determine the K_i values (±S.E.) as previously described[292] using the receptors solubilised in 0.1% DDM. All binding isotherms were best fit to a single site model.

4.4. Discussion

This chapter describes the application of INPHARMA[264,556] in determining the bound conformation of A-61603 on both α_{1A}- and α_{1B}-ARs relative to the predicted bound conformation of adrenaline, the binding of which is well characterised on the ARs by the extensive SAR studies[558] and X-ray crystallography[192]. Firstly, the competitive binding of the two ligands i.e. adrenaline and A-61603, was observed in STD-NMR experiments, suggesting that the binding of the two ligands occurs at the same site. The key experiment was Tr-NOESY in the presence of two drugs with the receptor which showed in addition to intra-ligand NOEs that describe the bound conformations, but also inter-ligand NOEs.

These inter-ligand NOEs could arise from the adjacent binding of the two drugs (ILOE[572,573]) forming a ternary complex or by consequent binding of the two ligands at the same site (INPHARMA) generating binary complexes. There are different ways suggested in the literature to differentiate between the two phenomena. First, by confirming that the two ligands under study are binding competitively. Krimm at al.[285] and Fruth *et al*.[574] used STD-NMR competition experiments, while Fredriksson *et al*.[303] used NOESY experiments in the presence of a high affinity known binder to confirm that the test ligands bind competitively to the receptor. We performed both STD-NMR with the two ligands and tr-NOESY in the presence of high affinity antagonist prazosin. We saw competition between the two ligands and also the

disappearance of intermolecular signals upon addition of prazosin, which indicates INPHARMA. This does not, however, exclude the possibility of observing allosteric interactions between the two ligands or the high affinity antagonist, and therefore, the contribution of ILOE cannot be ruled out definitively.

Sugiki *et al.*[575] have suggested that the mixing time, which is a critical parameter in the NOESY-based experiments, can be used to differentiate INPHARMA NOEs from ILOEs, stating that the ILOE method requires longer NOE mixing times when compared to the INPHARMA method[575]. Indeed Becattini *et al.*[266,576] observed ILOE intensities between weakly binding fragments obtained by "SAR by ILOE" methodology[266] at mixing times of 600 ms and Li *et al.*[572] observed ILOEs with mixing times ranging from 300 ms to 900 ms. INPHARMA NOEs, however, have been observed with a range of mixing times varying from 70 ms to 600 ms[264,302,310,577,578]. Sanchez-Pedregal *et al.*[264] and Fruth *et al.*[574] have observed INPHARMA intensities at 70 ms[264]. Bartoschek *et al.*[302] acquired STD-NMR and showed competition suggesting that the ligands bound to the same site supporting INPHARMA. However, tr-NOESY data showed no interligand NOEs at mixing times of 100 ms, which were only observed at longer mixing times. Sanchez-Pedregal *et al.*[579] and Fredriksson *et al.*[303] observed INPHARMA NOEs at 300 ms, but did not conduct NOE build-ups at short mixing times. Theoretical studies show that the optimal mixing time to observe INPHARMA depends on many factors including the correlation time of particularly the macromolecule, the internal dynamics of the complex, kinetics and the ratio between the ligand affinities[556]. Roughly, the larger the complex, the shorter the mixing time for which the intensity of the INPHARMA has reached its maximal value[556]. Given that, we think that the mixing time is not the definitive way to differentiate between the two phenomena. With our system, we recorded tr-NOESY ranging from 70 to 600 ms and observed maximal INPHARMA responses at 300 ms. At lower mixing times (70 ms), because of the low signal-to-noise ratio, intermolecular peaks could not be completely resolved.

The deuteration of the receptor has been proposed[284,285] to be another way of differentiating INPHARMA NOEs from ILOEs. INPHARMA is protein mediated NOE transfer between the ligands and when protein is deuterated, it can no longer retain the magnetisation resulting in the quenching of inter-ligand NOEs, while in ILOEs protein has no role in the transfer of magnetisation and hence deuteration has no effect on ILOEs. We fractionally deuterated the receptor (because full deuteration is difficult to achieve with GPCRs) which quenched the

inter-ligand NOEs, indicating that the phenomenon we are observing is resulting from INPHARMA, and not ILOE. To the best of our knowledge, deuteration to differentiate between the two phenomena, INPHARMA and ILOE, has never been performed before. Our study is the first successful example to show that the deuteration of a receptor, indeed can differentiate INPHARMA NOEs from ILOEs.

4.4.1. Computational approaches supporting the NMR data

After knowing that it is INPHARMA, the computer aided drug design approach was employed. The SpINPHARMA[307] program back calculated the INPHARMA spectra from the docked conformations as well as the MD simulation trajectory frames of A-61603 and then measured their correlation with the experimental INPHARMA data. This INPHARMA-SpINPHARMA-MD approach helped us identify the conformation of A-61603 correlating best with the experimental INPHARMA NOEs.

A similar computational approach has been adopted by one of the only two INPHARMA studies on GPCRs reported in the literature. Fredriksson *et al*.[303] determined the bound conformations of ligand poses inside the binding site of the $A_{2A}R$. The computational approach helped support the INPHARMA data, because their STD experiments were inconclusive as they had observed non-specific interactions between the ligands and the nanodiscs in which the receptor was incorporated, thereby masking the specific binding events. Another GPCR study, on GPR40 by Bartoschek *et al*.[302] used INPHARMA to determine the relative bound conformations of agonists, without necessarily needing any computational scoring. A reason that in part could account for this success is the use of proton-rich ligands, (~24 protons each ligand) resulting in a substantial number of INPHARMA signals, enough for determining the relative conformations of the ligands. This contrasts with our study where we had a reference ligand adrenaline with 6 protons and the test ligand A-61603 containing 16 protons. Our experience with the INPHARMA-SpINPHARMA-MD methodology suggests that it works best with the proton rich ligands. We performed similar studies with noradrenaline in place of adrenaline with A-61603. Noradrenaline lacks the methyl group of adrenaline. Although we did observe intermolecular NOEs between the pair, but because of the lack of protons, we did not obtain sufficient NOEs to be able to select a definitively docked conformation using SpINPHARMA.

4.4.2. The ligand optimal affinities for observing INPHARMA

INPHARMA is based on the observation of the protein mediated inter-ligand NOEs, in which ligand affinities, off-rates and residence times play a pivotal role[556]. INPHARMA NOEs have been mostly observed with ligand pairs with affinities in the μM range[264,285,574,580,581] and hence, with more or less equal concentrations of two ligands. Few studies report optimisation of the ligand concentrations according to the relative affinities of the ligands[302,579]. A particularly surprising study came from Fredriksson *et al.* where they have observed INPHARMA between the two ligands with a 1000-fold difference in affinities (8.65 μM and 1.60 nM (K_i)). Moreover, they could achieve it with equal ligand concentrations, which they attributed to the fact that the high degree of flexibility of the receptor binding pocket might led to increased k_{off} rates for the ligands leading to the observation of INPHARMA with these high affinity binders. While we were able to observe intermolecular NOEs with the two ligands with the 100-fold difference in affinity, it required considerable "tuning" of the experimental and sample conditions; most importantly the ligand and protein concentrations. Ligand concentrations were adjusted according to the relative affinities of the ligands (1000 μM adrenaline and 600 μM A-61603). The INPHARMA experiment was also performed with a mutant of α_{1A}-AR which shows higher affinities (100-fold) for both adrenaline and A-61603, but we could not observe any intermolecular NOEs in this case (Figure 4.9). Possibly further optimisation of the experimental conditions is needed to be able to observe the intermolecular NOEs with this "high-affinity receptor".

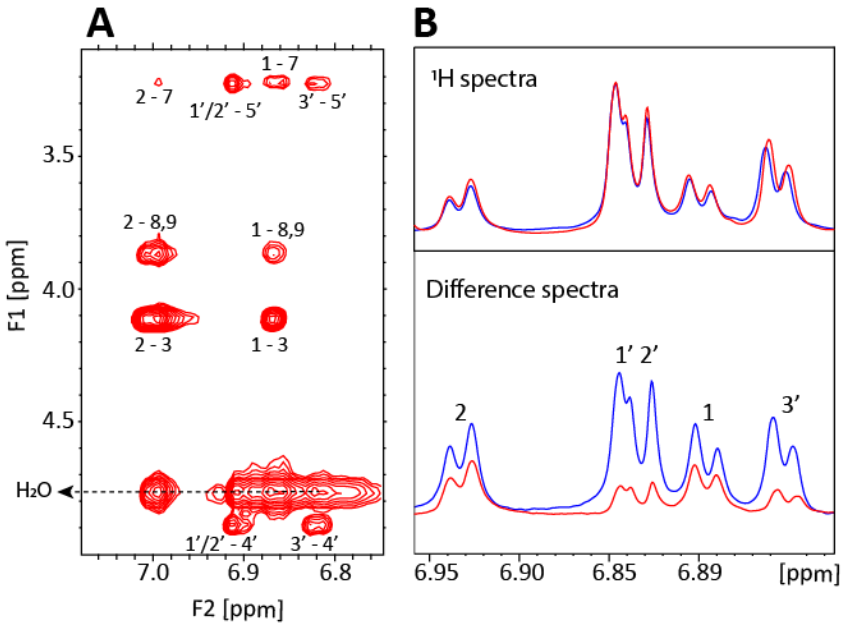

Figure 4.9. Experiments with α_{1A}-AR A4 L312F receptor. A. Tr-NOESY spectra of a ligand pair adrenaline (1 mM)/A-61603 (0.6 mM) with 20 μM α_{1A}-AR A4 L312F at 300 ms mixing

time. The colour of the cross peak (red) indicates the negative phase. B. STD-NMR experiment on the same sample (red spectra) compared with the STD-NMR in the presence of α_{1A}-AR A4 (in blue). All resonances are labelled according to the structures in Table 4.1.

4.4.3. Validating docked poses using MD simulations

In general, there are two components involved in generating a receptor-ligand complex structure *in silico*: docking and scoring. Docking places a ligand in the binding site of its macromolecular target, sampling the conformations and orientations of the ligand within the constraints of the receptor binding site. The scoring function ranks the docked poses in terms of the ligand conformation and orientation based on solvation[582,583], entropy of binding[305,584,585] or agreement with the known experimental data[307,273,305,586]. For better reliability, a "consensus scoring" is used, which involves multiple rescoring of a docked pose with a combination of different scoring functions[587]. The scoring function used in this study is SpINPHARMA[307], which ranks the docked conformations based on its agreement with the experimental INPHARMA NMR data. To be able to correctly predict a bound conformation, a large number of docked complexes should be given as an input in SpINPHARMA. A way to generate such an ensemble of conformations is by performing MD simulations, which, unlike most of the docking algorithms, take into account the flexibility of both the receptor and ligand. Our studies suggest that the docking poses that scored highly by SpINPHARMA do not necessarily generate poses that are stable in the MD. Instability is evident by the high ligand RMSDs when the top scoring docked poses on the homology models were used as the starting structure for the MD simulations. We attribute this to the fact that the ligand docking was performed on the homology models of the receptors. Ross and co-workers[588] have investigated the effect of input conformation on the accuracy of pose prediction[588]. Their unsurprising finding was that crystal structures used as an input mostly produced better overall results when compared to homology models. Since, in our case, there are no crystal structures available for α_{1A}- and α_{1B}-ARs, use of homology models based on the crystal structure of β_2-AR[561], with which these receptors share high sequence similarity (>60% in the TM region[589]) was the best approach. Moreover, the use of all-atom MD simulations and rescoring of the ensembles of scored docked poses enabled us to successfully select the best conformation in agreement with the experimental INPHARMA data, which could be validated by mutagenesis studies. Furthermore, the selected conformations informed well with the published SAR[292] data.

4.4.4. Importance of studying ligand stereochemistry

The stereochemistry of a ligand deserves special attention in protein-ligand interaction studies as it greatly influences the binding affinity[590] and plays a significant role in the determination of the binding thermodynamics[591]. The importance of studying stereochemistry is evident by the infamous case of the drug Thalidomide. It was introduced in Germany in 1957 and was marketed as a sedative drug for treating morning sickness in pregnant women[592–594]. In the following few years, about 10,000 infants worldwide were born with phocomelia (or limb malformation)[595,596] with > 50% mortality rate. It was later found out that the marketed drug was actually a racemic mixture, of (*R*)- and (*S*)-enantiomers of Thalidomide and that it was the (*R*)-enantiomer, which imparted sedative effects, whereas the (*S*)-isomer was teratogenic (an agent that can disturb the development of the embryo or foetus). The mechanism of which was not established, until the past few years[597,598]. In this study, the two ligands, adrenaline and A-61603 also contain chiral centres and hence, have (*R*)- and (*S*)-enantiomers. For adrenaline, it is well established that the (*R*) form is the only active form and hence, all our study is based on the (*R*) form of adrenaline. As for A-61603, both (*R*) and (*S*) forms are active, with (*R*) being more potent than (*S*) on WT α_{1A}-ARs, while both are equally potent on WT α_{1B}-ARs[228,571]. So, with the computational approach, the two enantiomers of A-61603 were studied separately and our results suggest that the binding conformations of the two enantiomers of A-61603 are different at both α_{1A}- and α_{1B}-ARs.

4.5. Conclusion

In conclusion, we have shown that the INPHARMA-SpINPHARMA-MD is a powerful approach for the determination of the receptor bound conformations of weak binding GPCR ligands, given there is a known conformation of another ligand on the same receptor. The knowledge would be valuable in the absence of direct information about the structure of the receptor, as is the case with α_{1A}- and α_{1B}-AR. The methodology described here could play a pivotal role in the fragment-based drug discovery (FBDD) and the ligand-based drug discovery (LBDD) approaches and can contribute significantly in the rational development of subtype-selective drugs in GPCRs.

ACKNOWLEDGMENTS

SpINPHARMA software, tested in this work, was provided by Christian Griesinger from Max Planck Institute for the Biophysical Chemistry, Göttingen.

CHAPTER 5 : GENERAL DISCUSSION

Elucidating the binding modes of ligands to their cognate GPCRs lays the foundation for understanding their biological signalling mechanisms and provides a framework for drug discovery. To date, however, there is a lack of structural information on GPCR ligands bound to their respective receptors. Most of the detailed insights have been provided by the ligand bound crystal structures of GPCRs[9,188,189,424,484] followed by a few cryo-EM[12–16] and NMR studies[295,297,301,599]. Specifically, for the adrenergic receptor class, only ligand bound structures of β_1- and β_2-ARs have been solved[11]. This lack of ligand-binding knowledge has hindered drug development with this class of receptors.

In general, all GPCRs share high sequence and structural conservation, and yet exhibit distinct tissue distributions and carry out different and at often times contrasting functions[600]. The two subtypes of α_1-AR, α_{1A} and α_{1B}, have been reported to be differently localised in human tissues, α_{1A}-ARs are known to be specifically expressed in the cerebellum, cerebral cortex, heart and prostate, while α_{1B}-ARs in the aorta and spleen[166,171,176,177]. The lack of subtype-selective drugs has hindered research of subtype-specific localisation and understanding of the physiological roles of each subtype and as a consequence, the selective targeting (blocking/activating) of these subtypes, which could be physiologically important and pharmacologically relevant[600] is challenging. To 'rationally' design subtype selectivity, a prior comprehensive knowledge of the bound conformation of the known ligands may be beneficial. In the case of the subtypes of α_1-AR, one of the few known α_{1A}-AR selective compounds is A-61603, the selectivity of which towards α_{1A}-AR is around 100-fold, which is good but not the best for therapeutic applications, which requires about 100- to 1000-fold difference. Of course, solving the crystal structure of α_{1A}-AR and α_{1B}-AR would be the most direct approach. But this project in part set out to explore methods to 'rapidly' i.e. within the timelines of the drug-discovery process without extensive data interpretation, determine the bound conformation of the weakly binding A-61603, and also the benzodiazepines, to further inform the development of subtype selective drugs on ARs.

Furthermore, majority of the crystal structures are solved in complex with high-affinity ligands. This is applicable not only to GPCRs but to all the proteins in general. The current scientific literature contains thousands of articles devoted to the study of protein–ligand interactions (e.g. searching PubMed with the term protein-ligand interactions yields > 40,000 articles), most of which focus on high-affinity complexes (typically with a $K_D < 10^{-6}$ M) that are easily detectable and therefore suitable to be studied by a variety of techniques[601–620], including X-ray crystallography and Cryo-EM studies. When an interaction is weak or very weak (e.g. $K_D > 10^{-4}$ M), many conventional approaches fail or become unreliable. Weak and transient complexes are extremely important[621] with respect to the signalling cascades in cells[622], regulation of biochemical pathways as well as allosteric regulation[622]. Among other techniques[623,624], NMR is indeed one of the most useful tools for investigating weak protein interactions with the added benefit of providing atomic level information on the binding site[284,625,626].

To study GPCR ligand interactions, NMR generally does not require suppressing the dynamics of the protein and does not require high-affinity ligands. Most of the structures solved with X-ray crystallography, as mentioned earlier, are in the presence of high-affinity ligands, mostly antagonists, which tend to reduce the flexibility of the receptor therefore benefiting crystallisation. In contrast, many agonists are weak-binding molecules and in addition, their binding can enhance the flexibility of the receptor, so obtaining the weak-agonist bound structure of a GPCR is not simple. There are a number of NMR methods[284,625] that are suited for the study of such conditions of weak binding ligands or more precisely ligands which are in the fast exchange regime i.e. exchanging fast (with off-rates > 10^2 s^{-1}) between bound and unbound states. The work constituting this thesis used these experiments constituting a variety of NOE-based ligand-based NMR methods including STD-NMR, Water-LOGSY, Tr-NOESY and INPHARMA. Using these methods, we studied the binding of a variety of ligands which includes endogenous agonists (adrenaline and noradrenaline), the biased agonist (A-61603) and allosteric compounds (benzodiazepines) to the α_{1A}- and α_{1B}-AR variants, which were thermostabilised using a directed evolution method CHESS[494]. The bound conformation of A-61603 was determined on α_{1A}- and α_{1B}-ARs based on the binding knowledge of adrenaline/noradrenaline, and the results were further supported by molecular dynamics simulation calculations. While the study with benzodiazepines confirms that these compounds do not specifically interact with α_{1A}-ARs, the results were very useful, in the sense that it validates our recently published work[235] which claims that the reported modulation of α_1-ARs

activity by benzodiazepines[209] in cell-based assays is not a result of direct ligand binding to α_1-ARs.

Conclusion and future directions

We have shown that the ligand-based NMR methods are highly useful for the study of weak binding ligands on GPCRs, which are otherwise difficult to study. Providing the sample conditions are optimal and the system requirements are met, the INPHARMA method is very useful for the determination of ligand binding poses on GPCRs. These methods can be supported by computational approaches, as done in this work, using SpINPHARMA and MD simulations. Such data would be highly valuable in the absence of direct information about the structure of the receptor, especially for fragment-based drug discovery (FBDD) and the ligand-based drug discovery (LBDD) approaches. Using this methodology, we are now characterising new fragments which have been screened for the selectivity towards either α_{1A}- or α_{1B}-AR and other α_{1A}-AR selective compounds, for example methoxamine[559]. Overall, the study shows that the methodology holds great potential in the rational development of subtype-selective drugs in GPCRs.

SUPPLEMENTARY FIGURES

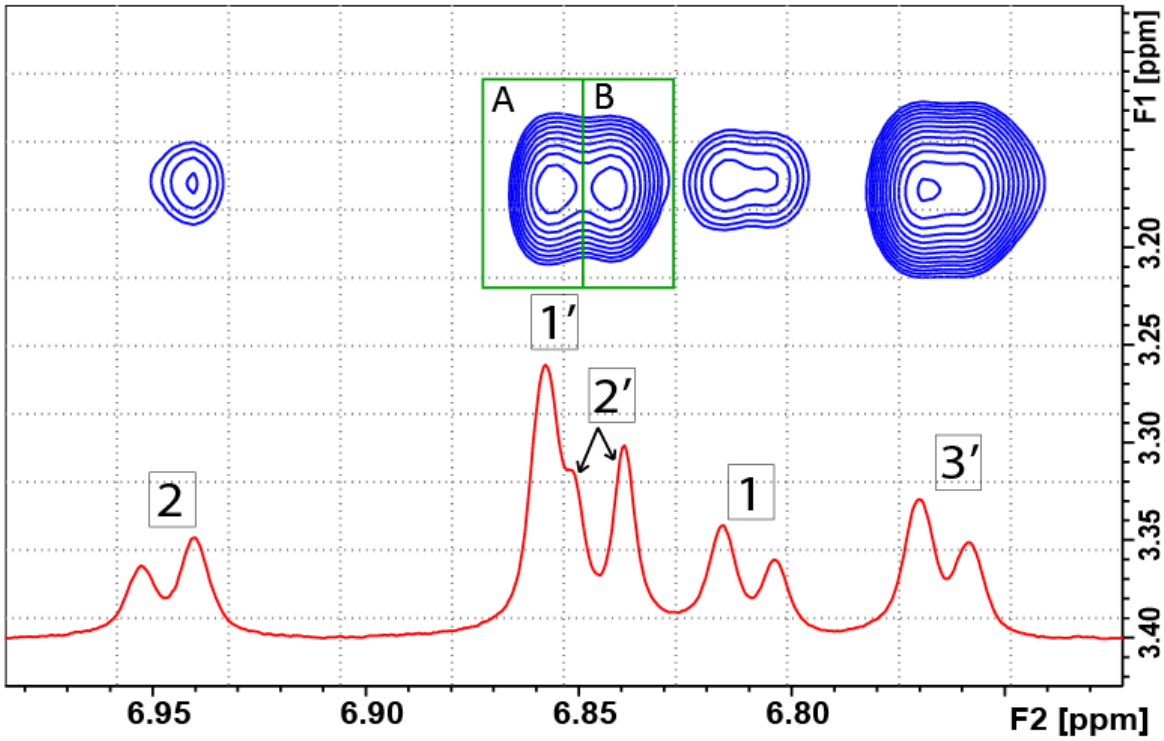

Supplementary Figure 1. Assigning the overlapping peaks in the Tr-NOESY spectra. Exemplary section of a 1D ^{1}H NMR spectrum overlaid on a Tr-NOESY spectrum of adrenaline and A-61603 in the presence of α_{1A}-AR A4. The numbering of the atoms corresponds to that shown in Table 4.1. All resonances from A-61603 are denoted by numbers, while those from adrenaline are denoted by the numbers followed by a prime symbol (’). A and B are the integration areas which were used to calculate the separated integrals of resonance 1’ and 2’ respectively from adrenaline/noradrenaline.

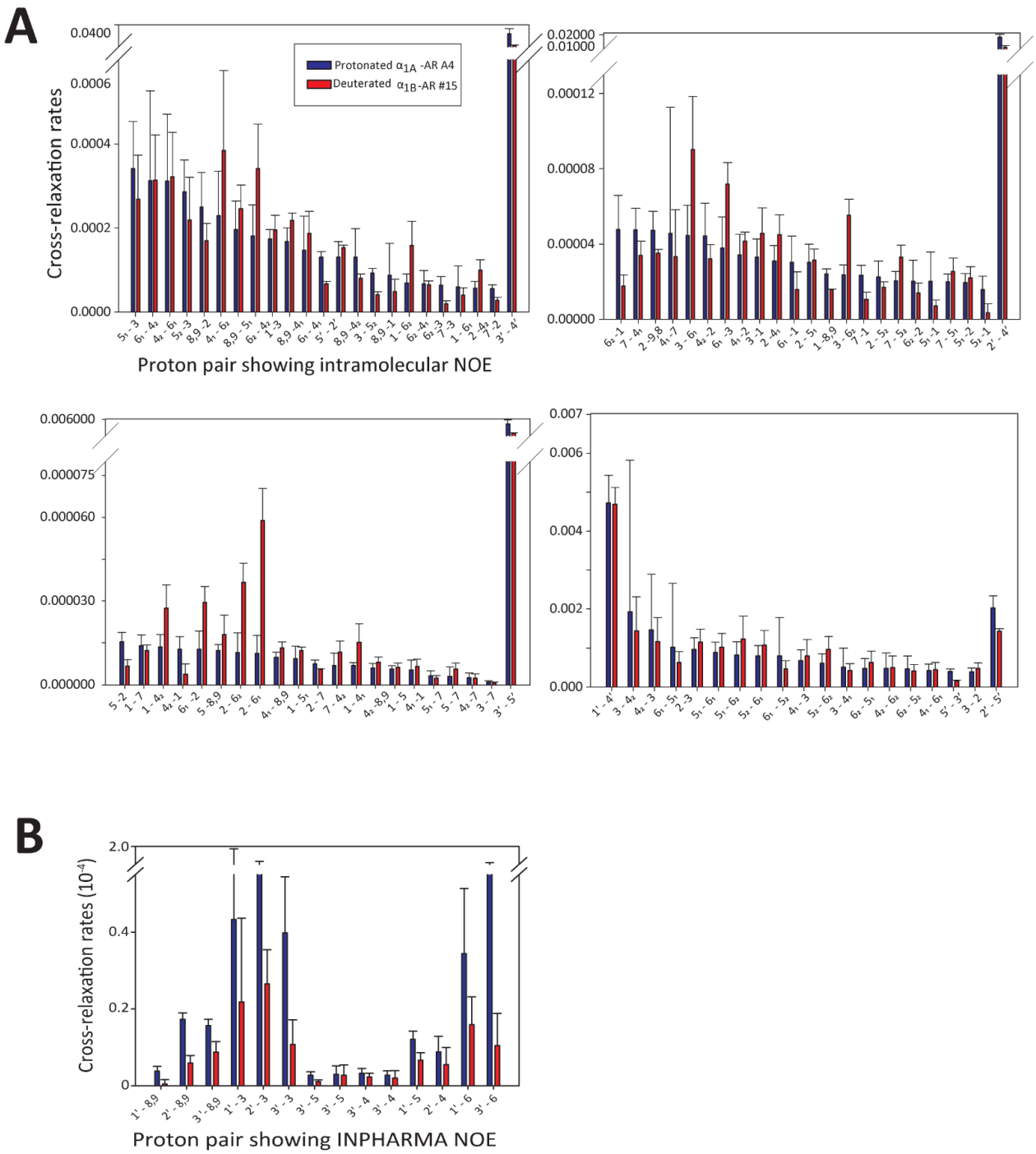

Supplementary Figure 2. Cross-relaxation rates comparison. Comparison of the cross-relaxation rates of noradrenaline and A-61603 intramolecular NOEs (A) and intermolecular NOEs (B) when bound either to protonated α_{1A}-AR A4 (in blue) or perdeuterated α_{1A}-AR A4 (in red). The protons pairs in the Y-axis are numbered according to the structures in Table 4.1.

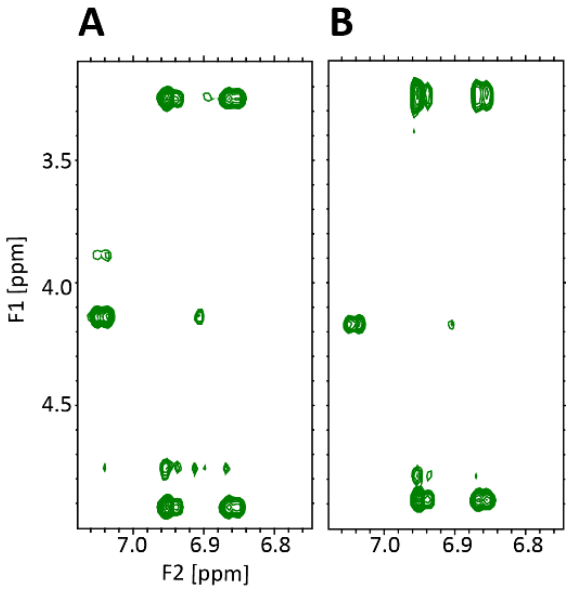

Supplementary Figure 3. Tr-NOESY experiment with two ligands and no receptor. A. 1 mM adrenaline and 0.6 mM A-61603. B. 1 mM noradrenaline and 0.6 mM A-61603. Mixing time: 800 ms. The colour of the cross peak (green) indicates the positive phase.

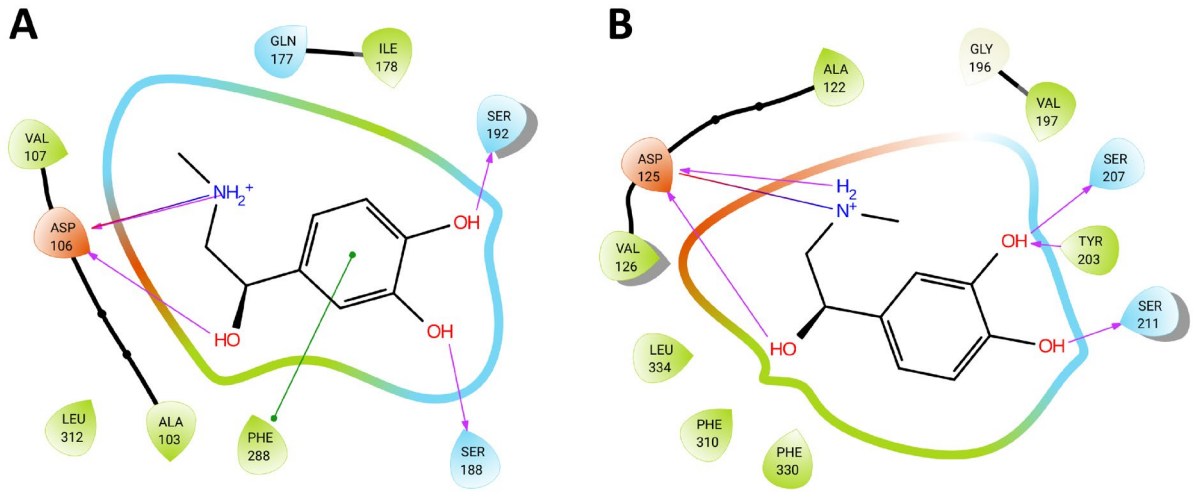

Supplementary Figure 4. Adrenaline docked conformations. Docked conformation of adrenaline on (A) α_{1A}-AR A4 and (B) α_{1B}-AR #15. All protein residues within 2.5 Å of the ligand are shown and plotted using Ligand Interaction Diagram tool in Maestro 11.7.012. Hydrophobic residues are coloured green, acidic residues are red, basic residues are purple, and polar residues are light blue. Connecting lines in purple: H-bond, green: π-π stacking, orange: π-cation.

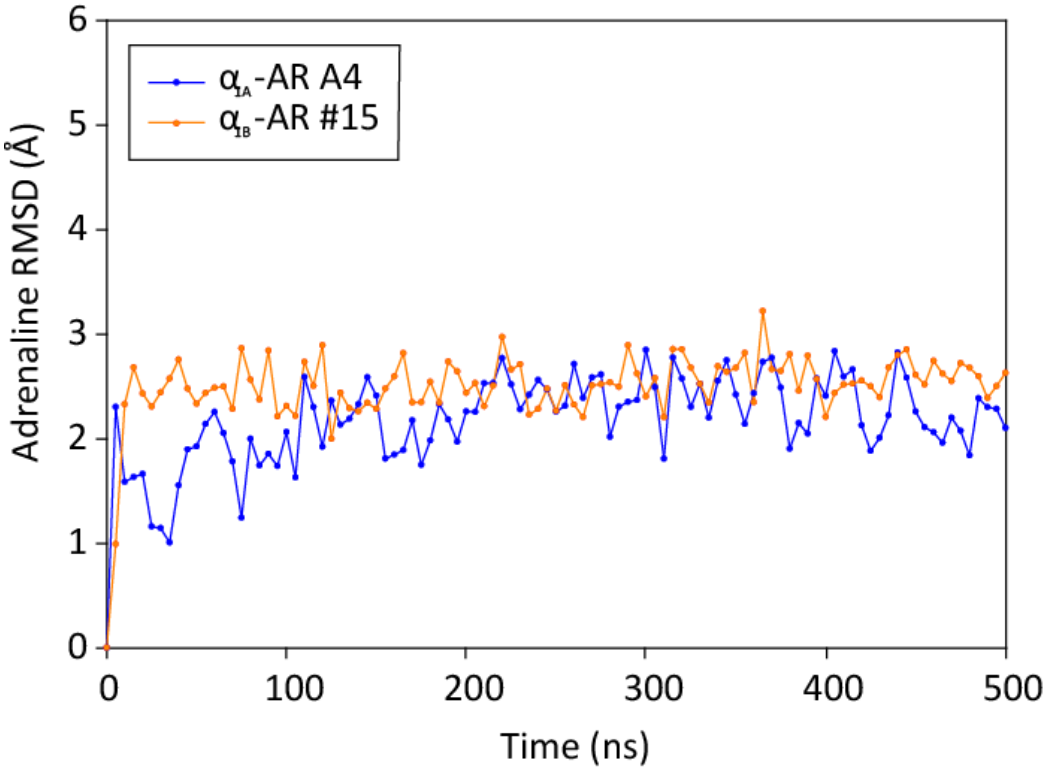

Supplementary Figure 5. Adrenaline RMSDs. The plot of the RMSD of the ligand, adrenaline over the course of the 500 ns MD simulations. The trajectories in blue and orange represent the simulations with α_{1A}-AR A4 and α_{1AB}-AR #15 respectively.

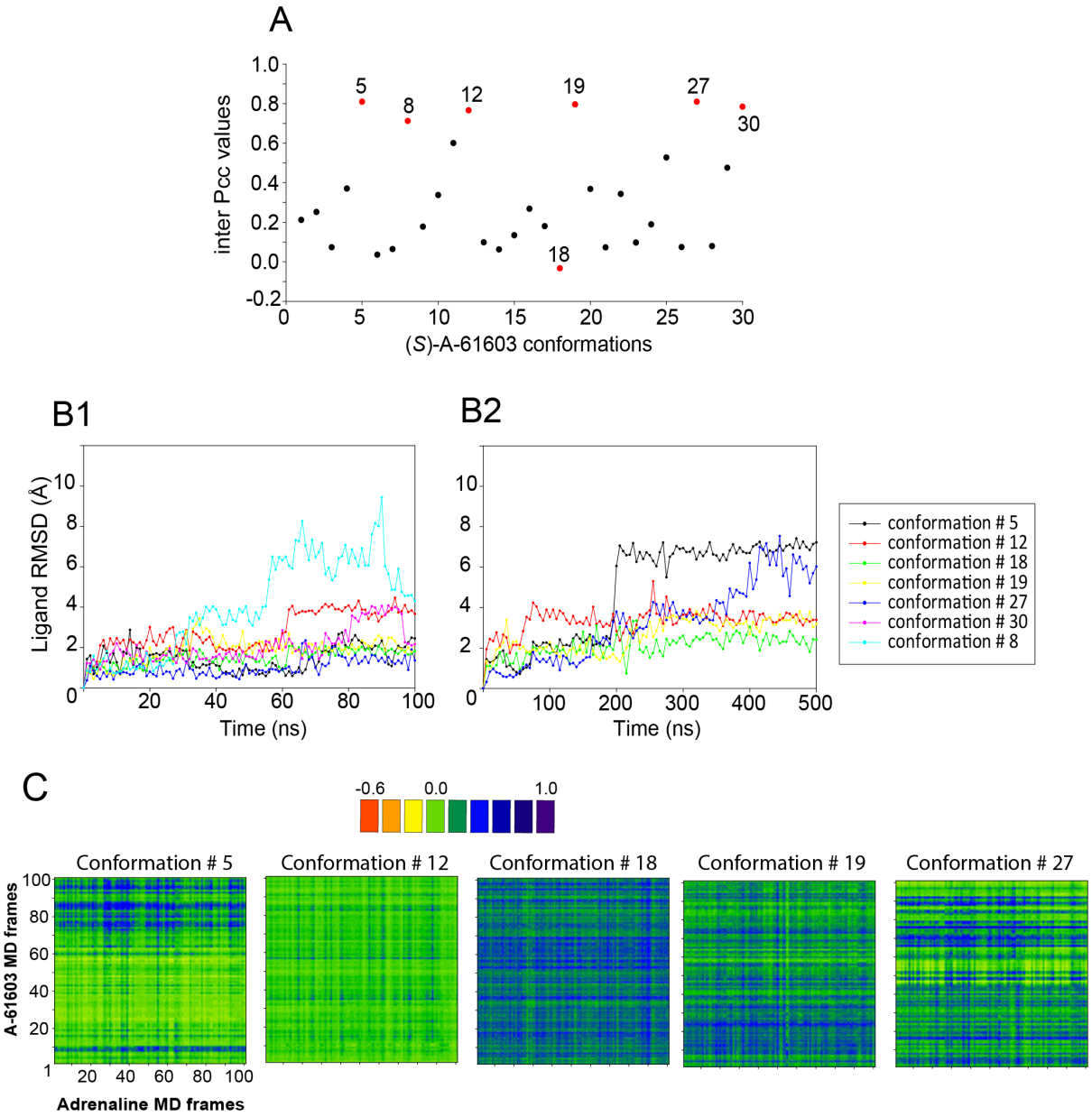

Supplementary Figure 6. Computational analysis of (*S*)-A-61603 binding to α_{1A}-AR A4. (A) A plot showing INPHARMA Pcc (Pearson correlation coefficient) score for each of the 30 (*S*)-A-61603 docked conformations on α_{1A}-AR A4. Selected conformations are marked in red and numbered. (B) RMSD plots of the selected (*S*)-A-61603 conformations. (B1) RMSD across 100 ns MD simulation. (B2) RMSD of the selected stable conformations across 500 ns MD. (C) Heat map representing the Pcc scores between the extracted MD frames. The values are arranged in the temporal order of the adrenaline and A-61603 simulation in the x- and y-dimension, respectively.

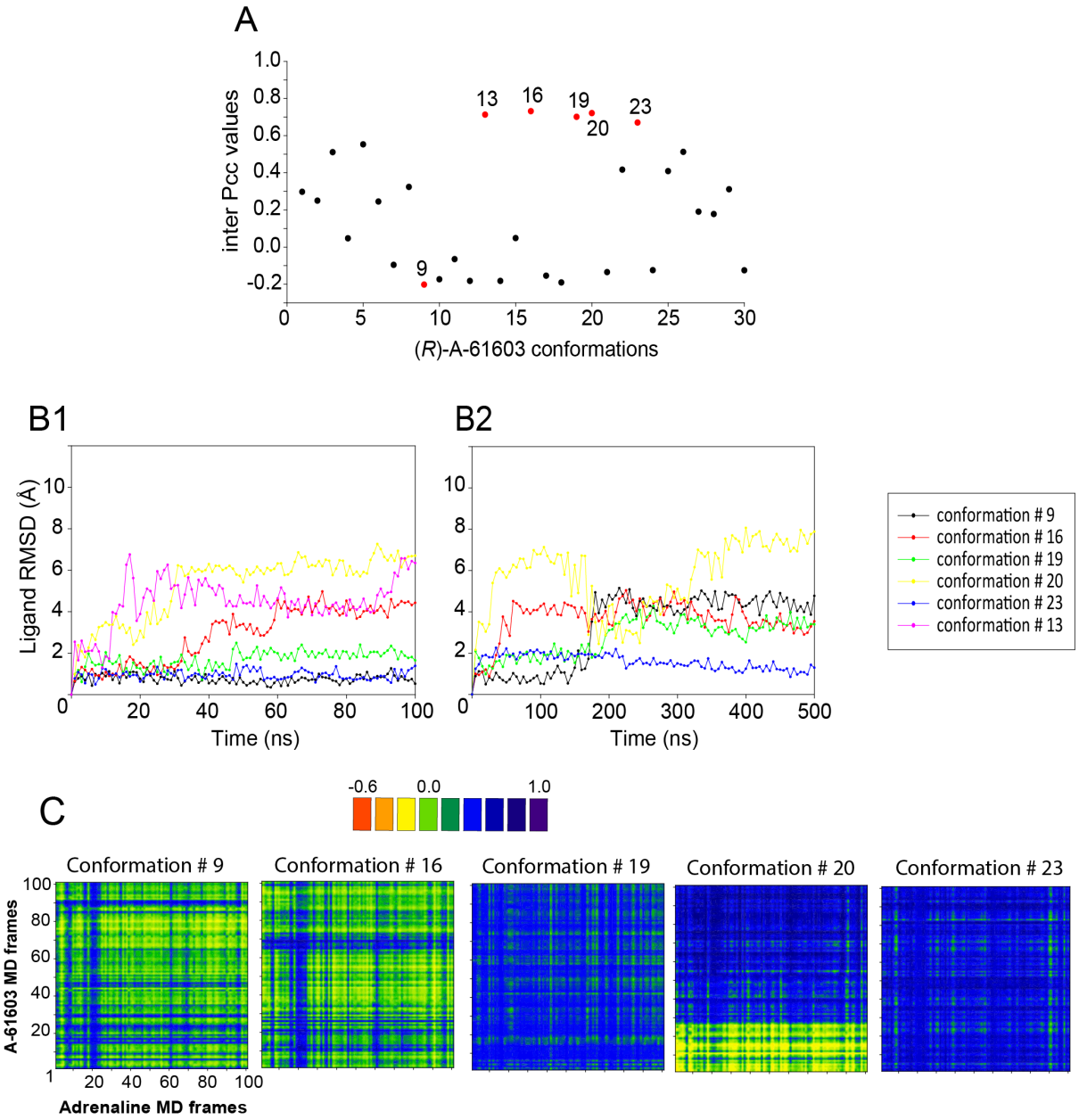

Supplementary Figure 7. Computational analysis of (*R*)-A-61603 binding to α_{1B}-AR #15. (A) A plot showing INPHARMA Pcc (Pearson correlation coefficient) score for each of the 30 (*R*)-A-61603 docked conformations on α_{1B}-AR #15. Selected conformations are marked in red and numbered. (B) RMSD plots of the selected (*R*)-A-61603 conformations. (B1) RMSD across 100 ns MD simulation. (B2) RMSD of the selected stable conformations across 500 ns MD. (C) Heat map representing the Pcc scores between the extracted MD frames. The values are arranged in the temporal order of the adrenaline and A-61603 simulation in the x- and y-dimension, respectively.

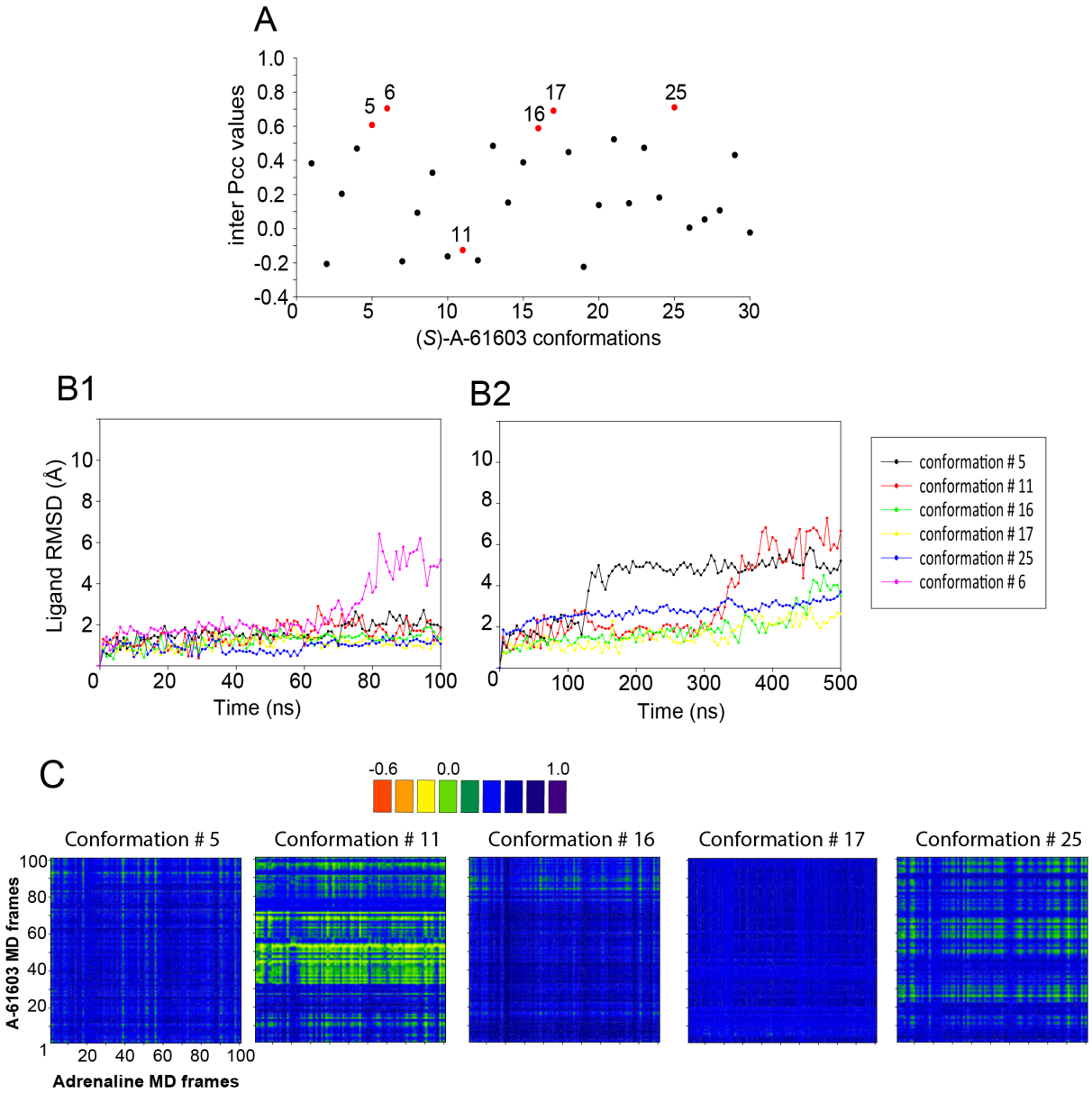

Supplementary Figure 8. Computational analysis of (*S*)-A-61603 binding to α_{1B}-AR #15. (A) A plot showing INPHARMA Pcc (Pearson correlation coefficient) score for each of the 30 (*R*)-A-61603 docked conformations on α_{1B}-AR #15. Selected conformations are marked in red and numbered. (B) RMSD plots of the selected (*S*)-A-61603 conformations. (B1) RMSD across 100 ns MD simulation. (B2) RMSD of the selected stable conformations across 500 ns MD. (C) Heat map representing the Pcc scores between the extracted MD frames. The values are arranged in the temporal order of the adrenaline and A-61603 simulation in the x- and y-dimension, respectively.

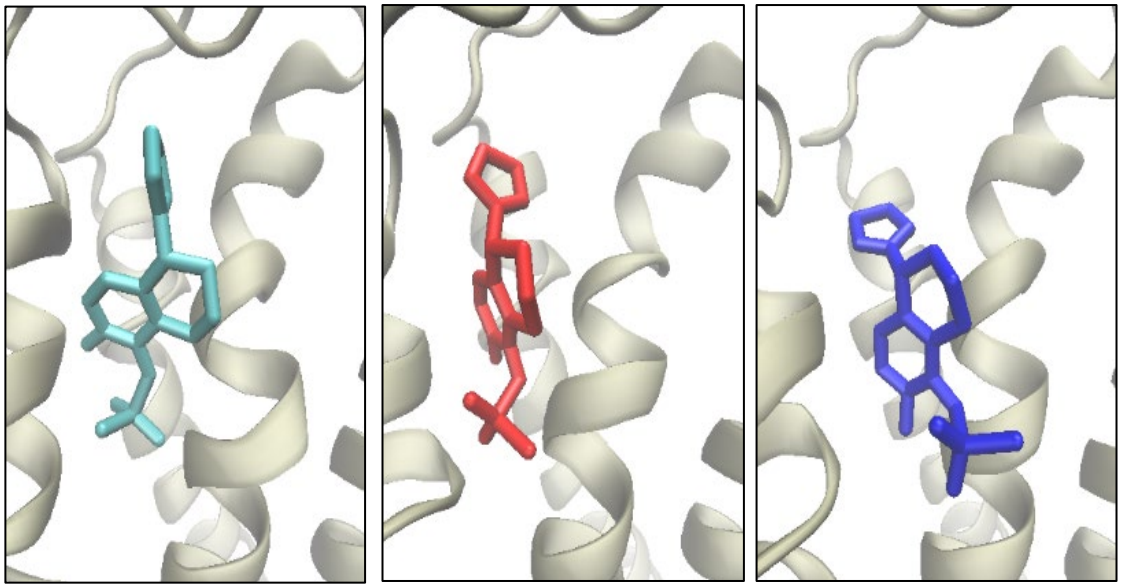

Supplementary Figure 9. Comparison of the high Pcc scoring poses of (*R*)-A-61603 on α_{1A}-AR A4. Conformation #3 in cyan, #12 in red and #25 in blue. All three poses are in the same orientation but distinct conformations.

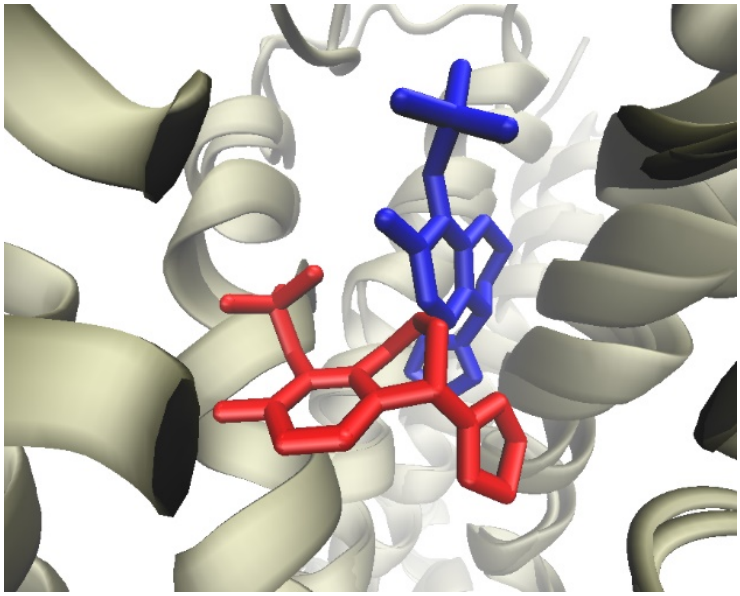

Supplementary Figure 10. (*S*)-A-61603 Conf #18 on α_{1A}-AR A4. In red, is the docked conformation before the relaxation phase in MD. In blue, the conformation of S-A-61603 after the relaxation in MD i.e. the first frame of the MD simulation.

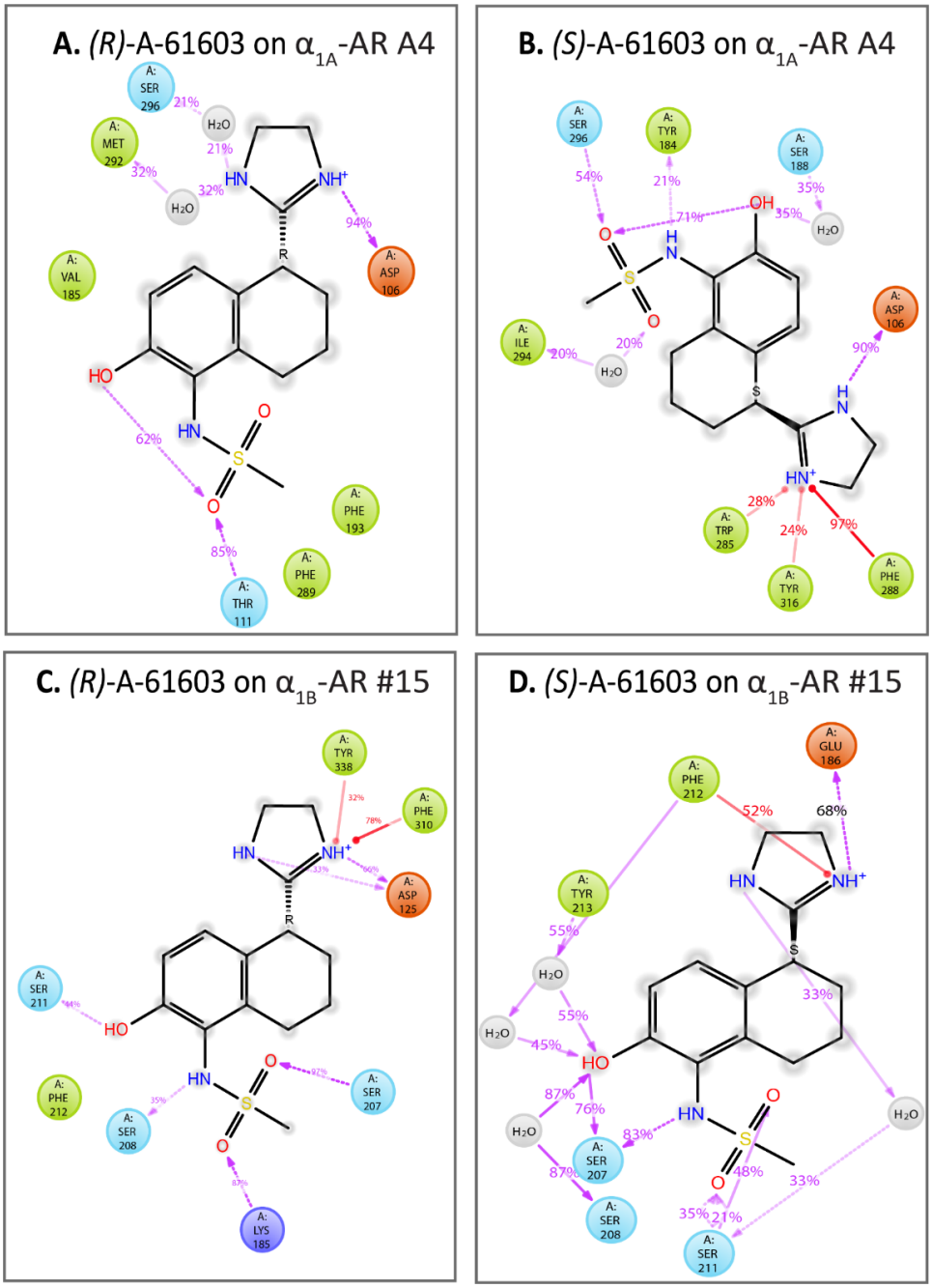

Supplementary Figure 11. Ligand Interaction maps. A schematic of ligand atom interactions of the selected conformations (A) #3 of (*R*)-A-61603 and (B) #18 of (*S*)-A-61603 with α_{1A}-AR A4 residues. And (C) #23 of (*R*)-A-61603 and (D) #17 of (*S*)-A-61603 with α_{1B}-AR #15 residues. Interactions that occur more than 20.0% of the simulation time in the selected trajectory (250.00 through 500.50 ns) are shown. The data are plotted using Simulation interactions diagram (SID) tool in Maestro 11.7.012. Hydrophobic residues are coloured green, acidic residues are red, basic residues are purple and polar residues are light blue. Connecting lines in purple: H-bond, green: π-π stacking, orange: π-cation.

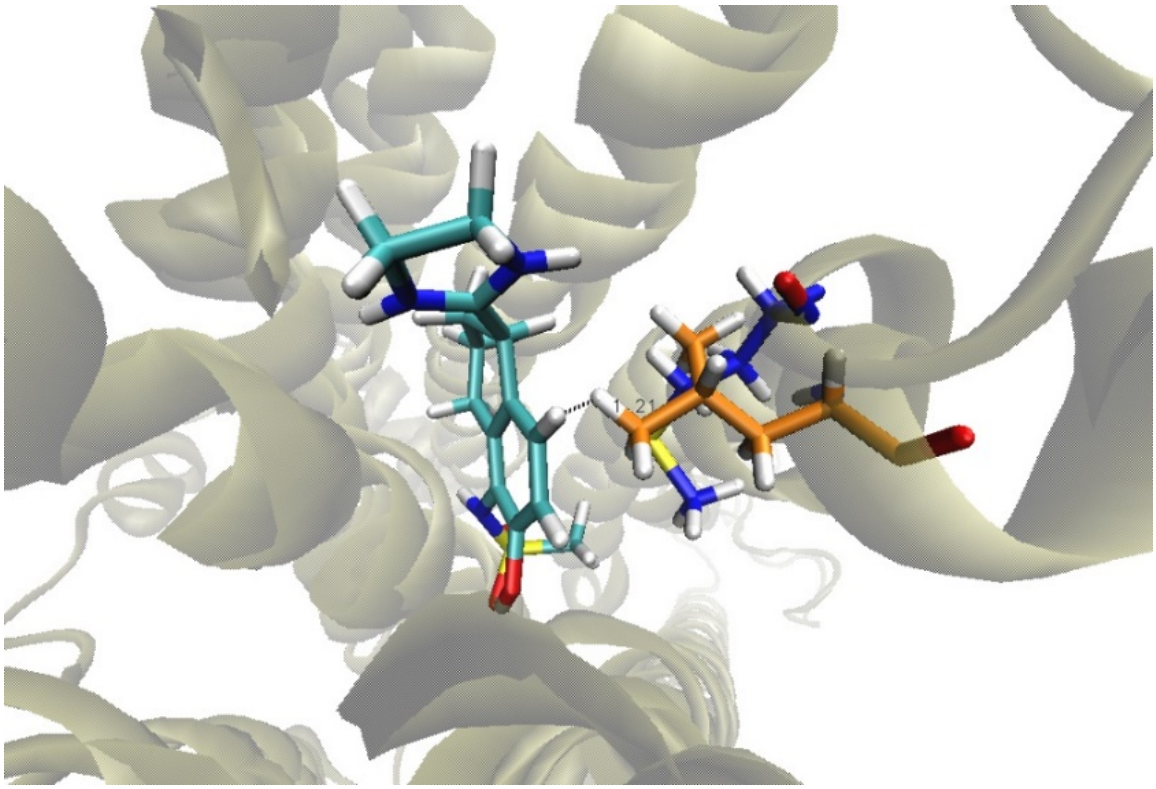

Supplementary Figure 12. The potential steric clash caused by the presence of Leu314$^{6.55x55}$ in α_{1B}-AR #15. (*R*)-A-61603 bound to α_{1A}-AR, superimposed to α_{1B}-AR #15. Key residue, M292$^{6.55x55}$ involved in the interaction of (*R*)-A-61603 with α_{1A}-AR A4 is shown in blue and the corresponding residue L314 in α_{1B}-AR #15 is shown in orange. The side chain of Leu314 is very close (1.21 Å) to the superimposed (*R*)-A-61603. The (*R*)-A-61603 conformation (in cyan) shown here is the top scoring MD pose of the selected conformation #3 on α_{1A}-AR.

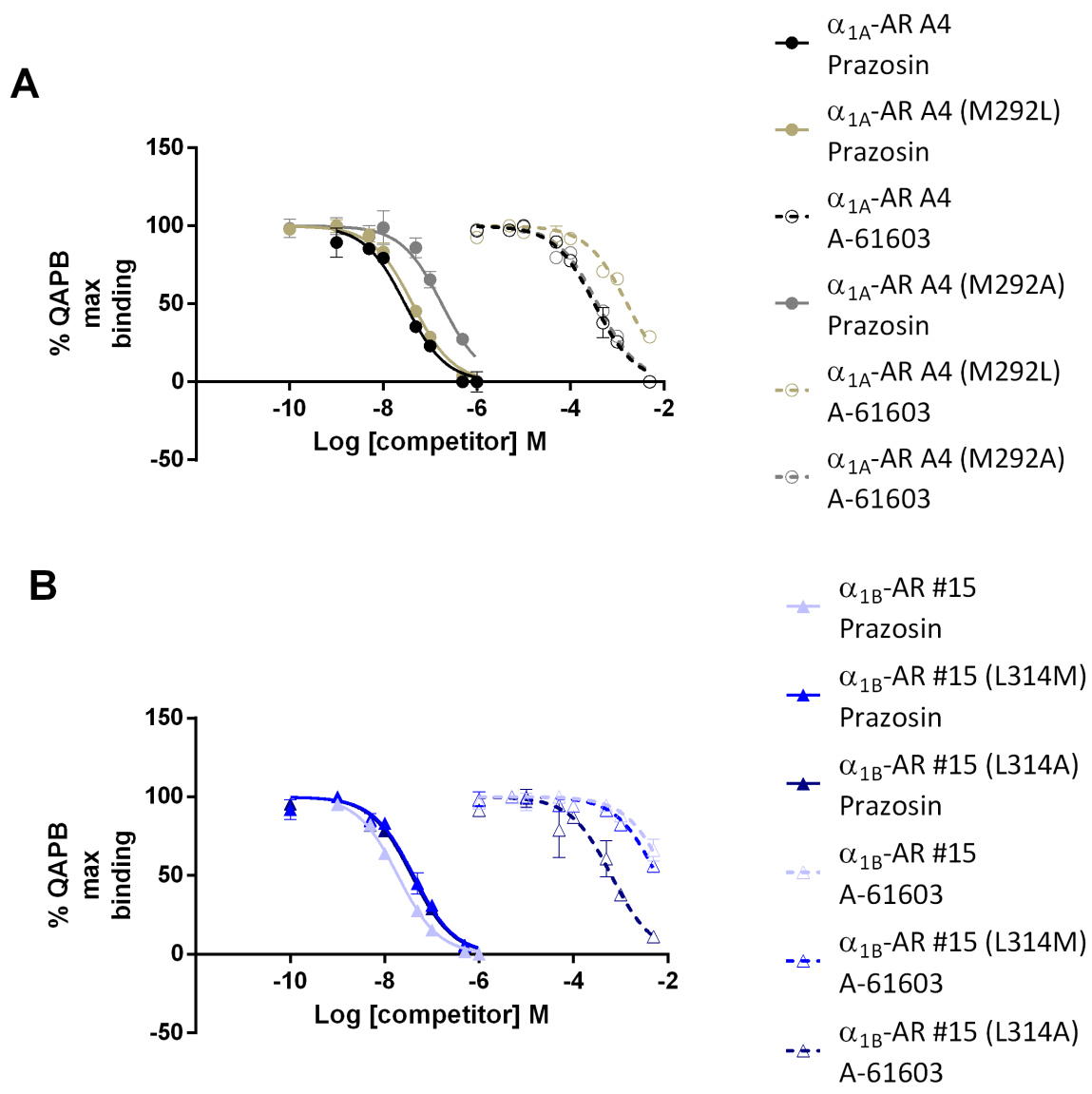

Supplementary Figure 13. QAPB competition binding experiments. (A) QAPB competition binding against purified α_{1A}-AR A4 (black circles and lines) α_{1A}-AR M292L (light brown circles and lines) and α_{1A}-AR M292A (grey circles and lines). (B) QAPB competition binding against purified α_{1B}-AR #15 (light purple triangles and lines) α_{1B}-AR #15 L314M (blue triangles and lines) and α_{1B}-AR #15 L314A (dark blue triangles and lines). Open symbols and dashed lines in (A) and (B) indicate competition with A-61603, whereas solid symbols and lines are from the competition with prazosin.

REFERENCES

1. Lefkowitz, R. J. A Brief History of G-Protein Coupled Receptors (Nobel Lecture). *Angewandte Chemie International Edition* **52**, 6366–6378 (2013).
2. Salon, J. A., Lodowski, D. T. & Palczewski, K. The Significance of G Protein-Coupled Receptor Crystallography for Drug Discovery. *Pharmacol Rev* **63**, 901–937 (2011).
3. Hargrave, P. A. & McDowell, J. H. Rhodopsin and phototransduction: a model system for G protein-linked receptors. *The FASEB Journal* **6**, 2323–2331 (1992).
4. Hanlon, C. D. & Andrew, D. J. Outside-in signaling – a brief review of GPCR signaling with a focus on the Drosophila GPCR family. *J Cell Sci* **128**, 3533–3542 (2015).
5. Venter, J. C. *et al.* The Sequence of the Human Genome. *Science* **291**, 1304–1351 (2001).
6. Katritch, V., Cherezov, V. & Stevens, R. C. Structure-Function of the G-protein-Coupled Receptor Superfamily. *Annu Rev Pharmacol Toxicol* **53**, 531–556 (2013).
7. Wettschureck, N. & Offermanns, S. Mammalian G proteins and their cell type specific functions. *Physiol Rev* **85**, 1159–204 (2005).
8. Pierce, K. L., Premont, R. T. & Lefkowitz, R. J. Signalling: Seven-transmembrane receptors. *Nature Reviews Molecular Cell Biology* **3**, 639–650 (2002).
9. Palczewski, K. *et al.* Crystal Structure of Rhodopsin: A G Protein-Coupled Receptor. *Science* **289**, 739–745 (2000).
10. Rasmussen, S. G. *et al.* Crystal structure of the beta2 adrenergic receptor-Gs protein complex. *Nature* **477**, 549–555 (2011).
11. Pándy-Szekeres, G. *et al.* GPCRdb in 2018: adding GPCR structure models and ligands. *Nucleic Acids Res* **46**, D440–D446 (2018).
12. Draper-Joyce, C. J. *et al.* Structure of the adenosine-bound human adenosine A1 receptor-Gi complex. *Nature* **558**, 559–563 (2018).
13. Zhang, Y. *et al.* Cryo-EM structure of the activated GLP-1 receptor in complex with a G protein. *Nature* **546**, 248–253 (2017).
14. Koehl, A. *et al.* Structure of the μ-opioid receptor-Gi protein complex. *Nature* **558**, 547–552 (2018).
15. Liang, Y.-L. *et al.* Phase-plate cryo-EM structure of a class B GPCR-G-protein complex. *Nature* **546**, 118–123 (2017).
16. García-Nafría, J., Nehmé, R., Edwards, P. C. & Tate, C. G. Cryo-EM structure of the serotonin 5-HT1B receptor coupled to heterotrimeric Go. *Nature* **558**, 620–623 (2018).

17. Kang, Y. *et al.* Cryo-EM structure of human rhodopsin bound to an inhibitory G protein. *Nature* **558**, 553–558 (2018).
18. Maeda, S., Qu, Q., Robertson, M. J., Skiniotis, G. & Kobilka, B. K. Structures of the M1 and M2 muscarinic acetylcholine receptor/G-protein complexes. *Science* **364**, 552–557 (2019).
19. Park, S. H. *et al.* Structure of the chemokine receptor CXCR1 in phospholipid bilayers. *Nature* **491**, 779–783 (2012).
20. Buchen, L. Cell signalling: It's all about the structure. *Nature* **476**, 387–390 (2011).
21. Downes, G. B. & Gautam, N. The G protein subunit gene families. *Genomics* **62**, 544–552 (1999).
22. Oldham, W. M., Van Eps, N., Preininger, A. M., Hubbell, W. L. & Hamm, H. E. Mechanism of the receptor-catalyzed activation of heterotrimeric G proteins. *Nature structural & molecular biology* **13**, 772 (2006).
23. Gutkind, J. S. Regulation of Mitogen-Activated Protein Kinase Signaling Networks by G Protein-Coupled Receptors. *Sci. STKE* **2000**, re1–re1 (2000).
24. Karnik, S. S., Gogonea, C., Patil, S., Saad, Y. & Takezako, T. Activation of G-protein-coupled receptors: a common molecular mechanism. *Trends in Endocrinology & Metabolism* **14**, 431–437 (2003).
25. Freissmuth, M., Casey, P. J. & Gilman, A. G. G proteins control diverse pathways of transmembrane signaling. *The FASEB Journal* **3**, 2125–2131 (1989).
26. Rosenbaum, D. M., Rasmussen, S. G. & Kobilka, B. K. The structure and function of G-protein-coupled receptors. *Nature* **459**, 356–63 (2009).
27. Palczewski, K., Buczy\lko, J., Kaplan, M. W., Polans, A. S. & Crabb, J. W. Mechanism of rhodopsin kinase activation. *Journal of Biological Chemistry* **266**, 12949–12955 (1991).
28. Luttrell, L. M. *et al.* β-Arrestin-Dependent Formation of β2 Adrenergic Receptor-Src Protein Kinase Complexes. *Science* **283**, 655–661 (1999).
29. Pitcher, J. A., Freedman, N. J. & Lefkowitz, R. J. G protein–coupled receptor kinases. *Annu. Rev. Biochem.* **67**, 653–692 (1998).
30. Drake Matthew T., Shenoy Sudha K. & Lefkowitz Robert J. Trafficking of G Protein–Coupled Receptors. *Circulation Research* **99**, 570–582 (2006).
31. Lefkowitz, R. J. & Shenoy, S. K. Transduction of receptor signals by \s s-arrestins. *Science* **308**, 512–517 (2005).
32. Irannejad, R. *et al.* Conformational biosensors reveal GPCR signalling from endosomes. *Nature* **495**, 534 (2013).

33. Nobles, K. N. *et al.* Distinct phosphorylation sites on the β2-adrenergic receptor establish a barcode that encodes differential functions of β-arrestin. *Sci. Signal.* **4**, ra51–ra51 (2011).
34. Tobin, A. B., Butcher, A. J. & Kong, K. C. Location, location, location…site-specific GPCR phosphorylation offers a mechanism for cell-type-specific signalling. *Trends in Pharmacological Sciences* **29**, 413–420 (2008).
35. Attwood, T. K. & Findlay, J. B. C. Fingerprinting G-protein-coupled receptors. *Protein Engineering, Design and Selection* **7**, 195–203 (1994).
36. Kolakowski, J. L. GCRDb: a G-protein-coupled receptor database. *Receptors & channels* **2**, 1–7 (1994).
37. Schiöth, H. B. & Fredriksson, R. The GRAFS classification system of G-protein coupled receptors in comparative perspective. *General and comparative endocrinology* **142**, 94–101 (2005).
38. Fredriksson, R., Lagerström, M. C., Lundin, L.-G. & Schiöth, H. B. The G-protein-coupled receptors in the human genome form five main families. Phylogenetic analysis, paralogon groups, and fingerprints. *Mol. Pharmacol.* **63**, 1256–1272 (2003).
39. Nordström, K. J. V., Sällman Almén, M., Edstam, M. M., Fredriksson, R. & Schiöth, H. B. Independent HHsearch, Needleman–Wunsch-Based, and Motif Analyses Reveal the Overall Hierarchy for Most of the G Protein-Coupled Receptor Families. *Mol Biol Evol* **28**, 2471–2480 (2011).
40. Lagerstrom, M. C. & Schioth, H. B. Structural diversity of G protein-coupled receptors and significance for drug discovery. *Nat Rev Drug Discov* **7**, 339–57 (2008).
41. Gloriam, D. E., Fredriksson, R. & Schiöth, H. B. The G protein-coupled receptor subset of the rat genome. *BMC genomics* **8**, 338 (2007).
42. Wacker, D., Stevens, R. C. & Roth, B. L. How Ligands Illuminate GPCR Molecular Pharmacology. *Cell* **170**, 414–427 (2017).
43. Ballesteros, J. A. & Weinstein, H. [19] Integrated methods for the construction of three-dimensional models and computational probing of structure-function relations in G protein-coupled receptors. in *Methods in neurosciences* **25**, 366–428 (Elsevier, 1995).
44. Deupi, X. & Standfuss, J. Structural insights into agonist-induced activation of G-protein-coupled receptors. *Current opinion in structural biology* **21**, 541–551 (2011).
45. Trzaskowski, B. *et al.* Action of Molecular Switches in GPCRs - Theoretical and Experimental Studies. *Curr Med Chem* **19**, 1090–1109 (2012).
46. Angel, T. E., Chance, M. R. & Palczewski, K. Conserved waters mediate structural and functional activation of family A (rhodopsin-like) G protein-coupled receptors. *Proceedings of the National Academy of Sciences* **106**, 8555–8560 (2009).

47. Fredriksson, R. & Schiöth, H. B. The Repertoire of G-Protein–Coupled Receptors in Fully Sequenced Genomes. *Mol Pharmacol* **67**, 1414–1425 (2005).
48. Bayliss, W. M. & Starling, E. H. The mechanism of pancreatic secretion. *The Journal of Physiology* **28**, 325–353 (1902).
49. Jensen, R. T. & Gardner, J. D. Identification and characterization of receptors for secretagogues on pancreatic acinar cells. in *Federation proceedings* **40**, 2486–2496 (1981).
50. Chang, T. & Chey, W. Y. Radioimmunoassay of secretin. *Digest Dis Sci* **25**, 529–552 (1980).
51. Watkins, H. A., Au, M. & Hay, D. L. The structure of secretin family GPCR peptide ligands: implications for receptor pharmacology and drug development. *Drug Discovery Today* **17**, 1006–1014 (2012).
52. Hoare, S. R. Mechanisms of peptide and nonpeptide ligand binding to Class B G-protein-coupled receptors. *Drug discovery today* **10**, 417–427 (2005).
53. Siu, F. Y. *et al.* Structure of the human glucagon class B G-protein-coupled receptor. *Nature* **499**, 444–449 (2013).
54. Koth, C. M. *et al.* Molecular basis for negative regulation of the glucagon receptor. *Proceedings of the National Academy of Sciences* **109**, 14393–14398 (2012).
55. Ishihara, T. *et al.* Molecular cloning and expression of a cDNA encoding the secretin receptor. *The EMBO Journal* **10**, 1635–1641 (1991).
56. Ishihara, T., Shigemoto, R., Mori, K., Takahashi, K. & Nagata, S. Functional expression and tissue distribution of a novel receptor for vasoactive intestinal polypeptide. *Neuron* **8**, 811–819 (1992).
57. Juppner, H. *et al.* AG protein-linked receptor for parathyroid hormone and parathyroid hormone-related peptide. *Science* **254**, 1024–1026 (1991).
58. Lin, H. Y. *et al.* Expression cloning of an adenylate cyclase-coupled calcitonin receptor. *Science* **254**, 1022–1024 (1991).
59. Hollenstein, K. *et al.* Structure of class B GPCR corticotropin-releasing factor receptor 1. *Nature* **499**, 438–443 (2013).
60. Tissir, F., Bar, I., Jossin, Y., Backer, O. D. & Goffinet, A. M. Protocadherin Celsr3 is crucial in axonal tract development. *Nature Neuroscience* **8**, 451 (2005).
61. Waller-Evans, H. *et al.* The Orphan Adhesion-GPCR GPR126 Is Required for Embryonic Development in the Mouse. *PLOS ONE* **5**, e14047 (2010).
62. Kuhnert, F. *et al.* Essential Regulation of CNS Angiogenesis by the Orphan G Protein–Coupled Receptor GPR124. *Science* **330**, 985–989 (2010).

63. Langenhan, T. *et al.* Latrophilin Signaling Links Anterior-Posterior Tissue Polarity and Oriented Cell Divisions in the C. elegans Embryo. *Developmental Cell* **17**, 494–504 (2009).
64. Lawrence, P. A., Struhl, G. & Casal, J. Planar cell polarity: one or two pathways? *Nature Reviews Genetics* **8**, 555–563 (2007).
65. Harmar, A. J. Family-B G-protein-coupled receptors. *Genome biology* **2**, reviews3013–1 (2001).
66. Bjarnadóttir, T. K. *et al.* The human and mouse repertoire of the adhesion family of G-protein-coupled receptors. *Genomics* **84**, 23–33 (2004).
67. Hamann, J. *et al.* International union of basic and clinical pharmacology. xciv. adhesion g protein–coupled receptors. *Pharmacological reviews* **67**, 338–367 (2015).
68. Araç, D. *et al.* A novel evolutionarily conserved domain of cell-adhesion GPCRs mediates autoproteolysis. *The EMBO journal* **31**, 1364–1378 (2012).
69. Langenhan, T., Aust, G. & Hamann, J. Sticky signaling—Adhesion class G protein–coupled receptors take the stage. *Sci. Signal.* **6**, re3–re3 (2013).
70. Bjarnadóttir, T. K., Fredriksson, R. & Schiöth, H. B. The gene repertoire and the common evolutionary history of glutamate, pheromone (V2R), taste (1) and other related G protein-coupled receptors. *Gene* **362**, 70–84 (2005).
71. Chun, L., Zhang, W. & Liu, J. Structure and ligand recognition of class C GPCRs. *Acta Pharmacologica Sinica* **33**, 312–323 (2012).
72. Meldrum, B. S. Glutamate as a neurotransmitter in the brain: review of physiology and pathology. *The Journal of nutrition* **130**, 1007S–1015S (2000).
73. Marek, G. J. Metabotropic glutamate 2/3 receptors as drug targets. *Current opinion in pharmacology* **4**, 18–22 (2004).
74. Swanson, C. J. *et al.* Metabotropic glutamate receptors as novel targets for anxiety and stress disorders. *Nature reviews Drug discovery* **4**, 131 (2005).
75. Bettler, B., Kaupmann, K., Mosbacher, J. & Gassmann, M. Molecular structure and physiological functions of GABAB receptors. *Physiological reviews* **84**, 835–867 (2004).
76. Bessis, A.-S. *et al.* Closure of the Venus flytrap module of mGlu8 receptor and the activation process: Insights from mutations converting antagonists into agonists. *PNAS* **99**, 11097–11102 (2002).
77. Morrill, G. A., Kostellow, A. B. & Gupta, R. K. Computational analysis of the extracellular domain of the Ca2+-sensing receptor: An alternate model for the Ca2+ sensing region. *Biochemical and biophysical research communications* **459**, 36–41 (2015).
78. Kunishima, N. *et al.* Structural basis of glutamate recognition by a dimeric metabotropic glutamate receptor. *Nature* **407**, 971 (2000).

79. Wu, H. *et al.* Structure of a class C GPCR metabotropic glutamate receptor 1 bound to an allosteric modulator. *Science* **344**, 58–64 (2014).
80. Doré, A. S. *et al.* Structure of class C GPCR metabotropic glutamate receptor 5 transmembrane domain. *Nature* **511**, 557–562 (2014).
81. Foord, S. M. *et al.* International Union of Pharmacology. XLVI. G protein-coupled receptor list. *Pharmacol. Rev.* **57**, 279–288 (2005).
82. Schulte, G. International union of basic and clinical pharmacology. LXXX. The class Frizzled receptors. *Pharmacological reviews* **62**, 632–667 (2010).
83. Willert, K. & Nusse, R. Wnt proteins. *Cold Spring Harbor perspectives in biology* **4**, a007864 (2012).
84. Kurayoshi, M., Yamamoto, H., Izumi, S. & Kikuchi, A. Post-translational palmitoylation and glycosylation of Wnt-5a are necessary for its signalling. *Biochemical Journal* **402**, 515–523 (2007).
85. Nichols, A. S., Floyd, D. H., Bruinsma, S. P., Narzinski, K. & Baranski, T. J. Frizzled receptors signal through G proteins. *Cellular signalling* **25**, 1468–1475 (2013).
86. Dijksterhuis, J. P., Petersen, J. & Schulte, G. WNT/Frizzled signalling: receptor–ligand selectivity with focus on FZD-G protein signalling and its physiological relevance: IUPHAR Review 3. *British journal of pharmacology* **171**, 1195–1209 (2014).
87. Schulte, G. & Bryja, V. The Frizzled family of unconventional G-protein-coupled receptors. *Trends in Pharmacological Sciences* **28**, 518–525 (2007).
88. Ruiz-Gómez, A., Molnar, C., Holguín, H., Mayor Jr, F. & de Celis, J. F. The cell biology of Smo signalling and its relationships with GPCRs. *Biochimica et Biophysica Acta (BBA)-Biomembranes* **1768**, 901–912 (2007).
89. Adler, E. *et al.* A novel family of mammalian taste receptors. *Cell* **100**, 693–702 (2000).
90. Foster, S. R. *et al.* Expression, regulation and putative nutrient-sensing function of taste GPCRs in the heart. *PLoS One* **8**, e64579 (2013).
91. Wang, C. *et al.* Structural basis for Smoothened receptor modulation and chemoresistance to anticancer drugs. *Nat Commun* **5**, 4355 (2014).
92. Wang, C. *et al.* Structure of the human smoothened receptor bound to an antitumour agent. *Nature* **497**, 338 (2013).
93. Weierstall, U. *Lipidic cubic phase injector facilitates membrane protein serial femtosecond crystallography (CXIDB ID 39)*. (Coherent X-ray Imaging Data Bank (Lawrence Berkeley National Laboratory …, 2016).

94. Zhang, X., Stevens, R. C. & Xu, F. The importance of ligands for G protein-coupled receptor stability. *Trends Biochem. Sci.* **40**, 79–87 (2015).
95. Hauser, A. S., Attwood, M. M., Rask-Andersen, M., Schiöth, H. B. & Gloriam, D. E. Trends in GPCR drug discovery: new agents, targets and indications. *Nature Reviews Drug Discovery* **16**, 829–842 (2017).
96. Roth, B. L. & Kroeze, W. K. Integrated Approaches for Genome-wide Interrogation of the Druggable Non-olfactory G Protein-coupled Receptor Superfamily. *J. Biol. Chem.* **290**, 19471–19477 (2015).
97. Rask-Andersen, M., Almén, M. S. & Schiöth, H. B. Trends in the exploitation of novel drug targets. *Nature Reviews Drug Discovery* **10**, 579–590 (2011).
98. Lafferty-Whyte, K., Mormeneo, D. & del Fresno Marimon, M. Trial watch: Opportunities and challenges of the 2016 target landscape. *Nature Reviews Drug Discovery* **16**, 10–11 (2016).
99. Moore, A. R. *et al.* Recurrent activating mutations of G-protein-coupled receptor *CYSLTR2* in uveal melanoma. *Nature Genetics* **48**, 675–680 (2016).
100. McAlear, S. D., Kraft, T. W. & Gross, A. K. 1 Rhodopsin Mutations in Congenital Night Blindness. in *Retinal Degenerative Diseases: Laboratory and Therapeutic Investigations* (eds. Anderson, R. E., Hollyfield, J. G. & LaVail, M. M.) 263–272 (Springer New York, 2010). doi:10.1007/978-1-4419-1399-9_30
101. Smit, M. J. *et al.* Pharmacogenomic and Structural Analysis of Constitutive G Protein–Coupled Receptor Activity. *Annu. Rev. Pharmacol. Toxicol.* **47**, 53–87 (2007).
102. Pan, Y., Metzenberg, A., Das, S., Jing, B. & Gitschier, J. Mutations in the V2 vasopressin receptor gene are associated with X–linked nephrogenic diabetes insipidus. *Nature Genetics* **2**, 103 (1992).
103. Becker, E. L., Kanaho, Y. & Kermode, J. C. Nature and functioning of the pertussis toxin-sensitive G protein of neutrophils. *Biomed Pharmacother* **41**, 289–297 (1987).
104. Lappano, R. & Maggiolini, M. G protein-coupled receptors: novel targets for drug discovery in cancer. *Nature Reviews Drug Discovery* **10**, 47–60 (2011).
105. Bhola, N. E. & Grandis, J. R. Crosstalk between G-protein-coupled receptors and epidermal growth factor receptor in cancer. *Frontiers in bioscience : a journal and virtual library* **13**, 1857–1865 (2008).
106. Roth, B. L., Sheffler, D. J. & Kroeze, W. K. Magic shotguns versus magic bullets: selectively non-selective drugs for mood disorders and schizophrenia. *Nature Reviews Drug Discovery* **3**, 353–359 (2004).

107. Rothman Richard B. *et al.* Evidence for Possible Involvement of 5-HT2B Receptors in the Cardiac Valvulopathy Associated With Fenfluramine and Other Serotonergic Medications. *Circulation* **102**, 2836–2841 (2000).
108. Roth, B. L. Drugs and Valvular Heart Disease. *New England Journal of Medicine* **356**, 6–9 (2007).
109. Overington, J. P., Al-Lazikani, B. & Hopkins, A. L. How many drug targets are there? *Nat Rev Drug Discov* **5**, 993–6 (2006).
110. Orzechowski, R. F., Currie, D. S. & Valancius, C. A. Comparative anticholinergic activities of 10 histamine H1 receptor antagonists in two functional models. *European journal of pharmacology* **506**, 257–264 (2005).
111. Snowman, A. M. & Snyder, S. H. Cetirizine: actions on neurotransmitter receptors. *Journal of Allergy and Clinical Immunology* **86**, 1025–1028 (1990).
112. Haraguchi, K., Ito, K., Kotaki, H., Sawada, Y. & Iga, T. Prediction of drug-induced catalepsy based on dopamine D1, D2, and muscarinic acetylcholine receptor occupancies. *Drug metabolism and disposition* **25**, 675–684 (1997).
113. Allen, J. A. & Roth, B. L. Strategies to Discover Unexpected Targets for Drugs Active at G Protein–Coupled Receptors. *Annu. Rev. Pharmacol. Toxicol.* **51**, 117–144 (2011).
114. Clark, A. J. The antagonism of acetyl choline by atropine. *The Journal of Physiology* **61**, 547–556 (1926).
115. Roth, B. L. DREADDs for Neuroscientists. *Neuron* **89**, 683–694 (2016).
116. Isberg, V. *et al.* Generic GPCR residue numbers - aligning topology maps while minding the gaps. *Trends Pharmacol. Sci.* **36**, 22–31 (2015).
117. Chan, H. C. S., Li, Y., Dahoun, T., Vogel, H. & Yuan, S. New Binding Sites, New Opportunities for GPCR Drug Discovery. *Trends in Biochemical Sciences* **44**, 312–330 (2019).
118. Guarnera, E. & Berezovsky, I. N. Allosteric sites: remote control in regulation of protein activity. *Current Opinion in Structural Biology* **37**, 1–8 (2016).
119. Burford, N. T. *et al.* Discovery of positive allosteric modulators and silent allosteric modulators of the μ-opioid receptor. *Proc Natl Acad Sci U S A* **110**, 10830–10835 (2013).
120. Christopoulos, A. *et al.* International Union of Basic and Clinical Pharmacology. XC. Multisite Pharmacology: Recommendations for the Nomenclature of Receptor Allosterism and Allosteric Ligands. *Pharmacol Rev* **66**, 918–947 (2014).
121. Fenalti, G. *et al.* Molecular control of δ-opioid receptor signalling. *Nature* **506**, 191–196 (2014).
122. Kenakin, T. & Boselli, C. Pharmacologic discrimination between receptor heterogeneity and allosteric interaction: resultant analysis of gallamine and pirenzepine antagonism of muscarinic responses in rat trachea. *J Pharmacol Exp Ther* **250**, 944–952 (1989).

123. Hawtin, S. R. *et al.* Charged Extracellular Residues, Conserved throughout a G-protein-coupled Receptor Family, Are Required for Ligand Binding, Receptor Activation, and Cell-surface Expression. *J. Biol. Chem.* **281**, 38478–38488 (2006).
124. Fan, Y., Li, C., Guo, J., Hu, G. & Wu, G. A Single Lys Residue on the First Intracellular Loop Modulates the Endoplasmic Reticulum Export and Cell-Surface Expression of α2A-Adrenergic Receptor. *PLOS ONE* **7**, e50416 (2012).
125. Ragnarsson, L., Andersson, \AAsa, Thomas, W. G. & Lewis, R. J. Extracellular surface residues of the α1B-adrenoceptor critical for G protein–coupled receptor function. *Molecular pharmacology* **87**, 121–129 (2015).
126. Audet, M. & Bouvier, M. Restructuring G-protein-coupled receptor activation. *Cell* **151**, 14–23 (2012).
127. Baker, J. G. & Hill, S. J. Multiple GPCR conformations and signalling pathways: implications for antagonist affinity estimates. *Trends in Pharmacological Sciences* **28**, 374–381 (2007).
128. Kruse, A. C. *et al.* Activation and allosteric modulation of a muscarinic acetylcholine receptor. *Nature* **504**, 101–106 (2013).
129. Srivastava, A. *et al.* High-resolution structure of the human GPR40 receptor bound to allosteric agonist TAK-875. *Nature* **513**, 124–127 (2014).
130. Cheng, R. K. Y. *et al.* Structural insight into allosteric modulation of protease-activated receptor 2. *Nature* **545**, 112–115 (2017).
131. Zhang, D. *et al.* Two disparate ligand-binding sites in the human $P2Y_1$ receptor. *Nature* **520**, 317–321 (2015).
132. Zheng, X., Gan, L., Wang, E. & Wang, J. Pocket-Based Drug Design: Exploring Pocket Space. *AAPS J* **15**, 228–241 (2013).
133. Robertson, N. *et al.* Structure of the complement C5a receptor bound to the extra-helical antagonist NDT9513727. *Nature* **553**, 111–114 (2018).
134. Lu, J. *et al.* Structural basis for the cooperative allosteric activation of the free fatty acid receptor GPR40. *Nature Structural & Molecular Biology* **24**, 570–577 (2017).
135. Liu, X. *et al.* Mechanism of intracellular allosteric β_2AR antagonist revealed by X-ray crystal structure. *Nature* **548**, 480–484 (2017).
136. Zheng, Y. *et al.* Structure of CC chemokine receptor 2 with orthosteric and allosteric antagonists. *Nature* **540**, 458–461 (2016).
137. Oswald, C. *et al.* Intracellular allosteric antagonism of the CCR9 receptor. *Nature* **540**, 462–465 (2016).

138. Liu, W. *et al.* Structural Basis for Allosteric Regulation of GPCRs by Sodium Ions. *Science* **337**, 232–236 (2012).
139. Katritch, V. *et al.* Allosteric sodium in class A GPCR signaling. *Trends in Biochemical Sciences* **39**, 233–244 (2014).
140. Yuan, S., Vogel, H. & Filipek, S. The Role of Water and Sodium Ions in the Activation of the μ-Opioid Receptor. *Angewandte Chemie International Edition* **52**, 10112–10115 (2013).
141. Hori, T. *et al.* Na^+-mimicking ligands stabilize the inactive state of leukotriene B_4 receptor BLT1. *Nature Chemical Biology* **14**, 262–269 (2018).
142. Chan, H. S. *et al.* Exploring a new ligand binding site of G protein-coupled receptors. *Chemical science* **9**, 6480–6489 (2018).
143. Urban, J. D. *et al.* Functional selectivity and classical concepts of quantitative pharmacology. *Journal of Pharmacology and Experimental Therapeutics* **320**, 1–13 (2007).
144. Zhou, X. E., Melcher, K. & Xu, H. E. Understanding the GPCR biased signaling through G protein and arrestin complex structures. *Current Opinion in Structural Biology* **45**, 150–159 (2017).
145. Warne, T., Edwards, P. C., Leslie, A. G. & Tate, C. G. Crystal Structures of a Stabilized Beta1-Adrenoceptor Bound to the Biased Agonists Bucindolol and Carvedilol. *Structure* **20**, 841 (2012).
146. Wacker, D. *et al.* Structural features for functional selectivity at serotonin receptors. *Science* **340**, 615–619 (2013).
147. Peng, Y. *et al.* 5-HT2C Receptor Structures Reveal the Structural Basis of GPCR Polypharmacology. *Cell* **172**, 719-730.e14 (2018).
148. Kruse, A. C. *et al.* Muscarinic acetylcholine receptors: novel opportunities for drug development. *Nature Reviews Drug Discovery* **13**, 549–560 (2014).
149. Thal, D. M. *et al.* Crystal structures of the M1 and M4 muscarinic acetylcholine receptors. *Nature* **531**, 335–340 (2016).
150. Kruse, A. C. *et al.* Structure and dynamics of the M3 muscarinic acetylcholine receptor. *Nature* **482**, 552–556 (2012).
151. Haga, K. *et al.* Structure of the human M2 muscarinic acetylcholine receptor bound to an antagonist. *Nature* **482**, 547–551 (2012).
152. Lee, S. M., Booe, J. M. & Pioszak, A. A. Structural insights into ligand recognition and selectivity for classes A, B, and C GPCRs. *Eur J Pharmacol* **763**, 196–205 (2015).
153. Butini, S. *et al.* Polypharmacology of dopamine receptor ligands. *Progress in Neurobiology* **142**, 68–103 (2016).

154. Korczynska, M. *et al.* Structure-based discovery of selective positive allosteric modulators of antagonists for the M2 muscarinic acetylcholine receptor. *Proceedings of the National Academy of Sciences* **115**, E2419–E2428 (2018).
155. Vecchio, E. A. *et al.* New paradigms in adenosine receptor pharmacology: allostery, oligomerization and biased agonism. *British Journal of Pharmacology* **175**, 4036–4046 (2018).
156. Livingston, K. E. & Traynor, J. R. Allostery at opioid receptors: modulation with small molecule ligands. *British Journal of Pharmacology* **175**, 2846–2856 (2018).
157. Graham, R. M. & Lanier, S. M. Identification and characterization of alpha-adrenergic receptors. *The Heart and Cardiovascular System. New York, Raven Press, Publishers* 1059–1096 (1986).
158. Ahlquist, R. P. A study of the adrenotropic receptors. *American Journal of Physiology-Legacy Content* **153**, 586–600 (1948).
159. Langer, S. Z. Presynaptic regulation of catecholamine release. *Biochemical Pharmacology* **23**, 1793–1800 (1974).
160. Lands, A. M., Arnold, A., Mcauliff, J. P., Luduena, F. P. & Brown, T. G. Differentiation of Receptor Systems activated by Sympathomimetic Amines. *Nature* **214**, 597 (1967).
161. Kaumann, A. J. Four β-adrenoceptor subtypes in the mammalian heart. *Trends in Pharmacological Sciences* **18**, 70–76 (1997).
162. Perez, D. M. *The adrenergic receptors: in the 21st century*. (Springer Science & Business Media, 2006).
163. Morrow, A. L. & Creese, I. Characterization of alpha 1-adrenergic receptor subtypes in rat brain: a reevaluation of [3H] WB4104 and [3H] prazosin binding. *Molecular Pharmacology* **29**, 321–330 (1986).
164. Cotecchia, S. *et al.* Molecular cloning and expression of the cDNA for the hamster alpha 1-adrenergic receptor. *Proceedings of the National Academy of Sciences* **85**, 7159–7163 (1988).
165. Schwinn, D. A. *et al.* Molecular cloning and expression of the cDNA for a novel alpha 1-adrenergic receptor subtype. *Journal of Biological Chemistry* **265**, 8183–8189 (1990).
166. Perez, D. M., Piascik, M. T., Malik, N., Gaivin, R. & Graham, R. M. Cloning, expression, and tissue distribution of the rat homolog of the bovine alpha 1C-adrenergic receptor provide evidence for its classification as the alpha 1A subtype. *Molecular Pharmacology* **46**, 823–831 (1994).
167. Laz, T. M. *et al.* The rat homologue of the bovine alpha 1c-adrenergic receptor shows the pharmacological properties of the classical alpha 1A subtype. *Molecular Pharmacology* **46**, 414–422 (1994).

168. Lomasney, J. W. *et al.* Molecular cloning and expression of the cDNA for the alpha 1A-adrenergic receptor. The gene for which is located on human chromosome 5. *Journal of Biological Chemistry* **266**, 6365–6369 (1991).
169. Perez, D. M., Piascik, M. T. & Graham, R. M. Solution-phase library screening for the identification of rare clones: isolation of an alpha 1D-adrenergic receptor cDNA. *Molecular Pharmacology* **40**, 876–883 (1991).
170. Hieble, J. P. *et al.* International Union of Pharmacology. X. Recommendation for nomenclature of alpha 1-adrenoceptors: consensus update. *Pharmacological Reviews* **47**, 267–270 (1995).
171. Graham, R. M., Perez, D. M., Hwa, J. & Piascik, M. T. α1-Adrenergic receptor subtypes: molecular structure, function, and signaling. *Circulation research* **78**, 737–749 (1996).
172. Cotecchia, S. The α1-adrenergic receptors: diversity of signaling networks and regulation. *Journal of Receptors and Signal Transduction* **30**, 410–419 (2010).
173. Schwinn, D. A. *et al.* The alpha 1C-adrenergic receptor: characterization of signal transduction pathways and mammalian tissue heterogeneity. *Mol Pharmacol* **40**, 619–626 (1991).
174. Graham C, Cook M R, Sastre A, Gerkovich M M & Kavet R. Cardiac autonomic control mechanisms in power-frequency magnetic fields: a multistudy analysis. *Environmental Health Perspectives* **108**, 737–742 (2000).
175. Perez, D. M. & Doze, V. A. Cardiac and neuroprotection regulated by alpha(1)-adrenergic receptor subtypes. *J Recept Signal Transduct Res* **31**, 98–110 (2011).
176. Weinberg, D. H. *et al.* Cloning, Expression and Characterization of Human α Adrenergic Receptors α1a, α1b and α1c. *Biochemical and Biophysical Research Communications* **201**, 1296–1304 (1994).
177. Faure, C., Pimoule, C., Vallancien, G., Langer, S. Z. & Graham, D. Identification of α1-adrenoceptor subtypes present in the human prostate. *Life Sciences* **54**, 1595–1605 (1994).
178. French, N. α2-Adrenoceptors and I2 sites in the mammalian central nervous system. *Pharmacology & Therapeutics* **68**, 175–208 (1995).
179. Lowell, B. B., MD, PhD & Flier, J. S., MD. BROWN ADIPOSE TISSUE, β3-ADRENERGIC RECEPTORS, AND OBESITY. *Annual Review of Medicine* **48**, 307–316 (1997).
180. Chapple, C. R. *et al.* Silodosin Therapy for Lower Urinary Tract Symptoms in Men with Suspected Benign Prostatic Hyperplasia: Results of an International, Randomized, Double-Blind, Placebo- and Active-Controlled Clinical Trial Performed in Europe. *European Urology* **59**, 342–352 (2011).

181. Lepor, H. & Hill, L. A. Silodosin for the Treatment of Benign Prostatic Hyperplasia: Pharmacology and Cardiovascular Tolerability. *Pharmacotherapy: The Journal of Human Pharmacology and Drug Therapy* **30**, 1303–1312 (2010).
182. Katzung, B. G. *Basic and Clinical Pharmacology*. (McGraw-Hill Education, 2017).
183. Buggy, D. J. *et al.* Prevention of spinal anaesthesia-induced hypotension in the elderly: i.m. methoxamine or combined hetastarch and crystalloid. *British Journal of Anaesthesia* **80**, 199–203 (1998).
184. Johnson, D. A. & Hricik, J. G. The Pharmacology of α-Adrenergic Decongestants. *Pharmacotherapy: The Journal of Human Pharmacology and Drug Therapy* **13**, 110S-115S (1993).
185. Carruthers, S. G. Adverse effects of alpha 1-adrenergic blocking drugs. *Drug Saf* **11**, 12–20 (1994).
186. James, P. A. *et al.* 2014 Evidence-Based Guideline for the Management of High Blood Pressure in Adults: Report From the Panel Members Appointed to the Eighth Joint National Committee (JNC 8). *JAMA* **311**, 507–520 (2014).
187. Freemantle, N., Cleland, J., Young, P., Mason, J. & Harrison, J. β Blockade after myocardial infarction: systematic review and meta regression analysis. *BMJ* **318**, 1730–1737 (1999).
188. Cherezov, V. *et al.* High Resolution Crystal Structure of an Engineered Human β2-Adrenergic G protein-Coupled Receptor. *Science* **318**, 1258–1265 (2007).
189. Warne, T. *et al.* Structure of a β_1-adrenergic G-protein-coupled receptor. *Nature* **454**, 486–491 (2008).
190. Rasmussen, S. G. F. *et al.* Structure of a nanobody-stabilized active state of the β(2) adrenoceptor. *Nature* **469**, 175–180 (2011).
191. Park, J. H., Scheerer, P., Hofmann, K. P., Choe, H.-W. & Ernst, O. P. Crystal structure of the ligand-free G-protein-coupled receptor opsin. *Nature* **454**, 183–187 (2008).
192. Ring, A. M. *et al.* Adrenaline-activated structure of beta2-adrenoceptor stabilized by an engineered nanobody. *Nature* **502**, 575–9 (2013).
193. Rosenbaum, D. M. *et al.* Structure and Function of an Irreversible Agonist-β2 Adrenoceptor complex. *Nature* **469**, 236–240 (2011).
194. Xu, F. *et al.* Structure of an agonist-bound human A2A adenosine receptor. *Science* **332**, 322–327 (2011).
195. White, J. F. *et al.* Structure of the agonist-bound neurotensin receptor. *Nature* **490**, 508–513 (2012).

196. Warne, T. *et al.* The structural basis for agonist and partial agonist action on a β(1)-adrenergic receptor. *Nature* **469**, 241–244 (2011).
197. Lebon, G. *et al.* Agonist-bound adenosine A 2A receptor structures reveal common features of GPCR activation. *Nature* **474**, 521 (2011).
198. Strader, C. D., Candelore, M. R., Hill, W. S., Sigal, I. S. & Dixon, R. A. Identification of two serine residues involved in agonist activation of the beta-adrenergic receptor. *J. Biol. Chem.* **264**, 13572–13578 (1989).
199. Liapakis, G. *et al.* The Forgotten Serine A CRITICAL ROLE FOR Ser-2035.42 IN LIGAND BINDING TO AND ACTIVATION OF THE β2-ADRENERGIC RECEPTOR. *Journal of Biological Chemistry* **275**, 37779–37788 (2000).
200. Hwa, J. & Perez, D. M. The unique nature of the serine interactions for alpha 1-adrenergic receptor agonist binding and activation. *J. Biol. Chem.* **271**, 6322–6327 (1996).
201. Porter, J. E., Hwa, J. & Perez, D. M. Activation of the α1b-Adrenergic Receptor Is Initiated by Disruption of an Interhelical Salt Bridge Constraint. *J. Biol. Chem.* **271**, 28318–28323 (1996).
202. Chen, S. *et al.* Phe310 in transmembrane VI of the α1B-adrenergic receptor is a key switch residue involved in activation and catecholamine ring aromatic bonding. *Journal of Biological Chemistry* **274**, 16320–16330 (1999).
203. Waugh, D. J., Zhao, M.-M., Zuscik, M. J. & Perez, D. M. Novel aromatic residues in transmembrane domains IV and V involved in agonist binding at α1A-adrenergic receptors. *Journal of Biological Chemistry* **275**, 11698–11705 (2000).
204. Wieland, K., Zuurmond, H. M., Krasel, C., Ijzerman, A. P. & Lohse, M. J. Involvement of Asn-293 in stereospecific agonist recognition and in activation of the beta 2-adrenergic receptor. *Proceedings of the National Academy of Sciences* **93**, 9276–9281 (1996).
205. Ahmed, M. *et al.* Mutational Analysis of the a1a-Adrenergic Receptor Binding Pocket of Antagonists by Radioligand Binding Assay. **31**, 4 (2008).
206. Waugh, D. J. J. *et al.* Phe-308 and Phe-312 in Transmembrane Domain 7 Are Major Sites of α1-Adrenergic Receptor Antagonist Binding IMIDAZOLINE AGONISTS BIND LIKE ANTAGONISTS. *J. Biol. Chem.* **276**, 25366–25371 (2001).
207. Zhao, M.-M., Hwa, J. & Perez, D. M. Identification of critical extracellular loop residues involved in alpha 1-adrenergic receptor subtype-selective antagonist binding. *Molecular pharmacology* **50**, 1118–1126 (1996).
208. Campbell, A. P., MacDougall, I. J. A., Griffith, R. & Finch, A. M. An aspartate in the second extracellular loop of the α1B adrenoceptor regulates agonist binding. *European Journal of Pharmacology* **733**, 90–96 (2014).

209. Waugh, D. J., Gaivin, R. J., Damron, D. S., Murray, P. A. & Perez, D. M. Binding, partial agonism, and potentiation of alpha(1)-adrenergic receptor function by benzodiazepines: A potential site of allosteric modulation. *J Pharmacol Exp Ther* **291**, 1164–71 (1999).
210. Jensen, B. C., O'Connell, T. D. & Simpson, P. C. Alpha-1-adrenergic receptors: Targets for agonist drugs to treat heart failure. *Journal of Molecular and Cellular Cardiology* **51**, 518–528 (2011).
211. Simpson, P. Norepinephrine-stimulated hypertrophy of cultured rat myocardial cells is an alpha 1 adrenergic response. *J Clin Invest* **72**, 732–738 (1983).
212. O-Uchi Jin *et al.* Interaction of α1-Adrenoceptor Subtypes With Different G Proteins Induces Opposite Effects on Cardiac L-type Ca2+ Channel. *Circulation Research* **102**, 1378–1388 (2008).
213. Rorabaugh, B. R. *et al.* α1A- but not α1B-adrenergic receptors precondition the ischemic heart by a staurosporine-sensitive, chelerythrine-insensitive mechanism. *Cardiovasc Res* **65**, 436–445 (2005).
214. Du, X.-J. *et al.* Genetic Enhancement of Ventricular Contractility Protects against Pressure-Overload-Induced Cardiac Dysfunction. *Journal of Molecular and Cellular Cardiology* **37**, 979–987 (2004).
215. Wang, B. H., Du, X.-J., Autelitano, D. J., Milano, C. A. & Woodcock, E. A. Adverse effects of constitutively active α1B-adrenergic receptors after pressure overload in mouse hearts. *American Journal of Physiology-Heart and Circulatory Physiology* **279**, H1079–H1086 (2000).
216. Lemire, I. *et al.* Cardiac-directed overexpression of wild-type α1B-adrenergic receptor induces dilated cardiomyopathy. *American Journal of Physiology-Heart and Circulatory Physiology* **281**, H931–H938 (2001).
217. Gupta, M. K. *et al.* α1-Adrenergic Receptors Regulate Neurogenesis and Gliogenesis. *Mol Pharmacol* **76**, 314–326 (2009).
218. Zuscik, M. J. *et al.* Overexpression of the α 1B -adrenergic receptor causes apoptotic neurodegeneration: Multiple system atrophy. *Nature Medicine* **6**, 1388 (2000).
219. Doze, V. A. *et al.* α1A- and α1B-adrenergic receptors differentially modulate antidepressant-like behavior in the mouse. *Brain Research* **1285**, 148–157 (2009).
220. Pizzanelli, C. *et al.* Lack of α1b-adrenergic receptor protects against epileptic seizures. *Epilepsia* **50**, 59–64 (2009).
221. Lubbe, W. F. & Hodge, J. V. Combined alpha- and beta-adrenoceptor antagonism with prazosin and oxprenolol in control of severe hypertension in pregnancy. *N Z Med J* **94**, 169–172 (1981).

222. Shibata, K. *et al.* KMD-3213, a novel, potent, alpha 1a-adrenoceptor-selective antagonist: characterization using recombinant human alpha 1-adrenoceptors and native tissues. *Mol Pharmacol* **48**, 250–258 (1995).
223. Hone, K., Obika, K., Foglar, R. & Tsujimoto, G. Selectivity of the imidazoline α-adrenoceptor agonists (oxymetazoline and cirazoline) for human cloned α1-adrenoceptor subtypes. *British Journal of Pharmacology* **116**, 1611–1618 (1995).
224. Ford, A. P. D. W. *et al.* Pharmacological pleiotropism of the human recombinant α1A-adrenoceptor: implications for α1-adrenoceptor classification. *British Journal of Pharmacology* **121**, 1127–1135 (1997).
225. Minneman, K. P., Han, C. & Abel, P. W. Comparison of alpha 1-adrenergic receptor subtypes distinguished by chlorethylclonidine and WB 4101. *Mol Pharmacol* **33**, 509–514 (1988).
226. Minneman, K. P. & Esbenshade, T. A. alpha1-Adrenergic Receptor Subtypes. *Annual Review of Pharmacology and Toxicology* **34**, 117–133 (1994).
227. Han, C., Abel, P. W. & Minneman, K. P. Heterogeneity of alpha 1-adrenergic receptors revealed by chlorethylclonidine. *Mol Pharmacol* **32**, 505–510 (1987).
228. Knepper, S. M. *et al.* A-61603, a potent alpha 1-adrenergic receptor agonist, selective for the alpha 1A receptor subtype. *J. Pharmacol. Exp. Ther.* **274**, 97–103 (1995).
229. Carroll, W. A. *et al.* In Vitro and In Vivo Characterization of Alpha-1A Selective Agonists and Their Utility for Stress Incontience. *Med Chem Res* **13**, 134–148 (2004).
230. Boer, R., Grassegger, A., Schudt, C. & Glossmann, H. (+)-Niguldipine binds with very high affinity to Ca2+ channels and to a subtype of α1-adrenoceptors. *European Journal of Pharmacology: Molecular Pharmacology* **172**, 131–145 (1989).
231. Hanft, G. & Gross, G. Subclassification of α1-adrenoceptor recognition sites by urapidil derivatives and other selective antagonists. *British Journal of Pharmacology* **97**, 691–700 (1989).
232. Marucci, G. *et al.* (+)-Cyclazosin, a selective α1B-adrenoceptor antagonist: Functional evaluation in rat and rabbit tissues. *European Journal of Pharmacology* **522**, 100–107 (2005).
233. Williams, T. J. *et al.* In vitroα1-adrenoceptor pharmacology of Ro 70–0004 and RS-100329, novel α1A-adrenoceptor selective antagonists. *British Journal of Pharmacology* **127**, 252–258 (1999).
234. Taniguchi, T., Inagaki, R., Murata, S., Akiba, I. & Muramatsu, I. Microphysiometric analysis of human alpha1a-adrenoceptor expressed in Chinese hamster ovary cells. *Br. J. Pharmacol.* **127**, 962–968 (1999).

235. Williams, L. M. *et al.* Diazepam is not a direct allosteric modulator of α1-adrenoceptors, but modulates receptor signaling by inhibiting phosphodiesterase-4. *Pharmacol Res Perspect* **7**, (2018).
236. Sharpe, I. A. *et al.* Allosteric α1-Adrenoreceptor Antagonism by the Conopeptide ρ-TIA. *J. Biol. Chem.* **278**, 34451–34457 (2003).
237. Lima, V. *et al.* Differential antagonism by conotoxin ρ-TIA of contractions mediated by distinct α1-adrenoceptor subtypes in rat vas deferens, spleen and aorta. *European Journal of Pharmacology* **508**, 183–192 (2005).
238. Campbell, A. P., Wakelin, L. P. G., Denny, W. A. & Finch, A. M. Homobivalent Conjugation Increases the Allosteric Effect of 9-aminoacridine at the α1-Adrenergic Receptors. *Mol Pharmacol* **91**, 135–144 (2017).
239. 9-aminoacridine (CHEBI:74789). Available at: https://www.ebi.ac.uk/chebi/searchId.do?chebiId=CHEBI:74789. (Accessed: 26th March 2019)
240. Hanson, M. A. *et al.* A specific cholesterol binding site is established by the 2.8 A structure of the human beta2-adrenergic receptor. *Structure* **16**, 897–905 (2008).
241. Latorraca, N. R., Venkatakrishnan, A. J. & Dror, R. O. GPCR Dynamics: Structures in Motion. *Chem. Rev.* **117**, 139–155 (2017).
242. Kumari, P., Ghosh, E. & Shukla, A. K. Emerging Approaches to GPCR Ligand Screening for Drug Discovery. *Trends Mol Med* **21**, 687–701 (2015).
243. Zou, Y., Weis, W. I. & Kobilka, B. K. N-terminal T4 lysozyme fusion facilitates crystallization of a G protein coupled receptor. *PLoS ONE* **7**, e46039 (2012).
244. Thompson, A. A. *et al.* Structure of the nociceptin/orphanin FQ receptor in complex with a peptide mimetic. *Nature* **485**, 395–399 (2012).
245. Doré, A. S. *et al.* Structure of the adenosine A(2A) receptor in complex with ZM241385 and the xanthines XAC and caffeine. *Structure* **19**, 1283–1293 (2011).
246. Carpenter, B., Nehmé, R., Warne, T., Leslie, A. G. W. & Tate, C. G. Structure of the adenosine A(2A) receptor bound to an engineered G protein. *Nature* **536**, 104–107 (2016).
247. Hino, T. *et al.* G-protein-coupled receptor inactivation by an allosteric inverse-agonist antibody. *Nature* **482**, 237–240 (2012).
248. Steyaert, J. & Kobilka, B. K. Nanobody stabilization of G protein-coupled receptor conformational states. *Curr. Opin. Struct. Biol.* **21**, 567–572 (2011).
249. Meyer, B. & Peters, T. NMR spectroscopy techniques for screening and identifying ligand binding to protein receptors. *Angew Chem Int Ed Engl* **42**, 864–90 (2003).

250. Hiroaki, H. Recent applications of isotopic labeling for protein NMR in drug discovery. *Expert Opin Drug Discov* **8**, 523–536 (2013).
251. Barile, E. & Pellecchia, M. NMR-based approaches for the identification and optimization of inhibitors of protein-protein interactions. *Chem. Rev.* **114**, 4749–4763 (2014).
252. Fernández, C. & Jahnke, W. New approaches for NMR screening in drug discovery. *Drug Discovery Today: Technologies* **1**, 277–283 (2004).
253. Vanwetswinkel, S. *et al.* TINS, target immobilized NMR screening: an efficient and sensitive method for ligand discovery. *Chem. Biol.* **12**, 207–216 (2005).
254. Benie, A. J., Moser, R., Bäuml, E., Blaas, D. & Peters, T. Virus−Ligand Interactions: Identification and Characterization of Ligand Binding by NMR Spectroscopy. *J. Am. Chem. Soc.* **125**, 14–15 (2003).
255. Gharbi-Benarous, J. *et al.* Epitope Mapping of the Phosphorylation Motif of the HIV-1 Protein Vpu Bound to the Selective Monoclonal Antibody Using TRNOESY and STD NMR Spectroscopy. *Biochemistry* **43**, 14555–14565 (2004).
256. Claasen, B., Axmann, M., Meinecke, R. & Meyer, B. Direct Observation of Ligand Binding to Membrane Proteins in Living Cells by a Saturation Transfer Double Difference (STDD) NMR Spectroscopy Method Shows a Significantly Higher Affinity of Integrin αIIbβ3 in Native Platelets than in Liposomes. *J. Am. Chem. Soc.* **127**, 916–919 (2005).
257. Meinecke, R. & Meyer, B. Determination of the Binding Specificity of an Integral Membrane Protein by Saturation Transfer Difference NMR: RGD Peptide Ligands Binding to Integrin αIIbβ3. *J. Med. Chem.* **44**, 3059–3065 (2001).
258. Bhunia, A., Bhattacharjya, S. & Chatterjee, S. Applications of saturation transfer difference NMR in biological systems. *Drug Discov. Today* **17**, 505–513 (2012).
259. Wagstaff, J. L., Taylor, S. L. & Howard, M. J. Recent developments and applications of saturation transfer difference nuclear magnetic resonance (STD NMR) spectroscopy. *Mol Biosyst* **9**, 571–577 (2013).
260. Hajduk, P. J. *et al.* SOS-NMR: a saturation transfer NMR-based method for determining the structures of protein-ligand complexes. *J. Am. Chem. Soc.* **126**, 2390–2398 (2004).
261. Dalvit, C. *et al.* Identification of compounds with binding affinity to proteins via magnetization transfer from bulk water*. *J Biomol NMR* **18**, 65–68 (2000).
262. Ludwig, C. *et al.* SALMON: solvent accessibility, ligand binding, and mapping of ligand orientation by NMR spectroscopy. *J. Med. Chem.* **51**, 1–3 (2008).
263. Ni, F. Recent developments in transferred NOE methods. *Progress in Nuclear Magnetic Resonance Spectroscopy* **26**, 517–606 (1994).

264. Sánchez-Pedregal, V. M. *et al.* The INPHARMA method: protein-mediated interligand NOEs for pharmacophore mapping. *Angew Chem Int Ed Engl* **44**, 4172–5 (2005).
265. Ono, K. *et al.* Structure-based approach to improve a small-molecule inhibitor by the use of a competitive peptide ligand. *Angew. Chem. Int. Ed. Engl.* **53**, 2597–2601 (2014).
266. Becattini, B. & Pellecchia, M. SAR by ILOEs: an NMR-based approach to reverse chemical genetics. *Chemistry* **12**, 2658–2662 (2006).
267. Hajduk, P. J., Olejniczak, E. T. & Fesik, S. W. One-Dimensional Relaxation- and Diffusion-Edited NMR Methods for Screening Compounds That Bind to Macromolecules. *J. Am. Chem. Soc.* **119**, 12257–12261 (1997).
268. Rossi, C., Donati, A. & Sansoni, M. R. Nuclear magnetic resonance as a tool for the identification of specific DNA—ligand interaction. *Chemical Physics Letters* **189**, 278–280 (1992).
269. Pellecchia, M., Sem, D. S. & Wüthrich, K. NMR in drug discovery. *Nat Rev Drug Discov* **1**, 211–219 (2002).
270. Bertini, I., Fragai, M., Lee, Y.-M., Luchinat, C. & Terni, B. Paramagnetic Metal Ions in Ligand Screening: The CoII Matrix Metalloproteinase 12. *Angewandte Chemie International Edition* **43**, 2254–2256 (2004).
271. Chen, A. & Shapiro, M. J. NOE Pumping: A Novel NMR Technique for Identification of Compounds with Binding Affinity to Macromolecules. *J. Am. Chem. Soc.* **120**, 10258–10259 (1998).
272. Chen, A. & Shapiro, M. J. NOE Pumping. 2. A High-Throughput Method To Determine Compounds with Binding Affinity to Macromolecules by NMR. *J. Am. Chem. Soc.* **122**, 414–415 (2000).
273. Jayalakshmi, V. & Krishna, N. R. Complete relaxation and conformational exchange matrix (CORCEMA) analysis of intermolecular saturation transfer effects in reversibly forming ligand-receptor complexes. *J. Magn. Reson.* **155**, 106–118 (2002).
274. Meyer, B. *et al.* Saturation Transfer Difference NMR Spectroscopy for Identifying Ligand Epitopes and Binding Specificities. in *Leucocyte Trafficking* (eds. Hamann, A., Asadullah, K. & Schottelius, A.) 149–167 (Springer Berlin Heidelberg, 2004).
275. Ma, R., Wang, P., Wu, J. & Ruan, K. Process of Fragment-Based Lead Discovery—A Perspective from NMR. *Molecules* **21**, 854 (2016).
276. Dalvit, C., Fogliatto, G., Stewart, A., Veronesi, M. & Stockman, B. WaterLOGSY as a method for primary NMR screening: Practical aspects and range of applicability. *J Biomol NMR* **21**, 349–359 (2001).

277. Huang, R. & Leung, I. K. Protein–Small Molecule Interactions by WaterLOGSY. *Methods in enzymology* **615**, 477–500 (2019).
278. Clore, G. M. & Gronenborn, A. M. Theory of the time dependent transferred nuclear Overhauser effect: Applications to structural analysis of ligand-protein complexes in solution. *Journal of Magnetic Resonance (1969)* **53**, 423–442 (1983).
279. Clore, G. M. & Gronenborn, A. M. Theory and applications of the transferred nuclear overhauser effect to the study of the conformations of small ligands bound to proteins. *Journal of Magnetic Resonance (1969)* **48**, 402–417 (1982).
280. Balaram, P., Bothner-By, A. A. & Breslow, E. Localization of tyrosine at the binding site of neurophysin II by negative nuclear Overhouser effects. *J. Am. Chem. Soc.* **94**, 4017–4018 (1972).
281. Balaram, P., Bothner-By, A. A. & Dadok, J. Negative nuclear Overhuaser effects as probes of macromolecular structure. *J. Am. Chem. Soc.* **94**, 4015–4017 (1972).
282. Moseley, H. N. B., Curto, E. V. & Krishna, N. R. Complete Relaxation and Conformational Exchange Matrix (CORCEMA) Analysis of NOESY Spectra of Interacting Systems; Two-Dimensional Transferred NOESY. *Journal of Magnetic Resonance, Series B* **108**, 243–261 (1995).
283. Dias, D. M. & Ciulli, A. NMR approaches in structure-based lead discovery: recent developments and new frontiers for targeting multi-protein complexes. *Prog. Biophys. Mol. Biol.* **116**, 101–112 (2014).
284. Cala, O., Guillière, F. & Krimm, I. NMR-based analysis of protein–ligand interactions. *Anal Bioanal Chem* **406**, 943–956 (2014).
285. Krimm, I. INPHARMA-based identification of ligand binding site in fragment-based drug design. *MedChemComm* **3**, 605–610 (2012).
286. *Protein-ligand interactions: methods and applications*. (Humana Press, 2013).
287. Andrews, S. P., Brown, G. A. & Christopher, J. A. Structure-Based and Fragment-Based GPCR Drug Discovery. *ChemMedChem* **9**, 256–275 (2014).
288. Chen, D. *et al.* Fragment Screening of GPCRs Using Biophysical Methods: Identification of Ligands of the Adenosine A2A Receptor with Novel Biological Activity. *ACS Chem. Biol.* **7**, 2064–2073 (2012).
289. Igonet, S. *et al.* Enabling STD-NMR fragment screening using stabilized native GPCR: A case study of adenosine receptor. *Scientific Reports* **8**, 8142 (2018).

290. Congreve, M. *et al.* Chapter Five - Fragment Screening of Stabilized G-Protein-Coupled Receptors Using Biophysical Methods. in *Methods in Enzymology* (ed. Kuo, L. C.) **493**, 115–136 (Academic Press, 2011).
291. Cox, B. D. *et al.* Structural analysis of CXCR4 – Antagonist interactions using saturation-transfer double-difference NMR. *Biochemical and Biophysical Research Communications* **466**, 28–32 (2015).
292. Yong, K. J. *et al.* Determinants of Ligand Subtype-Selectivity at α1A-Adrenoceptor Revealed Using Saturation Transfer Difference (STD) NMR. *ACS Chem. Biol.* **13**, 1090–1102 (2018).
293. Assadi-Porter, F. M. *et al.* Direct NMR Detection of the Binding of Functional Ligands to the Human Sweet Receptor, a Heterodimeric Family 3 GPCR. *J. Am. Chem. Soc.* **130**, 7212–7213 (2008).
294. Catoire, L. J. *et al.* Structure of a GPCR Ligand in Its Receptor-Bound State: Leukotriene B4 Adopts a Highly Constrained Conformation When Associated to Human BLT2. *J. Am. Chem. Soc.* **132**, 9049–9057 (2010).
295. Kofuku, Y. *et al.* Structural Basis of the Interaction between Chemokine Stromal Cell-derived Factor-1/CXCL12 and Its G-protein-coupled Receptor CXCR4. *J. Biol. Chem.* **284**, 35240–35250 (2009).
296. Yoshiura, C. *et al.* Elucidation of the CCR1- and CCR5-binding modes of MIP-1α by application of an NMR spectra reconstruction method to the transferred cross-saturation experiments. *J Biomol NMR* **63**, 333–340 (2015).
297. Yoshiura, C. *et al.* NMR Analyses of the Interaction between CCR5 and Its Ligand Using Functional Reconstitution of CCR5 in Lipid Bilayers. *J. Am. Chem. Soc.* **132**, 6768–6777 (2010).
298. Hajduk, P. J. & Greer, J. A decade of fragment-based drug design: strategic advances and lessons learned. *Nature Reviews Drug Discovery* **6**, 211–219 (2007).
299. O'Connor, C. *et al.* NMR structure and dynamics of the agonist dynorphin peptide bound to the human kappa opioid receptor. *PNAS* **112**, 11852–11857 (2015).
300. Brancaccio, D. *et al.* Ligand-Based NMR Study of C-X-C Chemokine Receptor Type 4 (CXCR4)–Ligand Interactions on Living Cancer Cells. *J. Med. Chem.* **61**, 2910–2923 (2018).
301. Inooka, H. *et al.* Conformation of a peptide ligand bound to its G-protein coupled receptor. *Nature Structural & Molecular Biology* **8**, 161–165 (2001).
302. Bartoschek, S. *et al.* Drug Design for G-Protein-Coupled Receptors by a Ligand-Based NMR Method. *Angewandte Chemie International Edition* **49**, 1426–1429 (2010).

303. Fredriksson, K. *et al.* Nanodiscs for INPHARMA NMR Characterization of GPCRs: Ligand Binding to the Human A2A Adenosine Receptor. *Angew. Chem. Int. Ed.* n/a-n/a (2017). doi:10.1002/anie.201612547
304. Korb, O., Möller, H. M. & Exner, T. E. NMR-Guided Molecular Docking of a Protein–Peptide Complex Based on Ant Colony Optimization. *ChemMedChem* **5**, 1001–1006 (2010).
305. Korb, O., Stützle, T. & Exner, T. E. Empirical Scoring Functions for Advanced Protein−Ligand Docking with PLANTS. *J. Chem. Inf. Model.* **49**, 84–96 (2009).
306. Jayalakshmi, V., Biet, T., Peters, T. & Krishna, N. R. Refinement of the Conformation of UDP−Galactose Bound to Galactosyltransferase Using the STD NMR Intensity-Restrained CORCEMA Optimization. *J. Am. Chem. Soc.* **126**, 8610–8611 (2004).
307. Skjærven, L. *et al.* Accounting for Conformational Variability in Protein–Ligand Docking with NMR-Guided Rescoring. *J. Am. Chem. Soc.* **135**, 5819–5827 (2013).
308. Zhang, W. *et al.* Identification of the binding site of an allosteric ligand using STD-NMR, docking, and CORCEMA-ST calculations. *ChemMedChem* **8**, 1629–1633 (2013).
309. Jayalakshmi, V. & Rama Krishna, N. CORCEMA refinement of the bound ligand conformation within the protein binding pocket in reversibly forming weak complexes using STD-NMR intensities. *Journal of Magnetic Resonance* **168**, 36–45 (2004).
310. Orts, J., Bartoschek, S., Griesinger, C., Monecke, P. & Carlomagno, T. An NMR-based scoring function improves the accuracy of binding pose predictions by docking by two orders of magnitude. *J Biomol NMR* **52**, 23–30 (2012).
311. Levitt, M. Growth of novel protein structural data. *PNAS* **104**, 3183–3188 (2007).
312. Bill, R. M. *et al.* Overcoming barriers to membrane protein structure determination. *Nature Biotechnology* **29**, 335–340 (2011).
313. Baker, M. Making membrane proteins for structures: a trillion tiny tweaks. *Nature Methods* **7**, 429–434 (2010).
314. Martí-Renom, M. A. *et al.* Comparative Protein Structure Modeling of Genes and Genomes. *Annual Review of Biophysics and Biomolecular Structure* **29**, 291–325 (2000).
315. Rost, B. Twilight zone of protein sequence alignments. *Protein Eng Des Sel* **12**, 85–94 (1999).
316. Doolittle, R. F. & Doolittle, R. F. *Of Urfs And Orfs: A Primer on How to Analyze Derived Amino Acid Sequences*. (University Science Books, 1986).
317. Eswar, N. *et al.* Comparative Protein Structure Modeling Using Modeller. *Current Protocols in Bioinformatics* **15**, 5.6.1-5.6.30 (2006).
318. Šali, A. & Blundell, T. L. Comparative Protein Modelling by Satisfaction of Spatial Restraints. *Journal of Molecular Biology* **234**, 779–815 (1993).

319. Arnold, K., Bordoli, L., Kopp, J. & Schwede, T. The SWISS-MODEL workspace: a web-based environment for protein structure homology modelling. *Bioinformatics* **22**, 195–201 (2006).
320. Bates, P. A., Kelley, L. A., MacCallum, R. M. & Sternberg, M. J. E. Enhancement of protein modeling by human intervention in applying the automatic programs 3D-JIGSAW and 3D-PSSM. *Proteins: Structure, Function, and Bioinformatics* **45**, 39–46 (2001).
321. Koehl, P. & Delarue, M. A self consistent mean field approach to simultaneous gap closure and side-chain positioning in homology modelling. *Nature Structural Biology* **2**, 163 (1995).
322. Petrey, D. *et al.* Using multiple structure alignments, fast model building, and energetic analysis in fold recognition and homology modeling. *Proteins: Structure, Function, and Bioinformatics* **53**, 430–435 (2003).
323. Illergård, K., Ardell, D. H. & Elofsson, A. Structure is three to ten times more conserved than sequence—A study of structural response in protein cores. *Proteins: Structure, Function, and Bioinformatics* **77**, 499–508 (2009).
324. Murzin, A. G., Brenner, S. E., Hubbard, T. & Chothia, C. SCOP: A structural classification of proteins database for the investigation of sequences and structures. *Journal of Molecular Biology* **247**, 536–540 (1995).
325. Andreeva, A. *et al.* Data growth and its impact on the SCOP database: new developments. *Nucleic Acids Res* **36**, D419–D425 (2008).
326. Jones, D. T., Taylort, W. R. & Thornton, J. M. A new approach to protein fold recognition. *Nature* **358**, 86 (1992).
327. Miller, R. T., Jones, D. T. & Thornton, J. M. Protein fold recognition by sequence threading: tools and assessment techniques. *The FASEB Journal* **10**, 171–178 (1996).
328. Xu, J., Li, M., Kim, D. & Xu, Y. Raptor: optimal protein threading by linear programming. *J. Bioinform. Comput. Biol.* **01**, 95–117 (2003).
329. Klepeis, J. L., Wei, Y., Hecht, M. H. & Floudas, C. A. Ab initio prediction of the three-dimensional structure of a de novo designed protein: A double-blind case study. *Proteins: Structure, Function, and Bioinformatics* **58**, 560–570 (2005).
330. Klepeis, J. L. & Floudas, C. A. ASTRO-FOLD: A Combinatorial and Global Optimization Framework for Ab Initio Prediction of Three-Dimensional Structures of Proteins from the Amino Acid Sequence. *Biophysical Journal* **85**, 2119–2146 (2003).
331. Liwo, A., Lee, J., Ripoll, D. R., Pillardy, J. & Scheraga, H. A. Protein structure prediction by global optimization of a potential energy function. *PNAS* **96**, 5482–5485 (1999).
332. Ołdziej, S. *et al.* Physics-based protein-structure prediction using a hierarchical protocol based on the UNRES force field: Assessment in two blind tests. *PNAS* **102**, 7547–7552 (2005).

333. Ponder, J. W. & Case, D. A. Force Fields for Protein Simulations. in *Advances in Protein Chemistry* **66**, 27–85 (Academic Press, 2003).
334. Jorgensen, W. L., Maxwell, D. S. & Tirado-Rives, J. Development and Testing of the OPLS All-Atom Force Field on Conformational Energetics and Properties of Organic Liquids. *J. Am. Chem. Soc.* **118**, 11225–11236 (1996).
335. Kaminski, G. A., Friesner, R. A., Tirado-Rives, J. & Jorgensen, W. L. Evaluation and Reparametrization of the OPLS-AA Force Field for Proteins via Comparison with Accurate Quantum Chemical Calculations on Peptides. *J. Phys. Chem. B* **105**, 6474–6487 (2001).
336. Brooks, B. R. *et al.* CHARMM: The Biomolecular Simulation Program. *J Comput Chem* **30**, 1545–1614 (2009).
337. Brooks, B. R. *et al.* CHARMM: A program for macromolecular energy, minimization, and dynamics calculations. *Journal of Computational Chemistry* **4**, 187–217 (1983).
338. MacKerell, A. D. *et al.* CHARMM: The Energy Function and Its Parameterization. in *Encyclopedia of Computational Chemistry* (American Cancer Society, 2002). doi:10.1002/0470845015.cfa007
339. Case, D. A. *et al.* The Amber biomolecular simulation programs. *Journal of Computational Chemistry* **26**, 1668–1688 (2005).
340. Jorgensen, W. L., Briggs, J. M. & Contreras, M. Leonor. Relative partition coefficients for organic solutes from fluid simulations. *J. Phys. Chem.* **94**, 1683–1686 (1990).
341. Christen, M. *et al.* The GROMOS software for biomolecular simulation: GROMOS05. *Journal of Computational Chemistry* **26**, 1719–1751 (2005).
342. Marrink, S. J., de Vries, A. H. & Mark, A. E. Coarse Grained Model for Semiquantitative Lipid Simulations. *J. Phys. Chem. B* **108**, 750–760 (2004).
343. Marrink, S. J., Risselada, H. J., Yefimov, S., Tieleman, D. P. & de Vries, A. H. The MARTINI Force Field: Coarse Grained Model for Biomolecular Simulations. *J. Phys. Chem. B* **111**, 7812–7824 (2007).
344. Monticelli, L. *et al.* The MARTINI Coarse-Grained Force Field: Extension to Proteins. *J. Chem. Theory Comput.* **4**, 819–834 (2008).
345. Hall, B. A. & Sansom, M. S. P. Coarse-Grained MD Simulations and Protein−Protein Interactions: The Cohesin−Dockerin System. *J. Chem. Theory Comput.* **5**, 2465–2471 (2009).
346. Tunbridge, I., Best, R. B., Gain, J. & Kuttel, M. M. Simulation of Coarse-Grained Protein−Protein Interactions with Graphics Processing Units. *J. Chem. Theory Comput.* **6**, 3588–3600 (2010).
347. Qin, M., Zhang, J. & Wang, W. Effects of Disulfide Bonds on Folding Behavior and Mechanism of the β-Sheet Protein Tendamistat. *Biophysical Journal* **90**, 272–286 (2006).

348. Clementi, C. Coarse-grained models of protein folding: toy models or predictive tools? *Current Opinion in Structural Biology* **18**, 10–15 (2008).
349. Thorpe, I. F., Zhou, J. & Voth, G. A. Peptide Folding Using Multiscale Coarse-Grained Models. *J. Phys. Chem. B* **112**, 13079–13090 (2008).
350. Markvoort, A. J., Smeijers, A. F., Pieterse, K., van Santen, R. A. & Hilbers, P. A. J. Lipid-Based Mechanisms for Vesicle Fission. *J. Phys. Chem. B* **111**, 5719–5725 (2007).
351. Smeijers, A. F., Pieterse, K., Markvoort, A. J. & Hilbers, P. A. J. Coarse-Grained Transmembrane Proteins: Hydrophobic Matching, Aggregation, and Their Effect on Fusion. *J. Phys. Chem. B* **110**, 13614–13623 (2006).
352. Bond, P. J., Holyoake, J., Ivetac, A., Khalid, S. & Sansom, M. S. P. Coarse-grained molecular dynamics simulations of membrane proteins and peptides. *Journal of Structural Biology* **157**, 593–605 (2007).
353. Scott, K. A. *et al.* Coarse-Grained MD Simulations of Membrane Protein-Bilayer Self-Assembly. *Structure* **16**, 621–630 (2008).
354. Gumbart, J. & Schulten, K. Structural Determinants of Lateral Gate Opening in the Protein Translocon. *Biochemistry* **46**, 11147–11157 (2007).
355. Treptow, W., Marrink, S.-J. & Tarek, M. Gating Motions in Voltage-Gated Potassium Channels Revealed by Coarse-Grained Molecular Dynamics Simulations. *J. Phys. Chem. B* **112**, 3277–3282 (2008).
356. Yefimov, S., van der Giessen, E., Onck, P. R. & Marrink, S. J. Mechanosensitive Membrane Channels in Action. *Biophysical Journal* **94**, 2994–3002 (2008).
357. McCammon, J. A., Gelin, B. R. & Karplus, M. Dynamics of folded proteins. *Nature* **267**, 585 (1977).
358. Levitt, M. & Sharon, R. Accurate simulation of protein dynamics in solution. *PNAS* **85**, 7557–7561 (1988).
359. Edholm, O., Berger, O. & Jähnig, F. Structure and Fluctuations of Bacteriorhodopsin in the Purple Membrane: A Molecular Dynamics Study. *Journal of Molecular Biology* **250**, 94–111 (1995).
360. Durrant, J. D., Oliveira, C. A. F. de & McCammon, J. A. Including receptor flexibility and induced fit effects into the design of MMP-2 inhibitors. *Journal of Molecular Recognition* **23**, 173–182 (2010).
361. Karplus, M. & Kuriyan, J. Molecular dynamics and protein function. *PNAS* **102**, 6679–6685 (2005).

362. Schäfer, L. V. *et al.* Lipid packing drives the segregation of transmembrane helices into disordered lipid domains in model membranes. *PNAS* **108**, 1343–1348 (2011).
363. Marrink, S. J., de Vries, A. H. & Tieleman, D. P. Lipids on the move: Simulations of membrane pores, domains, stalks and curves. *Biochimica et Biophysica Acta (BBA) - Biomembranes* **1788**, 149–168 (2009).
364. Dolenc, J., Missimer, J. H., Steinmetz, M. O. & van Gunsteren, W. F. Methods of NMR structure refinement: molecular dynamics simulations improve the agreement with measured NMR data of a C-terminal peptide of GCN4-p1. *J Biomol NMR* **47**, 221–235 (2010).
365. Subbotina, J. *et al.* Structural refinement of the hERG1 pore and voltage-sensing domains with ROSETTA-membrane and molecular dynamics simulations. *Proteins: Structure, Function, and Bioinformatics* **78**, 2922–2934 (2010).
366. Malde, A. K. & Mark, A. E. Binding and Enantiomeric Selectivity of Threonyl-tRNA Synthetase. *J. Am. Chem. Soc.* **131**, 3848–3849 (2009).
367. Klenin, K., Strodel, B., Wales, D. J. & Wenzel, W. Modelling proteins: Conformational sampling and reconstruction of folding kinetics. *Biochimica et Biophysica Acta (BBA) - Proteins and Proteomics* **1814**, 977–1000 (2011).
368. Khalili-Araghi, F. *et al.* Molecular dynamics simulations of membrane channels and transporters. *Current Opinion in Structural Biology* **19**, 128–137 (2009).
369. Lindahl, E. & Sansom, M. S. Membrane proteins: molecular dynamics simulations. *Current Opinion in Structural Biology* **18**, 425–431 (2008).
370. Gumbart, J., Wang, Y., Aksimentiev, A., Tajkhorshid, E. & Schulten, K. Molecular dynamics simulations of proteins in lipid bilayers. *Current Opinion in Structural Biology* **15**, 423–431 (2005).
371. Phillips, J. C. *et al.* Scalable molecular dynamics with NAMD. *Journal of Computational Chemistry* **26**, 1781–1802 (2005).
372. Hess, B., Kutzner, C., van der Spoel, D. & Lindahl, E. GROMACS 4: Algorithms for Highly Efficient, Load-Balanced, and Scalable Molecular Simulation. *J. Chem. Theory Comput.* **4**, 435–447 (2008).
373. Spoel, D. V. D. *et al.* GROMACS: Fast, flexible, and free. *Journal of Computational Chemistry* **26**, 1701–1718 (2005).
374. Bowers, K. J. *et al.* Scalable Algorithms for Molecular Dynamics Simulations on Commodity Clusters. in *SC '06: Proceedings of the 2006 ACM/IEEE Conference on Supercomputing* 43–43 (2006). doi:10.1109/SC.2006.54

375. Voelz, V. A., Bowman, G. R., Beauchamp, K. & Pande, V. S. Molecular simulation of ab initio protein folding for a millisecond folder NTL9(1-39). *J. Am. Chem. Soc.* **132**, 1526–1528 (2010).
376. Shaw, D. E. *et al.* Millisecond-scale Molecular Dynamics Simulations on Anton. in *Proceedings of the Conference on High Performance Computing Networking, Storage and Analysis* 39:1–39:11 (ACM, 2009). doi:10.1145/1654059.1654099
377. McRobb, F. M., Negri, A., Beuming, T. & Sherman, W. Molecular dynamics techniques for modeling G protein-coupled receptors. *Current Opinion in Pharmacology* **30**, 69–75 (2016).
378. Ciancetta, A., Sabbadin, D., Federico, S., Spalluto, G. & Moro, S. Advances in Computational Techniques to Study GPCR–Ligand Recognition. *Trends in Pharmacological Sciences* **36**, 878–890 (2015).
379. Johnston, J. M. & Filizola, M. Showcasing modern molecular dynamics simulations of membrane proteins through G protein-coupled receptors. *Current Opinion in Structural Biology* **21**, 552–558 (2011).
380. Ute F. Röhrig, Leonardo Guidoni, and & Ursula Rothlisberger*, ‡. Early Steps of the Intramolecular Signal Transduction in Rhodopsin Explored by Molecular Dynamics Simulations†. (2002). doi:10.1021/bi026011h
381. Crozier, P. S., Stevens, M. J., Forrest, L. R. & Woolf, T. B. Molecular Dynamics Simulation of Dark-adapted Rhodopsin in an Explicit Membrane Bilayer: Coupling between Local Retinal and Larger Scale Conformational Change. *Journal of Molecular Biology* **333**, 493–514 (2003).
382. Huber, T., Botelho, A. V., Beyer, K. & Brown, M. F. Membrane Model for the G-Protein-Coupled Receptor Rhodopsin: Hydrophobic Interface and Dynamical Structure. *Biophysical Journal* **86**, 2078–2100 (2004).
383. Michele Seeber, #, Pier G. De Benedetti, # and & Francesca Fanelli*, †. Molecular Dynamics Simulations of the Ligand-Induced Chemical Information Transfer in the 5-HT1A Receptor. (2003). doi:10.1021/ci034069c
384. Huang, X. *et al.* Molecular Dynamics Simulations on SDF-1α: Binding with CXCR4 Receptor. *Biophysical Journal* **84**, 171–184 (2003).
385. Zhang, Y., Sham, Y. Y., Rajamani, R., Gao, J. & Portoghese, P. S. Homology Modeling and Molecular Dynamics Simulations of the Mu Opioid Receptor in a Membrane–Aqueous System. *ChemBioChem* **6**, 853–859 (2005).
386. Manuela Iadanza, †, Monika Höltje, ‡, Giuseppe Ronsisvalle, † and & Hans-Dieter Höltje*, §. κ-Opioid Receptor Model in a Phospholipid Bilayer: Molecular Dynamics Simulation. (2002). doi:10.1021/jm0209127

387. Kohlhoff, K. J. *et al.* Cloud-based simulations on Google Exacycle reveal ligand modulation of GPCR activation pathways. *Nature Chemistry* **6**, 15–21 (2014).
388. Prioleau, C., Visiers, I., Ebersole, B. J., Weinstein, H. & Sealfon, S. C. Conserved Helix 7 Tyrosine Acts as a Multistate Conformational Switch in the 5HT2C Receptor IDENTIFICATION OF A NOVEL "LOCKED-ON" PHENOTYPE AND DOUBLE REVERTANT MUTATIONS. *J. Biol. Chem.* **277**, 36577–36584 (2002).
389. Sealfon, S. C. *et al.* Related Contribution of Specific Helix 2 and 7 Residues to Conformational Activation of the Serotonin 5-HT2A Receptor. *J. Biol. Chem.* **270**, 16683–16688 (1995).
390. Tiburu, E. K. *et al.* Solid-state NMR and molecular dynamics characterization of cannabinoid receptor-1 (CB1) helix 7 conformational plasticity in model membranes. *Biochimica et Biophysica Acta (BBA) - Biomembranes* **1788**, 1159–1167 (2009).
391. Venkatakrishnan, A. J. *et al.* Molecular signatures of G-protein-coupled receptors. *Nature* **494**, 185–194 (2013).
392. Dror, R. O. *et al.* Activation mechanism of the β2-adrenergic receptor. *PNAS* **108**, 18684–18689 (2011).
393. Schneider, S., Provasi, D. & Filizola, M. How Oliceridine (TRV-130) Binds and Stabilizes a μ-Opioid Receptor Conformational State That Selectively Triggers G Protein Signaling Pathways. *Biochemistry* **55**, 6456–6466 (2016).
394. Provasi, D. & Filizola, M. Putative Active States of a Prototypic G-Protein-Coupled Receptor from Biased Molecular Dynamics. *Biophysical Journal* **98**, 2347–2355 (2010).
395. Provasi, D., Artacho, M. C., Negri, A., Mobarec, J. C. & Filizola, M. Ligand-Induced Modulation of the Free-Energy Landscape of G Protein-Coupled Receptors Explored by Adaptive Biasing Techniques. *PLOS Computational Biology* **7**, e1002193 (2011).
396. Zia, S. R., Gaspari, R., Decherchi, S. & Rocchia, W. Probing Hydration Patterns in Class-A GPCRs via Biased MD: The A2A Receptor. (2016). doi:10.1021/acs.jctc.6b00475
397. Dror, R. O. *et al.* Pathway and mechanism of drug binding to G-protein-coupled receptors. *PNAS* **108**, 13118–13123 (2011).
398. Sabbadin, D. & Moro, S. Supervised Molecular Dynamics (SuMD) as a Helpful Tool To Depict GPCR–Ligand Recognition Pathway in a Nanosecond Time Scale. (2014). doi:10.1021/ci400766b
399. Deganutti, G., Cuzzolin, A., Ciancetta, A. & Moro, S. Understanding allosteric interactions in G protein-coupled receptors using Supervised Molecular Dynamics: A prototype study analysing the human A3 adenosine receptor positive allosteric modulator LUF6000. *Bioorganic & Medicinal Chemistry* **23**, 4065–4071 (2015).

400. Provasi, D., Bortolato, A. & Filizola, M. Exploring Molecular Mechanisms of Ligand Recognition by Opioid Receptors with Metadynamics. (2009). doi:10.1021/bi901494n
401. Dickson, C. J. *et al.* Uncoupling the Structure–Activity Relationships of β2 Adrenergic Receptor Ligands from Membrane Binding. (2016). doi:10.1021/acs.jmedchem.6b00358
402. Hedger, G. & Sansom, M. S. P. Lipid interaction sites on channels, transporters and receptors: Recent insights from molecular dynamics simulations. *Biochimica et Biophysica Acta (BBA) - Biomembranes* **1858**, 2390–2400 (2016).
403. Lee, J. Y. & Lyman, E. Predictions for Cholesterol Interaction Sites on the A2A Adenosine Receptor. (2012). doi:10.1021/ja307532d
404. Neale, C., Herce, H. D., Pomès, R. & García, A. E. Can Specific Protein-Lipid Interactions Stabilize an Active State of the Beta 2 Adrenergic Receptor? *Biophysical Journal* **109**, 1652–1662 (2015).
405. Xavier Periole, *, Thomas Huber, *, Siewert-Jan Marrink, † and & Sakmar‡, T. P. G Protein-Coupled Receptors Self-Assemble in Dynamics Simulations of Model Bilayers. (2007). doi:10.1021/ja0706246
406. Prasanna, X., Chattopadhyay, A. & Sengupta, D. Cholesterol Modulates the Dimer Interface of the β2-Adrenergic Receptor via Cholesterol Occupancy Sites. *Biophysical Journal* **106**, 1290–1300 (2014).
407. Provasi, D., Boz, M. B., Johnston, J. M. & Filizola, M. Preferred Supramolecular Organization and Dimer Interfaces of Opioid Receptors from Simulated Self-Association. *PLOS Computational Biology* **11**, e1004148 (2015).
408. Manna, M. *et al.* Mechanism of allosteric regulation of β2-adrenergic receptor by cholesterol. *eLife* **5**, e18432 (2016).
409. Velgy, N., Hedger, G. & Biggin, P. C. GPCRs: What Can We Learn from Molecular Dynamics Simulations? in *Computational Methods for GPCR Drug Discovery* (ed. Heifetz, A.) 133–158 (Springer New York, 2018). doi:10.1007/978-1-4939-7465-8_6
410. Ghosh, E., Kumari, P., Jaiman, D. & Shukla, A. K. Methodological advances: the unsung heroes of the GPCR structural revolution. *Nature Reviews Molecular Cell Biology* **16**, 69–81 (2015).
411. Gether, U. *et al.* Agonists induce conformational changes in transmembrane domains III and VI of the beta2 adrenoceptor. *EMBO J* **16**, 6737–6747 (1997).
412. Kobiilka, B. K. & Gether, U. Use of fluorescence spectroscopy to study conformational changes in the β2-adrenoceptor. in *Methods in Enzymology* **343**, 170–182 (Academic Press, 2002).
413. Day, P. W. *et al.* A monoclonal antibody for G protein–coupled receptor crystallography. *Nature Methods* **4**, 927–929 (2007).

414. Ostermeier, C., Iwata, S., Ludwig, B. & Michel, H. F v fragment-mediated crystallization of the membrane protein bacterial cytochrome c oxidase. *Nature Structural Biology* **2**, 842 (1995).
415. Hunte, C., Koepke, J., Lange, C., Rossmanith, T. & Michel, H. Structure at 2.3 A resolution of the cytochrome bc(1) complex from the yeast Saccharomyces cerevisiae co-crystallized with an antibody Fv fragment. *Structure* **8**, 669–684 (2000).
416. Padan, E., Venturi, M., Michel, H. & Hunte, C. Production and characterization of monoclonal antibodies directed against native epitopes of NhaA, the Na+/H+ antiporter of Escherichia coli. *FEBS Letters* **441**, 53–58 (1998).
417. Hunte, C. & Michel, H. Crystallisation of membrane proteins mediated by antibody fragments. *Current Opinion in Structural Biology* **12**, 503–508 (2002).
418. Screpanti, E., Padan, E., Rimon, A., Michel, H. & Hunte, C. Crucial Steps in the Structure Determination of the Na+/H+ Antiporter NhaA in its Native Conformation. *Journal of Molecular Biology* **362**, 192–202 (2006).
419. Shimamura, T. *et al.* Structure of the human histamine H1 receptor complex with doxepin. *Nature* **475**, 65–70 (2011).
420. Rosenbaum, D. M. *et al.* GPCR engineering yields high-resolution structural insights into beta2-adrenergic receptor function. *Science* **318**, 1266–1273 (2007).
421. Manglik, A. *et al.* Crystal structure of the μ-opioid receptor bound to a morphinan antagonist. *Nature* **485**, 321–326 (2012).
422. Zhang, C. *et al.* High-resolution crystal structure of human protease-activated receptor 1. *Nature* **492**, 387–392 (2012).
423. Granier, S. *et al.* Structure of the δ-opioid receptor bound to naltrindole. *Nature* **485**, 400–404 (2012).
424. Jaakola, V.-P. *et al.* The 2.6 angstrom crystal structure of a human A2A adenosine receptor bound to an antagonist. *Science* **322**, 1211–1217 (2008).
425. Chien, E. Y. T. *et al.* Structure of the human dopamine D3 receptor in complex with a D2/D3 selective antagonist. *Science* **330**, 1091–1095 (2010).
426. Wu, B. *et al.* Structures of the CXCR4 chemokine GPCR with small-molecule and cyclic peptide antagonists. *Science* **330**, 1066–1071 (2010).
427. Wu, H. *et al.* Structure of the human κ-opioid receptor in complex with JDTic. *Nature* **485**, 327–332 (2012).
428. Hanson, M. A. *et al.* Crystal structure of a lipid G protein-coupled receptor. *Science* **335**, 851–855 (2012).

429. Tan, Q. *et al.* Structure of the CCR5 chemokine receptor-HIV entry inhibitor maraviroc complex. *Science* **341**, 1387–1390 (2013).
430. Scott, K. Y. and D. Engineering Stabilised G Protein-coupled Receptors for Biochemical and Structural Studies.
431. Warne, T., Serrano-Vega, M. J., Tate, C. G. & Schertler, G. F. Development and crystallization of a minimal thermostabilised G protein-coupled receptor. *Protein Expr Purif* **65**, 204–213 (2009).
432. Tate, C. G. & Schertler, G. F. X. Engineering G protein-coupled receptors to facilitate their structure determination. *Curr. Opin. Struct. Biol.* **19**, 386–395 (2009).
433. Scott, D. J. & Pluckthun, A. Direct molecular evolution of detergent-stable G protein-coupled receptors using polymer encapsulated cells. *J Mol Biol* **425**, 662–77 (2013).
434. Maeda, S. & Schertler, G. F. X. Production of GPCR and GPCR complexes for structure determination. *Curr. Opin. Struct. Biol.* **23**, 381–392 (2013).
435. Venkatakrishnan, A. J. *et al.* Molecular signatures of G-protein-coupled receptors. *Nature* **494**, 185–194 (2013).
436. Granier, S. & Kobilka, B. A new era of GPCR structural and chemical biology. *Nat Chem Biol* **8**, 670–673 (2012).
437. Kolb, P. *et al.* Structure-based discovery of β2-adrenergic receptor ligands. *Proc Natl Acad Sci U S A* **106**, 6843–6848 (2009).
438. Carlsson, J. *et al.* Ligand Discovery from a Dopamine D3 Receptor Homology Model and Crystal Structure. *Nat Chem Biol* **7**, 769–778 (2011).
439. Carlsson, J. *et al.* Structure-Based Discovery of A2A Adenosine Receptor Ligands. *Journal of Medicinal Chemistry* **53**, 3748 (2010).
440. de Graaf, C. *et al.* Crystal structure-based virtual screening for novel fragment-like ligands of the human histamine H1 receptor. *J Med Chem* **54**, 8195–8206 (2011).
441. Christopher, J. A. *et al.* Biophysical Fragment Screening of the β1-Adrenergic Receptor: Identification of High Affinity Arylpiperazine Leads Using Structure-Based Drug Design. *J Med Chem* **56**, 3446–3455 (2013).
442. Singhal, A. *et al.* Insights into congenital stationary night blindness based on the structure of G90D rhodopsin. *EMBO reports* **14**, 520–526 (2013).
443. Warne, T., Edwards, P. C., Leslie, A. G. W. & Tate, C. G. Crystal Structures of a Stabilized β1-Adrenoceptor Bound to the Biased Agonists Bucindolol and Carvedilol. *Structure* **20–540**, 841–849 (2012).
444. Tate, C. G. Overexpression of mammalian integral membrane proteins for structural studies. *FEBS Letters* **504**, 94–98 (2001).

445. Okude, J. *et al.* Identification of a Conformational Equilibrium That Determines the Efficacy and Functional Selectivity of the μ-Opioid Receptor. *Angew. Chem. Int. Ed. Engl.* **54**, 15771–15776 (2015).
446. Kofuku, Y. *et al.* Functional Dynamics of Deuterated β2-Adrenergic Receptor in Lipid Bilayers Revealed by NMR Spectroscopy. *Angewandte Chemie International Edition* **53**, 13376–13379 (2014).
447. Kofuku, Y. *et al.* Efficacy of the β_2-adrenergic receptor is determined by conformational equilibrium in the transmembrane region. *Nature Communications* **3**, 1045 (2012).
448. Nygaard, R. *et al.* The dynamic process of β(2)-adrenergic receptor activation. *Cell* **152**, 532–542 (2013).
449. Solt, A. S. *et al.* Insight into partial agonism by observing multiple equilibria for ligand-bound and G s -mimetic nanobody-bound β 1 -adrenergic receptor. *Nature Communications* **8**, 1795 (2017).
450. Isogai, S. *et al.* Backbone NMR reveals allosteric signal transduction networks in the β1-adrenergic receptor. *Nature* **530**, 237–241 (2016).
451. Eddy, M. T. *et al.* Allosteric Coupling of Drug Binding and Intracellular Signaling in the A2A Adenosine Receptor. *Cell* **172**, 68-80.e12 (2018).
452. Sattler, M. & Fesik, S. W. Use of deuterium labeling in NMR: overcoming a sizeable problem. *Structure* **4**, 1245–1249 (1996).
453. Gardner, K. H. & Kay, L. E. The use of 2h, 13c, 15n multidimensional nmr gto study the structure and dynamics of proteins. *Annu. Rev. Biophys. Biomol. Struct.* **27**, 357–406 (1998).
454. Kerfah, R., Plevin, M. J., Sounier, R., Gans, P. & Boisbouvier, J. Methyl-specific isotopic labeling: a molecular tool box for solution NMR studies of large proteins. *Current Opinion in Structural Biology* **32**, 113–122 (2015).
455. Daniel Nietlispach, ⊥ *et al.* An Approach to the Structure Determination of Larger Proteins Using Triple Resonance NMR Experiments in Conjunction with Random Fractional Deuteration. (1996). doi:10.1021/ja952207b
456. Venters, R. A. *et al.* High-level 2H/13C/15N labeling of proteins for NMR studies. *J Biomol NMR* **5**, 339–344 (1995).
457. Pervushin, K., Riek, R., Wider, G. & Wüthrich, K. Attenuated T2 relaxation by mutual cancellation of dipole–dipole coupling and chemical shift anisotropy indicates an avenue to NMR structures of very large biological macromolecules in solution. *PNAS* **94**, 12366–12371 (1997).

458. Pachter, R., Arrowsmith, C. H. & Jardetzky, O. The effect of selective deuteration on magnetization transfer in larger proteins. *J. Biomol. NMR* **2**, 183–194 (1992).
459. Casiraghi, M., Damian, M., Lescop, E., Banères, J.-L. & Catoire, L. J. Illuminating the Energy Landscape of GPCRs: The Key Contribution of Solution-State NMR Associated with Escherichia coli as an Expression Host. *Biochemistry* **57**, 2297–2307 (2018).
460. Opitz, C., Isogai, S. & Grzesiek, S. An economic approach to efficient isotope labeling in insect cells using homemade 15N-, 13C- and 2H-labeled yeast extracts. *J. Biomol. NMR* **62**, 373–385 (2015).
461. Salom, D. *et al.* Isotopic labeling of mammalian G protein-coupled receptors heterologously expressed in Caenorhabditis elegans. *Anal. Biochem.* **472**, 30–36 (2015).
462. Clark, L. D. *et al.* Ligand modulation of sidechain dynamics in a wild-type human GPCR. *eLife* **6**, e28505 (2017).
463. Miyazawa-Onami, M. *et al.* Perdeuteration and methyl-selective (1)H, (13)C-labeling by using a Kluyveromyces lactis expression system. *J. Biomol. NMR* **57**, 297–304 (2013).
464. Clark, L. *et al.* Methyl labeling and TROSY NMR spectroscopy of proteins expressed in the eukaryote Pichia pastoris. *J. Biomol. NMR* **62**, 239–245 (2015).
465. Crespi, H. L., Conrad, S. M., Uphaus, R. A. & Katz, J. J. Cultivation of Microorganisms in Heavy Water*. *Annals of the New York Academy of Sciences* **84**, 648–666 (1960).
466. Franke, B. *et al.* Production of isotope-labeled proteins in insect cells for NMR. *J. Biomol. NMR* **71**, 173–184 (2018).
467. Warschawski, D. E. *et al.* Choosing membrane mimetics for NMR structural studies of transmembrane proteins. *Biochimica et Biophysica Acta (BBA) - Biomembranes* **1808**, 1957–1974 (2011).
468. Egloff, P., Deluigi, M., Heine, P., Balada, S. & Plückthun, A. A cleavable ligand column for the rapid isolation of large quantities of homogeneous and functional neurotensin receptor 1 variants from E. coli. *Protein Expression and Purification* **108**, 106–114 (2015).
469. Seddon, A. M., Curnow, P. & Booth, P. J. Membrane proteins, lipids and detergents: not just a soap opera. *Biochim. Biophys. Acta* **1666**, 105–117 (2004).
470. Egloff, P. *et al.* Structure of signaling-competent neurotensin receptor 1 obtained by directed evolution in Escherichia coli. *PNAS* **111**, E655–E662 (2014).
471. Warne, T., Chirnside, J. & Schertler, G. F. X. Expression and purification of truncated, non-glycosylated turkey beta-adrenergic receptors for crystallization. *Biochim. Biophys. Acta* **1610**, 133–140 (2003).

472. Park, S. H. *et al.* Optimization of purification and refolding of the human chemokine receptor CXCR1 improves the stability of proteoliposomes for structure determination. *Biochim. Biophys. Acta* **1818**, 584–591 (2012).
473. Huang, W. *et al.* Structural insights into μ-opioid receptor activation. *Nature* **524**, 315–321 (2015).
474. Weiss, H. M. & Grisshammer, R. Purification and characterization of the human adenosine A(2a) receptor functionally expressed in Escherichia coli. *Eur. J. Biochem.* **269**, 82–92 (2002).
475. Ye, L., Van Eps, N., Zimmer, M., Ernst, O. P. & Prosser, R. S. Activation of the A2A adenosine G-protein-coupled receptor by conformational selection. *Nature* **533**, 265–268 (2016).
476. Vukoti, K., Kimura, T., Macke, L., Gawrisch, K. & Yeliseev, A. Stabilization of Functional Recombinant Cannabinoid Receptor CB2 in Detergent Micelles and Lipid Bilayers. *PLOS ONE* **7**, e46290 (2012).
477. Valley, C. C. *et al.* The methionine-aromatic motif plays a unique role in stabilizing protein structure. *J. Biol. Chem.* **287**, 34979–34991 (2012).
478. Grisshammer, R., Averbeck, P. & Sohal, A. K. Improved purification of a rat neurotensin receptor expressed in Escherichia coli. *Biochemical Society Transactions* **27**, 899–903 (1999).
479. Yin, J., Mobarec, J. C., Kolb, P. & Rosenbaum, D. M. Crystal structure of the human OX2 orexin receptor bound to the insomnia drug suvorexant. *Nature* **519**, 247–250 (2015).
480. Grisshammer, R. Purification of recombinant G-protein-coupled receptors. *Meth. Enzymol.* **463**, 631–645 (2009).
481. Bornhorst, J. A. & Falke, J. J. [16] Purification of Proteins Using Polyhistidine Affinity Tags. *Methods Enzymol* **326**, 245–254 (2000).
482. Einhauer, A. & Jungbauer, A. Affinity of the monoclonal antibody M1 directed against the FLAG peptide. *J Chromatogr A* **921**, 25–30 (2001).
483. Molday, L. L. & Molday, R. S. 1D4: A Versatile Epitope Tag for the Purification and Characterization of Expressed Membrane and Soluble Proteins. in *Protein Affinity Tags: Methods and Protocols* (eds. Giannone, R. J. & Dykstra, A. B.) 1–15 (Springer New York, 2014). doi:10.1007/978-1-4939-1034-2_1
484. Rasmussen, S. G. F. *et al.* Crystal structure of the human beta2 adrenergic G-protein-coupled receptor. *Nature* **450**, 383–387 (2007).
485. Kobilka, B. K. Amino and carboxyl terminal modifications to facilitate the production and purification of a G protein-coupled receptor. *Anal. Biochem.* **231**, 269–271 (1995).
486. Huang, J., Chen, S., Zhang, J. J. & Huang, X.-Y. Crystal structure of oligomeric β1-adrenergic G protein-coupled receptors in ligand-free basal state. *Nat. Struct. Mol. Biol.* **20**, 419–425 (2013).

487. Manglik, A. *et al.* Structural Insights into the Dynamic Process of beta2-Adrenergic Receptor Signaling. *Cell* **161**, 1101–11 (2015).
488. Caron, M. G., Srinivasan, Y., Pitha, J., Kociolek, K. & Lefkowitz, R. J. Affinity chromatography of the beta-adrenergic receptor. *J. Biol. Chem.* **254**, 2923–2927 (1979).
489. Lefkowitz, R. J., Haber, E. & O'Hara, D. Identification of the cardiac beta-adrenergic receptor protein: solubilization and purification by affinity chromatography. *Proc Natl Acad Sci U S A* **69**, 2828–2832 (1972).
490. Perreault, M. L., Hasbi, A., O'Dowd, B. F. & George, S. R. Heteromeric Dopamine Receptor Signaling Complexes: Emerging Neurobiology and Disease Relevance. *Neuropsychopharmacology* **39**, 156–168 (2014).
491. Denisov, I. G., Grinkova, Y. V., Lazarides, A. A. & Sligar, S. G. Directed self-assembly of monodisperse phospholipid bilayer Nanodiscs with controlled size. *J. Am. Chem. Soc.* **126**, 3477–3487 (2004).
492. Baicu, S. C. & Taylor, M. J. Acid-base buffering in organ preservation solutions as a function of temperature: new parameters for comparing buffer capacity and efficiency. *Cryobiology* **45**, 33–48 (2002).
493. Grisshammer, R., Duckworth, R. & Henderson, R. Expression of a rat neurotensin receptor in Escherichia coli. *Biochem J* **295**, 571–576 (1993).
494. Yong, K. J. & Scott, D. J. Rapid directed evolution of stabilized proteins with cellular high-throughput encapsulation solubilization and screening (CHESS). *Biotechnol. Bioeng.* **112**, 438–446 (2015).
495. Marley, J., Lu, M. & Bracken, C. A method for efficient isotopic labeling of recombinant proteins. *Journal Of Biomolecular NMR* **20**, 71–75 (2001).
496. Cai, M. *et al.* An efficient and cost-effective isotope labeling protocol for proteins expressed in Escherichia coli. *J. Biomol. NMR* **11**, 97–102 (1998).
497. Rath, A., Glibowicka, M., Nadeau, V. G., Chen, G. & Deber, C. M. Detergent binding explains anomalous SDS-PAGE migration of membrane proteins. *Proc. Natl. Acad. Sci. U.S.A.* **106**, 1760–1765 (2009).
498. Mackenzie, J. F., Daly, C. J., Pediani, J. D. & McGrath, J. C. Quantitative imaging in live human cells reveals intracellular alpha(1)-adrenoceptor ligand-binding sites. *J. Pharmacol. Exp. Ther.* **294**, 434–443 (2000).
499. Johnson, R. E. *et al.* 4,5-Dihydro-3-(methanesulfonamidophenyl)-1-phenyl-1H-2,4-benzodiazepines: A Novel Class III Antiarrhythmic Agents. *J. Med. Chem.* **38**, 2551–2556 (1995).

500. Johnson, R. E. *et al.* 4,5-Dihydro-1-phenyl-1H-2,4-benzodiazepines: Novel antiarrhythmic agents. *J. Med. Chem.* **36**, 3361–3370 (1993).
501. Butcher, J. W. *et al.* Novel 5-cyclopropyl-1,4-benzodiazepin-2-ones as potent and selective IKs-blocking class III antiarrhythmic agents. *Bioorganic & Medicinal Chemistry Letters* **13**, 1165–1168 (2003).
502. Seebohm, G. *et al.* Molecular Determinants of KCNQ1 Channel Block by a Benzodiazepine. *Mol Pharmacol* **64**, 70–77 (2003).
503. Shvets, N., Terletskaya, A., Dimoglo, A. & Chumakov, Yu. Study of the electronic and structural features characteristic of 4,5-dihydro-1-phenyl-1H-2,4-benzodiazepines demonstrating antiarrhythmic activity. *Journal of Molecular Structure: THEOCHEM* **463**, 105–110 (1999).
504. Liebman, J. M. *et al.* CGS 7525A, A new, centrally active alpha2 adrenoceptor antagonist. *Life Sciences* **32**, 355–363 (1983).
505. Gupta, S. P. Quantitative Structure-Activity Relationship Studies on Cholecystokinin Antagonists. *Current Pharmaceutical Design* (2001). Available at: http://www.eurekaselect.com/64254/article. (Accessed: 25th March 2019)
506. Ursini, A. *et al.* Synthesis and SAR of New 5-Phenyl-3-ureido-1,5-benzodiazepines as Cholecystokinin-B Receptor Antagonists. *J. Med. Chem.* **43**, 3596–3613 (2000).
507. Evans, B. E. *et al.* Design of potent, orally effective, nonpeptidal antagonists of the peptide hormone cholecystokinin. *PNAS* **83**, 4918–4922 (1986).
508. Haynes, S. W., Gao, X., Tang, Y. & Walsh, C. T. Assembly of Asperlicin Peptidyl Alkaloids from Anthranilate and Tryptophan: A Two-Enzyme Pathway Generates Heptacyclic Scaffold Complexity in Asperlicin E. *J. Am. Chem. Soc.* **134**, 17444–17447 (2012).
509. Kukla, M. J. *et al.* Synthesis and anti-HIV-1 activity of 4,5,6,7-tetrahydro-5-methylimidazo[4,5,1-jk][1,4]benzodiazepin-2(1H)-one (TIBO) derivatives. *J. Med. Chem.* **34**, 746–751 (1991).
510. Zhou, Z. & Madura, J. D. CoMFA 3D-QSAR Analysis of HIV-1 RT Nonnucleoside Inhibitors, TIBO Derivatives Based on Docking Conformation and Alignment. *J. Chem. Inf. Comput. Sci.* **44**, 2167–2178 (2004).
511. Ho, W. *et al.* Synthesis and Anti-HIV-1 Activity of 4,5,6,7-Tetrahydro-5-methylimidazo[4,5,1-jk][1,4]benzodiazepin-2(1H)-one (TlBO) Derivatives. 4. *J. Med. Chem.* **38**, 794–802 (1995).
512. Breslin, H. J. *et al.* Synthesis and anti-HIV activity of 1,3,4,5-tetrahydro-2H-1,4-benzodiazepin-2-one (TBO) derivatives. truncated

4,5,6,7-tetrahydro-5-methylimidazo[4,5,1-jk][1,4]benzodiazepin-2(1H)-ones (TIBO) analogues. *Bioorganic & Medicinal Chemistry* **7**, 2427–2436 (1999).

513. Balestrieri, M., Oriani, M. G., Simoncini, A. & Bellantuono, C. Psychotropic Drug Treatment in Anorexia Nervosa. Search for Differences in Efficacy/Tolerability Between Adolescent and Mixed-age Population. *European Eating Disorders Review* **21**, 361–373 (2013).
514. Dunican, K. C. & DelDotto, D. The Role of Olanzapine in the Treatment of Anorexia Nervosa. *Ann Pharmacother* **41**, 111–115 (2007).
515. Piggott, M. *et al.* Comparative distribution of binding of the muscarinic receptor ligands pirenzepine, AF-DX 384, (R,R)-I-QNB and (R,S)-I-QNB to human brain. *Journal of Chemical Neuroanatomy* **24**, 211–223 (2002).
516. Cappelli, A. *et al.* Synthesis, Biological Evaluation, and Quantitative Receptor Docking Simulations of 2-[(Acylamino)ethyl]-1,4-benzodiazepines as Novel Tifluadom-like Ligands with High Affinity and Selectivity for κ-Opioid Receptors. *J. Med. Chem.* **39**, 860–872 (1996).
517. Anzini, M. *et al.* Synthesis, Biological Evaluation, and Receptor Docking Simulations of 2-[(Acylamino)ethyl]-1,4-benzodiazepines as κ-Opioid Receptor Agonists Endowed with Antinociceptive and Antiamnesic Activity. *J. Med. Chem.* **46**, 3853–3864 (2003).
518. Burkard, W. P. [3H]tifluadom binding in guinea-pig brain membranes. *European Journal of Pharmacology* **97**, 337–338 (1984).
519. Römer, D. *et al.* Unexpected opioid activity in a known class of drug. *Life Sciences* **31**, 1217–1220 (1982).
520. Kesäniemi, Y. A. & Miettinen, T. A. Inhibition of cholesterol absorption by neomycin, benzodiazepine derivatives and ketoconazole. *Eur J Clin Pharmacol* **40**, S65–S67 (1991).
521. Ilango, S. S., Remya, P. U. & Ponnuswamy, S. Synthesis and antimicrobial activity of novel 1,5-benzodiazepines. 5
522. Nallan, L. *et al.* Protein Farnesyltransferase Inhibitors Exhibit Potent Antimalarial Activity. *J. Med. Chem.* **48**, 3704–3713 (2005).
523. Chen, C.-Y. *et al.* Synthesis, DNA-binding abilities and anticancer activities of triazole-pyrrolo[2,1-c][1,4]benzodiazepines hybrid scaffolds. *Bioorganic & Medicinal Chemistry Letters* **23**, 6854–6859 (2013).
524. Cortes Eduardo, C. *et al.* Anticancer Activity and Anti-inflammatory Studies of 5-Aryl-1,4-benzodiazepine Derivatives. *Anti-Cancer Agents in Medicinal Chemistry* **12**, 611–618 (2012).
525. Costa, E., Guidotti, A. & Mao, C. C. Evidence for involvement of GABA in the action of benzodiazepines: studies on rat cerebellum. *Adv Biochem Psychopharmacol* 113–30 (1975).

526. Olsen, R. W. GABAA receptor: Positive and negative allosteric modulators. *Neuropharmacology* **136**, 10–22 (2018).
527. $GABA_A$ receptor positive allosteric modulator. *Wikipedia* (2019).
528. Sternbach, L. H. 1,4-benzodiazepines. Chemistry and some aspects of the structure-activity relationship. *Angew Chem Int Ed Engl* **10**, 34–43 (1971).
529. Mayer, M. & Meyer, B. Group Epitope Mapping by Saturation Transfer Difference NMR To Identify Segments of a Ligand in Direct Contact with a Protein Receptor. *Journal of the American Chemical Society* **123**, 6108–6117 (2001).
530. Hwang, T. L. & Shaka, A. J. Water Suppression That Works. Excitation Sculpting Using Arbitrary Wave-Forms and Pulsed-Field Gradients. *Journal of Magnetic Resonance, Series A* **112**, 275–279 (1995).
531. Dalvit, C. Efficient multiple-solvent suppression for the study of the interactions of organic solvents with biomolecules. 8
532. Optimization and CH methionine labeling of a signaling competent neurotensin receptor 1 variant for NMR studies. *PubFacts* Available at: https://www.pubfacts.com/detail/29596791/Optimization-and-CH-methionine-labeling-of-a-signaling-competent-neurotensin-receptor-1-variant-for-. (Accessed: 1st February 2019)
533. Cambridge, D., Davey, M. J. & Massingham, R. Prazosin, a selective antagonist of post-synaptic alpha-adrenoceptors [proceedings]. *Br J Pharmacol* **59**, 514P-515P (1977).
534. Pubchem. Spiperone. Available at: https://pubchem.ncbi.nlm.nih.gov/compound/5265. (Accessed: 13th December 2018)
535. Spiperone. *Wikipedia* (2018).
536. Ivanović, M. T., Bruetzel, L. K., Lipfert, J. & Hub, J. S. Temperature-Dependent Atomic Models of Detergent Micelles Refined against Small-Angle X-Ray Scattering Data. *Angew. Chem. Int. Ed.* **57**, 5635–5639 (2018).
537. Plati, J., Tsomaia, N., Piserchio, A. & Mierke, D. F. Structural Features of Parathyroid Hormone Receptor Coupled to GαS-Protein. *Biophysical Journal* **92**, 535–540 (2007).
538. Vom, A. *et al.* Detection and Prevention of Aggregation-based False Positives in STD-NMR-based Fragment Screening. *Aust. J. Chem.* **66**, 1518–1524 (2013).
539. LaPlante, S. R. *et al.* Compound Aggregation in Drug Discovery: Implementing a Practical NMR Assay for Medicinal Chemists. *J. Med. Chem.* **56**, 5142–5150 (2013).
540. Sassano, M. F., Doak, A. K., Roth, B. L. & Shoichet, B. K. Colloidal Aggregation Causes Inhibition of G Protein-Coupled Receptors. *J Med Chem* **56**, 2406–2414 (2013).

541. Dalvit, C., Caronni, D., Mongelli, N., Veronesi, M. & Vulpetti, A. NMR-Based Quality Control Approach for the Identification of False Positives and False Negatives in High Throughput Screening. (2006). Available at: https://www.ingentaconnect.com/content/ben/cddt/2006/00000003/00000002/art00003. (Accessed: 16th May 2019)
542. Seidler, J., McGovern, S. L., Doman, T. N. & Shoichet, B. K. Identification and prediction of promiscuous aggregating inhibitors among known drugs. *J. Med. Chem.* **46**, 4477–4486 (2003).
543. Scott, D. E. *et al.* Using a fragment-based approach to target protein-protein interactions. *Chembiochem* **14**, 332–342 (2013).
544. Silvestre, H. L., Blundell, T. L., Abell, C. & Ciulli, A. Integrated biophysical approach to fragment screening and validation for fragment-based lead discovery. *Proc. Natl. Acad. Sci. U.S.A.* **110**, 12984–12989 (2013).
545. Cala, O. & Krimm, I. Ligand-Orientation Based Fragment Selection in STD NMR Screening. *J Med Chem* **58**, 8739–42 (2015).
546. Sledz, P. *et al.* Optimization of the interligand Overhauser effect for fragment linking: application to inhibitor discovery against Mycobacterium tuberculosis pantothenate synthetase. *J. Am. Chem. Soc.* **132**, 4544–4545 (2010).
547. Santos, R. *et al.* A comprehensive map of molecular drug targets. *Nat Rev Drug Discov* **16**, 19–34 (2017).
548. Garland, S. L. Are GPCRs still a source of new targets? *J Biomol Screen* **18**, 947–966 (2013).
549. Nygaard, R., Frimurer, T. M., Holst, B., Rosenkilde, M. M. & Schwartz, T. W. Ligand binding and micro-switches in 7TM receptor structures. *Trends in Pharmacological Sciences* **30**, 249–259 (2009).
550. Chalothorn, D. *et al.* Differences in the Cellular Localization and Agonist-Mediated Internalization Properties of the α1-Adrenoceptor Subtypes. *Mol Pharmacol* **61**, 1008–1016 (2002).
551. García-Sáinz, J. A., Vázquez-Prado, J. & del Carmen Medina, L. α1-Adrenoceptors: function and phosphorylation. *European Journal of Pharmacology* **389**, 1–12 (2000).
552. Piascik, M. T. & Perez, D. M. Alpha1-adrenergic receptors: new insights and directions. *J. Pharmacol. Exp. Ther.* **298**, 403–410 (2001).
553. Robison, G. A., Butcher, R. W. & Sutherland, E. W. ADENYL CYCLASE AS AN ADRENERGIC RECEPTOR*. *Annals of the New York Academy of Sciences* **139**, 703–723 (1967).
554. Renaud, J.-P. *et al.* Biophysics in drug discovery: impact, challenges and opportunities. *Nat Rev Drug Discov* **15**, 679–698 (2016).

555. Li, D., DeRose, E. F. & London, R. E. The inter-ligand Overhauser effect: A powerful new NMR approach for mapping structural relationships of macromolecular ligands. *J Biomol NMR* **15**, 71–76 (1999).
556. Orts, J., Griesinger, C. & Carlomagno, T. The INPHARMA technique for pharmacophore mapping: A theoretical guide to the method. *J Magn Reson* **200**, 64–73 (2009).
557. Ring, A. M. *et al.* Adrenaline-activated structure of beta2-adrenoceptor stabilized by an engineered nanobody. *Nature* **502**, 575–9 (2013).
558. Perez, D. M. Structure-Function of α1-Adrenergic Receptors. *Biochem Pharmacol* **73**, 1051–1062 (2007).
559. Hwa, J., Graham, R. M. & Perez, D. M. Identification of Critical Determinants of α1-Adrenergic Receptor Subtype Selective Agonist Binding. *J. Biol. Chem.* **270**, 23189–23195 (1995).
560. Zhang, J., Yang, J., Jang, R. & Zhang, Y. GPCR-I-TASSER: A Hybrid Approach to G Protein-Coupled Receptor Structure Modeling and the Application to the Human Genome. *Structure* **23**, 1538–1549 (2015).
561. Staus, D. P. *et al.* Allosteric nanobodies reveal the dynamic range and diverse mechanisms of G-protein-coupled receptor activation. *Nature* **535**, 448–452 (2016).
562. Kim, S. *et al.* PubChem Substance and Compound databases. *Nucleic Acids Res* **44**, D1202–D1213 (2016).
563. Greenwood, J. R., Calkins, D., Sullivan, A. P. & Shelley, J. C. Towards the comprehensive, rapid, and accurate prediction of the favorable tautomeric states of drug-like molecules in aqueous solution. *J. Comput. Aided Mol. Des.* **24**, 591–604 (2010).
564. Cavanagh, J., Fairbrother, W. J., III, A. G. P. & Skelton, N. J. *Protein NMR Spectroscopy: Principles and Practice*. (Elsevier, 1995).
565. Strop, P. & Brunger, A. T. Refractive index-based determination of detergent concentration and its application to the study of membrane proteins. *Protein Science* **14**, 2207–2211 (2005).
566. Desmond 2.2 User Manual. *Schrödinger Press* 152
567. Strahan, G. D., Keniry, M. A. & Shafer, R. H. NMR structure refinement and dynamics of the K+-[d(G3T4G3)]2 quadruplex via particle mesh Ewald molecular dynamics simulations. *Biophys. J.* **75**, 968–981 (1998).
568. Humphrey, W., Dalke, A. & Schulten, K. VMD: visual molecular dynamics. *J Mol Graph* **14**, 33–38, 27–28 (1996).
569. Maïga, A. *et al.* Molecular exploration of the α1A-adrenoceptor orthosteric site: Binding site definition for epinephrine, HEAT and prazosin. *FEBS Letters* **588**, 4613–4619 (2014).

570. Ishiguro, M. *et al.* Identification of binding sites of prazosin, tamsulosin and KMD-3213 with α1-adrenergic receptor subtypes by molecular modeling. *Life Sciences* **71**, 2531–2541 (2002).
571. Meyer, M. D. *et al.* Synthesis and *in Vitro* Characterization of *N* -[5-(4,5-Dihydro-1 *H* -imidazol-2-yl)- 2-hydroxy-5,6,7,8-tetrahydronaphthalen-1-yl]methanesulfonamide and Its Enantiomers: A Novel Selective α_{1A} Receptor Agonist [1]. *Journal of Medicinal Chemistry* **39**, 4116–4119 (1996).
572. Li, D., DeRose, E. F. & London, R. E. The inter-ligand Overhauser effect: a powerful new NMR approach for mapping structural relationships of macromolecular ligands. *J. Biomol. NMR* **15**, 71–76 (1999).
573. Leone, M., Freeze, H. H. & Pellecchia, C. S. C. and M. The Nuclear Overhauser Effect in the Lead Identification Process Pharmacophore Models. *Current Drug Discovery Technologies* (2006). Available at: http://www.eurekaselect.com/89726/article. (Accessed: 28th May 2019)
574. Fruth, M. *et al.* Binding mode characterization of novel RNA polymerase inhibitors using a combined biochemical and NMR approach. *ACS Chem Biol* **9**, 2656–63 (2014).
575. Sugiki, T., Furuita, K., Fujiwara, T. & Kojima, C. Current NMR Techniques for Structure-Based Drug Discovery. *Molecules* **23**, 148 (2018).
576. Becattini, B. *et al.* Structure-activity relationships by interligand NOE-based design and synthesis of antiapoptotic compounds targeting Bid. *Proc Natl Acad Sci U S A* **103**, 12602–6 (2006).
577. Orts, J. *et al.* Crystallography-Independent Determination of Ligand Binding Modes. *Angewandte Chemie International Edition* **47**, 7736–7740 (2008).
578. Orts, J. *et al.* Specific Methyl Group Protonation for the Measurement of Pharmacophore-Specific Interligand NOE Interactions. *Chemistry – A European Journal* **14**, 7517–7520 (2008).
579. Sanchez-Pedregal, V. M. *et al.* The tubulin-bound conformation of discodermolide derived by NMR studies in solution supports a common pharmacophore model for epothilone and discodermolide. *Angew Chem Int Ed Engl* **45**, 7388–94 (2006).
580. Reese, M. *et al.* Structural basis of the activity of the microtubule-stabilizing agent epothilone a studied by NMR spectroscopy in solution. *Angew Chem Int Ed Engl* **46**, 1864–8 (2007).
581. Kubicek, K., Grimm, S. K., Orts, J., Sasse, F. & Carlomagno, T. The tubulin-bound structure of the antimitotic drug tubulysin. *Angew Chem Int Ed Engl* **49**, 4809–12 (2010).
582. Fong, P., McNamara, J. P., Hillier, I. H. & Bryce, R. A. Assessment of QM/MM Scoring Functions for Molecular Docking to HIV-1 Protease. *J. Chem. Inf. Model.* **49**, 913–924 (2009).

583. Cincilla, G., Vidal, D. & Pons, M. An improved scoring function for suboptimal polar ligand complexes. *J Comput Aided Mol Des* **23**, 143–152 (2009).
584. Englebienne, P. & Moitessier, N. Docking Ligands into Flexible and Solvated Macromolecules. 5. Force-Field-Based Prediction of Binding Affinities of Ligands to Proteins. *J. Chem. Inf. Model.* **49**, 2564–2571 (2009).
585. Tarasov, D. & Tovbin, D. How sophisticated should a scoring function be to ensure successful docking, scoring and virtual screening? *J Mol Model* **15**, 329–341 (2009).
586. González-Ruiz, D. & Gohlke, H. Steering Protein−Ligand Docking with Quantitative NMR Chemical Shift Perturbations. *J. Chem. Inf. Model.* **49**, 2260–2271 (2009).
587. Charifson, P. S., Corkery, J. J., Murcko, M. A. & Walters, W. P. Consensus Scoring: A Method for Obtaining Improved Hit Rates from Docking Databases of Three-Dimensional Structures into Proteins. *J. Med. Chem.* **42**, 5100–5109 (1999).
588. Cross, J. B. *et al.* Comparison of Several Molecular Docking Programs: Pose Prediction and Virtual Screening Accuracy. *J. Chem. Inf. Model.* **49**, 1455–1474 (2009).
589. Munk, C. *et al.* GPCRdb: the G protein-coupled receptor database – an introduction. *Br J Pharmacol* **173**, 2195–2207 (2016).
590. Jozwiak, K. *et al.* The effect of fenoterol stereochemistry on the β2 adrenergic receptor system: ligand directed chiral recognition. *Chirality* **23**, E1–E6 (2011).
591. Comba, P. The relation between ligand structures, coordination stereochemistry, and electronic and thermodynamic properties. *Coordination Chemistry Reviews* **123**, 1–48 (1993).
592. Bartlett, J. B., Dredge, K. & Dalgleish, A. G. The evolution of thalidomide and its IMiD derivatives as anticancer agents. *Nature Reviews Cancer* **4**, 314 (2004).
593. Shortt, J., Hsu, A. K. & Johnstone, R. W. Thalidomide-analogue biology: immunological, molecular and epigenetic targets in cancer therapy. *Oncogene* **32**, 4191–4202 (2013).
594. Melchert, M. & List, A. The thalidomide saga. *The International Journal of Biochemistry & Cell Biology* **39**, 1489–1499 (2007).
595. McBride, W. G. Thalidomide and Congenital Abnormalities. 3
596. Lenz, W. Thalidomide and Congenital Abnormalities. in *Problems of Birth Defects: From Hippocrates to Thalidomide and After* (ed. Persaud, T. V. N.) 199–199 (Springer Netherlands, 1977). doi:10.1007/978-94-011-6621-8_28
597. Fischer, E. S. *et al.* Structure of the DDB1–CRBN E3 ubiquitin ligase in complex with thalidomide. *Nature* **512**, 49–53 (2014).
598. Lopez-Girona, A. *et al.* Cereblon is a direct protein target for immunomodulatory and antiproliferative activities of lenalidomide and pomalidomide. *Leukemia* **26**, 2326–2335 (2012).

599. Lopez, J. J. *et al.* The structure of the neuropeptide bradykinin bound to the human G-protein coupled receptor bradykinin B2 as determined by solid-state NMR spectroscopy. *Angew. Chem. Int. Ed. Engl.* **47**, 1668–1671 (2008).
600. Perez, D. M. & Doze, V. A. Cardiac and neuroprotection regulated by alpha(1)-adrenergic receptor subtypes. *J Recept Signal Transduct Res* **31**, 98–110 (2011).
601. Schlichting, I. X-Ray Crystallography of Protein-Ligand Interactions. in *Protein-Ligand Interactions: Methods and Applications* (ed. Ulrich Nienhaus, G.) 155–165 (Humana Press, 2005). doi:10.1385/1-59259-912-5:155
602. Rodger, A., Marrington, R., Roper, D. & Windsor, S. Circular Dichroism Spectroscopy for the Study of Protein-Ligand Interactions. in *Protein-Ligand Interactions: Methods and Applications* (ed. Ulrich Nienhaus, G.) 343–363 (Humana Press, 2005). doi:10.1385/1-59259-912-5:343
603. Hassan, S. A., Gracia, L., Vasudevan, G. & Steinbach, P. J. Computer Simulation of Protein-Ligand Interactions. in *Protein-Ligand Interactions: Methods and Applications* (ed. Ulrich Nienhaus, G.) 451–492 (Humana Press, 2005). doi:10.1385/1-59259-912-5:451
604. Urbanke, C., Witte, G. & Curth, U. Sedimentation Velocity Method in the Analytical Ultracentrifuge for the Study of Protein-Protein Interactions. in *Protein-Ligand Interactions: Methods and Applications* (ed. Ulrich Nienhaus, G.) 101–113 (Humana Press, 2005). doi:10.1385/1-59259-912-5:101
605. Gesellchen, F., Zimmermann, B. & Herberg, F. W. Direct Optical Detection of Protein-Ligand Interactions. in *Protein-Ligand Interactions: Methods and Applications* (ed. Ulrich Nienhaus, G.) 17–45 (Humana Press, 2005). doi:10.1385/1-59259-912-5:017
606. Jennissen, H. P. Hydrophobic Interaction Chromatography. in *Protein-Ligand Interactions: Methods and Applications* (ed. Ulrich Nienhaus, G.) 81–99 (Humana Press, 2005). doi:10.1007/978-1-59259-912-7_5
607. Janshoff, A. & Steinem, C. Label-Free Detection of Protein-Ligand Interactions by the Quartz Crystal Microbalance. in *Protein-Ligand Interactions: Methods and Applications* (ed. Ulrich Nienhaus, G.) 47–63 (Humana Press, 2005). doi:10.1385/1-59259-912-5:047
608. Lewis, E. A. & Murphy, K. P. Isothermal Titration Calorimetry. in *Protein-Ligand Interactions: Methods and Applications* (ed. Ulrich Nienhaus, G.) 1–15 (Humana Press, 2005). doi:10.1385/1-59259-912-5:001
609. Mandell, J. G., Baerga-Ortiz, A., Falick, A. M. & Komives, E. A. Measurement of Solvent Accessibility at Protein-Protein Interfaces. in *Protein-Ligand Interactions: Methods and Applications* (ed. Ulrich Nienhaus, G.) 65–79 (Humana Press, 2005). doi:10.1385/1-59259-912-5:065

610. Strange, R. W. & Hasnain, S. S. Combined Use of XAFS and Crystallography for Studying Protein-Ligand Interactions in Metalloproteins. in *Protein-Ligand Interactions: Methods and Applications* (ed. Ulrich Nienhaus, G.) 167–196 (Humana Press, 2005). doi:10.1385/1-59259-912-5:167
611. Nienhaus, K. & Nienhaus, G. U. Probing Heme Protein-Ligand Interactions by UV/Visible Absorption Spectroscopy. in *Protein-Ligand Interactions: Methods and Applications* (ed. Ulrich Nienhaus, G.) 215–241 (Humana Press, 2005). doi:10.1385/1-59259-912-5:215
612. Lim, M. & Anfinrud, P. A. Ultrafast Time-Resolved IR Studies of Protein-Ligand Interactions. in *Protein-Ligand Interactions: Methods and Applications* (ed. Ulrich Nienhaus, G.) 243–259 (Humana Press, 2005). doi:10.1385/1-59259-912-5:243
613. Kötting, C. & Gerwert, K. Monitoring Protein-Ligand Interactions by Time-Resolved FTIR Difference Spectroscopy. in *Protein-Ligand Interactions: Methods and Applications* (ed. Ulrich Nienhaus, G.) 261–285 (Humana Press, 2005). doi:10.1385/1-59259-912-5:261
614. Samuni, U. & Friedman, J. M. Proteins in Motion. in *Protein-Ligand Interactions: Methods and Applications* (ed. Ulrich Nienhaus, G.) 287–300 (Humana Press, 2005). doi:10.1385/1-59259-912-5:287
615. Jameson, D. M. & Mocz, G. Fluorescence Polarization/Anisotropy Approaches to Study Protein-Ligand Interactions. in *Protein-Ligand Interactions: Methods and Applications* (ed. Ulrich Nienhaus, G.) 301–322 (Humana Press, 2005). doi:10.1385/1-59259-912-5:301
616. Hargrove, M. S. Ligand Binding With Stopped-Flow Rapid Mixing. in *Protein-Ligand Interactions: Methods and Applications* (ed. Ulrich Nienhaus, G.) 323–341 (Humana Press, 2005). doi:10.1385/1-59259-912-5:323
617. Zemanová, L., Schenk, A., Valler, M. J., Nienhaus, G. U. & Heilker, R. High-Throughput Screening of Interactions Between G ProteinCoupled Receptors and Ligands Using Confocal Optics Microscopy. in *Protein-Ligand Interactions: Methods and Applications* (ed. Ulrich Nienhaus, G.) 365–383 (Humana Press, 2005). doi:10.1385/1-59259-912-5:365
618. Lu, H. P. Single-Molecule Study of Protein-Protein and Protein-DNA Interaction Dynamics. in *Protein-Ligand Interactions: Methods and Applications* (ed. Ulrich Nienhaus, G.) 385–413 (Humana Press, 2005). doi:10.1385/1-59259-912-5:385
619. Hazlett, T. L., Ruan, Q. & Tetin, S. Y. Application of Fluorescence Correlation Spectroscopy to Hapten-Antibody Binding. in *Protein-Ligand Interactions: Methods and Applications* (ed. Ulrich Nienhaus, G.) 415–438 (Humana Press, 2005). doi:10.1385/1-59259-912-5:415

620. Eibl, R. H. & Moy, V. T. Atomic Force Microscopy Measurements of Protein-Ligand Interactions on Living Cells. in *Protein-Ligand Interactions: Methods and Applications* (ed. Ulrich Nienhaus, G.) 439–449 (Humana Press, 2005). doi:10.1385/1-59259-912-5:439
621. Qin, J. & Gronenborn, A. M. Weak protein complexes: challenging to study but essential for life. *The FEBS Journal* 1948–1949 (2014). doi:10.1111/febs.12744@10.1002/(ISSN)1742-4658(CAT)MinireviewSeries(VI)WeakProteinInteracts
622. Luna, R. E., Akabayov, S. R., Ziarek, J. J. & Wagner, G. Examining weak protein-protein interactions in start codon recognition via nuclear magnetic resonance spectroscopy. *FEBS J* **281**, 1965–1973 (2014).
623. Tuukkanen, A. T. & Svergun, D. I. Weak protein-ligand interactions studied by small-angle X-ray scattering. *FEBS J* **281**, 1974–1987 (2014).
624. Neumann, T., Junker, H.-D., Schmidt, K. & Sekul, R. SPR-based Fragment Screening: Advantages and Applications. (2007). Available at: https://www.ingentaconnect.com/content/ben/ctmc/2007/00000007/00000016/art00007. (Accessed: 25th May 2019)
625. Harner, M. J., Mueller, L., Robbins, K. J. & Reily, M. D. NMR in drug design. *Archives of Biochemistry and Biophysics* **628**, 132–147 (2017).
626. Qin, J., Vinogradova, O. & Gronenborn, A. M. Protein-protein interactions probed by nuclear magnetic resonance spectroscopy. *Methods Enzymol* **339**, 377–389 (2001).